Photon Transfer

DN → λ

Photon Transfer

DN → λ

James R. Janesick

SPIE
PRESS

Bellingham, Washington USA

Library of Congress Cataloging-in-Publication Data

Janesick, James R.
Photon transfer : DN --> [lambda] / James R. Janesick.
p. cm.
Includes bibliographical references and index.
ISBN 978-0-8194-6722-5
1. Image converters--Calibration. 2. Image processing--Digital techniques--Mathematics. 3. Photon transport theory. 4. Engineering mathematics--Formulae. I. Title.

TK8316.J36 2007
621.36'7--dc22

2007021671

Published by

SPIE
P.O. Box 10
Bellingham, Washington 98227-0010 USA
Phone: +1 360.676.3290
Fax: +1 360.647.1445
Email: Books@SPIE.org
spie.org

Printed in the United States of America.

To the other Universes.

Contents

Acronyms and Abbreviations

ADC	analog-to-digital converter
AR	antireflection
CCD	charge-coupled device
CCE	charge collection efficiency
CDS	correlated double sampler
DCDS	digital CDS
DN	digital number
DPTC	dark photon transfer curve
DTC	dark transfer curve
EUV	extreme ultraviolet
FF	flat fielding
FPN	fixed pattern noise
IR	infrared
LED	light-emitting diode
LTC	lux transfer curve
MLTC	modulation lux transfer curve
MOSFET	metal-oxide-semiconductor field-effect transistor
MPTC	modulation photon transfer curve
MTF	modulation transfer function
PT	photon transfer
PTC	photon transfer curve
QE	quantum efficiency
RTS	random telegraph signal
S/N	signal-to-noise
TDI	time-delayed integration
UV	ultraviolet
VPTC	variance photon transfer curve
XDR	extended dynamic range

Preface

This book was prompted by engineers, scientists, and hardware managers who attended short courses held on CCD and CMOS imagers at UCLA Extension, SPIE conferences, and various seminars. Roughly 20% of course material presented is typically allocated to the *photon transfer characterization technique* necessary to set the stage for other sessions that require its application. Course evaluation forms generated by students requested more in-depth discussions about the measurement standard, and they suggested that a reference book on photon transfer be written. Encouraged by these recommendations, after 25 years of teaching these courses, this short book finally materialized.

Photon Transfer is designed for a wide audience—from the novice to the advanced user already familiar with the method. For first-time users, the book's primary purpose is to give sufficient guidelines to accurately generate, calibrate, and understand imaging data products made through the photon transfer method. With this goal in mind, Chapters 2–4 represent background and theoretical material necessary to fundamentally demonstrate how the technique works. Chapter 5 then discusses the mechanics of generating photon transfer curves before proceeding into more-complex photon transfer products.

Experienced users may find the material presented in Chapters 6–12 to be new territory. As this book was written, the author discovered many new photon-transfer characteristics, even after more than 30 years of previous study and use (e.g., Chapter 7 on the subject of V/e^- nonlinearity, Chapter 8 on flat fielding, and Chapter 9 on the modulation photon transfer curve). It is likely that readers will also discover new ways to apply photon transfer on future imaging technologies and applications.

The book contains more than 230 figures that present experimental CCD and CMOS data products and modeling simulations connected to photon transfer. Contents also provide hundreds of relations that support photon transfer theory, simulations, and data presented. For the more-important equations, 57 example problems are presented to demonstrate how the relations are used. Appendix A presents a spreadsheet of experimental CMOS data used to exercise the photon transfer method and produce numerous products and transfer curves. Appendices B–D present example computer photon transfer simulation programs utilized throughout the book.

The author would like to acknowledge Margaret Thayer, Timothy Lamkins, and Scott Schrum of SPIE for giving life to my English. Thanks goes to Joseph Altebrando and Rich Lobdill for first seeing and reacting with welcomed criticisms to the manuscript. I wish to express my thanks to Tom Elliott for helping me pioneer—over the many years we have worked together—the photon transfer technique and the presented x-ray data products. I especially want to thank my wife Linda and daughter Amanda, my sister Barb, and Mom and Dad for their timely support in many ways.

Photon Transfer

DN → λ

Chapter 1
Introduction

1.1 Photon Transfer History and Application

Photon transfer (PT) is a valuable testing methodology employed in the design, operation, characterization, optimization, calibration, specification, and application of solid state imagers and camera systems (most notably CCD and CMOS). As far as the author knows, PT began its evolution during the era of vidicon tubes used by NASA's early planetary imaging missions. The noise floor for these imagers was typically constant with light level, although a slight noise elevation near saturation was occasionally observed. Researchers speculated that the noise increase was associated with photon shot noise and prepared rudimentary plots to graph the noise source and better understand its nature. These plots may have been the first photon transfer curves (PTCs) generated by an area array imager in which noise was plotted against signal.

In the mid-1970s the charge-coupled device (CCD) began to replace the vidicon to become the premier imager for NASA and the imaging world.[1] This new solid state imager exhibited a read noise floor considerably lower than that of the vidicon (40 times less at that time). Photon shot noise was clearly observed, and the title "shot noise limited" was given to the sensor to signify its ideal performance. At the same time the CCD and PTC were immediately married. Although the formal name "photon transfer curve" would come a few years later, the new testing technique was formally born and would become an important measurement standard for the imaging community. Today PT is routinely used and continues to evolve along with the multitude of new imaging technologies in development.

The PT technique is applicable to all imaging disciplines. For example, CCD and CMOS solid state physicists as well as design and fabrication/process engineers rely on PT feedback to assist in the development and production of quality imagers. Table 1.1 lists key sensor performance parameters that are measured and optimized by PT and the chapters in this book where they are discussed.

Camera companies and their customers also regularly use a PTC for trouble shooting, characterization, optimization, and calibration purposes. The system level performance parameters listed in Table 1.2 depend on PT results.

Table 1.1 Detector performance parameters.

Performance parameter	Symbol	Unit	Chapter
Interacting quantum efficiency	QE_I	interacting photons/ incident photons	2
Quantum efficiency	QE	e^-/incident photons	2
Quantum yield	η_i	electrons/interacting photons	2
Fano factor	F_F		3
Pixel FPN quality factor	P_N		3
Charge collection efficiency	CCE		4
Effective quantum yield	η_E	e^-/photon	4
Sense node capacitance	C_{SN}	F	4
Sense node gain	A_{SN}	V/e^-	4
Charge capacity	S_{FW}	e^-	5
Dynamic range	DR		5
Image lag factor	I_{LAG}		5
Read noise	σ_{READ}	e^- rms	5
V/V nonlinearity	NL		7
V/e^- signal nonlinearity	NL_S		7
V/e^- noise nonlinearity	NL_N		7
Dark current figure of merit	D_{FM}	nA/cm^2 at 300 K	11
Dark current FPN quality factor	D_N		11
Dark current nonlinearity	NL_D		11
Offset fixed pattern noise	σ_{OFF}	e^- rms	11
Pixel source follower noise	σ_{SF}	e^- rms	11
Reset noise	σ_{RESET}	e^- rms	11
Pixel responsivity	R_e	e^-/lux-sec	12

Note that the performance parameters listed in Tables 1.1 and 1.2 are specified in absolute units (e.g., electrons). In contrast, sensor and camera systems that use relative units to specify performance can be very puzzling. For example, it is impossible to discern if a pixel's charge capacity is satisfactory if it is specified in output volts. But there is no misunderstanding about a full-well specification given in electron units. Some parameters may be encountered that fool one's intuition. For example, a low read noise voltage generated by a detector may seem to achieve better signal-to-noise (S/N) performance relative to a higher noise floor. However, when the same noise is measured in electrons, the higher noise voltage may prove to be superior (e.g., refer to Chapter 11 on reset noise). The absolute scientific units provided by PT take the guesswork out of properly specifying performance.

Raw data generated by a camera system are measured in the form of relative digital numbers, or DNs (i.e., a pixel's signal is encoded in DN). The DN is phys-

Table 1.2 Camera system performance parameters.

Performance parameter	Symbol	Units	Chapter
Analog to digital converter (ADC) sensitivity	$K_{\mathrm{ADC}}(\mathrm{e}^-/\mathrm{DN})$	e^-/DN	4
ADC offset	$S_{\mathrm{ADC\_OFF}}(\mathrm{DN})$	DN	4
ADC sensitivity variance	σ_{K}	e^-/DN rms	6
ADC noise sensitivity	$N_{\mathrm{ADC}}(\mathrm{e}^-/\mathrm{DN})$	e^-/DN	7
ADC signal sensitivity	$S_{\mathrm{ADC}}(\mathrm{e}^-/\mathrm{DN})$	e^-/DN	7
Flat-fielding quality factor	Q_{FF}	e^-	8
Flat-field S/N	$(\mathrm{S/N})_{\mathrm{FF}}$		10
Image S/N	$(\mathrm{S/N})_{\mathrm{I}}$		10
Maximum image S/N	$(\mathrm{S/N})_{\mathrm{I\_MAX}}$		10
ADC quantizing noise	σ_{ADC}	e^- rms	11
System noise	σ_{SYS}	e^- rms	11
Absolute flat-field S/N	$[\mathrm{S/N}]_{\mathrm{L\_FF}}$		12
Absolute image S/N	$[\mathrm{S/N}]_{\mathrm{L\_I}}$		12
Minimum detectable luminance	L_{MIN}	lux	12
Image luminance required for S/N = 10	L_{Q}	lux	12

ically meaningless. Therefore, it is essential that a constant be found that converts DN units to absolute electron units. Deriving this constant may seem like a daunting task considering the multitude of transfer functions associated with a camera system, especially if the accuracy required for this constant must sometimes be better than 1% for scientific work. Luckily, PT can treat a camera system, no matter how complex it is, as a black box and determine the desired conversion constant with very little effort. The user needs only to expose the camera to a light source and measure the signal and noise output DN responses for a small group of pixels. From there PT is applied, and almost magically, the desired e^-/DN constant is obtained.

Photon transfer is one of the first go/no-go tests performed to determine the health of a new camera system. Frequently, PTC plots are disappointing on the first try because a new camera may be filled with problems. PT aids troubleshooting with routines to identify issues ranging from solid state sensor problems to software data acquisition deficiencies. PT keeps everyone honest (including software engineers!) by providing absolute information each step of the way. Dozens of PTCs may be generated before a camera can be declared "operational," and even more curves to title it "optimized." But in the end, the efforts will be worthwhile to ensure that a camera is achieving the most reliable high performance possible.

Fortunately, testers have prior knowledge about what a PTC should look like before beginning the process. PTC "shape" is dictated by Mother Nature, who herself is described by a few PT relations. Many PTCs presented in this text are computer simulated using derived theoretical PT relations (e.g., refer to the appendix for

example computer programs). Textbook experimental PTCs will precisely follow simulation results only when a system is in perfect working order as judged by PT.

When executing PT, initially it may seem like a lifetime before good results materialize. However, as experience is gained with PTC, data will be generated in short order (experts can generate PTCs in less than a minute). The necessity for high-speed PT testing is warranted because each camera modification requires a new e^-/DN calibration. For example, when attempting to lower the read noise through a camera change, the DN noise level must be converted to electrons through e^-/DN in order to verify if the fix worked (recall that a lower DN noise change could actually mean a higher electron noise level). Similar to peeling an onion, read noise sources are eliminated one by one through the routine. Therefore, it is desirable to run PT experiments quickly. PT also enables testers to tweak most other parameters for optimum performance with a fast turnaround.

The end user will also find PT valuable. For example, generating a PTC will verify if a camera purchase meets specifications before serious application in the field takes place. An application may require absolute calibration to measure signals with very high accuracy (a $<1\%$ photometry error is routine for astronomers). PTCs will demonstrate and confirm that a camera system is stable and reliable. Image processing algorithms are often applied to remove fixed pattern noise (FPN) sources to obtain high S/N performance, especially when working with low-contrast images. PTCs validate that the software and hardware for this important purpose are in order. As will be shown in Chapter 12, PT is also a valuable tool that joins commercial photometric and scientific radiometric measurement units.

1.2 Photon Transfer Family

It is remarkable that only two measurements—average signal and rms noise—can produce the amount of information contained in this book. In addition to the data products presented in Tables 1.1 and 1.2, different transfer curves can be generated from the same two parameters for further characterization results. As it turns out, format is an important factor in extracting the most information from a PTC; therefore, specific plotting routines have been invented for this purpose. Collectively, these routines are called the "photon transfer family." Tables 1.3–1.17 present the principal transfer curves contained for the family. By far the most exercised plot is the classical PTC (Table 1.3) and the variance PTC (Table 1.4). This data will give the user significant insight about whether a camera system is in proper working order as well as supply many of the performance parameters listed in Tables 1.1 and 1.2. Note that some PTCs are composed of multiple plots that differentiate noise sources (grouped as "sets"). Also, PTC data are usually plotted in both DN and electron units, which produces supplementary information.

Each performance parameter and transfer curve presented in Tables 1.1–1.17 will be encountered in this book, including many others. Theoretical PT relations are also derived for each curve to support the experimental data taken.

Table 1.3 Photon transfer curve (PTC).

Set	Plots	Units	Chapter
Set 1	read, shot, FPN (total noise) vs. signal	log rms DN vs. log DN	5
Set 1	read, shot noise vs. signal	log rms DN vs. log DN	5
Set 1	shot noise vs. signal	log rms DN vs. log DN	5
Set 1	FPN vs. signal	log rms DN vs. log DN	5
Set 2	read, shot, FPN (total noise) vs. signal	log rms e^- vs. log e^-	5
Set 2	read, shot noise vs. signal	log rms e^- vs. log e^-	5
Set 2	shot noise vs. signal	log rms e^- vs. log e^-	5
Set 2	FPN vs. signal	log rms e^- vs. log e^-	5

Table 1.4 Variance photon transfer curve (VPTC).

Set	Plots	Units	Chapter
Set 1	shot noise variance vs. signal	(rms DN)^2 vs. DN	5

Table 1.5 V/V nonlinearity.

Set	Plots	Units	Chapter
Set 1	K_{ADC}(e^-/DN) vs. signal	e^-/DN vs. log DN	7
Set 2	K_{ADC}(e^-/DN) vs. signal	e^-/DN vs. log e^-	7

Table 1.6 V/e^- nonlinearity.

Set	Plots	Units	Chapter
Set 1	S_{ADC}(e^-/DN) vs. signal	signal e^-/DN vs. log DN	7
Set 1	N_{ADC}(e^-/DN) vs. signal	noise e^-/DN vs. log DN	7
Set 2	S_{ADC}(e^-/DN) vs. signal	signal e^-/DN vs. log e^-	7
Set 2	N_{ADC}(e^-/DN) vs. signal	noise e^-/DN vs. log e^-	7

Table 1.7 Nonlinearity residuals.

Set	Plots	Units	Chapter
Set 1	nonlinearity vs. signal	% vs. log DN	7
Set 2	nonlinearity vs. signal	% vs. log e^-	7

Table 1.8 K_{ADC}(e^-/DN) histogram.

Set	Plots	Units	Chapter
Set 1	occurrences vs. K_{ADS}(e^-/DN)	occurrences vs. e^-/DN	6

Table 1.9 Quantum yield.

Set	Plots	Units	Chapter
Set 1	quantum yield vs. wavelength	e^-/interacting photon vs. wavelength	2

Table 1.10 Flat-fielding photon transfer curve (FFPTC).

Set	Plots	Units	Chapter
Set 1	read, shot, FPN (total noise) vs. signal	log rms DN vs. log DN	8
Set 1	read, shot noise vs. signal	log rms DN vs. log DN	8
Set 1	read, shot noise vs. signal (after FF)	log rms DN vs. log DN	8
Set 2	read, shot noise, FPN vs. signal	log rms e^- vs. log e^-	8
Set 2	read, shot noise (total noise) vs. signal	log rms e^- vs. log e^-	8
Set 2	read, shot noise vs. signal (after FF)	log rms e^- vs. log e^-	8

Table 1.11 Modulation photon transfer curve (MPTC).

Set	Plots	Units	Chapter
Set 1	image modulation vs. signal	log rms DN vs. log DN	9
Set 1	read, shot, FPN vs. signal	log rms DN vs. log DN	9
Set 1	read, shot noise vs. signal	log rms DN vs. log DN	9
Set 2	image modulation vs. signal	log rms e^- vs. log e^-	9
Set 2	read, shot, FPN vs. signal	log rms e^- vs. log e^-	9
Set 2	read, shot noise vs. signal	log rms e^- vs. log e^-	9

Table 1.12 Signal-to-noise transfer curve.

Set	Plots	Units	Chapter
Set 1	read, shot, FPN (total noise) S/N vs. signal	log S/N vs. log DN	10
Set 1	read, shot S/N vs. signal	log S/N vs. log DN	10
Set 2	read, shot, FPN (total noise) S/N vs. signal	log S/N vs. log e^-	10
Set 2	read, shot S/N vs. signal	log S/N vs. log e^-	10

Table 1.13 Flat-fielding signal-to-noise transfer curve.

Set	Plots	Units	Chapter
Set 1	S/N vs. signal (after FF)	log S/N vs. log DN	10
Set 2	S/N vs. signal (after FF)	log S/N vs. log e^-	10

Table 1.14 Image signal-to-noise transfer curve.

Set	Plots	Units	Chapter
Set 1	Image S/N vs. signal (with FPN)	log S/N vs. log DN	10
Set 1	Image S/N vs. signal (without FPN)	log S/N vs. log DN	10
Set 2	Image S/N vs. signal (with FPN)	log S/N vs. log e^-	10
Set 2	Image S/N vs. signal (without FPN)	log S/N vs. log e^-	10

Table 1.15 Dark transfer curve (DTC).

Set	Plots	Units	Chapter
Set 1	Dark read, shot, FPN (total noise) vs. signal	log DN vs. log DN	11
Set 1	Dark read, shot noise vs. signal	log DN vs. log DN	11
Set 2	Dark read, shot, FPN (total noise) vs. signal	log e^- vs. log e^-	11
Set 2	Dark read, shot noise vs. signal	log e^- vs. log e^-	11

Table 1.16 Lux transfer curve (LTC).

Set	Plots	Units	Chapter
Set 1	S/N vs. luminance (with FPN)	log S/N vs. log lux	12
Set 1	S/N vs. luminance (without FPN)	log S/N vs. log lux	12

Table 1.17 Modulation lux transfer curve (MLTC).

Set	Plots	Units	Chapter
Set 1	S/N vs. luminance (with FPN)	log S/N vs. log lux	12
Set 1	S/N vs. luminance (without FPN)	log S/N vs. log lux	12

1.3 Chapter Review

This section summarizes each chapter in this book:

Chapter 2, *Photon Interaction*, briefly reviews the photoelectric effect as applied to semiconductors stimulated with energetic particles. Although varieties of particles, carriers, and semiconductors can be involved in the PT process, this book assumes that photons, electrons, and silicon are responsible for generating electronic images. PT plays a role in measuring the number of photons that interact photoelectrically with the silicon, a performance parameter referred to as *quantum efficiency* (QE). For energetic photons, multiple electrons are generated, a performance parameter referred to as *quantum yield*. This characteristic is important because a PT response is dependent on photon wavelength, which allows incident photon energy and related quantum yield to be determined.

Chapter 3, *Photon Transfer Noise Sources*, introduces four fundamental noise sources measured by PT. Two sources, shot noise and Fano noise, are related to initial photo-carrier generation. Photon shot noise plays a major role in providing the information necessary to determine the e^-/DN conversion constant found by the PTC. The third noise source, pixel FPN, is present because charge collection from pixel to pixel is different. Although FPN seems to be insignificant (only 1% pixel nonuniformity is measured for CCD and CMOS detectors), the noise source dominates the sensor's dynamic range and has a dramatic limiting effect on S/N performance. The last noise source, read noise, limits the accuracy for all measurements made by PT.

Chapter 4, *Photon Transfer Theory,* presents transfer functions for a typical camera system with the photon as the input and DN as the output. General PT equations are derived for the various sensitivity functions internal to the system that relate DN, volt, electron, and photon measurement units (e.g., e^-/DN). We demonstrate how quantum efficiency, quantum yield, and charge collection efficiency (CCE) are measured by manipulating the sensitivity constants.

Chapter 5, *Photon Transfer Curve*, reviews camera and software setup requirements to perform PT experiments. Experimental data is used to show a step-by-step procedure used to generate a PTC. The classical PTC is introduced, showing four distinct noise regimes in the plots (read noise, shot noise, FPN, and full well). PTC computer simulations are employed to exercise PT equations derived for the plots. Various performance parameters are then extracted from the PTCs, including the important e^-/DN conversion constant. Common signal processing errors that add uncertainty to the ideal PTC response are reviewed and demonstrated. An advanced measuring technique is described that generates a full PTC from a single frame of data. The variance PTC, an alternate graphing format, is presented to graphically determine e^-/DN in the presence of read noise. The last section of the chapter includes many sample experimental PTC data products.

Chapter 6, e^-/DN *Variance*, theoretically derives the formulas required to determine the e^-/DN constant to a specific degree of accuracy. PTC simulations and data products verify the precision achieved for the relations presented. The analysis is also applicable to other camera sensitivity parameters that require a desired degree of accuracy.

Chapter 7, *Nonlinearity*, discusses V/V gain nonlinearity common to CCD and CMOS sensors. The problem is quantified by taking a standard PTC data set and plotting e^-/DN as a function of signal. Signal processing algorithms are presented that remove the nonlinearity problem. This chapter also deals with V/e^- nonlinearity, a more serious gain problem associated with CMOS detectors. Detailed analysis presents the impact of V/e^- gain nonlinearity on PTC results. The last section shows that PTC can separate the effects of V/V and V/e^- nonlinearity issues when both problems are present.

Chapter 8, *Flat Fielding*, demonstrates a popular image signal processing technique used to remove FPN in images to achieve shot noise limited performance (the best possible performance). The chapter begins by demonstrating the mechanics of the flat-fielding technique through simulation. A general formula is derived that predicts the resultant noise contained in an image after flat fielding is performed. Various before and after flat-field simulations are presented that demonstrate the flat-fielding routine. The PTC is then used to verify expected results.

Chapter 9, *Modulation Photon Transfer*, derives the response generated by a detector stimulated by a sinusoidal light source. Important results from analysis and simulations show that the average sinusoidal shot noise and FPN are approximately equivalent to a uniform light response with the same average signal level. Similar conclusions are extended to real images. The "modulation PTC" plots image modulation as a function of average signal. An "image modulation constant" is extracted from the curve, a product of incoming scene contrast and system modulation transfer function (MTF). The parameter is used to quantify image S/N performance in the following chapter.

Chapter 10, *Signal-to-noise Performance*, replots PTC data as S/N as a function of signal. Image S/N plots are generated from modulation PTC data. An important relation is also derived to show that S/N for an image is the product of the flat-field S/N and the image modulation constant. Simulated images are presented to demonstrate that quality images required S/N $>$ 10. Analysis includes S/N improvements achieved when FPN is removed through flat fielding. The chapter closes by showing S/N improvements made when multiple frames of an image are averaged.

Chapter 11, *Read Noise*, discusses important noise sources found in CCD and CMOS cameras that are collectively called the read noise floor. Noise sources analyzed include pixel source follower noise, sense node reset noise, thermal dark current noise, ADC quantizing noise, offset FPN, and system noise. Relations are given for each source and show their unique influence on PTC results.

Chapter 12, *Lux Transfer*, describes a powerful extension of the PTC that plots S/N as a function of absolute light level. The LTC is a valuable standard that collects all detector and camera performance parameters into a single performance curve. Also presented is the "modulation LTC," an extension of modulation PTC that plots image S/N as a function of absolute light level. Numerous data products are derived from these two curves, including minimum detectable luminance level, luminance required for image S/N $>$ 10, and pixel responsivity (e^-/lux-sec). Radiometric and photometric units are married by the LTC.

Appendix A presents tables containing raw experimental data generated by a CMOS imager. Discussions take the user through a step-by-step process to generate various PTC results from the data. Appendixes B, C, and D contain MatLab simulation programs that generate PTCs and LTCs.

Chapter 2
Photon Interaction

2.1 Photoelectric Effect

Photons incident on a semiconductor generate electron-hole pairs through a process known as the *photoelectric absorption effect* or simply the *photoelectric effect* (refer to Fig. 2.1). Once created, the carriers are free to move in the semiconductor lattice, where they are quickly collected by pixel elements (pixels). The majority of silicon CCD and CMOS imagers are designed and fabricated to generate electrons and discard holes through a device ground return. Particles other than photons can also produce signal carriers by ionizing silicon atoms as they travel through the lattice, including high-energy electrons, protons, ions, etc. Any high-energy particle that is in a charged state can free primary valence electrons that collide with other silicon atoms to generate secondary electrons (e.g., refer to Fig. 4.5, which shows proton ionizing events). For PT discussions in this text, it will be assumed that photons, electrons, and silicon are responsible for generating electronic pictures.

Figure 2.1(a) shows the photoelectric effect taking place when an interacting photon has adequate energy to overcome the silicon bandgap energy by removing a valence electron into the conduction band. Figure 2.1(b) shows an energetic photon that has extra energy to generate multiple electrons by the conduction band electron, which is explained in Sec. 2.3. For silicon, the minimum photon energy requirement to free a valence electron is approximately 1.14 eV, or in terms of wavelength,

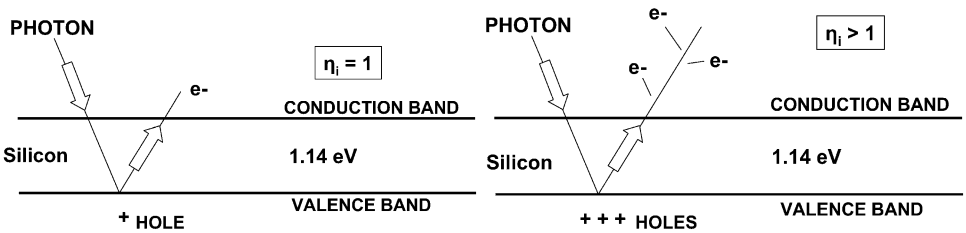

Figure 2.1 (a) Photoelectric effect where a single electron-hole pair and (b) multiple electron holes are generated per interacting photon.

$$\lambda = \frac{12{,}390}{h_\nu}, \tag{2.1}$$

where h_ν is the energy of the photon (eV), and λ is its wavelength (A).

Example 2.1

What is the corresponding wavelength for a 1.14 eV photon? Calculate the solution in units of A, nm, μm, and cm.

Solution:
From Eq. (2.1),

$$\lambda = \frac{12{,}390}{1.14} = 10,868\text{A} \quad (1086.8\ \text{nm}, 1.0868\ \mu\text{m}, \text{ and } 1.0868 \times 10^{-4}\ \text{cm}).$$

For photon energies less than 1.14 eV, the photoelectric effect does not take place and the silicon is transparent. Therefore, direct imagery is not possible for wavelengths beyond 10,868 A.

The photoelectric effect for silicon extends over a very wide photon energy range, from 1 to 10 keV (10,000 to 1 A). For example, Fig. 2.2 plots the photon interacting efficiency of silicon as a function of photon energy (eV) and wavelength (A) for a backside-illuminated silicon detector of 10-μm thickness. As labeled in the figure, the spectral sensitivity covers the near infrared (IR), visible, ultraviolet (UV), extreme UV (EUV), and soft x-ray regions. The response is IR-limited by the silicon bandgap energy and by the photon's cross-section in the hard x-ray. Sensitivity at the IR/x-ray edges is solely dependent on the silicon thickness' ability to capture incident photons.

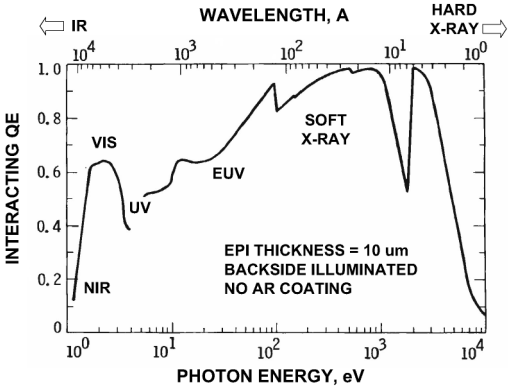

Figure 2.2 Broadband interacting QE for a backside illuminated silicon imager as a function of wavelength and photon energy.

2.2 Quantum Efficiency

The ability of a semiconductor to produce electrons from incident photons is referred to as its *quantum efficiency* (QE)—e^-/incident photon—which is defined as

$$\mathrm{QE} = \eta_i \mathrm{QE_I}, \tag{2.2}$$

where η_i is the quantum yield gain (e^-/interacting photon) discussed in Sec. 2.3, and $\mathrm{QE_I}$ is called the *interacting QE*. $\mathrm{QE_I}$ is defined as

$$\mathrm{QE_I} = \frac{P_\mathrm{I}}{P}, \tag{2.3}$$

where P is the average number of incident photons per pixel, and P_I is the average number of interacting photons per pixel. Note that QE can be greater than unity because of quantum yield gain, whereas $\mathrm{QE_I}$ is always less than unity. $\mathrm{QE_I}$ provides a figure of merit to show the user how well the sensor manufacturer has allowed incident photons to interact with the semiconductor.

Although $\mathrm{QE_I}$ data sheets are usually provided by the manufacturer, the performance parameters can also be verified by the user. Figure 2.3 shows a QE test configuration using a calibrated silicon photodiode that covers a spectral range of 2,500 to 11,000 A. The diode and sensor in question are in close proximity to intercept the same number of incident photons. The illumination shown in the figure is provided by a 100-W quartz lamp in conjunction with a diffuser to scatter light uniformly across both devices (monochrometers also can be used to make detailed

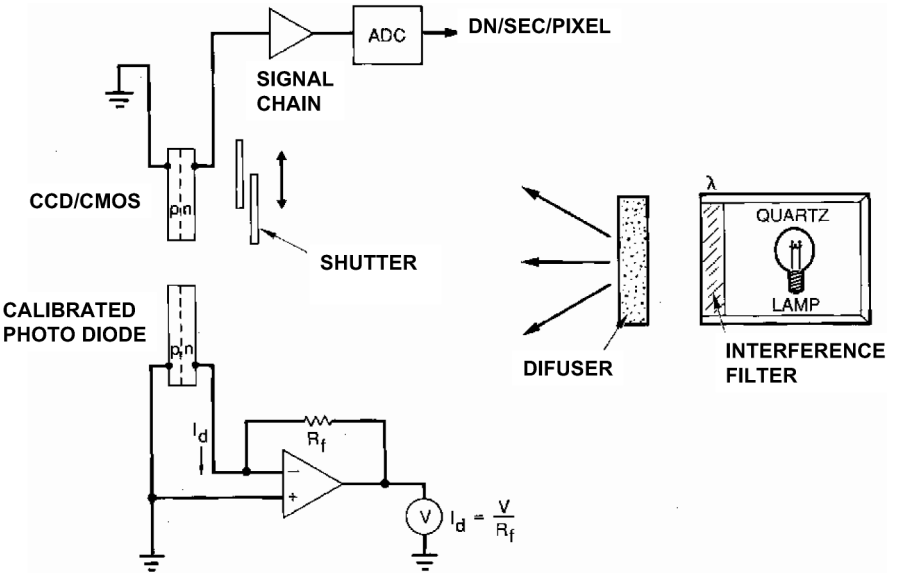

Figure 2.3 QE measurement set-up.

QE measurements). Interference filters are used to filter light and measure QE as a function of wavelength. QE is determined by comparing responses of the sensor and standard diode through the relation

$$\mathrm{QE} = \frac{A_\mathrm{D} S(\mathrm{DN}) K_\mathrm{ADC}(\mathrm{e}^-/\mathrm{DN}) \mathrm{QE}_\mathrm{D}}{P_\mathrm{A} S_\mathrm{D} t_\mathrm{I}}, \tag{2.4}$$

where A_D is the active area of a standard photodiode (cm^2), QE_D is the quantum efficiency of the standard diode, P_A is the area of a pixel (cm^2), S_D is the photo signal generated by the diode (e^-/sec), t_I is the exposure or integration time for the sensor (sec), and $K_\mathrm{ADC}(\mathrm{e}^-/\mathrm{DN})$ is a constant found through PT that converts the DN to electron units (refer to Chapter 4). The term QE_D in Eq. (2.4) is the QE of the standard diode. These data are often supplied by the manufacturer in the form of spectral responsivity (ampere/watt) as a function of wavelength. This quantity can be converted to QE_D by the equation

$$\mathrm{QE}_\mathrm{D} = \frac{12{,}390 R_\mathrm{e}}{\lambda}, \tag{2.5}$$

where R_e is the standard diode responsivity (A/W). Figure 2.4 shows a typical response generated by a silicon photodiode. The responsivity covers the near-UV (2500 A) to the near IR (11,000 A).

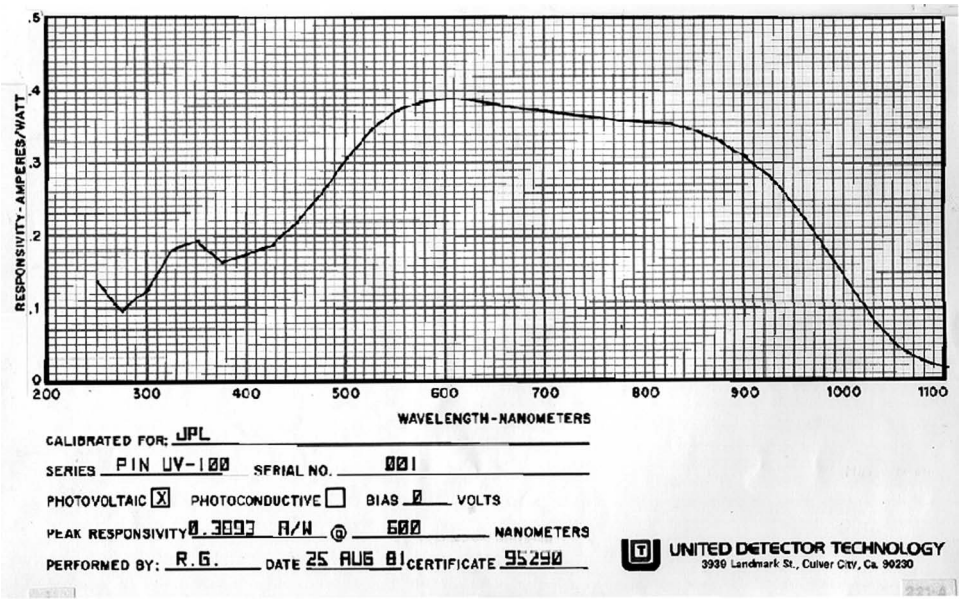

Figure 2.4 Standard silicon-calibrated photodiode used for QE measurement.

Example 2.2

Determine QE, assuming the following test data and parameters:

$$S(\mathrm{DN}) = 25{,}000$$

$$K_{\mathrm{ADC}}(\mathrm{e^-/DN}) = 10$$

$$A_{\mathrm{D}} = 1\ \mathrm{cm}^2$$

$$P_{\mathrm{A}} = 4 \times 10^{-6}\ \mathrm{cm}^2$$

$$\mathrm{QE_D} = 0.75$$

$$S_{\mathrm{D}} = 6.25 \times 10^{10}\ \mathrm{e^-/sec}$$

$$t_{\mathrm{I}} = 1.5\ \mathrm{sec}$$

Solution:
From Eq. (2.4),

$$\mathrm{QE} = \frac{1 \times (2.5 \times 10^4) \times 10 \times 0.75}{(4 \times 10^{-6}) \times (6.25 \times 10^{10}) \times 1.5} = 0.5.$$

For backside-illuminated sensors, one can cross-check the appropriate QE and $\mathrm{QE_I}$ measurements through the equation

$$\mathrm{QE_I} = (1 - R_{\mathrm{REF}})\Big(1 - e^{-(T_{\mathrm{EPI}}/L_{\mathrm{A}})}\Big), \tag{2.6}$$

where R_{REF} is the silicon reflection coefficient factor, T_{EPI} is the optical active thickness of the sensor (typically the epitaxial silicon thickness in μm), and L_{A} is the silicon photon absorption length (μm). Table 2.1 provides approximate values for R_{REF} and L_{A} as a function of wavelength.

When the sensor has an antireflection (AR) coating, the QE is approximated through

$$\mathrm{QE_I} = E_{\mathrm{AR}}\Big(1 - e^{-(T_{\mathrm{EPI}}/L_{\mathrm{A}})}\Big), \tag{2.7}$$

where E_{AR} is the AR efficiency factor, which varies depending on which coating is used.

Table 2.1 Approximate values for R_{REF} and L_{A} as a function of wavelength.

Wavelength (nm)	Absorption Length (μm)	Reflection Coefficient	AR Coating Efficiency Factor
300	.0065	.63	.46
320	.00851	.58	.47
340	.0115	.58	.48
360	.0286	.60	.72
380	.0667	.55	.8
400	.2	.5	.85
420	.2976	.48	.89
440	.43	.46	.92
460	.5814	.44	.94
480	.7752	.42	.95
500	.9804	.405	.96
520	1.2048	.39	.963
540	1.4265	.38	.962
560	1.6666	.37	.961
580	1.9305	.36	.960
600	2.2472	.355	.959
620	2.5773	.354	.958
640	2.9851	.353	.957
660	3.4722	.352	.956
680	4.0650	.351	.955
700	4.7619	.350	.954
720	5.5555	.349	.953
740	6.4935	.348	.952
760	7.6336	.347	.951
780	8.9285	.346	.950
800	10.5263	.345	.949
820	12.7388	.344	.948
840	15.3846	.343	.947
860	18.6915	.342	.946
880	22.9985	.341	.945
900	28.5714	.340	.944
920	35.08	.338	.943
940	43.47	.336	.942
960	54.34	.334	.941
980	70.42	.332	.941
1000	93.45	.330	.940

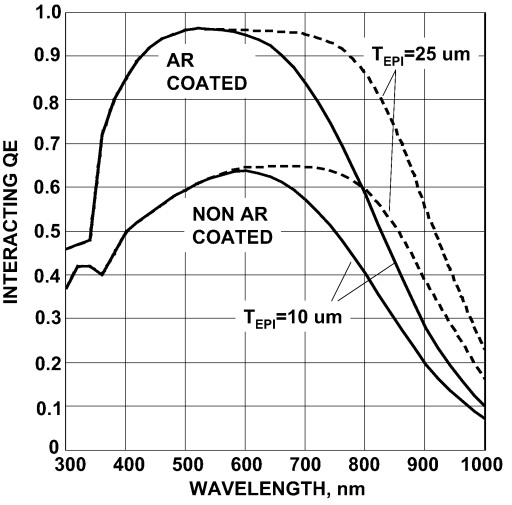

Figure 2.5 QE-modeled response with and without an antireflection coating.

Example 2.3

Plot Eqs. (2.6) and (2.7) using the data supplied in Table 2.1. Assume $T_{\mathrm{EPI}} = 10$ and 25 μm.

Solution:
Figure 2.5 shows the desired QE plots.

The average number of electrons generated per pixel as a function of incident photons is

$$S = \mathrm{QE_I}\eta_{\mathrm{i}}P = \eta_{\mathrm{i}}P_{\mathrm{I}}, \tag{2.8}$$

where S is the signal (e^-).

2.3 Quantum Yield

For silicon, photon energy that ranges from 1.14 to 3.1 eV (11,868–4,000 A) will generate a single electron. This spectral range covers the near-IR (i.e., 7,000–11,000 A) and visible (i.e., 4,000–7,000 A) regions. Energies greater than approximately 3.1 eV will produce multiple electrons because the energetic electron injected will collide with other silicon atoms and free additional electrons [refer to Fig. 2.1(b)]. Figure 2.6 presents quantum yield data from a CCD showing that multiple electron generation begins to take place beyond 4000 A. The critical wavelength at the onset of the effect is dependent on the internal electric fields within the

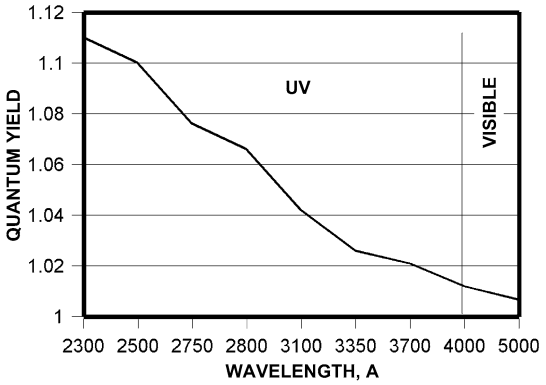

Figure 2.6 Measured quantum yield in the UV by photon transfer.

sensor and therefore varies from sensor to sensor because of processing differences. Chapter 4 will describe how quantum yield is measured with the PT technique.

The quantum yield gain for interacting photon energies > 10 eV is given by the relation

$$\eta_{\mathrm{i}} = \frac{h_{\nu}}{E_{\text{e-h}}}. \tag{2.9}$$

This relation in terms of wavelength is

$$\eta_{\mathrm{i}} = \frac{12{,}390}{E_{\text{e-h}}\lambda}, \tag{2.10}$$

where $E_{\text{e-h}}$ is the energy required to generate an electron-hole pair (which for silicon is approximately 3.65 eV/e^- at room temperature). This energy requirement is greater than the silicon bandgap (i.e., 1.14 eV) because the conservation of momentum principle requires that some energy transfers to the excitation of the lattice vibrations and phonons (i.e., heat). Equation (2.9) is valid only for photon energies > 10 eV. Unfortunately, a simple quantum yield relation for the 3.1–10 eV range is not possible.

Example 2.4

Find the quantum yield gain for 10 eV and 5.9 keV photons.

Solution:
From Eq. (2.9),

$$\eta_{\mathrm{i}} = \frac{10}{3.65} = 2.74\ \mathrm{e}^-/\text{interacting photon} \quad \text{at } 10\ \mathrm{eV},$$

and

$$\eta_{\mathrm{i}} = \frac{5900}{3.65} = 1620\ \mathrm{e}^-/\text{interacting photon} \quad \text{at } 5.9\ \mathrm{keV}.$$

Important Points

1. The photoelectric effect for silicon imagers extends over a useful photon energy range of 1–10,000 eV (1–10,000 A).
2. QE performance is the fraction of the incident photons that interact multiplied by the quantum yield. Interacting QE is only specified by the percentage of photons that interact.
3. The quantum yield gain is unity for visible and near-IR light and increases when the photon energy is > 3.1 eV (4000 A).
4. The PT conversion constant e^-/DN is necessary to measure QE, QE_I, and η_i.

Chapter 3
Photon Transfer Noise Sources

When photons strike a detector, interactions immediately produce a signal variance or *noise* from pixel-to-pixel. This chapter introduces four fundamental noise sources important to PT work. The first two sources, *signal shot noise* and *Fano noise*, are related to photon interaction. The third noise source, *fixed pattern noise*, is associated with pixel-to-pixel sensitivity nonuniformity. The fourth source, *read noise*, encompasses all other noise sources that are not dependent on signal strength. Shot noise increases by the square root of signal, whereas FPN increases proportionally with signal. Fano noise increases by the square root of photon energy (or quantum yield).

3.1 Photon Shot Noise

Signal shot noise is fundamentally connected to the way photons spatially arrive on a detector. For example, Fig. 3.1 shows a Monte Carlo simulation where 200 photons are randomly interacting with a 20×20 pixel region. As can be seen, the number of photon interactions varies from zero to four interactions per pixel. The standard deviation (or rms) for the number of interactions per pixel is called *photon shot noise*.

Photon shot noise—a spatially and temporally random phenomenon described by Bose-Einstein statistics—is expressed by

$$\sigma_{\mathrm{SHOT}}(P_{\mathrm{I}})^2 = P_{\mathrm{I}} \frac{e^{hc/\lambda kT}}{e^{hc/\lambda kT} - 1}, \tag{3.1}$$

where $\sigma_{\mathrm{SHOT}}(P_{\mathrm{I}})^2$ is the interacting photon shot noise variance, h is Planck's constant (6.626×10^{-34} J-s), λ is the photon wavelength (cm), k is Boltzmann's constant (1.38×10^{-23} J/K), c is the speed of light (2.99×10^{8} m/sec), and T is absolute temperature (K).[2–4]

Figure 3.2 plots Eq. (3.1) as a function of wavelength (μm) and the temperature of the semiconductor. For wavelengths greater than 10 μm, photons couple with phonons (i.e., lattice vibrations in a solid) that increase the shot noise. As the operating temperature is reduced, the semiconductor produces less coupling action and variance as seen in the plot. However, for silicon detectors this phenomenon is not observed since the photoelectric effect for wavelengths >1 μm can not take

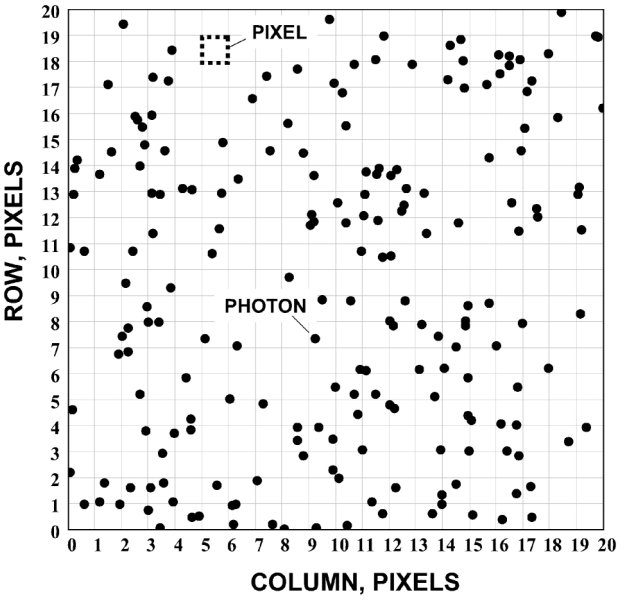

Figure 3.1 Monte Carlo simulation showing photons interacting with pixels.

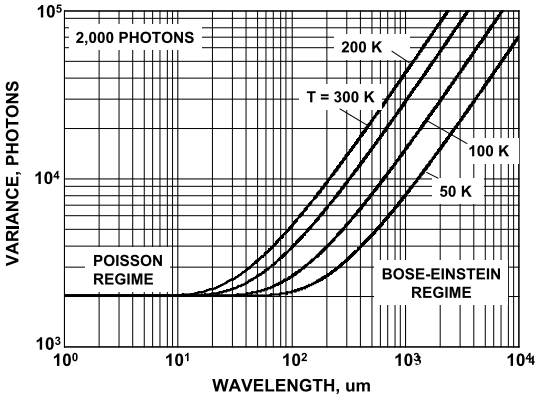

Figure 3.2 Photon shot noise variance as a function of wavelength.

place. Assuming that $hc/\lambda \gg kT$, Eq. (3.1) reduces to the familiar shot noise relation characteristic of visible imagers as

$$\sigma_{\mathrm{SHOT}}(P_{\mathrm{I}}) = P_{\mathrm{I}}^{1/2}. \tag{3.2}$$

Photon shot noise is described by the classical Poisson probability distribution,

$$p_i = \frac{P_{\mathrm{I}}^i}{i!} e^{-P_{\mathrm{I}}}, \tag{3.3}$$

where p_i is the probability that there are i interactions per pixel.

Example 3.1

Find the probability that 0, 1, 2, and 3 photons interact with a pixel, assuming an average of 1 interacting photon per pixel.

Solution:
From Eq. (3.3):

$$p_0 = \frac{1^0}{0!}e^{-1} = 0.368 \quad \text{0 photon interactions}$$

$$p_1 = \frac{1^1}{1!}e^{-1} = 0.368 \quad \text{1 photon interaction}$$

$$p_2 = \frac{1^2}{2!}e^{-1} = 0.184 \quad \text{2 photon interactions}$$

$$p_3 = \frac{1^3}{3!}e^{-1} = 0.0613 \quad \text{3 photon interactions}$$

Figure 3.3 shows results from a random number generator governed by Poisson statistics. The histogram plots occurrences as a function of interacting photons per pixel, assuming 90,000 pixels and 90,000 interacting photons (i.e., $P_{\mathrm{I}} = 1$). The resultant distribution follows the Poisson formula given by Eq. (3.3). For example, 33,200 pixels have one photon interaction, whereas 33,070 pixels show no interactions. The results are expanded and plotted in Fig. 3.4 on a log curve that shows six pixels with seven events.

Figure 3.3 also shows a Gaussian curve to fit data for Example 3.1 that follows

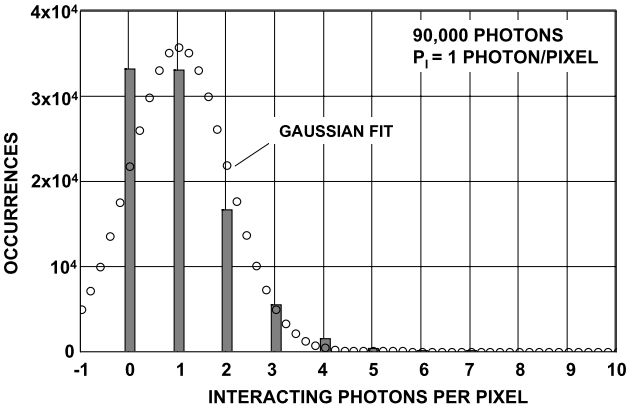

Figure 3.3 Interacting-photons-per-pixel histogram for Fig. 3.1 assuming 1 photon/pixel average.

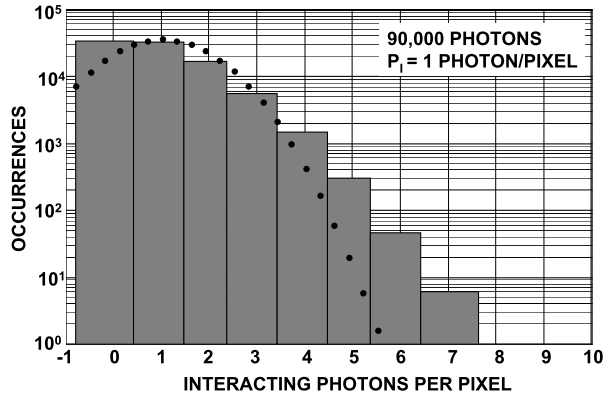

Figure 3.4 Logarithmic histogram for Fig. 3.3.

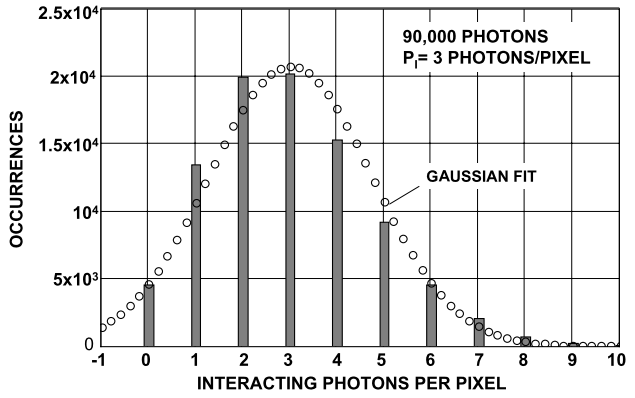

Figure 3.5 Interacting-photons-per-pixel histogram assuming 3 photons/pixel average.

the relation

$$p_i = \frac{1}{(2\pi)^{1/2}\sigma_{\mathrm{PI}}} e^{-(i-P_{\mathrm{I}})^2/2\sigma_{\mathrm{PI}}^2}. \tag{3.4}$$

A Gaussian distribution approximates a Poisson distribution when the number of interacting photons per pixel is large. For example, Fig. 3.5 is a histogram plot that assumes $P_{\mathrm{I}} = 3$, which exhibits a better fit to the Poisson distribution. Figure 3.6 is a histogram for $P_{\mathrm{I}} = 20$ and shows a near-perfect normal distribution.

3.2 Signal Shot Noise

The signal shot noise generated by interacting photons is given by

$$\sigma_{\mathrm{SHOT}} = \eta_{\mathrm{i}}(P_{\mathrm{I}})^{1/2}, \tag{3.5}$$

where σ_{SHOT} is the signal shot noise (rms e^-). Substituting Eq. (2.8) into Eq. (3.5) yields

$$\sigma_{\mathrm{SHOT}} = (\eta_{\mathrm{i}} S)^{1/2}. \tag{3.6}$$

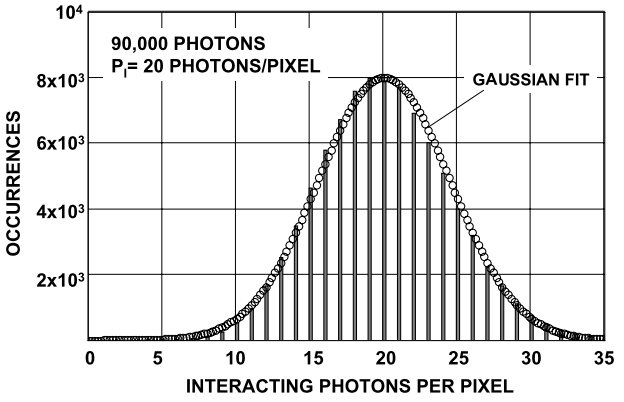

Figure 3.6 Interacting-photon-per-pixel histogram assuming 20 photons/pixel average.

Equation (3.6) is used extensively throughout this book. The relation will be verified through simulation in Figs. 3.9–3.11.

Example 3.2

Assume from Example 3.1 that each interacting photon generates an electron. Add random noise to the response histogram shown in Fig. 3.3 to produce histograms for the following noise levels: 0.1, 0.2, 0.3, 0.4, and 0.5 e^- rms.

Solution:
Figure 3.7 shows the desired histograms. Note that the noise degrades the resolution between electron peaks. Although some CCD and CMOS imagers exhibit read noise levels slightly less than 1 e^-, the noise level is still too high to resolve single-photon interactions. Is it coincidental that the detector's noise level is just shy of doing this?

3.3 Fano Noise

If all the energy of an interacting photon was spent in the production of electron-hole (e-h) pairs, then there would be no variation in the number of e-h pairs produced. On the other hand, if the energy was partitioned between breaking covalent bonds and lattice vibrations, or if phonon production was uncorrelated, Poisson statistics would apply. But neither is the case in nature. The variance in multiple electron-hole charge generation, called *Fano noise*, is empirically described by

$$\sigma_{\mathrm{FN}} = (F_{\mathrm{F}}\eta_{\mathrm{i}})^{1/2} = \left(F_{\mathrm{F}}\frac{h_\nu}{E_{\text{e-h}}}\right)^{1/2}, \tag{3.7}$$

where σ_{FN} is the Fano noise (e^- rms), and F_{F} is referred to as the *Fano factor*, which is defined by the variance in the number of electrons generated divided by

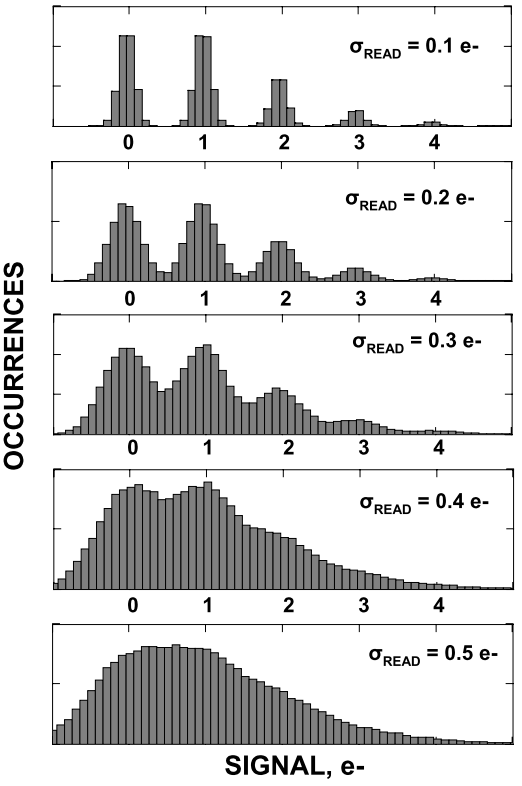

Figure 3.7 Histograms showing influence of different read noise levels on Fig. 3.3.

the average number of electrons generated per interacting photon. The Fano factor is approximately 0.1 for silicon and is applicable for photon energies greater than 10 eV.[1] Figure 3.8 plots Fano noise as a function of photon energy and wavelength. Note that Fano noise becomes appreciable in the soft x-ray regime (i.e., when greater than the read noise floor of 1 e^- rms). Ultra-low read noise CCD and CMOS imagers and cameras are Fano noise-limited through out the x-ray spectrum (and are referred to as such).

Example 3.3

Determine the Fano noise, assuming a quantum yield of 1620 e^- per interacting photon ($h_\nu = 5.9$ keV).

Solution:
From Eq. (3.7),

$$\sigma_{\mathrm{FN}} = (0.1 \times 1620)^{1/2} = 12.7\ \mathrm{e}^-.$$

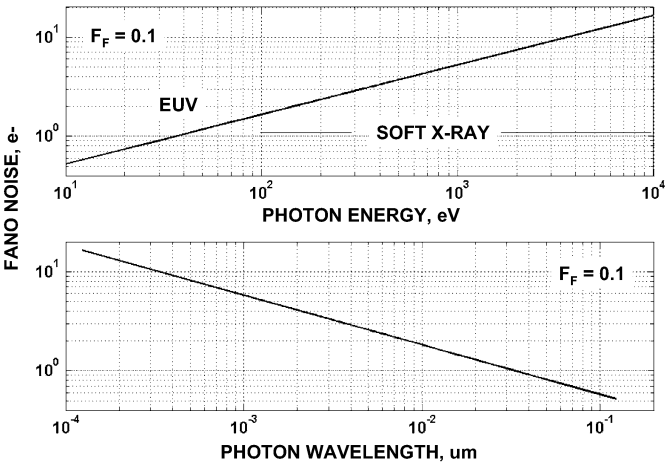

Figure 3.8 Fano noise as a function of photon energy and wavelength.

Figure 3.9 presents a simulation experiment where 90,000 pixels are exposed to an average photon flux of three interacting photons/pixel with $\eta_{\mathrm{i}} = 10\ \mathrm{e}^{-}$/interacting photons. Note that the signal peaks that define the Poisson envelope are separated by 10 e^{-} at locations given by

$$S_{\mathrm{PEAK}} = N_{\mathrm{P}}\eta_{\mathrm{i}}, \tag{3.8}$$

where S_{PEAK} is the signal charge peak level, and N_{P} is the number of multiple photon interactions per pixel that take place. For example, $N_{\mathrm{P}} = 4$ produces a signal peak at 40 e^{-}.

The corresponding standard deviation caused by Fano noise about each signal peak is given by

$$\sigma_{\mathrm{FN\_PEAK}} = (N_{\mathrm{P}}F_{\mathrm{F}}\eta_{\mathrm{i}})^{1/2}. \tag{3.9}$$

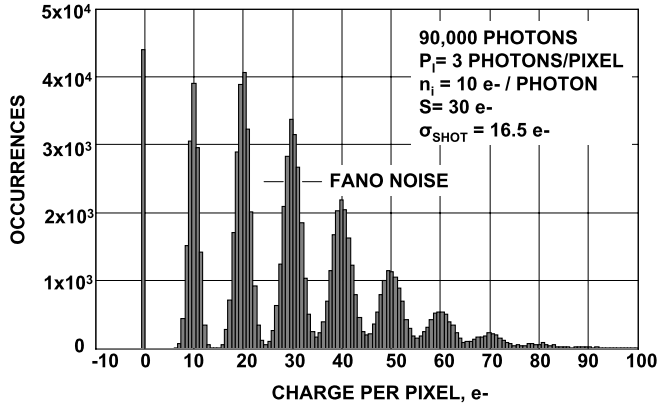

Figure 3.9 Charge-generated-per-pixel histogram with Fano noise present ($n_{\mathrm{i}} = 10\ \mathrm{e}^{-}$/ photon, $P_{\mathrm{I}} = 3$ photons/pixel).

Note that the noise about each peak increases with N_{P} because the Fano noise for multiple pixel-photon interactions is added in quadrature by $(N_{\mathrm{P}})^{1/2}$. This broadening effect is seen in Fig. 3.9, where the separation between signal peaks is less pronounced. Figure 3.10 shows a similar histogram where the average photon flux rate is increased from three to 10 interacting photons/pixel. Note that the signal peaks are unresolved for large N_{P} because of Fano noise. Figure 3.11 shows how the resolution improves when the quantum yield is increased from 10 to 30 electrons/interacting photon.

When signal shot noise and Fano noise are added in quadrature, the net noise is

$$\sigma_{\mathrm{SHOT+FN}} = (\sigma^2_{\mathrm{SHOT}} + \sigma^2_{\mathrm{FN}})^{1/2}. \tag{3.10}$$

Substituting Eqs. (3.6) and (3.7) into Eq. (3.10) yields

$$\sigma_{\mathrm{SHOT+FN}} = \left(\eta_{\mathrm{i}}(S + F_{\mathrm{F}})\right)^{1/2}. \tag{3.11}$$

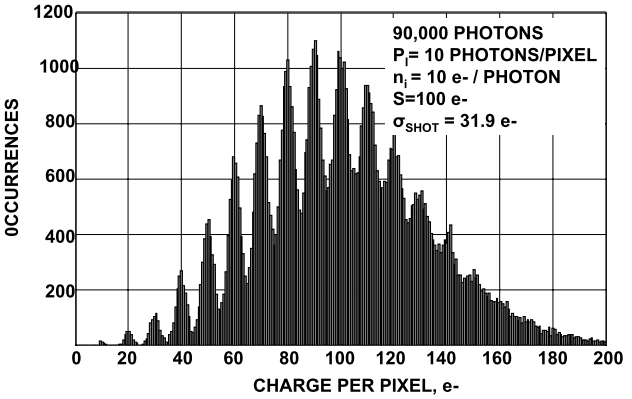

Figure 3.10 Charge-generated-per-pixel histogram with Fano noise ($n_{\mathrm{i}} = 10$ e$^-$/photon, $P_{\mathrm{I}} = 10$ photons/pixel).

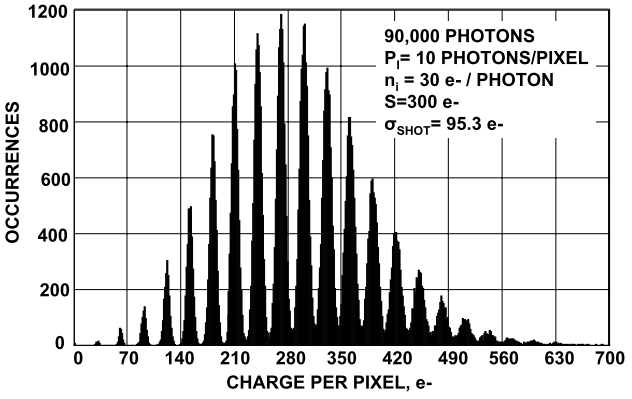

Figure 3.11 Charge-generated-per-pixel histogram with Fano noise ($n_{\mathrm{i}} = 30$ e$^-$/photon, $P_{\mathrm{I}} = 10$ photons/pixel).

Note that relative to signal shot noise, Fano noise is only important when the number of photon interactions per pixel is very small (i.e., when the average signal is small). Figure 3.12 shows a PTC plot of σ_{SHOT} and $\sigma_{\mathrm{SHOT+FN}}$ as a function of signal and different quantum yields. Fano noise is only significant in the plots when $S < 1\,\mathrm{e}^-$. This condition takes place for single photon detection x-ray applications.

Example 3.4

Determine the signal shot noise and Fano noise for the histograms shown in Figs. 3.9–3.11.

Solution:
From Eqs. (3.6) and (3.7),
Figure 3.9 ($\eta_{\mathrm{i}} = 10$, $P_{\mathrm{I}} = 3$)

$$\begin{aligned} \sigma_{\mathrm{SHOT}} &= 10(3)^{1/2} = 17.32\,\mathrm{e}^- \\ \sigma_{\mathrm{FN}} &= (0.1 \times 10)^{1/2} = 1\,\mathrm{e}^- \end{aligned}$$

Figure 3.10 ($\eta_{\mathrm{i}} = 10$, $P_{\mathrm{I}} = 10$)

$$\begin{aligned} \sigma_{\mathrm{SHOT}} &= 10(10)^{1/2} = 31.63\,\mathrm{e}^- \\ \sigma_{\mathrm{FN}} &= (0.1 \times 10)^{1/2} = 1\,\mathrm{e}^- \end{aligned}$$

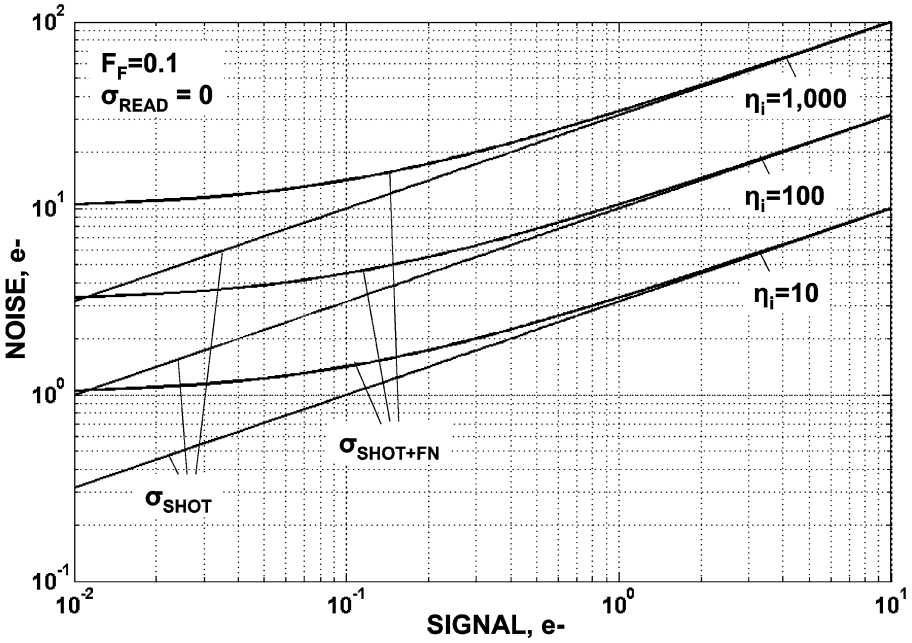

Figure 3.12 PTCs showing Fano noise dominating shot noise for small average signals.

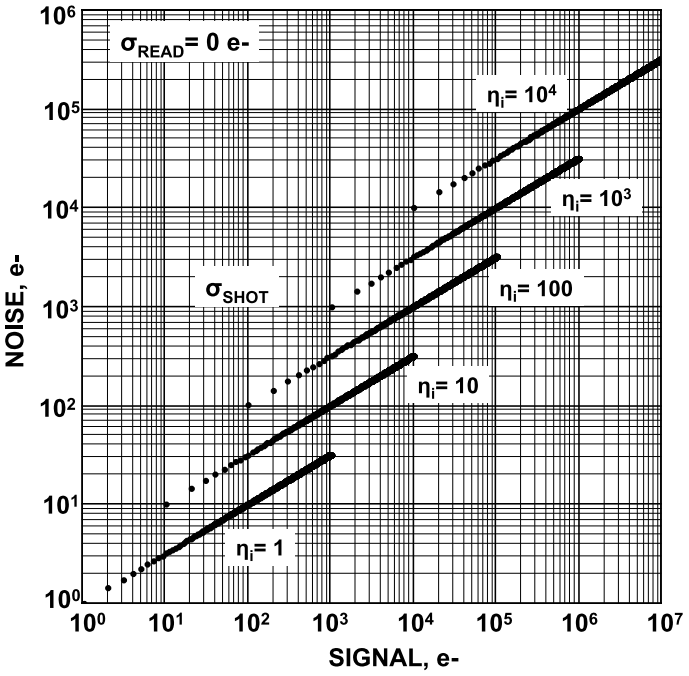

Figure 3.13 Shot noise versus signal PTCs for different quantum yields.

Figure 3.11 ($\eta_{\rm i} = 30$, $P_{\rm I} = 10$)

$$\begin{aligned} \sigma_{\rm SHOT} &= 30(10)^{1/2} = 95\ {\rm e}^- \\ \sigma_{\rm FN} &= (0.1 \times 30)^{1/2} = 1.732\ {\rm e}^- \end{aligned}$$

Figure 3.13 plots $\sigma_{\rm SHOT}$ as a function of S and different $\eta_{\rm i}$. Note that for a given signal level, the signal shot noise increases by the square root of quantum yield [i.e., Eq. (3.6)].

3.4 Fixed Pattern Noise

After the photoelectric effect takes place, the pixels collect the photoelectrons generated. The charge collection process is not perfect because some pixels collect charge more efficiently than others, resulting in pixel-to-pixel sensitivity differences. The effect generates FPN in an image.[1] This noise is called "fixed" because it is not random—it is spatially the same pattern from image to image.

FPN is defined by the relation

$$\sigma_{\rm FPN} = P_{\rm N} S, \tag{3.12}$$

where $\sigma_{\rm FPN}$ is the FPN (rms e^-), and $P_{\rm N}$ is the FPN quality factor, which is approximately 0.01 (1%) for CCD and CMOS sensors.

P_{N} is one of the first data products produced by a PTC (refer to Chapter 5). It is measured by the ratio of rms noise to the mean signal for a uniform light stimulus. For example, a 1% FPN implies that the rms noise is 1% of the mean signal level.

Unlike shot noise, which varies as the square root of signal [i.e., Eq. (3.6)], FPN is proportional to signal. It is for this reason that FPN for visible and near-IR applications will dominate signal shot noise over most of a sensor's dynamic range. This characteristic will be very important to signal-to-noise performance discussions in Chapter 10.

Example 3.5

Compare signal shot noise and FPN for a signal level of 2×10^5 e^-. Assume $\eta_{\mathrm{i}} = 1$ and $P_{\mathrm{N}} = 0.05$.

Solution:
From Eq. (3.6), the shot noise is

$$\sigma_{\mathrm{SHOT}} = (2 \times 10^5)^2 = 447\ \mathrm{e}^-.$$

From Eq. (3.12), the FPN is

$$\sigma_{\mathrm{FPN}} = (2 \times 10^5) \times 0.05 = 10{,}000\ \mathrm{e}^-.$$

Figure 3.14 presents a sinusoidal image that possesses maximum and minimum signal excursions of 200,000 and 0 e^-, respectively, assuming $P_{\mathrm{N}} = 5\%$. The images demonstrate the signal-to-noise difference when FPN dominates.

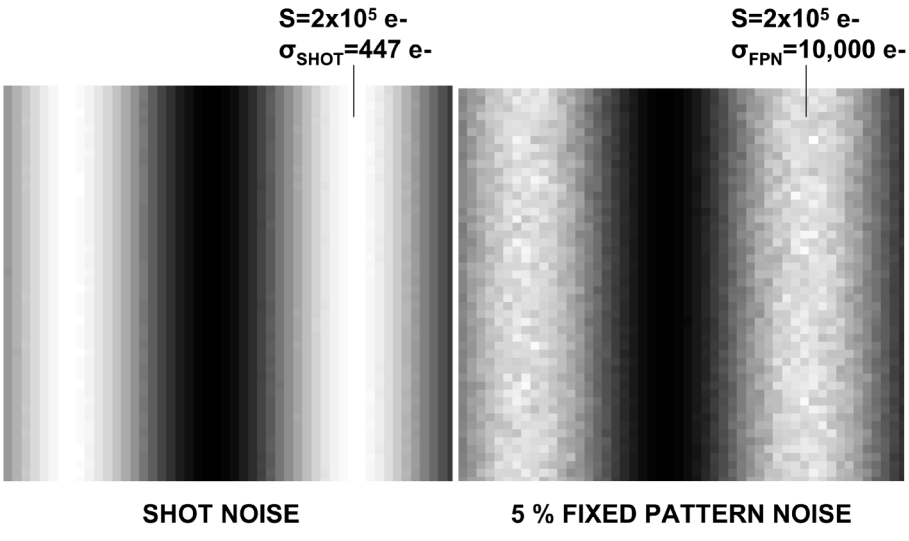

Figure 3.14 Sinusoidal images with and without FPN at the same average signal level.

FPN and shot noise can be compared by their ratio [i.e., Eqs. (3.12) and (3.6)] as

$$\frac{\sigma_{\mathrm{FPN}}}{\sigma_{\mathrm{SHOT}}} = P_{\mathrm{N}}\left(\frac{S}{\eta_{\mathrm{i}}}\right)^{1/2}. \tag{3.13}$$

Figure 3.15 plots this ratio as a function of signal and quantum yield.

The signal level where FPN equals signal shot noise is found by setting Eq. (3.13) to unity and solving for signal to produce

$$S_{\mathrm{SHOT=FPN}} = \frac{\eta_{\mathrm{i}}}{P_{\mathrm{N}}^2}; \tag{3.14}$$

or, in terms of photon energy,

$$S_{\mathrm{SHOT=FPN}} = \frac{h_\nu}{3.65P_{\mathrm{N}}^2}. \tag{3.15}$$

Example 3.6

Determine the signal level when $\sigma_{\mathrm{FPN}} = \sigma_{\mathrm{SHOT}}$ for $\eta_{\mathrm{i}} = 1$ and 100. Assume $P_{\mathrm{N}} = 0.01$.

Solution:
From Eq. (3.14),

$$S_{\mathrm{SHOT=FPN}} = \frac{1}{0.01^2} = 10{,}000\ \mathrm{e}^-, \quad \eta_{\mathrm{i}} = 1;$$

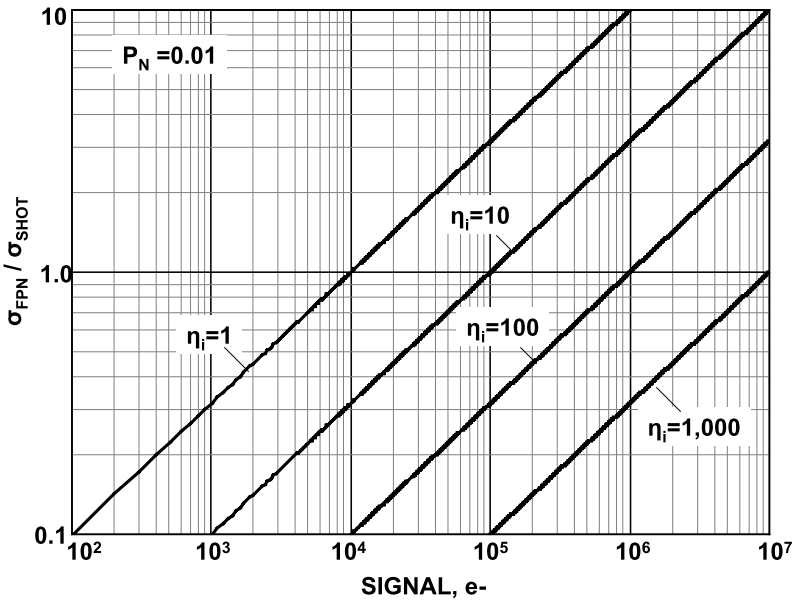

Figure 3.15 FPN/shot noise ratio as a function of signal at different quantum yields.

and

$$S_{\mathrm{SHOT=FPN}} = \frac{100}{0.01^2} = 10^6 \ \mathrm{e}^-, \quad \eta_{\mathrm{i}} = 100.$$

These results are also shown in Fig. 3.15.

Most CMOS and CCD detectors do not exhibit a charge capacity as large as 10^6 e^-. Therefore, x-ray sensors will be dominated by signal shot noise instead of FPN common to visible detectors (also refer to Fig. 10.3).

As mentioned above, the minimum FPN for CCD and CMOS imagers is approximately 1% of the signal level. Many other FPN sources contribute to a measurement increase of P_{N} above the ideal. For example, dust particles situated above pixels block the incoming light and generate additional FPN. A few particulates within a region of interest can have a dramatic effect on PT statistics. When FPN noise is limited by this problem, P_{N} represents a measurement of device cleanliness and not the detector itself. Optical effects such as vignetting, shading, and interference fringing also fall into the category of FPN sources. For example, Fig. 3.16 shows a 5461 A flat-field image with deep fringes generated by a CCD. The interference pattern is caused by light reflections between the sensor's surface and the optical window, which are nearly perfectly flat to one another. This image exhibits a FPN of approximately 10%—10 times greater than the ideal pixel-to-pixel FPN nonuniformity. Fortunately, all FPN sources can be readily removed through the process of flat fielding (see Chapter 8).

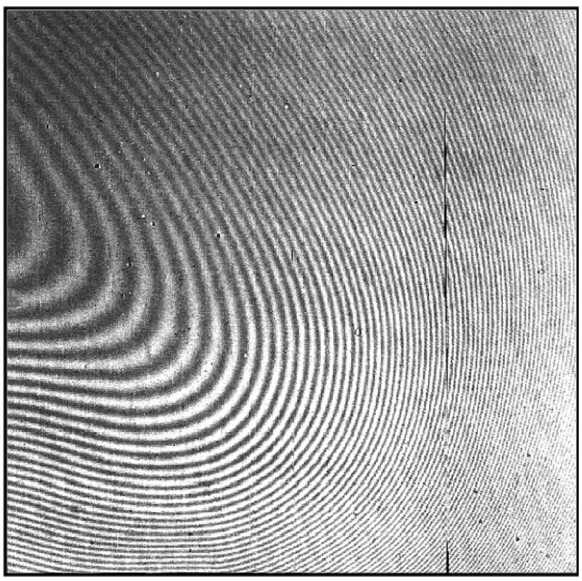

Figure 3.16 Optical interference fringes and dust spots resulting in high FPN.

3.5 Read Noise

Chapter 11 is devoted to important read noise sources encountered in CCD and CMOS imagers and camera systems. *Read noise* is defined as any noise source that is not a function of signal.

Shot noise, FPN, and Fano noise can be added in quadrature with read noise to produce the total noise equation,

$$\sigma_{\mathrm{TOTAL}} = (\sigma^2_{\mathrm{READ}} + \sigma^2_{\mathrm{FN}} + \sigma^2_{\mathrm{SHOT}} + \sigma^2_{\mathrm{FPN}})^{1/2}; \tag{3.16}$$

or, equivalently,

$$\sigma_{\mathrm{TOTAL}} = (\sigma^2_{\mathrm{READ}} + \eta_{\mathrm{i}} F_{\mathrm{F}} + \eta_{\mathrm{i}} S + (P_{\mathrm{N}} S)^2)^{1/2}, \tag{3.17}$$

where σ_{TOTAL} is the total noise (e^- rms), and σ_{READ} is the read noise (rms e^-). The four noise sources are Gaussian distributed. The PTCs generated in Chapter 5 plot each noise source separately as a function of signal.

Important Points

1. Shot and Fano noise are fundamentally related to the charge generated by a photon's interaction with a semiconductor.
2. Shot noise increases by the square root of the signal and quantum yield, whereas Fano noise increases by the square root of the quantum yield.
3. Fano noise is observed in PTCs when the number of interacting photons is less than the number of pixels.
4. FPN is associated with pixel-to-pixel sensitivity differences that increase directly with signal.
5. The minimum FPN noise achieved by CCD and CMOS imagers is approximately 1% of the signal level.
6. For wavelengths > 4000 A, FPN begins to dominate shot noise at a signal level of approximately 10,000 e^- (i.e., $1/P^2_{\mathrm{N}}$). For wavelengths < 4000 A, shot noise increases relative to FPN by the quantum yield gain.
7. Read noise encompasses all noise sources that are signal independent.

Chapter 4
Photon Transfer Theory

4.1 Photon Transfer Relation

A functional block diagram for a typical CCD/CMOS camera system is illustrated in Fig. 4.1. The system shown is described by the six transfer functions related to the semiconductor, pixel detector, and electronics that process the video signal. The input to the camera is expressed in units of the average number of incident photons per pixel (P), and the final output signal is given as the average DN encoded for each pixel. The output is related to the input gain relation

$$\frac{S(\mathrm{DN})}{P} = \mathrm{QE_I}\eta_\mathrm{i} A_\mathrm{SN} A_\mathrm{SF} A_\mathrm{CDS} A_\mathrm{ADC}, \tag{4.1}$$

where the individual gain functions are given in Table 4.1.

The signal and shot noise parameters at each point in the block diagram are listed in Table 4.2.

The gain functions contained in Eq. (4.1) are difficult to measure individually with good precision ($<$1% rms), especially those parameters related to the internal workings of the sensor. The PT method provides us with a solution to find the overall camera transfer function [Eq. (4.1)] accurately without knowing individual transfer functions. However, the PT technique is only fully applicable if a detector's response is shot noise-limited as explained below. Fortunately, this is the case for solid state sensors such as CCD and CMOS imagers.

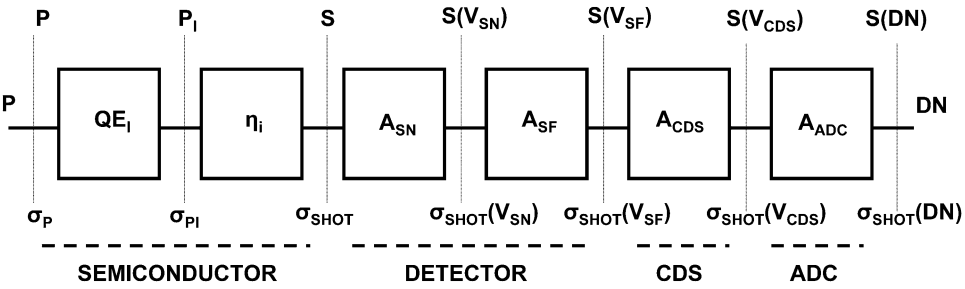

Figure 4.1 Typical solid state camera system showing internal gain functions and signal and noise parameters.

Table 4.1 Camera gain functions.

Parameter	Gain Function	Symbol
Quantum efficiency	P_{I}/P	$\mathrm{QE_I}$
Quantum yield gain	S/P_{I}	η_{i}
Sense node gain	$S(V_{\mathrm{SN}})/S$	A_{SN}
Source follower gain	$S(V_{\mathrm{SF}})/S(V_{\mathrm{SN}})$	A_{SF}
CDS gain	$S(V_{\mathrm{CDS}})/S(V_{\mathrm{SF}})$	A_{CDS}
ADC gain	$S(\mathrm{DN})/S(V_{\mathrm{CDS}})$	A_{ADC}

Table 4.2 Camera signal and noise parameters.

Parameter	Average Signal	Noise (rms)
Incident photons	P	$\sigma_{\mathrm{SHOT}}(P)$
Interacting photons	P_{I}	$\sigma_{\mathrm{SHOT}}(P_{\mathrm{I}})$
Sense node electrons	S	σ_{SHOT}
Sense node voltage	$S(V_{\mathrm{SN}})$	$\sigma_{\mathrm{SHOT}}(V_{\mathrm{SN}})$
Source follower voltage	$S(V_{\mathrm{SF}})$	$\sigma_{\mathrm{SHOT}}(V_{\mathrm{SF}})$
CDS voltage	$S(V_{\mathrm{CDS}})$	$\sigma_{\mathrm{SHOT}}(V_{\mathrm{CDS}})$
ADC signal	$S(\mathrm{DN})$	$\sigma_{\mathrm{SHOT}}(\mathrm{DN})$

The general PT formula will now be derived. Figure 4.2 shows a general camera block diagram where the input signal exhibits shot noise characteristics. That is, from Eq. (3.2),

$$\sigma_{\mathrm{A}} = A^{1/2}, \tag{4.2}$$

where A is the mean input signal level, and σ_{A} is the input noise standard deviation (or rms).

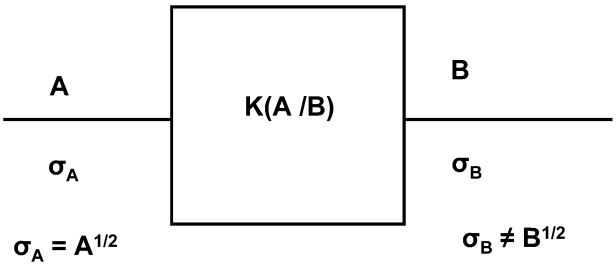

Figure 4.2 Black box camera system with a constant $K(A/B)$ used to transfer output signal (B) and noise (σ_{B}) measurements to the input.

A sensitivity constant defined as $K(A/B)$ relates and transfers output signal and noise measurements to the input. In other words,

$$A = BK(A/B) \tag{4.3}$$

and

$$\sigma_{\mathrm{A}} = \sigma_{\mathrm{B}} K(A/B), \tag{4.4}$$

where B and σ_{B} are the measured output mean signal level and noise standard deviation, respectively. Units for output B and input A will be different; generally, A is specified in absolute physical units that describe shot noise characteristics (photons and electrons), whereas B is specified in relative nonphysical units generated by an amplifier or analog-to-digital converter (volt and DN).

At this point in the analysis $K(A/B)$ is unknown. However, substituting Eqs. (4.3) and (4.4) into Eq. (4.2) and solving for $K(A/B)$ yields the desired result:

$$K(A/B) = \frac{B}{\sigma_{\mathrm{B}}^2}, \tag{4.5}$$

where $K(A/B)$ is referred to the sensitivity constant of the system. Equation (4.5) is called the *PT relation*, an important equation that is the basis of the PT technique. Note that $K(A/B)$ is simply found by measuring output statistics (i.e., mean and noise variance) without knowledge of the individual camera transfer functions.

For a given set of measured B and σ_{B} output quantities, there is only one unique value for $K(A/B)$ that will satisfy the special input condition $\sigma_{\mathrm{A}} = A^{1/2}$. It is also important to note from Eq. (4.5) that $\sigma_{\mathrm{B}} \neq B^{1/2}$, because if that were the case, $K(A/B)$ would be forced to unity. As will be shown later, this would be an extremely rare setting for a camera system (mere coincidence). Also, it will be shown that $K(A/B)$ is adjusted to achieve optimum camera performance. $K(A/B)$ is usually tuned optimally by changing the voltage gain of an amplifier stage (typically block 5 in Fig. 4.1). Note that increasing the gain between A and B causes the sensitivity constant $K(A/B)$ to decrease.

It should be emphasized that gain functions are employed when referring the input of a measuring device to its output (i.e., from left to right in Fig. 4.1). Sensitivity functions are used to transfer output measurements to the input (i.e., from

Table 4.3 Sense node sensitivities ($\eta_{\mathrm{i}} = 1$).

Sensitivity Parameter	Symbol	Sensitivity	Gain
Sense node	$K_{\mathrm{SN}}(\mathrm{e}^-/V_{\mathrm{SN}})$	$S(V_{\mathrm{SN}})/\sigma_{\mathrm{SHOT}}(V_{\mathrm{SN}})^2$	A_{SN}
Source follower	$K_{\mathrm{SF}}(\mathrm{e}^-/V_{\mathrm{SF}})$	$S(V_{\mathrm{SF}})/\sigma_{\mathrm{SHOT}}(V_{\mathrm{SF}})^2$	$A_{\mathrm{SN}}A_{\mathrm{SF}}$
CDS	$K_{\mathrm{CDS}}(\mathrm{e}^-/V_{\mathrm{CDS}})$	$S(V_{\mathrm{CDS}})/\sigma_{\mathrm{SHOT}}(V_{\mathrm{CDS}})^2$	$A_{\mathrm{SN}}A_{\mathrm{SF}}A_{\mathrm{CDS}}$
ADC	$K_{\mathrm{ADC}}(\mathrm{e}^-/\mathrm{DN})$	$S(\mathrm{DN})/\sigma_{\mathrm{SHOT}}(\mathrm{DN})^2$	$A_{\mathrm{SN}}A_{\mathrm{SF}}A_{\mathrm{CDS}}A_{\mathrm{ADC}}$

Table 4.4 Interacting photon sensitivities ($\eta_i \geq 1$).

Sensitivity Parameter	Symbol	Sensitivity	Gain
Interacting photon	$K_{SN}(P_I/e^-)$	$S(V_{SN})/\sigma_{SHOT}(V_{SN})^2$	η_i
ADC	$K_{ADC}(P_I/DN)$	$S(DN)/\sigma_{SHOT}(DN)^2$	$\eta_i A_{SN} A_{SF} A_{CDS} A_{ADC}$

Table 4.5 Incident photon sensitivities ($\eta_i \geq 1$).

Sensitivity Parameter	Symbol	Sensitivity	Gain
Incident photon	$K_{PI}(P/P_I)$	$(QE_I)^{-1}$	QE_I
ADC	$K_{ADC}(P/DN)$	$(QE_I)^{-1} S(DN)/\sigma_{SHOT}(DN)^2$	$QE_I \eta_i A_{SN} A_{SF} A_{CDS} A_{ADC}$

right to left in Fig. 4.1). For example, to convert output units to input units, multiply the output by the sensitivity factor $K(A/B)$. Equation (4.5) can now be applied to derive the most commonly applied sensitivity camera constants listed in Tables 4.3–4.5.

4.2 Sense Node Sensitivities

4.2.1 Sense node sensitivity

Figure 4.3 shows the sense node region, common to all CCD and CMOS detectors, where signal charge is converted to a working voltage and buffered by a source follower amplifier (i.e., the third block shown in Fig. 4.1). Relationships linking sense node capacitance, V/e$^-$ sense node gain, e$^-$/V sensitivity, and charge and voltage on this node are related through the differential equation

$$C_{SN} = q\frac{dS}{dV_{SN}}, \tag{4.6}$$

where C_{SN} is the sense node capacitance (F), V_{SN} is the sense node voltage, S is the signal (e$^-$), and q is the charge of an electron (1.6×10^{-19}C).

Integrating Eq. (4.6) with respect to V_{SN} yields

$$S = \frac{1}{q}\int_{V_{SN}}^{V_{REF}} C_{SN} dV_{SN}, \tag{4.7}$$

where V_{REF} is the reference voltage on the sense node after the sense node is reset. The limits of integration are set for negative (i.e., electron) changing signals on the sense node.

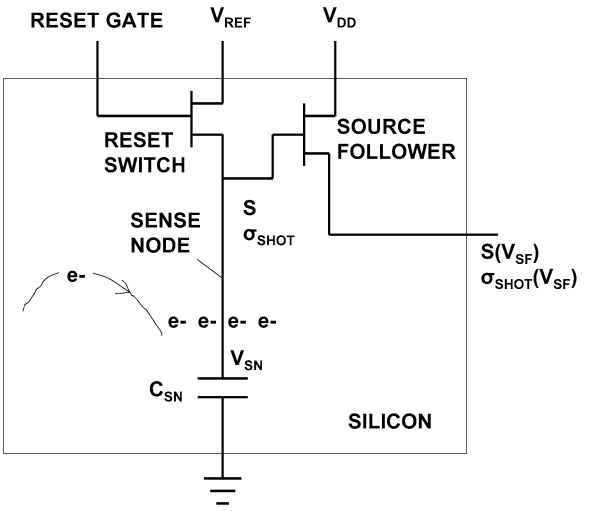

Figure 4.3 Typical CCD/CMOS sense node region where signal charge and related noise are converted to a working output voltage.

For linear detectors, $C_{\rm SN}$ is a constant and invariant to signal. Chapter 7 analyzes the situation when the sense node capacitance varies with signal. Integrating Eq. (4.7) with a fixed $C_{\rm SN}$ yields

$$S = \frac{C_{\rm SN}(V_{\rm REF} - V_{\rm SN})}{q}. \tag{4.8}$$

The sense node voltage is

$$V_{\rm SN} = V_{\rm REF} - S(V_{\rm SN}), \tag{4.9}$$

where $S(V_{\rm SN})$ is the sense node signal voltage.

Equation (4.9) reduces Eq. (4.8) to

$$S = \frac{C_{\rm SN} S(V_{\rm SN})}{q}. \tag{4.10}$$

From Eq. (4.10), the sense node sensitivity is

$$K_{\rm SN}(\mathrm{e}^-/V_{\rm SN}) = \frac{S}{S(V_{\rm SN})} = \frac{C_{\rm SN}}{q} = \frac{1}{A_{\rm SN}}. \tag{4.11}$$

From the PT Eq. (4.5), the shot noise voltage on the sense node is

$$\sigma_{\rm SHOT}(V_{\rm SN}) = \left[\frac{S(V_{\rm SN})}{K_{\rm SN}(\mathrm{e}^-/V_{\rm SN})}\right]^{1/2}; \quad \eta_{\rm i} = 1. \tag{4.12}$$

4.2.2 Sense node to source follower sensitivity

The source follower output voltage is given by

$$V_{\mathrm{SF}} = V_{\mathrm{SF\_OFF}} - S(V_{\mathrm{SF}}), \tag{4.13}$$

where V_{SF} is the source follower output voltage, $S(V_{\mathrm{SF}})$ is the source follower signal voltage, and $V_{\mathrm{SF\_OFF}}$ is the DC source follower offset voltage.

The sense node to source follower sensitivity node is found through the PT Eq. (4.5), which yields

$$K_{\mathrm{SF}}(\mathrm{e}^-/V_{\mathrm{SF}}) = \frac{S(V_{\mathrm{SF}})}{\sigma_{\mathrm{SHOT}}(V_{\mathrm{SF}})^2}; \quad \eta_{\mathrm{i}} = 1. \tag{4.14}$$

In terms of sense node sensitivity,

$$K_{\mathrm{SF}}(\mathrm{e}^-/V_{\mathrm{SF}}) = \frac{K_{\mathrm{SN}}(\mathrm{e}^-/V_{\mathrm{SN}})}{A_{\mathrm{SF}}}, \tag{4.15}$$

where A_{SF} is the source follower voltage gain.

Example 4.1

Determine $K_{\mathrm{SF}}(\mathrm{e}^-/V_{\mathrm{SF}})$, S, σ_{SHOT}, $K_{\mathrm{SN}}(\mathrm{e}^-/V_{\mathrm{SN}})$, A_{SN}, and C_{SN} from the following data measurements made at the output of the source follower:

$$S(V_{\mathrm{SF}}) = 0.016 \text{ V}$$

$$\sigma_{\mathrm{SHOT}}(V_{\mathrm{SF}}) = 0.000315 \text{ V}$$

Assume $A_{\mathrm{SF}} = 0.9$ V/V, and $\eta_{\mathrm{i}} = 1$ (i.e., visible or near IR light).

Solution:
Applying Eq. (4.14) to the data yields

$$K_{\mathrm{SF}}(\mathrm{e}^-/V_{\mathrm{SF}}) = \frac{0.016}{0.000315^2} = 1.61 \times 10^5 \text{ e}^-/\text{V}.$$

Converting the source follower signal voltage to electrons,

$$S = K_{\mathrm{SF}}(\mathrm{e}^-/V_{\mathrm{SF}}) \times S(V_{\mathrm{SF}}) = 2560 \text{ e}^-.$$

Converting the source follower noise voltage to electrons,

$$\sigma_{\mathrm{SHOT}} = K_{\mathrm{SF}}(\mathrm{e}^-/V_{\mathrm{SF}}) \times \sigma_{\mathrm{SHOT}}(V_{\mathrm{SF}}) = 51 \text{ e}^- \text{ rms}.$$

From Eq. (4.15), the sense node sensitivity is

$$K_{\mathrm{SN}}(\mathrm{e}^-/V_{\mathrm{SN}}) = (1.61 \times 10^5) \times 0.9 = 1.45 \times 10^5 \text{ e}^-/\text{V}.$$

The reciprocal of the sense node sensitivity is the sense node gain,

$$A_{\mathrm{SN}} = \frac{1}{K_{\mathrm{SN}}(\mathrm{e}^-/V_{\mathrm{SN}})} = 6.9 \times 10^{-6}\ \mathrm{V/e}^-.$$

From Eqs. (4.10) and (4.15), the sense node capacitance is

$$C_{\mathrm{SN}} = (1.6 \times 10^{-19}) \times 0.9 \times (1.45 \times 10^{5}) = 2.01 \times 10^{-14}\ \mathrm{F}.$$

It is amazing that only two relative measurements (signal and noise voltages) at the output of the source follower produce such a wealth of absolute information through the PT technique.

4.2.3 Sense node to CDS sensitivity

For positive going signals, the CDS output voltage is given by

$$V_{\mathrm{CDS}} = V_{\mathrm{CDS\_OFF}} + S(V_{\mathrm{CDS}}), \tag{4.16}$$

where V_{CDS} is the CDS output voltage, $S(V_{\mathrm{CDS}})$ is the CDS signal voltage, and $V_{\mathrm{CDS\_OFF}}$ is the CDS offset voltage.

The sense node to CDS sensitivity is found through the PT Eq. (4.5), which yields

$$K_{\mathrm{CDS}}(\mathrm{e}^-/V_{\mathrm{CDS}}) = \frac{S(V_{\mathrm{CDS}})}{\sigma_{\mathrm{SHOT}}(V_{\mathrm{CDS}})^2}; \quad \eta_{\mathrm{i}} = 1. \tag{4.17}$$

In terms of sense node sensitivity,

$$K_{\mathrm{CDS}}(\mathrm{e}^-/V_{\mathrm{CDS}}) = \frac{K_{\mathrm{SN}}(\mathrm{e}^-/V_{\mathrm{SN}})}{A_{\mathrm{SF}} A_{\mathrm{CDS}}}, \tag{4.18}$$

where A_{CDS} is the CDS voltage gain.

4.2.4 Sense node to ADC sensitivity

For positive going signals, the ADC output signal is

$$\mathrm{DN}_{\mathrm{ADC}} = S_{\mathrm{ADC\_OFF}}(\mathrm{DN}) + S(\mathrm{DN}), \tag{4.19}$$

where $\mathrm{DN}_{\mathrm{ADC}}$ is the raw ADC output signal, $S(\mathrm{DN})$ is the true signal, and $S_{\mathrm{ADC\_OFF}}(\mathrm{DN})$ is the ADC offset level.

From PT, the sense node to ADC sensitivity is

$$K_{\mathrm{ADC}}(\mathrm{e}^-/\mathrm{DN}) = \frac{S(\mathrm{DN})}{\sigma_{\mathrm{SHOT}}(\mathrm{DN})^2}; \quad \eta_{\mathrm{i}} = 1. \tag{4.20}$$

In terms of sense node sensitivity,

$$K_{\mathrm{ADC}}(\mathrm{e}^-/\mathrm{DN}) = \frac{K_{\mathrm{SN}}(\mathrm{e}^-/V_{\mathrm{SN}})}{A_{\mathrm{SF}} A_{\mathrm{CDS}} A_{\mathrm{ADC}}}. \tag{4.21}$$

Example 4.2

Find $K_{\mathrm{ADC}}(\mathrm{e}^-/\mathrm{DN})$, S, σ_{SHOT}, $K_{\mathrm{SN}}(\mathrm{e}^-/V_{\mathrm{SN}})$, C_{SN}, and A_{SN} from the following data taken at the output of the ADC:

$$\mathrm{DN}_{\mathrm{ADC}} = 10{,}800$$

$$S_{\mathrm{ADC\_OFF}}(\mathrm{DN}) = 800$$

$$\sigma_{\mathrm{SHOT}}(\mathrm{DN}) = 50$$

Assume $A_{\mathrm{SF}} = 0.9$ V/V, $A_{\mathrm{CDS}} = 10$ V/V, $A_{\mathrm{ADC}} = 3250$ DN/V, and $\eta_{\mathrm{i}} = 1$. Convert DN signal and noise levels to electrons.

Solution:
From Eq. (4.19), the ADC signal is

$$S(\mathrm{DN}) = 10{,}800 - 800 = 10{,}000.$$

From Eq. (4.20), the ADC sensitivity is

$$K_{\mathrm{ADC}}(\mathrm{e}^-/\mathrm{DN}) = \frac{10{,}000}{50^2} = 4.$$

Signal and noise in electrons are

$$S = 4 \times 10{,}000 = 40{,}000\ \mathrm{e}^-$$

$$\sigma_{\mathrm{SHOT}} = 40{,}000^{1/2} = 200\ \mathrm{e}^-$$

From Eq. (4.21), the sense node sensitivity is

$$K_{\mathrm{SN}}(\mathrm{e}^-/V_{\mathrm{SN}}) = 0.9 \times 10 \times 3250 \times 4 = 1.17 \times 10^5\ \mathrm{e}^-/\mathrm{V}.$$

From Eq. (4.11), the sense node capacitance is

$$C_{\mathrm{SN}} = (1.6 \times 10^{-19}) \times 1.17 \times 10^5 = 1.87 \times 10^{-14}\ \mathrm{F}.$$

The sense node gain is

$$A_{\mathrm{SN}} = \frac{1}{K_{\mathrm{SN}}(\mathrm{e}^-/V_{\mathrm{SN}})} = \frac{1}{1.17 \times 10^5\ \mathrm{e}^-/\mathrm{V}} = 8.54 \times 10^{-6}\ \mathrm{V/e}^-.$$

4.3 Interacting Photon Sensitivities

4.3.1 Interacting photon sensitivity

The interacting photon sensitivity is defined by the quantum yield,

$$K_{\mathrm{SN}}(P_{\mathrm{I}}/\mathrm{e}^-) = (\eta_{\mathrm{i}})^{-1}. \tag{4.22}$$

4.3.2 Interacting photon to ADC sensitivity

The interacting photon to ADC sensitivity, from PT Eq. (4.5), is

$$K_{\mathrm{ADC}}(P_{\mathrm{I}}/\mathrm{DN}) = \frac{S(\mathrm{DN})}{\sigma_{\mathrm{SHOT}}(\mathrm{DN})^2} \quad \text{for all } \eta_{\mathrm{i}}. \tag{4.23}$$

Noting that

$$K_{\mathrm{ADC}}(P_{\mathrm{I}}/\mathrm{DN}) = \frac{K_{\mathrm{ADC}}(\mathrm{e}^-/\mathrm{DN})}{\eta_{\mathrm{i}}}, \tag{4.24}$$

and solving for η_{i} yields

$$\eta_{\mathrm{i}} = \frac{K_{\mathrm{ADC}}(\mathrm{e}^-/\mathrm{DN})}{K_{\mathrm{ADC}}(P_{\mathrm{I}}/\mathrm{DN})} = \frac{K_{\mathrm{ADC}}(\mathrm{e}^-/\mathrm{DN})\sigma_{\mathrm{SHOT}}(\mathrm{DN})^2}{S(\mathrm{DN})}. \tag{4.25}$$

Example 4.3

Find $K_{\mathrm{ADC}}(P_{\mathrm{I}}/\mathrm{DN})$, $K_{\mathrm{ADC}}(\mathrm{e}^-/\mathrm{DN})$, η_{i}, and the photon energy for the following data taken at the output of the ADC:

$\eta_{\mathrm{i}} = 1$ (i.e., visible or near IR stimulus)
$S(\mathrm{DN}) = 10{,}000$
$\sigma_{\mathrm{SHOT}}(\mathrm{DN}) = 70$

$\eta_{\mathrm{i}} > 1$ (working wavelength)
$S(\mathrm{DN}) = 25{,}000$
$\sigma_{\mathrm{SHOT}}(\mathrm{DN}) = 700$

Solution:

$$\eta_{\mathrm{i}} = 1$$

From Eq. (4.20),

$$K_{\mathrm{ADC}}(\mathrm{e}^-/\mathrm{DN}) = \frac{10{,}000}{70^2} = 2.04;$$

$$\eta_{\mathrm{i}} > 1.$$

From Eq. (4.23),

$$K_{\mathrm{ADC}}(P_{\mathrm{I}}/\mathrm{DN}) = \frac{25{,}000}{700^2} = 0.051.$$

From Eq. (4.25), the quantum yield is

$$\eta_{\mathrm{i}} = \frac{2.04}{0.051} = 40\ \mathrm{e}^-/\text{interacting photon}.$$

The quantum yield corresponds to a photon energy of approximately $40 \times 3.65 = 146$ eV [Eq. (2.9)].

4.4 Incident Photon Sensitivities

4.4.1 Incident photon sensitivity

The incident photon sensitivity is equal to the interacting QE found experimentally [i.e., Eq. (2.4)]:

$$K_{\mathrm{PI}}(P/P_{\mathrm{I}}) = \mathrm{QE}_{\mathrm{I}}^{-1}. \tag{4.26}$$

4.4.2 Incident photon to ADC sensitivity

Incident photon to ADC sensitivity is given by

$$K_{\mathrm{ADC}}(P/\mathrm{DN}) = \frac{K_{\mathrm{ADC}}(P_{\mathrm{I}}/\mathrm{DN})}{\mathrm{QE}_{\mathrm{I}}} \quad \text{for all } \eta_{\mathrm{i}}. \tag{4.27}$$

Example 4.4

From Example 4.3, find $K_{\mathrm{ADC}}(P/\mathrm{DN})$ assuming $\mathrm{QE}_{\mathrm{I}} = 0.5$.

Solution:
From Eq. (4.27),

$$K_{\mathrm{ADC}}(P/\mathrm{DN}) = \frac{0.051}{0.5} = 0.102.$$

4.5 Photon Transfer General Derivation

$K_{\mathrm{ADC}}(\mathrm{e}^-/\mathrm{DN})$ in terms of output DN statistics can be derived on first principles starting with the equation

$$S(\mathrm{DN}) = \frac{P_{\mathrm{I}}}{K_{\mathrm{ADC}}(\mathrm{e}^-/\mathrm{DN})}, \tag{4.28}$$

where unity quantum yield is assumed. The variance of Eq. (4.28) is found by the propagation of errors formula, i.e.,

$$\sigma^2_{\mathrm{SHOT}}(\mathrm{DN}) = \left[\frac{\partial S(\mathrm{DN})}{\partial P_{\mathrm{I}}}\right]^2 \sigma^2_{P_{\mathrm{I}}} + \left[\frac{\partial S(\mathrm{DN})}{\partial K_{\mathrm{ADC}}(\mathrm{e}^-/\mathrm{DN})}\right]^2 \sigma^2_{K_{\mathrm{ADC}}(\mathrm{e}^-/\mathrm{DN})}. \tag{4.29}$$

Performing the differentiation yields

$$\sigma_{\mathrm{SHOT}}(\mathrm{DN})^2 = \left[\frac{1}{K_{\mathrm{ADC}}(\mathrm{e}^-/\mathrm{DN})}\right]^2 \sigma^2_{P_{\mathrm{I}}} + \left[\frac{-P_{\mathrm{I}}}{K_{\mathrm{ADC}}(\mathrm{e}^-/\mathrm{DN})^2}\right]^2 \sigma^2_{K_{\mathrm{ADC}}(\mathrm{e}^-/\mathrm{DN})}. \tag{4.30}$$

Assuming $\sigma^2_{K(\mathrm{e^-/DN})} = 0$ (i.e., if a sufficient number of pixels are sampled) and $\sigma^2_{P_\mathrm{I}} = P_\mathrm{I}$, Eq. (4.30) reduces to

$$\sigma_{\mathrm{SHOT}}(\mathrm{DN})^2 = \left[\frac{1}{K_{\mathrm{ADC}}(\mathrm{e^-/DN})}\right]^2 P_\mathrm{I}. \tag{4.31}$$

Substituting Eq. (4.28) into Eq. (4.31) and solving for $K_{\mathrm{ADC}}(\mathrm{e^-/DN})$ yields

$$K_{\mathrm{ADC}}(\mathrm{e^-/DN}) = \frac{S(\mathrm{DN})}{\sigma^2_{\mathrm{SHOT}}(\mathrm{DN})}. \tag{4.32}$$

4.6 Effective Quantum Yield

4.6.1 Photon event charge sharing

As long as all of the charge generated by a photon is collected by the target pixel and not by neighboring pixels, Eq. (4.25) can be applied to determine the quantum yield. However, charge may be shared if the diameter of the initial electron cloud immediately after a photon interacts is comparable to the pixel size. This effect may take place for high-energy soft x-rays where cloud diameter increases with photon energy.

Charge sharing also occurs when a pixel's active volume is only partially depleted—that is, regions of the pixel where electric fields do not exist, allowing electrons to wander into neighboring pixels.[1] The charge diffusion problem is presented in Figs. 4.4 through 4.5. Figure 4.4 shows 5.9-keV soft x-ray photon events (1620 $\mathrm{e^-}$) generated by a CCD that exhibits a significant charge diffusion problem. Photons that penetrate and interact below the pixel's depletion region diffuse into many pixels around the target pixel. Figure 4.5 shows the charge diffusion problem for three 9-MeV grazing incident protons that interact with the same CCD. The protons ionize the silicon atoms, generating a signal charge that initially collects in single pixels along the track. However, as the proton goes deeper into the silicon, beyond the depletion region, the charge cloud grows in size and occupies more than a dozen pixels before the proton finally stops.

The quantum yield measured will be lower than expected if electrons from a photon event are shared among the pixels. The measurement effect is a reduction of the true, measured shot noise. That is,

$$\sigma_{\mathrm{SHOT}} = (\eta_\mathrm{E} S)^{1/2}, \tag{4.33}$$

where η_E is the effective quantum yield that is measured. If charge sharing takes place, the effective quantum yield will always be less than the ideal quantum yield (i.e., $\eta_\mathrm{E} < \eta_\mathrm{i}$).

Quantum yield is measured more accurately with larger pixel sensors because the pixels represent a larger target for the charge cloud to collect. Also, pixels can be summed to improve the measurement (e.g., 2×2 sum). This can be achieved either on-chip for a CCD or off-chip for a CMOS sensor.

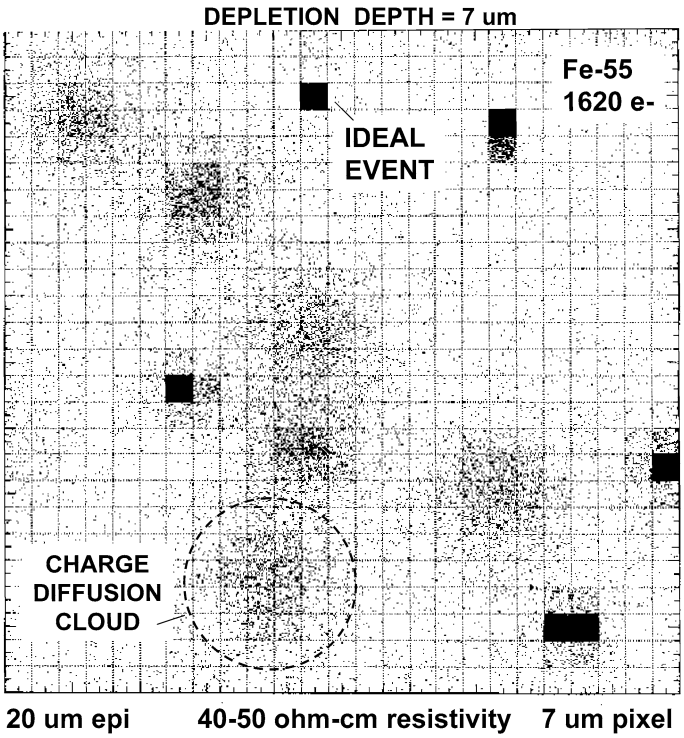

Figure 4.4 Fe-55 1620 e^- x-ray photons taken from a CCD that exhibits charge diffusion and collection problems.

4.6.2 Charge collection efficiency

The effective quantum yield measured represents a figure of merit for how well pixels collect signal charge. Charge collection efficiency (CCE) is defined as[1]

$$\mathrm{CCE} = \frac{\eta_\mathrm{E}}{\eta_\mathrm{i}}. \tag{4.34}$$

Figure 4.6 shows a 5.9-keV x-ray quantum yield histogram taken from a CCD with 15-μm pixels. The array was uniformly illuminated with x-rays (approximately five x-rays per pixel). The quantum yield was calculated using Eq. (4.25) for many different 40×40 pixel subarrays across the sensor. Data were then displayed in the histogram shown. The average effective quantum yield measured was 900 e^- significantly less than the ideal quantum yield of 1620 e^-. The less-than-optimum response was caused by field-free silicon that resulted in charge diffusion and sharing as well as some recombination loss within the substrate of the device.

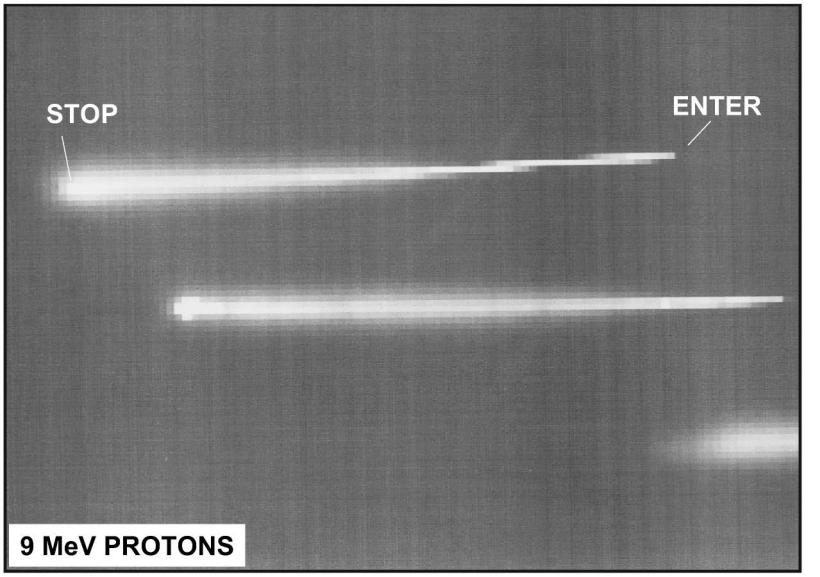

Figure 4.5 9 MeV proton events showing charge diffusion characteristics by the same CCD in Fig. 4.4.

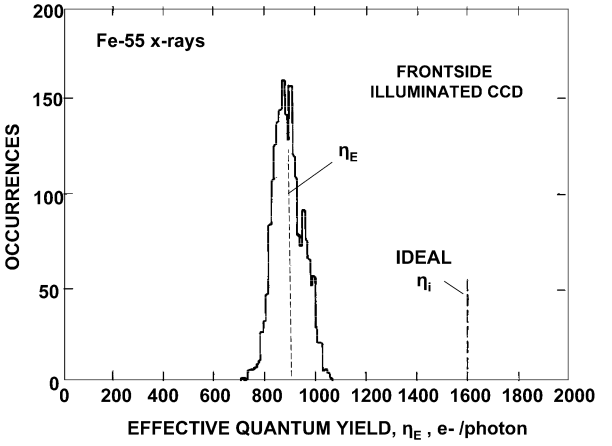

Figure 4.6 CCD Fe-55 histogram showing that the effective quantum yield is less than the ideal quantum yield because of charge collection problems.

Example 4.5

Calculate the CCE for the PT results in Fig. 4.6.

Solution:
From Eq. (4.34),

$$\mathrm{CCE} = \frac{900}{1620} = 0.556.$$

Important Points

1. PT relations [e.g., $K_{\mathrm{ADC}}(\mathrm{e}^-/\mathrm{DN})$] are found by measuring the output signal statistics. When finding the relations, the camera can be treated as a black box as long as the input exhibits shot noise behavior.
2. Given the output mean and variance quantities, only one unique PT relation satisfies the input shot noise statistics (i.e., $\mathrm{noise} = \mathrm{signal}^{1/2}$).
3. The PT relation allows relative output measurement units (DN, volt) to be converted to absolute input physical units (electrons and photons).
4. The PT relation is used to determine internal camera transfer functions [e.g., sense node gain (V/e^-) and sense node capacitance].
5. Quantum efficiency and quantum yield performance parameters are found through the PT relation.
6. Charge sharing between pixels lowers shot noise and quantum yield measurements.
7. The PT relation is used to measure pixel CCE performance of a detector.

Chapter 5
Photon Transfer Curve

5.1 PTC Setup and Generation

This chapter opens by discussing the mechanics of generating a PTC. An ideal PTC response from a camera system exposed to a uniform light source is illustrated in Fig. 5.1. For a subarray of pixels, rms noise is plotted as a function of average signal at different light levels (or exposure times). Four distinct noise regimes are identified in a PTC. The first regime, read noise, represents the random noise measured under totally dark conditions, which often includes several different noise contributors (refer to Chapter 12). As the light illumination is increased, read noise gives way to photon shot noise, which represents the middle region of the curve. Since the plot in Fig. 5.1 is on log-log coordinates, shot noise is characterized by a line with a slope of $1/2$. The third regime is associated with pixel FPN, which produces a characteristic slope of unity because signal and FPN scale together.

The fourth region occurs when the subarray of pixels enters the full-well regime. In this region the noise modulation typically decreases as saturation is approached. Although shot noise always decreases, for some arrays the FPN may actually increase (CMOS detectors often exhibit this characteristic). This happens because some columns of the array may reach full well before others, generating a

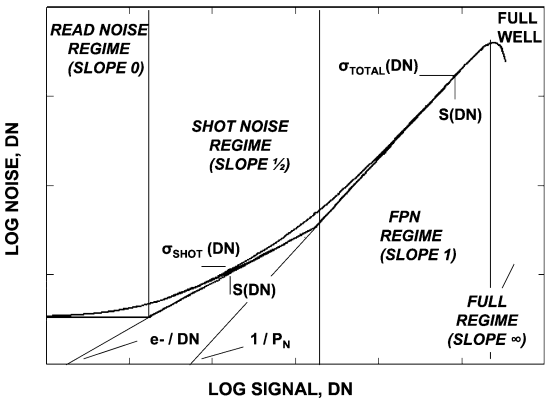

Figure 5.1 Ideal total noise PTC illustration showing the four classical noise regimes.

fixed-pattern, column-to-column noise. In either case, a rapid noise deviation from the $1/2$ or 1 slope curves indicates that full well has taken place. In general, PTC represents a very sensitive test tool for detecting full-well conditions.

PTC measurements are made initially in computer DN units that will be converted to electron units later. For statistical reasons, it is desirable to include as many pixels in a PTC measurement as possible. Chapter 6 will show that measurement accuracy is proportional to the square root of the number of pixels sampled. For example, a 20×20 pixel subarray will exhibit a 7% standard deviation for the data products produced. When greater accuracy is required, additional pixels must be interrogated (20,000 pixels will yield 1% accuracy).

Usually, the exposure time is varied for a PTC sequence, letting the charge integration period and frame readout time remain constant. For fast PTC generation, the exposure time is increased logarithmically to cover the dynamic range more quickly. Exposure time can be controlled by a mechanical shutter or a pulsed light source. It is also possible to vary the light intensity and keep the exposure time constant by allowing the computer to control the power supply voltage to a light source. A low-cost light-emitting diode (LED) is often utilized for start-up systems. LEDs can be turned "on" and "off" very quickly, which allows for very short exposure periods (a few microseconds is possible). This feature is advantageous because fast exposures are necessary to cover the full dynamic range of the sensor. A response of four to five orders of magnitude may be required for high-end/scientific camera systems. Several LEDs can be run in parallel to provide an intense flat-field light source. The color of the LED is not critical for PTC work; however, FPN typically shows some wavelength dependence. Light uniformity across the subarray of pixels being sampled needs to be better that 1%, or FPN measurements will be in error; shot noise is insensitive to field flatness.

The average signal level is plotted only after a fixed average electrical offset level is removed from the raw pixel values that were initially stored in the computer (refer to Fig. 5.2). In equation form,

$$S(\mathrm{DN}) = \frac{\sum_{i=1}^{N_{\mathrm{PIX}}} \mathrm{DN}_{i\_\mathrm{ADC}}}{N_{\mathrm{PIX}}} - S_{\mathrm{ADC\_OFF}}(\mathrm{DN}), \tag{5.1}$$

where $S(\mathrm{DN})$ is the average signal level, $\mathrm{DN}_{i\_\mathrm{ADC}}$ is the raw signal value of the ith raw video pixel, N_{PIX} is the number of pixels contained in the subarray, and $S_{\mathrm{ADC\_OFF}}(\mathrm{DN})$ is the ADC offset level [refer to Eq. (4.19)].

Strictly speaking, the absolute offset level represents the signal measured from a region on the array where electrons are not generated. This includes "background electrons" generated by sources other than photo-generated charge, such as thermal dark current. For CCDs, the zero electron level is readily found by "over scanning" the sensor's horizontal register. The "virtual pixels" that follow the last horizontal video pixel of each line represent the best measurement of zero charge and offset. The overscanned pixels from each line are stored in a computer along with

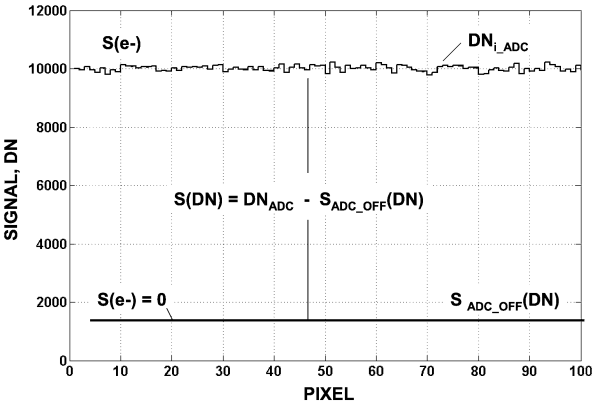

Figure 5.2 Illustration showing the raw signal and offset levels for a row of pixels.

the raw video pixels. The average of the over-scanned pixels represents the desired ADC offset level. The single offset value produced [i.e., $S_{\mathrm{ADC\_OFF}}(\mathrm{DN})$] is subtracted from the averaged raw video pixel values to find the true average signal level, $S(\mathrm{DN})$ [i.e., Eq. (5.1)].

For CMOS sensors, finding a pixel region in absence of electrons is not possible because all pixels are active. In this case, the offset value is determined from several dark frames that are averaged to reduce the random noise they contain (read noise, dark current shot noise, etc.). That is,

$$\mathrm{OFF}_i(\mathrm{DN}) = \frac{\sum_{j=1}^{N_\mathrm{F}} \mathrm{off}_j(\mathrm{DN})}{N_\mathrm{F}}, \tag{5.2}$$

where $\mathrm{OFF}_i(\mathrm{DN})$ is the averaged offset subarray based on j dark frames, $\mathrm{off}_j(\mathrm{DN})$ is the jth offset frame, and N_F is the number of offset frames averaged.

The resultant offset subarray described by Eq. (5.2) is stored and later subtracted pixel by pixel from subsequent raw video subarrays to obtain the true photogenerated signal, i.e.,

$$S(\mathrm{DN}) = \frac{\sum_{i=1}^{N_\mathrm{PIX}} \mathrm{DN}_{i\_\mathrm{ADC}} - \mathrm{OFF}_i(\mathrm{DN})}{N_\mathrm{PIX}}, \tag{5.3}$$

where $\mathrm{OFF}_i(\mathrm{DN})$ is the offset signal level of the ith offset pixel.

Noise for the ordinate of Fig. 5.1 is found by calculating the standard deviation (or rms) of the pixel values from the subarray after the offset value is removed. That is,

$$\sigma_\mathrm{TOTAL}(\mathrm{DN}) = \left\{ \frac{\sum_{i=1}^{N_\mathrm{PIX}} [S_i(\mathrm{DN}) - S(\mathrm{DN})]^2}{N_\mathrm{PIX}} \right\}^{1/2}, \tag{5.4}$$

where $\sigma_\mathrm{TOTAL}(\mathrm{DN})$ is the total noise (read noise, shot noise, and FPN) plotted in Fig. 5.1, and $S_i(\mathrm{DN})$ is the signal value of the ith raw video pixel without offset.

The FPN must be removed to obtain the shot/read noise response. FPN is eliminated by differencing, pixel by pixel, two identical frames taken back-to-back at the same exposure level, which is illustrated in Fig. 5.3. The standard of the difference is given by

$$\sigma_{\Delta}(\mathrm{DN}) = \left[\frac{\sum_{i=1}^{N_{\mathrm{PIX}}}(\mathrm{DN1}_{i\_\mathrm{ADC}} - \mathrm{DN2}_{i\_\mathrm{ADC}})^2}{N_{\mathrm{PIX}}}\right]^{1/2}, \tag{5.5}$$

where $\mathrm{DN1}_{i\_\mathrm{ADC}}$ and $\mathrm{DN2}_{i\_\mathrm{ADC}}$ are the raw signal values of the ith raw video pixel for the first frame and the second subarrays taken back-to-back.

It is important to divide the result in Eq. (5.5) by $2^{1/2}$ because random noise increases by this amount: when two identical frames are either subtracted (as in this case) or added, the random noise component of the resultant frame increases by $2^{1/2}$. Therefore, the true random noise from the differencing process is

$$\sigma_{\mathrm{READ+SHOT}}(\mathrm{DN}) = \frac{\sigma_{\Delta}}{2^{1/2}}, \tag{5.6}$$

where $\sigma_{\mathrm{READ+SHOT}}(\mathrm{DN})$ is the read noise and shot noise.

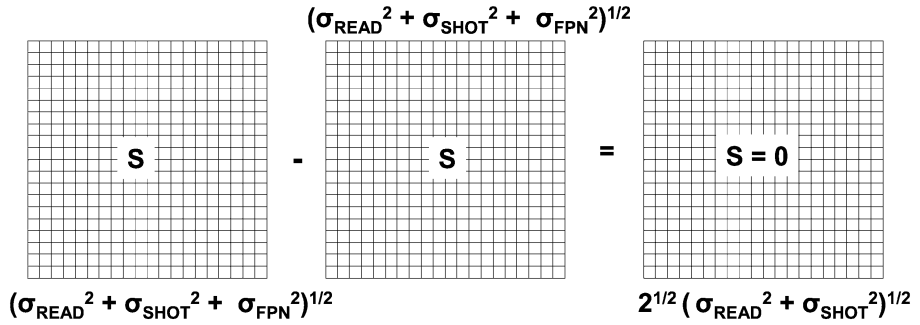

Figure 5.3 Illustration showing how FPN is removed by subtracting two back-to-back frames.

5.2 PTC Family

Individual PTCs for each noise component are typically plotted as a family (refer to Fig. 5.4). For example, from the PT Eq. (4.20), the shot noise is given by

$$\sigma_{\mathrm{SHOT}}(\mathrm{DN}) = \left[\frac{S(\mathrm{DN})}{K_{\mathrm{ADC}}(\mathrm{e^-/DN})}\right]^{1/2}. \tag{5.7}$$

From Eq. (3.12), the FPN is given as

$$\sigma_{\mathrm{FPN}}(\mathrm{DN}) = P_{\mathrm{N}} S(\mathrm{DN}). \tag{5.8}$$

The total noise shown in Fig. 5.1, which includes read noise, shot noise, and FPN, is found by the quadrature sum of the individual noise sources:

$$\sigma_{\mathrm{TOTAL}}(\mathrm{DN}) = \left\{\sigma_{\mathrm{READ}}(\mathrm{DN})^2 + \frac{S(\mathrm{DN})}{K_{\mathrm{ADC}}(\mathrm{e^-/DN})} + [P_{\mathrm{N}} S(\mathrm{DN})]^2\right\}^{1/2}. \tag{5.9}$$

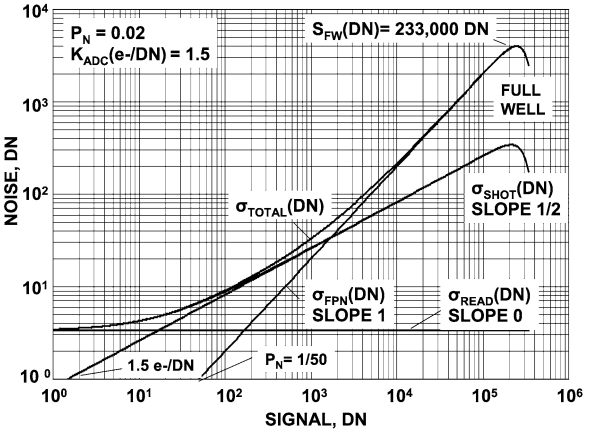

Figure 5.4 Classical PTC set plotted in DN units showing various data products.

Shot and read noise are separated from total noise by

$$\sigma_{\mathrm{SHOT+READ}}(\mathrm{DN}) = \left[\sigma_{\mathrm{TOTAL}}(\mathrm{DN})^2 - \sigma_{\mathrm{FPN}}(\mathrm{DN})^2\right]^{1/2}. \tag{5.10}$$

Shot noise is separated from $\sigma_{\mathrm{SHOT+READ}}(\mathrm{DN})$ by

$$\sigma_{\mathrm{SHOT}}(\mathrm{DN}) = \left[\sigma_{\mathrm{SHOT+READ}}(\mathrm{DN})^2 - \sigma_{\mathrm{READ}}(\mathrm{DN})^2\right]^{1/2}. \tag{5.11}$$

The next two examples demonstrate how $\sigma_{\mathrm{TOTAL}}(\mathrm{DN})$, $\sigma_{\mathrm{READ}}(\mathrm{DN})$, $\sigma_{\mathrm{SHOT}}(\mathrm{DN})$, and $\sigma_{\mathrm{FPN}}(\mathrm{DN})$ are plotted as a family to form the "classical PTC set."

Example 5.1

Using the equations above, generate PTCs for $\sigma_{\mathrm{TOTAL}}(\mathrm{DN})$, $\sigma_{\mathrm{READ}}(\mathrm{DN})$, $\sigma_{\mathrm{SHOT}}(\mathrm{DN})$, and $\sigma_{\mathrm{FPN}}(\mathrm{DN})$ as a function of $S(\mathrm{DN})$. Validate $K_{\mathrm{ADC}}(\mathrm{e^-/DN})$ for a single point on the shot noise curve. Also confirm P_{N} using a single point on the FPN curve. Determine the sensor's dynamic range. On a separate graph, plot each noise source in electron units. Assume $\sigma_{\mathrm{READ}}(\mathrm{DN}) = 3.33\,\mathrm{DN}$, $K_{\mathrm{ADC}}(\mathrm{e^-/DN}) = 1.5$, $\eta_{\mathrm{i}} = 1\ \mathrm{e^-}$/photon, $P_{\mathrm{N}} = 0.02$ (2%), and a charge capacity of $S_{\mathrm{FW}}(\mathrm{DN}) = 233{,}000\ \mathrm{DN}$.

Solution:
From Eqs. (5.7) and (5.8), the shot noise and FPN are

$$\sigma_{\mathrm{SHOT}}(\mathrm{DN}) = \left[\frac{S(\mathrm{DN})}{1.5}\right]^{1/2}$$

and

$$\sigma_{\mathrm{FPN}}(\mathrm{DN}) = 0.02 \times S(\mathrm{DN}).$$

From Eq. (5.9), the total noise is given by

$$\sigma_{\mathrm{TOTAL}}(\mathrm{DN}) = \left\{3.33^2 + \frac{S(\mathrm{DN})}{1.5} + [0.02 \times S(\mathrm{DN})]^2\right\}^{1/2}.$$

Each noise source is plotted in Fig. 5.4. The read noise, shot noise, and FPN show slopes of 0, $1/2$, and unity, respectively.

$K_{\mathrm{ADC}}(\mathrm{e}^-/\mathrm{DN})$ is calculated from a single data point on the shot noise curve shown in Fig. 5.4. For example, a signal level of 10,000 DN corresponds to a shot noise level of approximately 82 DN. From Eq. (4.20),

$$K_{\mathrm{ADC}}(\mathrm{e}^-/\mathrm{DN}) = \frac{10{,}000}{82^2} = 1.5.$$

The FPN quality factor, P_{N}, is found from a single data point on the FPN curve and by applying Eq. (5.8). For example, a signal level of 10,000 DN corresponds to a FPN of 200 DN to produce a P_{N} of

$$P_{\mathrm{N}} = \frac{200}{10{,}000} = 0.02\ (2\%).$$

The PTC shows that the shot and FPN noise are rapidly turning over at approximately 233,000 DN, indicating the full-well condition. The corresponding charge capacity in electron units is

$$S_{\mathrm{FW}} = 233{,}000\ \mathrm{DN} \times 1.5\ \mathrm{e}^-/\mathrm{DN} = 350{,}000\ \mathrm{e}^-,$$

and the read noise in electron is

$$\sigma_{\mathrm{READ}} = 3.3\ \mathrm{DN} \times 1.5\ \mathrm{e}^-/\mathrm{DN} = 5\ \mathrm{e}^-.$$

The dynamic range is defined as the ratio of full well to read noise, which yields

$$\mathrm{DR} = \frac{S_{\mathrm{FW}}}{\sigma_{\mathrm{READ}}} = \frac{350{,}000}{5} = 70{,}000.$$

The dynamic range can also be given in db units by

$$\mathrm{DR(db)} = 20 \times \log_{10}(\mathrm{DR}) = 20 \times \log(70{,}000) = 97.$$

Figure 5.5 converts the PTCs shown in Fig. 5.4 into units of electrons using $K_{\mathrm{ADC}}(\mathrm{e}^-/\mathrm{DN}) = 1.5$. Note that the FPN curve does not shift during the conversion process, as does the shot noise curve. Also, the shot noise tracks the square root of signal (i.e., $\sigma_{\mathrm{SHOT}} = S^{1/2}$), which is not the case for the DN shot noise plot (i.e., $\sigma_{\mathrm{SHOT}}(\mathrm{DN}) \neq S(\mathrm{DN})^{1/2}$).

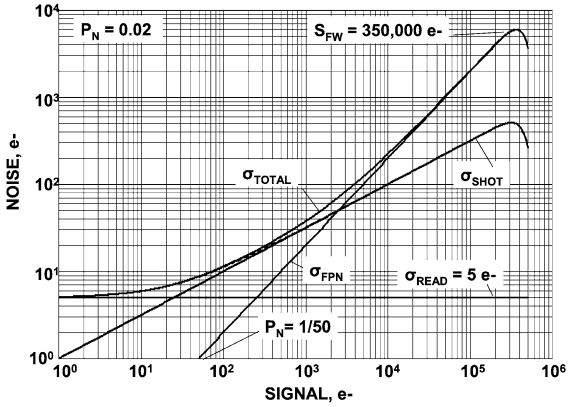

Figure 5.5 Classical PTC data set plotted in electron units.

$K_{\mathrm{ADC}}(\mathrm{e}^{-}/\mathrm{DN})$ can also be found graphically by extending the slope $1/2$ shot noise line back to the signal axis as shown in Figs. 5.1 and 5.4. The signal intercept represents the value $K_{\mathrm{ADC}}(\mathrm{e}^{-}/\mathrm{DN})$ [i.e., $K_{\mathrm{ADC}}(\mathrm{e}^{-}/\mathrm{DN}) = S(\mathrm{DN})$]. This result is proved by first taking the logarithm of Eq. (4.20) to produce

$$\log K_{\mathrm{ADC}}(\mathrm{e}^{-}/\mathrm{DN}) = \log S(\mathrm{DN}) - 2\log \sigma_{\mathrm{SHOT}}(\mathrm{DN}); \tag{5.12}$$

letting $\sigma_{\mathrm{SHOT}}(\mathrm{DN}) = 1$ and solving for $K_{\mathrm{ADC}}(\mathrm{e}^{-}/\mathrm{DN})$ yields

$$\log K_{\mathrm{ADC}}(\mathrm{e}^{-}/\mathrm{DN}) = \log S(\mathrm{DN}) - 2\log 1 = \log S(\mathrm{DN}); \tag{5.13}$$

and taking the antilog of both sides yields

$$K_{\mathrm{ADC}}(\mathrm{e}^{-}/\mathrm{DN}) = S(\mathrm{DN}). \tag{5.14}$$

Also note that the FPN curve intercept on the signal axis is equal to $1/P_{\mathrm{N}}$. This is shown by taking the logarithm of Eq. (5.8) to produce

$$\log \sigma_{\mathrm{FPN}}(\mathrm{DN}) = \log P_N + \log S(\mathrm{DN}). \tag{5.15}$$

Letting $\sigma_{\mathrm{FPN}}(\mathrm{DN}) = 1$ and solving for P_{N} yields

$$P_N = \frac{1}{S(\mathrm{DN})}. \tag{5.16}$$

$K_{\mathrm{ADC}}(\mathrm{e}^{-}/\mathrm{DN})$ and P_{N} are both graphically determined in Figs. 5.1 and 5.4.

Example 5.2

From the data table below, generate PTCs for $\sigma_{\mathrm{TOTAL}}(\mathrm{DN})$, $\sigma_{\mathrm{READ+SHOT}}(\mathrm{DN})$, $\sigma_{\mathrm{SHOT}}(\mathrm{DN})$, and $\sigma_{\mathrm{FPN}}(\mathrm{DN})$. Plot the results in DN units. Determine $K_{\mathrm{ADC}}(\mathrm{e}^{-}/\mathrm{DN})$, P_{N}, σ_{READ}, S_{FW}, and dynamic range.

Raw signal $\mathrm{DN_{ADC}}$	Offset $S_{\mathrm{ADC\_OFF}}$ (DN)	Signal $S(\mathrm{DN})$	Total Noise σ_{TOTAL} (DN)	Δ Noise (DN)	Shot Noise σ_{SHOT} (DN)	FPN $\sigma_{\mathrm{FPN}}(\mathrm{DN})$
1.03E+02	1.02E+02	1.00E+00	4.95E+00	5.08E+00	8.73E−01	2.00E−02
1.04E+02	1.02E+02	1.62E+00	5.26E+00	5.18E+00	1.35E+00	3.20E−02
1.05E+02	1.02E+02	2.63E+00	4.93E+00	4.95E+00	7.16E−01	5.30E−02
1.06E+02	1.02E+02	4.27E+00	5.24E+00	5.20E+00	1.41E+00	8.50E−02
1.09E+02	1.02E+02	6.92E+00	5.36E+00	5.17E+00	1.30E+00	1.38E−01
1.13E+02	1.02E+02	1.12E+01	5.56E+00	5.33E+00	1.86E+00	2.24E−01
1.20E+02	1.02E+02	1.82E+01	6.33E+00	6.15E+00	3.58E+00	3.64E−01
1.32E+02	1.02E+02	2.95E+01	6.39E+00	6.51E+00	4.17E+00	5.90E−01
1.50E+02	1.02E+02	4.79E+01	7.87E+00	7.93E+00	6.16E+00	9.57E−01
1.80E+02	1.02E+02	7.76E+01	9.19E+00	8.96E+00	7.44E+00	1.55E+00
2.28E+02	1.02E+02	1.26E+02	1.08E+01	1.05E+01	9.22E+00	2.52E+00
3.06E+02	1.02E+02	2.04E+02	1.36E+01	1.27E+01	1.16E+01	4.08E+00
4.33E+02	1.02E+02	3.31E+02	1.76E+01	1.57E+01	1.49E+01	6.62E+00
6.39E+02	1.02E+02	5.37E+02	2.23E+01	1.95E+01	1.89E+01	1.07E+01
9.73E+02	1.02E+02	8.71E+02	2.98E+01	2.46E+01	2.41E+01	1.74E+01
1.51E+03	1.02E+02	1.41E+03	4.27E+01	3.06E+01	3.02E+01	2.83E+01
2.39E+03	1.02E+02	2.29E+03	5.92E+01	3.83E+01	3.80E+01	4.58E+01
3.82E+03	1.02E+02	3.72E+03	9.16E+01	5.13E+01	5.11E+01	7.43E+01
6.13E+03	1.02E+02	6.03E+03	1.39E+02	6.41E+01	6.39E+01	1.20E+02
9.87E+03	1.02E+02	9.77E+03	2.15E+02	7.75E+01	7.73E+01	1.95E+02
1.60E+04	1.02E+02	1.58E+04	3.28E+02	1.02E+02	1.02E+02	3.13E+02
2.58E+04	1.02E+02	2.57E+04	5.06E+02	1.18E+02	1.18E+02	4.87E+02
4.18E+04	1.02E+02	4.17E+04	6.79E+02	1.33E+02	1.33E+02	6.63E+02
6.77E+04	1.02E+02	6.76E+04	5.24E+02	8.35E+01	8.33E+01	5.09E+02
1.10E+05	1.02E+02	1.10E+05	3.51E+01	4.20E+00	2.71E+00	3.39E+01
1.78E+05	1.02E+02	1.78E+05	0.00E+00	0.00E+00	5.00E+00	0.00E+00

Solution:
The raw signal values are given in the first column of the table. The ADC offset level is tabulated in the second column and is subtracted from the first column to produce the true signal level, $S(\mathrm{DN})$, tabulated in the third column. The fourth column is the standard deviation of $S(\mathrm{DN})$, which represents the total noise, $\sigma_{\mathrm{TOTAL}}(\mathrm{DN})$, and is plotted in Fig. 5.6. From this curve, the read noise, $\sigma_{\mathrm{READ}}(\mathrm{DN})$, is approximately 5 DN for the lowest signal level taken. The slope 1 portion of the curve is used to find P_{N} [graphically or through Eq. (5.8)], which yields $P_{\mathrm{N}} = 0.02$.

FPN is eliminated by differencing, pixel by pixel, two identical images taken back to back at the same exposure level illustrated in Fig. 5.3. The standard deviation of the frame difference (divided by $2^{1/2}$ as discussed above) is

tabulated in the fifth column and represents only random noise (i.e., $\sigma_{\mathrm{READ+SHOT}}$). $\sigma_{\mathrm{READ+SHOT}}$ noise is plotted in Fig. 5.6. Shot noise without read noise is found through Eq. (5.11) as

$$\sigma_{\mathrm{SHOT}}(\mathrm{DN}) = (\sigma_{\mathrm{READ+SHOT}}(\mathrm{DN})^2 - 5^2)^{1/2},$$

which is tabulated in the sixth column and plotted in Fig. 5.6.

The FPN curve is found from

$$\sigma_{\mathrm{FPN}}(\mathrm{DN}) = 0.02 \times S(\mathrm{DN}).$$

This data is contained in the seventh column and plotted in Fig. 5.6.

$K_{\mathrm{ADC}}(\mathrm{e}^-/\mathrm{DN})$ is determined from a data point on the shot noise curve. For example, when $\sigma_{\mathrm{SHOT}}(\mathrm{DN}) = 100$ DN and $S(\mathrm{DN}) = 15{,}000$ DN, they yield

$$K_{\mathrm{ADC}}(\mathrm{e}^-/\mathrm{DN}) = \frac{15{,}000}{100^2} = 1.5\ \mathrm{e}^-/\mathrm{DN}.$$

Full well is found where the noise begins to decrease with signal and deviates either from the shot noise slope $1/2$ curve or the FPN slope 1 curve. In electron units, full well is approximately

$$S_{\mathrm{FW}} = K_{\mathrm{ADC}}(\mathrm{e}^-/\mathrm{DN}) \times S_{\mathrm{FW}}(\mathrm{DN}) = 1.5 \times 40{,}000 = 60{,}000\ \mathrm{e}^-.$$

Read noise in electron units is

$$\sigma_{\mathrm{READ}} = K_{\mathrm{ADC}}(\mathrm{e}^-/\mathrm{DN}) \times \sigma_{\mathrm{READ}}(\mathrm{DN}) = 1.5 \times 5 = 7.5\ \mathrm{e}^-.$$

The dynamic range is

$$\mathrm{DR} = \frac{S_{\mathrm{FW}}}{\sigma_{\mathrm{READ}}} = \frac{60{,}000}{7.5} = 8000.$$

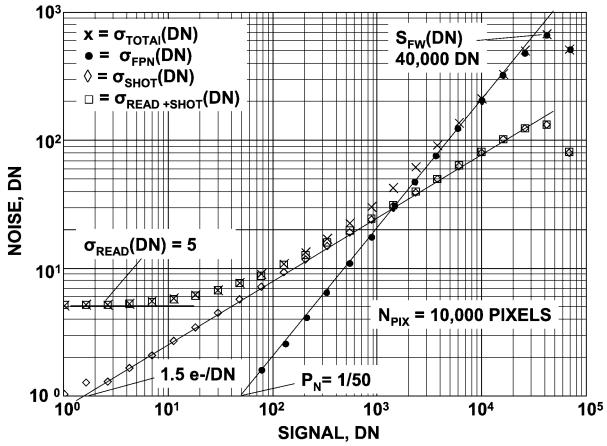

Figure 5.6 Experimental PTC set.

In db,

$$\mathrm{DR(db)} = 20\log_{10}(8000) = 78.$$

For PTC measurements when the quantum yield is greater than unity, the shot noise in DN units from Eq. (4.23) is

$$\sigma_{\mathrm{SHOT}}(\mathrm{DN}) = \left[\frac{S(\mathrm{DN})}{K_{\mathrm{ADC}}(P_{\mathrm{I}}/\mathrm{DN})}\right]^{1/2} = \left[\frac{\eta_i S(\mathrm{DN})}{K_{\mathrm{ADC}}(\mathrm{e^-/DN})}\right]^{1/2}. \tag{5.17}$$

The total noise is

$$\sigma_{\mathrm{TOTAL}}(\mathrm{DN}) = \left[\sigma_{\mathrm{READ}}(\mathrm{DN})^2 + \frac{\eta_{\mathrm{i}} S(\mathrm{DN})}{K_{\mathrm{ADC}}(\mathrm{e^-/DN})} + [P_{\mathrm{N}} S(\mathrm{DN})]^2\right]^{1/2}. \tag{5.18}$$

Example 5.3

From Example 5.1, generate total noise PTCs when assuming $\eta_{\mathrm{i}} = 1$, 3, 10, 25, 50, and 100 $\mathrm{e^-}$/interacting photon. Plot the results in DN units. Find the signal level where FPN and shot noise are equal for each case. Also, graphically determine η_{i}. Assume perfect CCE (i.e., $\eta_{\mathrm{E}} = \eta_{\mathrm{i}}$).

Solution:
From Eq. (5.18), the total noise is

$$\sigma_{\mathrm{TOTAL}}(\mathrm{DN}) = \left\{3.33^2 + \eta_{\mathrm{i}}\frac{S(\mathrm{DN})}{1.5} + [0.02 \times S(\mathrm{DN})]^2\right\}^{1/2}$$

and is plotted in Fig. 5.7 for each quantum yield factor. Note that FPN gives way to shot noise as the quantum yield increases.

The signal level where FPN and shot noise are equal for each quantum yield factor is found through Eq. (3.14), i.e.,

$$\begin{aligned}
S &= \frac{1}{(0.02)^2} = 2500\ \mathrm{e^-} && \eta_{\mathrm{i}} = 1\\
S &= \frac{3}{(0.02)^2} = 7500\ \mathrm{e^-} && \eta_{\mathrm{i}} = 3\\
S &= \frac{10}{(0.02)^2} = 25{,}000\ \mathrm{e^-} && \eta_{\mathrm{i}} = 10\\
S &= \frac{25}{(0.02)^2} = 62{,}500\ \mathrm{e^-} && \eta_{\mathrm{i}} = 25\\
S &= \frac{50}{(0.02)^2} = 125{,}000\ \mathrm{e^-} && \eta_{\mathrm{i}} = 50\\
S &= \frac{100}{(0.02)^2} = 250{,}000\ \mathrm{e^-} && \eta_{\mathrm{i}} = 100
\end{aligned}$$

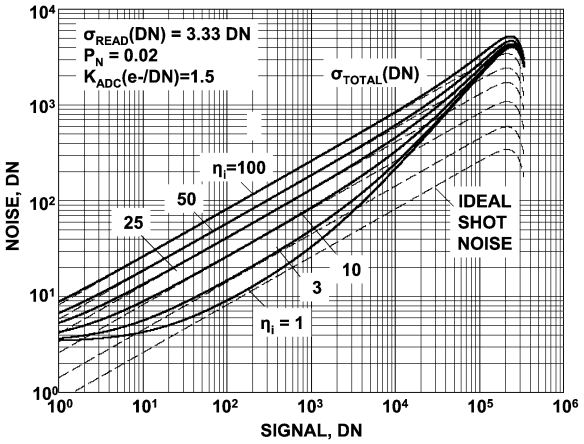

Figure 5.7 Total noise and shot noise PTC responses for different quantum yields.

Figure 5.8 presents a magnified view of Fig. 5.7 that shows the $K_{\mathrm{ADC}}(P_{\mathrm{I}}/\mathrm{DN})$ and $K_{\mathrm{ADC}}(\mathrm{e}^{-}/\mathrm{DN})$ intercept values. The quantum yield is determined from an intercept value using Eq. (4.25):

$$\eta_{\mathrm{i}} = \frac{K_{\mathrm{ADC}}(\mathrm{e}^{-}/\mathrm{DN})}{K_{\mathrm{ADC}}(P_{\mathrm{I}}/\mathrm{DN})},$$

where $K_{\mathrm{ADC}}(\mathrm{e}^{-}/\mathrm{DN}) = 1.5$, and $K_{\mathrm{ADC}}(P_{\mathrm{I}}/\mathrm{DN})$ is the signal level when $\sigma_{\mathrm{SHOT}}(\mathrm{DN}) = 1$. The quantum yields from this equation are

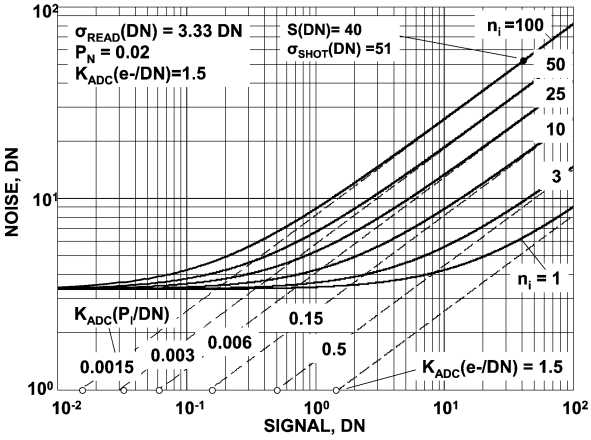

Figure 5.8 Magnified plots for Fig. 5.7 used to graphically determine the quantum yield through $K(P_{\mathrm{I}}/\mathrm{DN})$ and $K_{\mathrm{ADC}}(\mathrm{e}^{-}/\mathrm{DN})$.

$$\eta_i = \frac{1.5}{1.500} = 1 \quad e^-/\text{interacting photon}$$
$$\eta_i = \frac{1.5}{0.500} = 3$$
$$\eta_i = \frac{1.5}{0.150} = 10$$
$$\eta_i = \frac{1.5}{0.060} = 25$$
$$\eta_i = \frac{1.5}{0.030} = 50$$
$$\eta_i = \frac{1.5}{0.015} = 100.$$

Quantum yield can also determined directly from Eq. (4.25) through

$$\eta_i = \frac{K_{ADC}(e^-/DN)\sigma_{SHOT}(DN)^2}{S(DN)}.$$

For example, the $\eta_i = 100$ shot noise curve contains a data point shown at $S(DN) = 40$, $\sigma_{SHOT}(DN) = 51$, which yields approximately

$$\eta_i = 1.5 \times \frac{51^2}{40} = 98\ e^-.$$

5.3 PTC Errors

As discussed at the beginning of this chapter, it is critically important that the offset $[S_{ADC\_OFF}(DN)]$ be removed from the raw signal with good precision. It is also essential to track the offset level regularly because it can fluctuate. How often an offset measurement is required comes through experience with one's camera system (offset stability varies significantly between cameras and is considered to be an important figure-of-merit for system reliability).

A few DN of error in offset can significantly alter PT results. For example, Fig. 5.9 shows the effect of offset error on the $\sigma_{READ+SHOT}$ curve when an insufficient amount of offset is subtracted. Figure 5.10 presents the influence of the error only on the σ_{SHOT} curve. Note that the offset error shifts data from the ideal slope $1/2$ shot noise curve. When the curve bends, $K_{ADC}(e^-/DN)$ cannot be determined, which is mainly a problem for low signal levels. For example, Fig. 5.11 plots $K_{ADC}(e^-/DN)$ with signal for Fig. 5.10. Note that the signal level must be at least 10 times greater than the offset error before $K_{ADC}(e^-/DN)$ exhibits reasonable accuracy.

For low signals, read noise must also be eliminated, or $K_{ADC}(e^-/DN)$ will be in error. Figure 5.12 presents PTCs for various read noise subtractions. The ideal

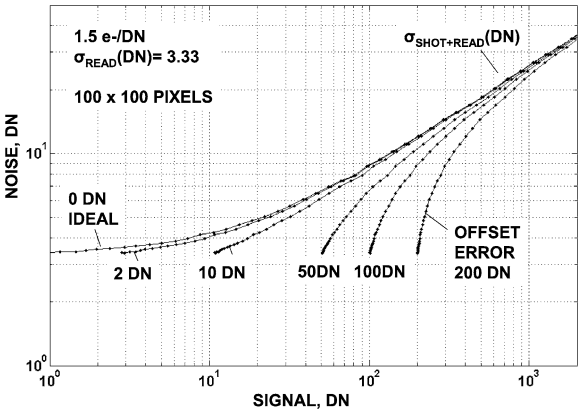

Figure 5.9 PTCs showing the affect of various offset errors on read and shot noise measurements.

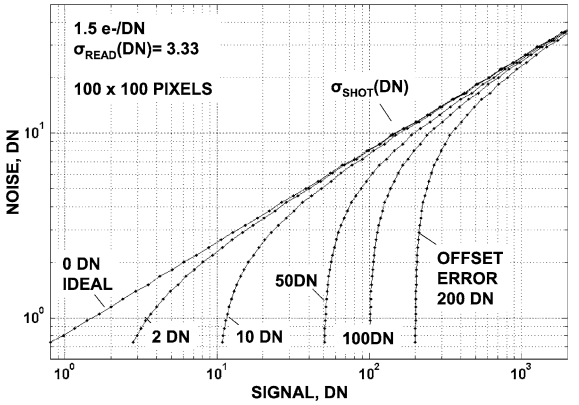

Figure 5.10 PTCs showing the affect of various offset errors on shot noise.

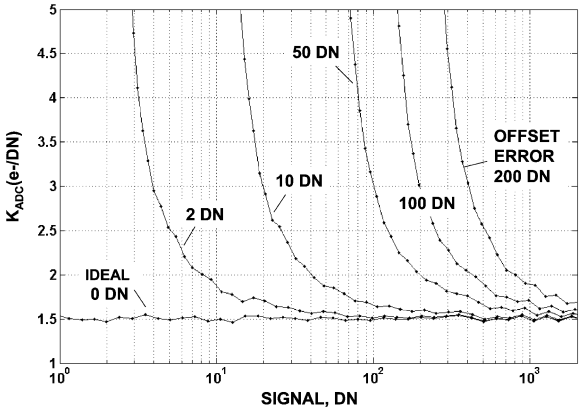

Figure 5.11 Offset error influence on $K_{\mathrm{ADC}}(\mathrm{e}^{-}/\mathrm{DN})$ measurement.

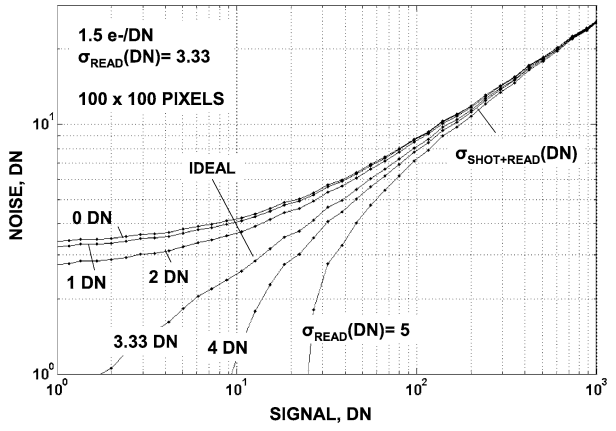

Figure 5.12 PTCs showing the affect of a read noise error on shot noise measurement.

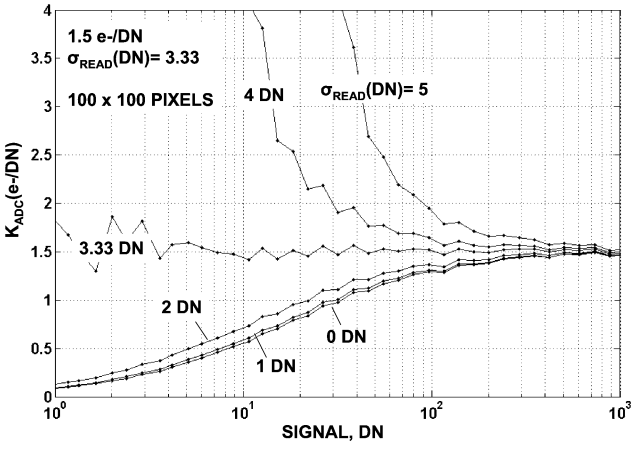

Figure 5.13 Read noise error affect on $K_{\mathrm{ADC}}(\mathrm{e}^{-}/\mathrm{DN})$ measurement.

shot noise curve is obtained when $\sigma_{\mathrm{READ}} = 3.33$ DN is deducted. As Fig. 5.13 demonstrates, $K_{\mathrm{ADC}}(\mathrm{e}^{-}/\mathrm{DN})$ will be greater than the true value if too much read noise is removed, and it will be underestimated if not enough is taken. Note that the signal level must be 10 times greater than the noise error to ensure reasonable accuracy for $K_{\mathrm{ADC}}(\mathrm{e}^{-}/\mathrm{DN})$.

FPN also needs to be removed for an accurate $K_{\mathrm{ADC}}(\mathrm{e}^{-}/\mathrm{DN})$ reading. FPN can be removed either by differencing frames, as in Fig. 5.3, or through flat fielding, a process discussed in Chapter 8. Figure 5.14 presents PTCs for $\sigma_{\mathrm{TOTAL}}(\mathrm{DN})$ and $\sigma_{\mathrm{SHOT}}(\mathrm{DN})$. Note that only a small segment of the dynamic range is shot noise limited for the total noise curve. Figure 5.15 plots $K_{\mathrm{ADC}}(\mathrm{e}^{-}/\mathrm{DN})$ based on the total noise without read noise subtraction or FPN removal [i.e., $K_{\mathrm{ADC}}(\mathrm{e}^{-}/\mathrm{DN}) =$

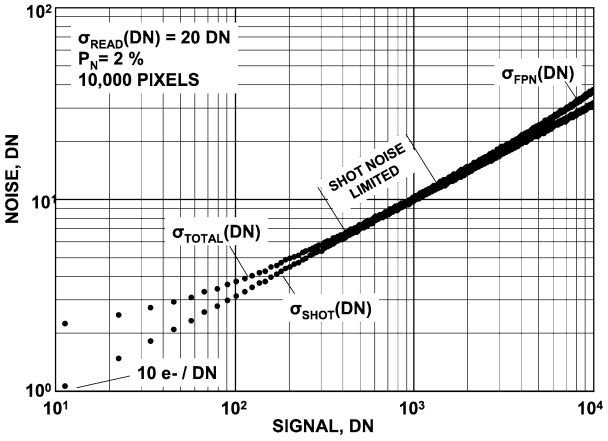

Figure 5.14 PTC showing a limited shot noise region for the total noise curve.

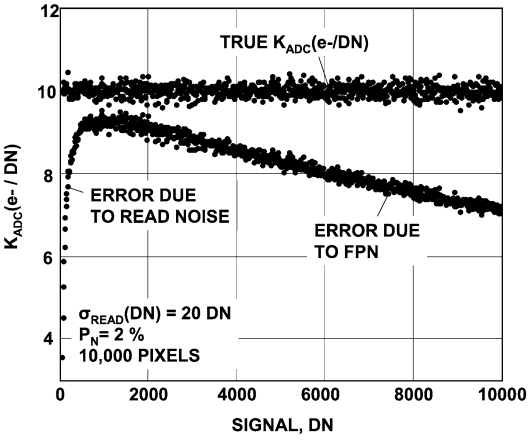

Figure 5.15 $K_{\mathrm{ADC}}(\mathrm{e}^-/\mathrm{DN})$ error when FPN or read noise are present.

$S(\mathrm{DN})/\sigma_{\mathrm{TOTAL}}(\mathrm{DN})^2]$. As can be seen, $K_{\mathrm{ADC}}(\mathrm{e}^-/\mathrm{DN})$ is in error when either noise source is present and will always produce a smaller result than the true value.

The accuracy of $K_{\mathrm{ADC}}(\mathrm{e}^-/\mathrm{DN})$ can be confirmed by converting a PTC generated in DN units into electron units. Shot noise should precisely follow the square root of signal if $K_{\mathrm{ADC}}(\mathrm{e}^-/\mathrm{DN})$ is correct. For example, Fig. 5.16 shows PTC electron plots based on DN data generated with $K_{\mathrm{ADC}}(\mathrm{e}^-/\mathrm{DN}) = 2.0$. Note that if $K_{\mathrm{ADC}}(\mathrm{e}^-/\mathrm{DN}) \neq 2$, the DN-to-electron conversion is in error, and the shot noise relation does not apply (i.e., $S \neq (\sigma_{\mathrm{SHOT}})^{1/2}$). One can fine-tune $K_{\mathrm{ADC}}(\mathrm{e}^-/\mathrm{DN})$ by forcing the relationship.

PT is also sensitive to charge transfer problems related to CCD and CMOS arrays. Numerous deferred charge and image lag difficulties have been identified. In

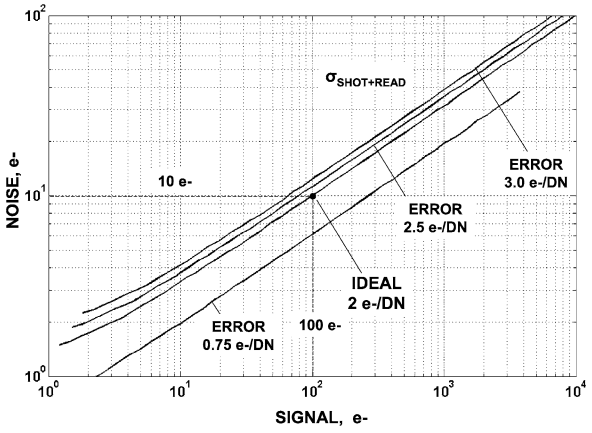

Figure 5.16 PTC shot noise responses in electron units for different $K_{\mathrm{ADC}}(\mathrm{e}^{-}/\mathrm{DN})$ errors compared to the ideal.

general, these problems reduce the measured shot noise without influencing the average signal. For example, Fig. 5.17 presents a PTC generated by a CMOS imager that exhibits an image lag problem. Note that for low-level signals, shot noise values are below the slope $1/2$ curve. Figure 5.18 plots $K_{\mathrm{ADC}}(\mathrm{e}^{-}/\mathrm{DN})$ with signal showing that $K_{\mathrm{ADC}}(\mathrm{e}^{-}/\mathrm{DN})$ is greater than the true value of 19 e^{-}/DN for low signal levels. Typically, when a PTC exhibits an initial decrease in $K_{\mathrm{ADC}}(\mathrm{e}^{-}/\mathrm{DN})$ with signal, it indicates that a charge transfer problem is present.

Image lag is quantified from a PTC through the relation

$$I_{\mathrm{LAG}} = \frac{\sigma_{\mathrm{M\_SHOT}}}{\sigma_{\mathrm{SHOT}}} = \frac{\sigma_{\mathrm{M\_SHOT}}(\mathrm{DN})}{\sigma_{\mathrm{SHOT}}(\mathrm{DN})}. \tag{5.19}$$

When the measured shot noise modulation is perfect (i.e. $I_{\mathrm{LAG}} = 1$), then it is fairly safe to assume that a camera system will perfectly preserve the modulation

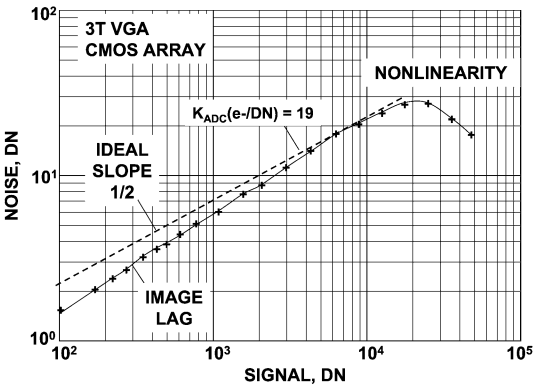

Figure 5.17 PTC shot noise response when image lag is present.

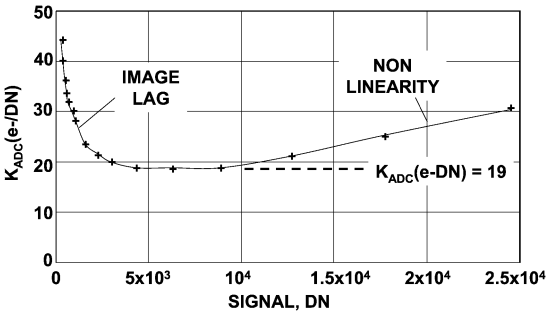

Figure 5.18 $K_{\mathrm{ADC}}(\mathrm{e}^{-}/\mathrm{DN})$ plot for Fig. 5.17.

produced by a real image, at least in terms of reading that image out. Hence, it is important that a PTC responce be ideal before acquiring images.

Example 5.4

The measured shot noise for the experimental CMOS data presented in Fig. 5.17 can be curve fitted with the equation

$$\sigma_{\mathrm{M\_SHOT}}(\mathrm{DN}) = \sigma_{\mathrm{SHOT}}(\mathrm{DN})\left\{1 - 0.29 \times \exp\left[-\frac{S(\mathrm{DN})}{1579}\right]\right\}. \quad \text{(E5.1)}$$

Use this relation to generate a PTC and an image lag factor plot as a function of signal.

Solution:
Figure 5.19 shows the required PTC.

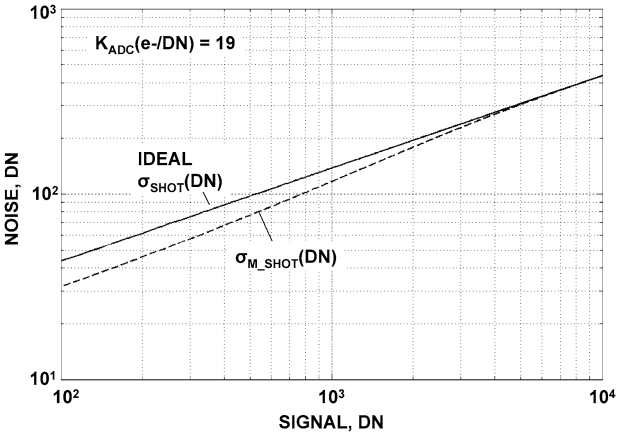

Figure 5.19 Ideal and measured image lag PTC responses as a function of signal.

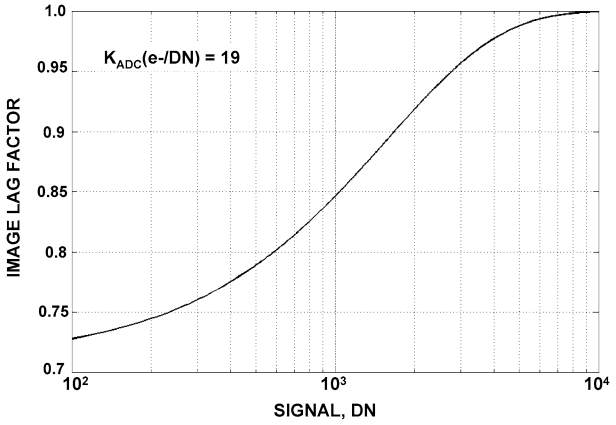

Figure 5.20 Image lag factor as a function of signal for Fig. 5.19.

Substituting Eq. (E5.1) into Eq. (E5.19) produces the image lag factor:

$$I_{\mathrm{LAG}} = \left[1 - 0.29 \times \exp\left(-\frac{S}{1579}\right)\right].$$

The image lag factor is plotted in Fig. 5.20.

It is advantageous to measure the image lag factor since clock and bias to a detector are varied to achieve optimum performance.

5.4 Shutterless (Time-Delayed Integration) PTC

For CCD imagers, it is possible to generate a full PTC from a single frame of data using the "shutterless" PTC method. In this method, the curve is generated without a mechanical shutter or pulsed light source. Instead, the CCD is continuously exposed to light and readout without an integration or shuttering cycle. The readout mode is similar to the *time-delayed integration* (TDI) used by CCD cameras.

In the shutterless method, illumination is provided by a nonuniform light source projected onto the CCD. For example, Fig. 5.21 shows a sinusoidal stimulus used to generate a PTC. After the light is adjusted to slightly above full well (66,670 DN in this case), and the video is stabilized, a specific number of data lines are read and stored in a computer. Then $S(\mathrm{DN})$ and $\sigma_{\mathrm{SHOT+READ}}(\mathrm{DN})$ are calculated for each column of the array. Continuous readout and exposure eliminates FPN since charge is smeared over many pixels during readout. Therefore, frame differencing as performed above (Fig. 5.3) to obtain shot noise data is not required.

Figure 5.22 shows a simulated shutterless PTC for the sinusoidal light source shown in Fig. 5.21. Signal and noise are measured for 1000 columns, thus producing 1000 data points that range from the read noise floor to full well. The number

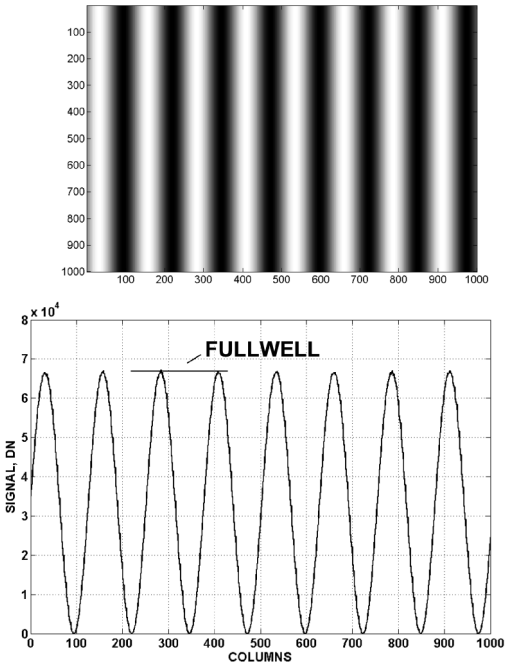

Figure 5.21 Sinusoidal stimulus used to generate a shutterless PTC.

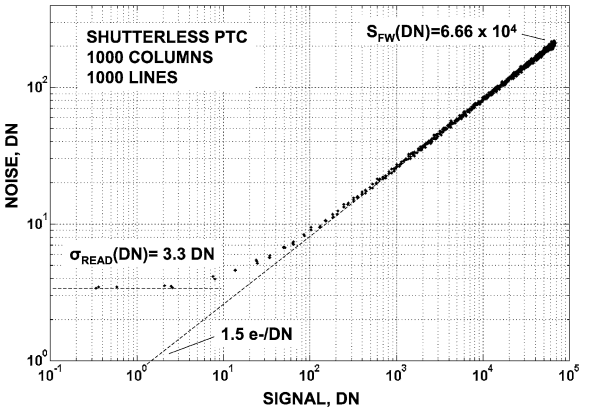

Figure 5.22 Shutterless PTC using the stimulus shown in Fig. 5.21.

of lines read into the computer depends on the measurement accuracy required. For example, a 1000-line reading yields a 5% measurement accuracy of $K_{\mathrm{ADC}}(\mathrm{e}^{-}/\mathrm{DN})$ (a parameter derived in Chapter 6).

It should be pointed out that FPN and related P_{N} information is lost with the shutterless PTC technique. However, linearity information is preserved through the $K_{\mathrm{ADC}}(\mathrm{e}^{-}/\mathrm{DN})$ plot, as shown in Fig. 5.23 for the PTC in Fig. 5.22.

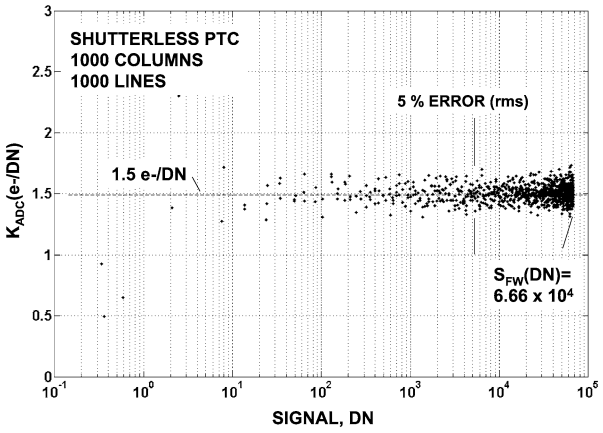

Figure 5.23 $K_{\mathrm{ADC}}(\mathrm{e}^{-}/\mathrm{DN})$ plot for Fig. 5.22.

5.5 Variance PTC

Noise variance can also be plotted as a function of signal instead of the standard deviation. Assuming FPN is removed through frame differencing (i.e., Fig. 5.3), the noise variance from Eq. (5.9) is

$$\sigma_{\mathrm{READ+SHOT}}(\mathrm{DN})^2 = \sigma_{\mathrm{READ}}(\mathrm{DN})^2 + \frac{S(\mathrm{DN})}{K_{\mathrm{ADC}}(\mathrm{e}^{-}/\mathrm{DN})}. \tag{5.19}$$

Note that this is a linear equation with the form

$$y = \text{constant} + \frac{x}{K_{\mathrm{ADC}}(\mathrm{e}^{-}/\mathrm{DN})}, \tag{5.20}$$

with slope $[K_{\mathrm{ADC}}(\mathrm{e}^{-}/\mathrm{DN})]^{-1}$. The read noise is the y-intercept value. Example 5.5 demonstrates how $K_{\mathrm{ADC}}(\mathrm{e}^{-}/\mathrm{DN})$ and read noise are extracted from a variance PTC.

Example 5.5

From Example 5.1, plot the noise variance as a function of signal on linear coordinates. Determine $K_{\mathrm{ADC}}(\mathrm{e}^{-}/\mathrm{DN})$ and the read noise from the plot.

Solution:
Figure 5.24 plots $\sigma_{\mathrm{SHOT}}(\mathrm{DN})^2$ with signal. A single data point from the linear portion of the curve (i.e., below full well) yields the slope. For example,

$$\begin{aligned} S(\mathrm{DN}) &= 90{,}000 \text{ DN and } \sigma_{\mathrm{SHOT}}(\mathrm{DN})^2 = 60{,}000; \\ \text{slope} &= \frac{60{,}000}{90{,}000} = 0.666. \end{aligned}$$

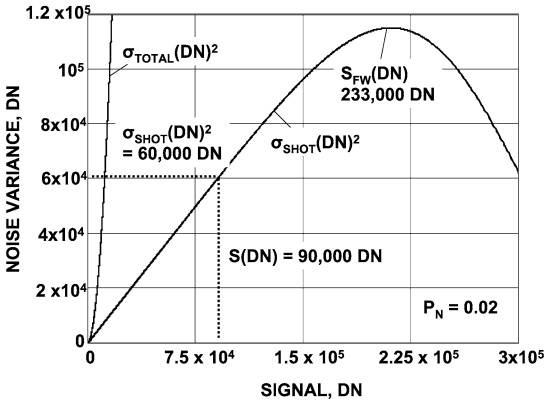

Figure 5.24 Variance PTCs.

The corresponding ADC sensitivity is the reciprocal of the slope:

$$K_{\mathrm{ADC}}(\mathrm{e}^{-}/\mathrm{DN}) = \frac{1}{0.666} = 1.5.$$

Figure 5.25 plots $\sigma_{\mathrm{READ+SHOT}}(\mathrm{DN})$ and $\sigma_{\mathrm{SHOT}}(\mathrm{DN})$ for low signal levels, showing identical slopes for the two curves. Read noise is determined from the intercept on the noise axis from the $\sigma_{\mathrm{READ+SHOT}}(\mathrm{DN})$ curve. The plot yields

$$\begin{aligned} \sigma_{\mathrm{READ}}(\mathrm{DN})^2 &= 11, \\ \sigma_{\mathrm{READ}}(\mathrm{DN}) &= 3.33, \end{aligned}$$

and

$$\sigma_{\mathrm{READ}} = 3.33 \times 1.5 = 5\ \mathrm{e}^{-}.$$

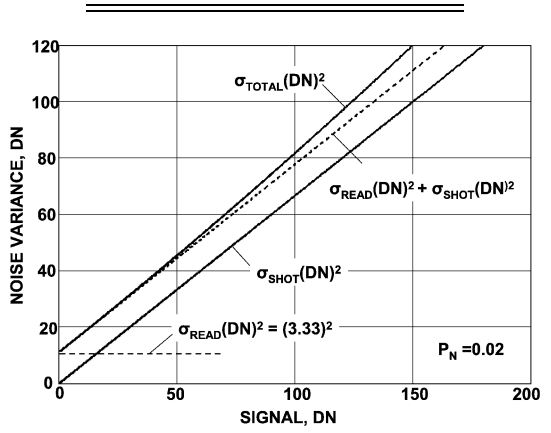

Figure 5.25 Magnified variance PTC responses for Fig. 5.24.

Figures 5.26 and 5.27 compare the standard deviation and variance PTCs. Both figures plot $\sigma_{\mathrm{READ+SHOT}}(\mathrm{DN})$ for different read noise floors that vary from 2–400 e^-, assuming $K_{\mathrm{ADC}}(\mathrm{e}^-/\mathrm{DN}) = 100$. Note that for high noise levels, it is impossible to graphically find $K_{\mathrm{ADC}}(\mathrm{e}^-/\mathrm{DN})$ from the standard deviation PTC, whereas the slope from the variance response is readily determined. Figure 5.28 shows results when read noise is subtracted from the PTCs in Fig. 5.26, thereby producing the $\sigma_{\mathrm{SHOT}}(\mathrm{DN})$ curve. Two noise levels are shown ($\sigma_{\mathrm{READ}} = 200$ and 400 e^-) for clarity only. Fitting a slope $1/2$ line through the data points now yields $K_{\mathrm{ADC}}(\mathrm{e}^-/\mathrm{DN})$. It should be mentioned that the accuracy in determining $K_{\mathrm{ADC}}(\mathrm{e}^-/\mathrm{DN})$ for a given data set is identical for the variance and standard deviation PTC methods (refer to Chapter 6).

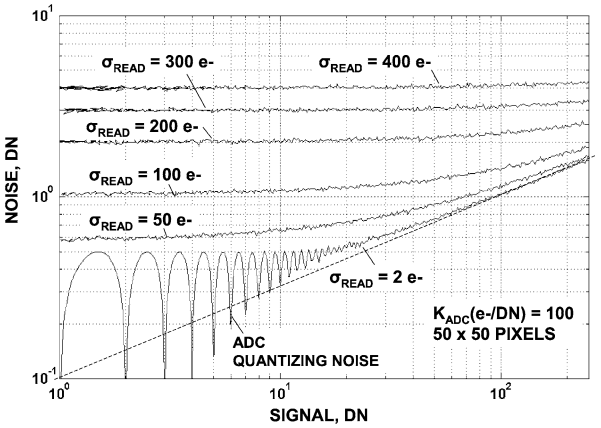

Figure 5.26 PTCs for different read noise floors.

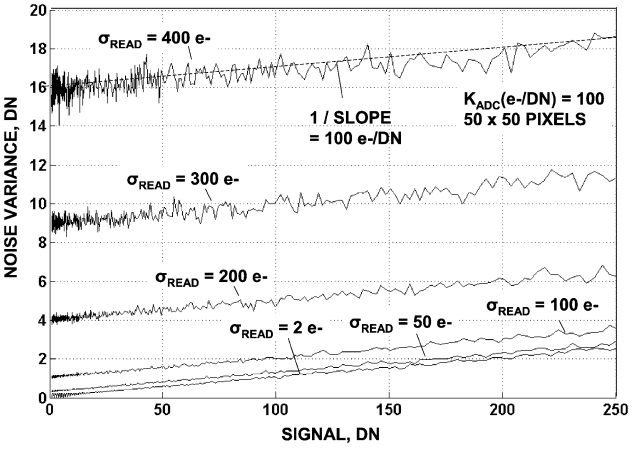

Figure 5.27 Corresponding variance PTCs for Fig. 5.26.

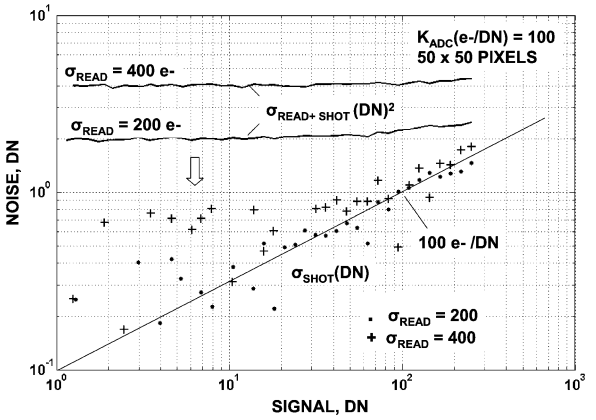

Figure 5.28 Read noise removal for selected PTCs shown in Fig. 5.26, allowing $K_{\mathrm{ADC}}(\mathrm{e}^-/\mathrm{DN})$ to be graphically measured.

When the quantum yield is greater than unity, the total noise variance is

$$\sigma_{\mathrm{TOTAL}}(\mathrm{DN})^2 = \sigma_{\mathrm{READ}}(\mathrm{DN})^2 + \frac{\eta_{\mathrm{i}} S(\mathrm{DN})}{K_{\mathrm{ADC}}(\mathrm{e}^-/\mathrm{DN})}, \tag{5.21}$$

which is a linear equation having a slope of $\eta_{\mathrm{i}}[K_{\mathrm{ADC}}(\mathrm{e}^-/\mathrm{DN})]^{-1}$. That is, the slope increases proportionally to the quantum yield.

Example 5.6

Plot the noise variance as a function of signal for $\eta_{\mathrm{i}} = 1$ and 10. Assume $K_{\mathrm{ADC}}(\mathrm{e}^-/\mathrm{DN}) = 100$.

Solution:
Figure 5.29 shows the desired curves. The quantum yield is found by the ratio of the two slopes, i.e.,

$$\eta_{\mathrm{i}} = \frac{K_{\mathrm{ADC}}(P_{\mathrm{I}}/\mathrm{DN})\ \text{slope}}{K_{\mathrm{ADC}}(\mathrm{e}^-/\mathrm{DN})\ \text{slope}},$$

and

$$\eta_{\mathrm{i}} = \frac{0.1}{0.01} = 10\ \mathrm{e}^-/\text{interacting photon}.$$

5.6 Example Experimental PTC Data

Figure 5.30 presents a $\sigma_{\mathrm{READ+SHOT}}$ PTC generated by a Hubble Space Telescope CCD (WF/PC I).[1] $K_{\mathrm{ADC}}(\mathrm{e}^-/\mathrm{DN})$ is found from any data point on the slope $1/2$

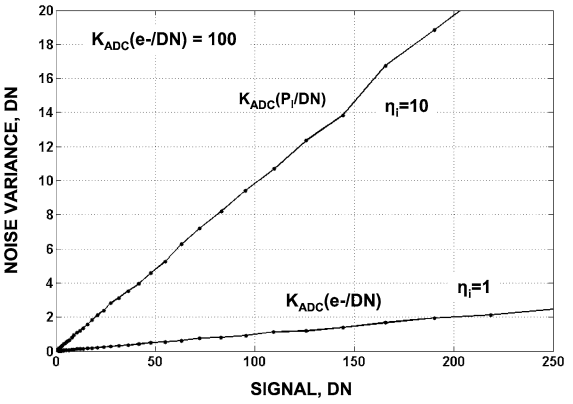

Figure 5.29 Variance PTCs used to measure quantum yield.

curve, which yields 2 e^-/DN. Using this constant, full well and read noise (in DN units) are converted to 60,000 e^- and 16 e^- rms, respectively. It is worth noting that CCD performance has improved dramatically since the early Hubble CCDs. For example, charge capacity for the same size pixel (15 μm) has increased to 500,000 e^-. Read noise has improved by a factor of 10 for the same signal-processing parameters. PT has played a major role in increasing the CCD's dynamic range in terms of design, fabrication, and operating parameters.

It is a rare occasion when a satisfactory PTC is generated for a new camera system that is powered for the first time. Hardware and software problems usually stand in the way of good PTCs that are resolved one by one. For example, Figure 5.31 shows a CCD PTC that exhibits an undesired "kink" caused by an improper vertical clock voltage setting that limits full-well performance to 240,000 e^-. The problem was fixed by lowering the clock voltage by 1.5 V, which in turn increased the charge capacity to 350,000 e^-. PTC anomalies like this are usually critical to

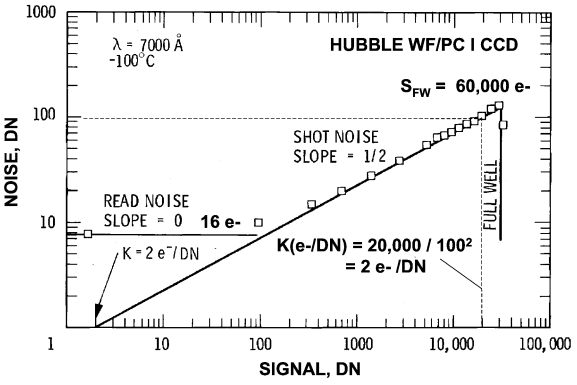

Figure 5.30 Early Hubble Space Telescope WF/PC I CCD PTC with FPN removed.

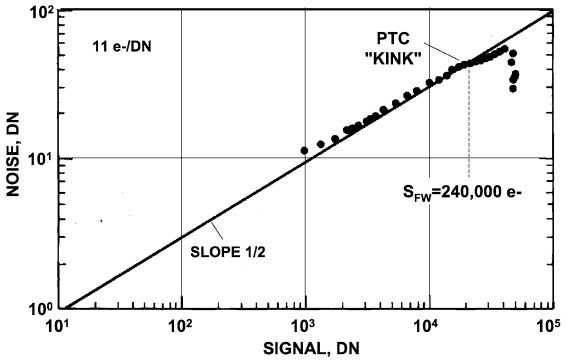

Figure 5.31 Shot noise PTC showing a "kink" in the response indicative of an improper clock voltage setting.

camera performance and should not be ignored. CCD and CMOS clock and voltage optimization rely heavily on PT results.

Figure 5.32 shows $\sigma_{\mathrm{READ+SHOT}}(\mathrm{DN})$ PTC responses generated by a CMOS imager that incorporates two pixel architectures with different sense node V/e$^-$ gains. The high and low gains produce ADC sensitivity values of 0.05 e^-/DN and 0.18 e^-/DN, respectively. As indicated, the read noise is 3 DN for both pixels because the noise is generated downstream of the sense node (hence voltage and DN read noise are identical). The shot noise curves are well separated because their $K_{\mathrm{ADC}}(\mathrm{e}^-/\mathrm{DN})$ values are different. The DN data of Fig. 5.32 are converted to electrons and plotted in Fig. 5.33. Note that the shot noise curves now overlap, whereas the read noise curves separate. The shot noise for both curves is equal to the square root of the signal and independent of $K_{\mathrm{ADC}}(\mathrm{e}^-/\mathrm{DN})$. However, the read noise in electron units is different for two pixels because read noise varies inversely

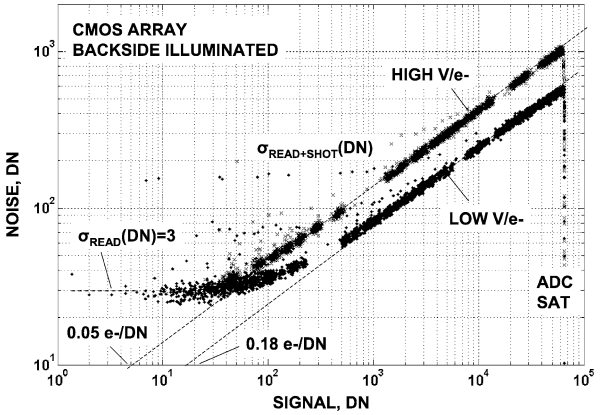

Figure 5.32 CMOS PTCs for two different pixel architectures with low and high sense node gains showing the same read noise floor of 3 DN rms.

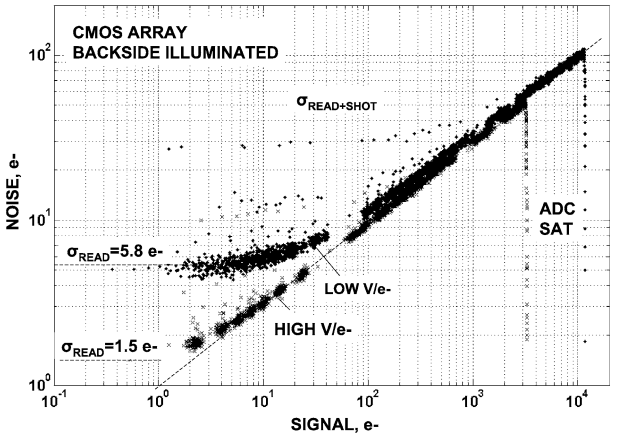

Figure 5.33 Corresponding PTCs for Fig. 5.32 measured in electron units showing read noise levels of 5.8 e^- and 1.5 e^-.

with $K_{\mathrm{ADC}}(\mathrm{e}^-/\mathrm{DN})$. Read noise levels of 5.8 e^- and 1.5 e^- are measured for each pixel type.

PTC is a useful tool to characterize many unique and unusual camera features offered by CMOS imagers (a book could be written on the subject). For example, the dynamic range for a CMOS pixel camera can be increased by using the reset timing diagram shown in Fig. 5.34. Conventional timing, shown in Fig. 5.35(a), resets the pixel once per charge-integration period. Timing for an "extended dynamic range (XDR)" mode is shown in Fig. 5.35(b), where an additional reset clock is applied during the charge-integration period. The amplitude of the second reset clock is adjusted to "clip" the signal on the sense node at a given level (labeled as S_{XDR}) and time period. After the second reset is applied, charge is allowed to integrate until the conventional reset is applied. For example, Fig. 5.35 plots the sense node charge throughout the integration period both with and without an XDR reset ap-

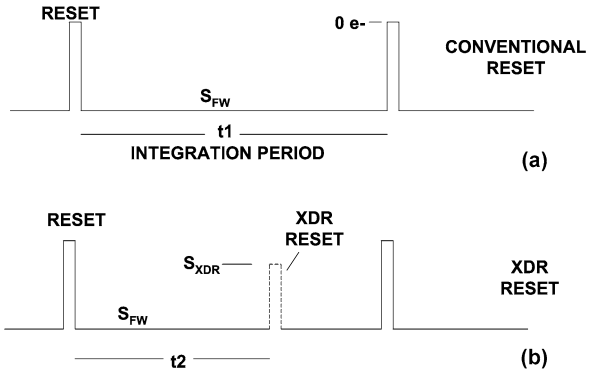

Figure 5.34 CMOS XDR set-up timing diagram.

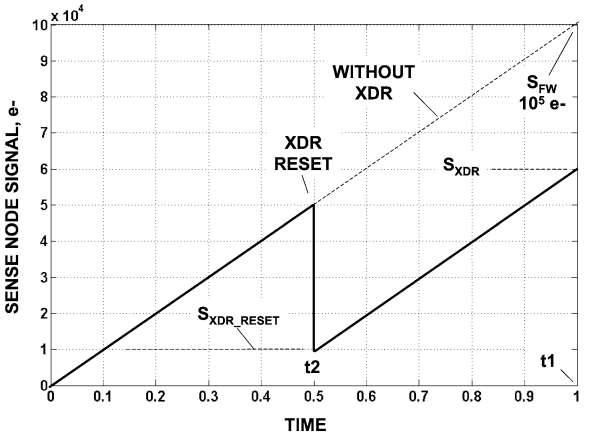

Figure 5.35 XDR sense node signal as a function of time.

plied. Note that without XDR, the charge level reaches 10^5 e^-, whereas the XDR signal only increases to 6×10^4 e^- and thereby compresses the signal. Figure 5.36 shows the response to a sinusoidal input, also with and without XDR applied. The compression on the sine wave is apparent when the signal level becomes greater than $S_{\mathrm{XDR\_RESET}}$.

The maximum signal level generated by an XDR compressor is given by

$$S_{\mathrm{XDR}} = S_{\mathrm{XDR\_RESET}} + \frac{t1 - t2}{t1} S_{\mathrm{FW}}, \tag{5.22}$$

where $S_{\mathrm{XDR\_RESET}}$ is the signal level immediately after XDR reset takes place, S_{FW} is the full-well signal of the detector, $t1$ is the integration time, and $t2$ represents the time when the XDR reset is applied. Both $S_{\mathrm{XDR\_RESET}}$ and $t2$ are

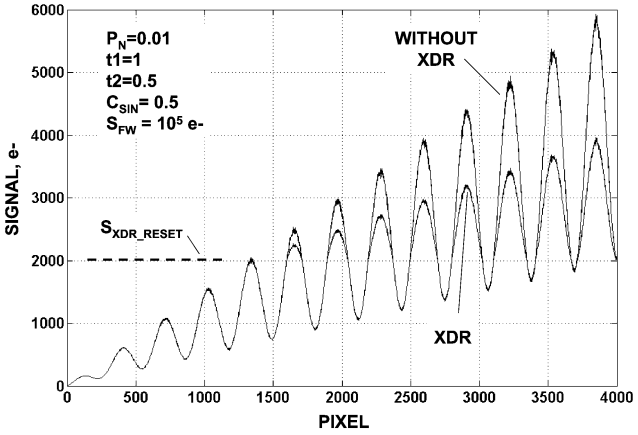

Figure 5.36 XDR response compared to conventional response.

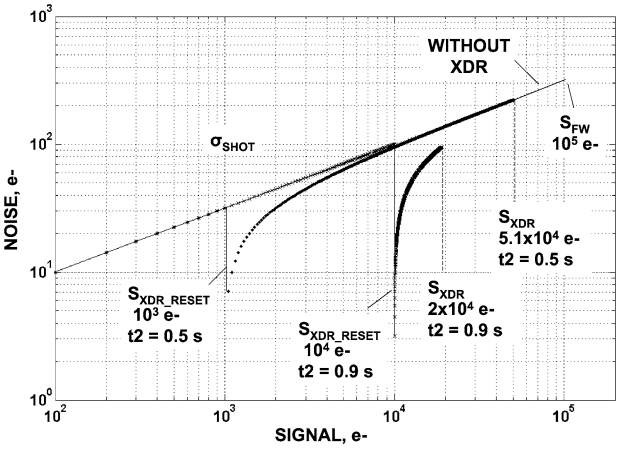

Figure 5.37 PTCs for two different XDR timing conditions in comparison to a conventional response.

usually set external to the sensor by the user. The compression achieved is given simply by

$$C_{\mathrm{XDR}} = \frac{\mathrm{S_{FW}}}{\mathrm{S_{XDR}}}. \tag{5.23}$$

A simulated PTC shot-noise response for XDR is demonstrated in Fig. 5.37 for two different XDR settings. The next example will determine the compression achieved from the curves.

Example 5.7

Determine the maximum XDR signal generated for the PT shown in Fig. 5.37 with the two settings:

XDR setting #1:

$$S_{\mathrm{XDR\_RESET}} = 1000\ \mathrm{e}^-,$$
$$t1 = 1,\ t2 = 0.5.$$

XDR setting #2:

$$S_{\mathrm{XDR\_RESET}} = 10000\ \mathrm{e}^-,$$
$$t1 = 1,\ t2 = 0.9.$$

Assume $S_{\mathrm{FW}} = 10^5\ \mathrm{e}^-$ and determine the compression achieved for each setting.

Solution:
From Eqs. (5.22) and (5.23), the maximum XDR signals and compression ratios are:

XDR setting #1:

$$S_{\mathrm{XDR}} = 10^3 + 0.5 \times 10^5 = 5.1 \times 10^4 \ \mathrm{e}^-,$$

$$C_{\mathrm{XDR}} = \frac{10^5}{5.1 \times 10^4} = 1.96.$$

XDR setting #2:

$$S_{\mathrm{XDR}} = 10^4 + 0.1 \times 10^5 = 2.0 \times 10^4 \ \mathrm{e}^-,$$

$$C_{\mathrm{XDR}} = \frac{10^5}{2 \times 10^4} = 5.0.$$

Important Points

1. A PTC contains four noise regimes: read noise, shot noise, fixed pattern noise, and full well.
2. A PTC is plotted on log-log coordinates to cover the full dynamic range of a camera system.
3. PTC is initially plotted in DN units. To convert the PTC to electron units, $K_{\mathrm{ADC}}(\mathrm{e}^-/\mathrm{DN})$ must be determined first.
4. Before a PTC can be generated, the ADC offset must be removed from raw video pixel values to obtain the true signal level.
5. Absolute ADC offset represents a signal level of zero electrons.
6. FPN measurements are dependent on the uniformity of a light source ($<1\%$ nonuniformity flatness is required). Shot noise measurements do not require a uniform light source.
7. FPN can be removed by pixel-by-pixel differencing of two identical frames taken back to back. The resultant frame contains only random noise (read and shot noise). The resultant frame must be divided by $2^{1/2}$ to find the true random noise.
8. Full well is usually exceeded by a detector when either shot noise or FPN rapidly decrease with signal.
9. The classical PTC contains individual plots for total noise, shot noise, and fixed pattern noise.
10. $K_{\mathrm{ADC}}(\mathrm{e}^-/\mathrm{DN})$ and P_{N} can be determined graphically from a PTC or through the PT relation.
11. Full well and read noise are converted to electrons after $K_{\mathrm{ADC}}(\mathrm{e}^-/\mathrm{DN})$ is found.

12. For a PTC expressed in electron units, shot noise equals the square root of signal.
13. Offset, read noise, and FPN must be precisely removed in order to determine $K_{\mathrm{ADC}}(\mathrm{e}^{-}/\mathrm{DN})$.
14. Charge transfer problems are quantified by PTC. Charge transfer issues lower the measured shot noise.
15. The shutterless PTC technique allows a shot noise PTC to be generated from a single frame of data.
16. The variance PTC is advantageous in finding $K_{\mathrm{ADC}}(\mathrm{e}^{-}/\mathrm{DN})$ in the presence of read noise.

Chapter 6
e^{-}/DN Variance

This chapter derives a formula used to determine the measurement accuracy of $K_{\mathrm{ADC}}(\mathrm{e}^{-}/\mathrm{DN})$. To show the error's origin graphically, a shot noise PTC plotted on linear scales is presented in Fig. 6.1. The data were simulated using a random number generator based on a 500-pixel subarray. The data points are scattered about the ideal solid shot noise curve; the variance in data about the curve reflects upon the error in measuring $K_{\mathrm{ADC}}(\mathrm{e}^{-}/\mathrm{DN})$. A histogram of $K_{\mathrm{ADC}}(\mathrm{e}^{-}/\mathrm{DN})$ with a standard deviation of 0.645 is shown in Fig. 6.2. The histogram in Fig. 6.3 shows an improved standard deviation of 0.141 DN when 10,000 pixels are sampled. These results suggest that the uncertainty in ADC sensitivity decreases by the square root of the number of pixels sampled. It would also be informative to know how read noise and signal level influence measurement accuracy. The analysis below includes these variables when $K_{\mathrm{ADC}}(\mathrm{e}^{-}/\mathrm{DN})$ variance is calculated.

The error behind $K_{\mathrm{ADC}}(\mathrm{e}^{-}/\mathrm{DN})$ is determined by applying the propagation of errors formula to the equation

$$K = \frac{S}{N^2 - R^2}, \tag{6.1}$$

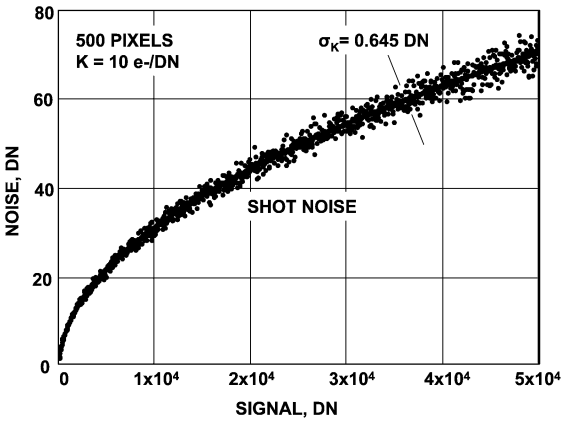

Figure 6.1 Linear PTC showing shot noise build up with signal.

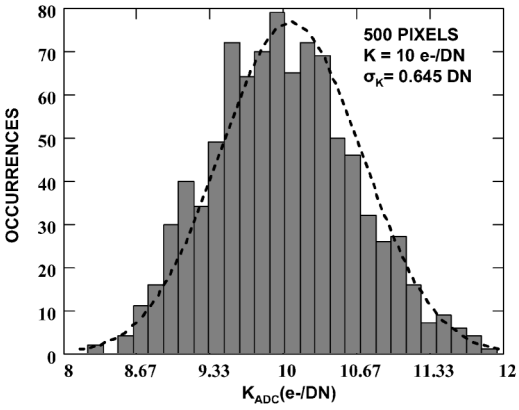

Figure 6.2 K_{ADC}(e$^-$/DN) histogram for Fig. 6.1 with 0.645 e$^-$/DN rms variation.

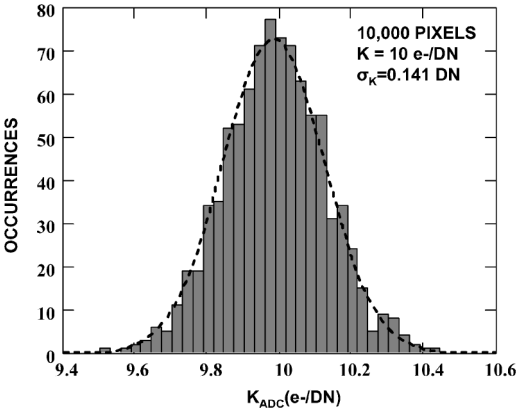

Figure 6.3 K_{ADC}(e$^-$/DN) histogram with 0.141 e$^-$/DN rms variation.

where for short-hand notation we let $K = K_{\mathrm{ADC}}(\mathrm{e}^-/\mathrm{DN})$, $N = \sigma_{\mathrm{READ+SHOT}}(\mathrm{DN})$, $R = \sigma_{\mathrm{READ}}(\mathrm{DN})$, and $S = S(\mathrm{DN})$.

Applying the formula yields

$$\sigma_{\mathrm{K}}^2 = \left[\frac{\partial K}{\partial S}\right]^2 \sigma_{\mathrm{S}}^2 + \left[\frac{\partial K}{\partial N}\right]^2 \sigma_{\mathrm{N}}^2 + \left[\frac{\partial K}{\partial R}\right]^2 \sigma_{\mathrm{R}}^2, \tag{6.2}$$

where σ_{K}^2 is the variance of K.

Differentiating produces

$$\sigma_{\mathrm{K}}^2 = \left[\frac{1}{N^2 - R^2}\right]^2 \sigma_{\mathrm{S}}^2 + \left[\frac{-2SN}{(N^2 - R^2)^2}\right]^2 \sigma_{\mathrm{N}}^2 + \left[\frac{2SR}{(N^2 - R^2)^2}\right]^2 \sigma_{\mathrm{R}}^2. \tag{6.3}$$

Assuming photon statistics [i.e., $K\sigma_{\mathrm{S}} = (KS)^{1/2}$], the uncertainty in the signal measured is

$$\sigma_{\mathrm{S}}^2 = \frac{S}{KN_{\mathrm{PIX}}}, \tag{6.4}$$

where N_{PIX} is the number of pixels sampled. The uncertainties in the noise sources are

$$\sigma_{\mathrm{N}}^2 = \frac{N^2}{2N_{\mathrm{PIX}}} \tag{6.5}$$

and

$$\sigma_{\mathrm{R}}^2 = \frac{R^2}{2N_{\mathrm{PIX}}}. \tag{6.6}$$

By substituting Eqs. (6.4)–(6.6) and noting that

$$N^2 = \frac{S}{K} + R^2, \tag{6.7}$$

we find

$$\sigma_{\mathrm{K}}^2 = \frac{1}{N_{\mathrm{PIX}}}\left(\frac{K}{S} + \frac{2\left(\frac{S}{K} + R^2\right)^2 K^4}{S^2} + \frac{2R^4K^4}{S^2}\right). \tag{6.8}$$

If the read noise is negligible relative to signal shot noise, Eq. (6.8) simplifies to

$$\sigma_{\mathrm{K}}^2 = \frac{K}{N_{\mathrm{PIX}}}\left(\frac{1}{S} + 2K\right). \tag{6.9}$$

And if $1/S \ll 2K$, then Eq. (6.9) reduces further to

$$\sigma_{\mathrm{K}}^2 = \frac{2K^2}{N_{\mathrm{PIX}}}. \tag{6.10}$$

The error of K in percent is

$$\%\sigma_{\mathrm{K}} = \frac{\sigma_{\mathrm{K}}}{K} \times 100. \tag{6.11}$$

Substituting Eq. (6.10) into Eq. (6.11) produces

$$\%\sigma_{\mathrm{K}} = \left(\frac{2}{N_{\mathrm{PIX}}}\right)^{1/2} \times 100. \tag{6.12}$$

Note that K can be held to a 1% error when 20,000 pixels are sampled.

Example 6.1

Given the following parameters, determine the standard deviation of K:

$K = 0.2\,\mathrm{e^-/DN}$
$N_{\mathrm{PIX}} = 1000$ pixels
$S = 1000$ DN

Assume read noise is negligible. Also calculate the percent error in K.

Solution:
From Eq. (6.9),

$$\sigma_{\mathrm{K}} = \left[\frac{0.2}{1000} \times \left(\frac{1}{1000} + 2 \times 0.2\right)\right]^{1/2} = 0.00895$$

From Eq. (6.12), the percent error of $K_{\mathrm{ADC}}(\mathrm{e}^-/\mathrm{DN})$ is

$$\%\sigma_{\mathrm{K}} = \left(\frac{2}{1000}\right)^{1/2} \times 100 = 4.47\% \text{ rms.}$$

Figure 6.4 plots Eq. (6.1) [i.e., $K = S/(N^2 - R^2)$] as a function of S(DN). The data is simulated by a random number generator based on the following assumptions: 500 pixels, $R = 250$ DN, and $K = 0.2$ e$^-$/DN. Note that the variation in data points about 0.2 e$^-$/DN increases dramatically for low signal levels as the read noise becomes influential. Figure 6.5 plots σ_{K} for various noise levels, including the $R = 250$ DN assumed in Fig. 6.4. For high signal levels where read noise is not a factor, $\sigma_{\mathrm{K}} = 0.0126$ ($\%\sigma_{\mathrm{K}} = 6.3\%$). Note also from the zero read noise curve that signal level does not significantly influence e$^-$/DN measurement accuracy, as long as $1/S < 2K$ as assumed by Eq. (6.10).

Figure 6.6 shows individual PTCs for 108 pixels taken from an experimental CMOS array. Each data point plotted is based on 512 samples/pixel. Note that the read noise level for each pixel is different, a characteristic related to CMOS arrays.[5,6] The data saturates at 65,000 DN—the limit of the 16-bit analog-to-digital converter used for this measurement. Figure 6.7 plots K as a function of signal for each pixel. The results are similar to the simulation presented in Fig. 6.4, where the

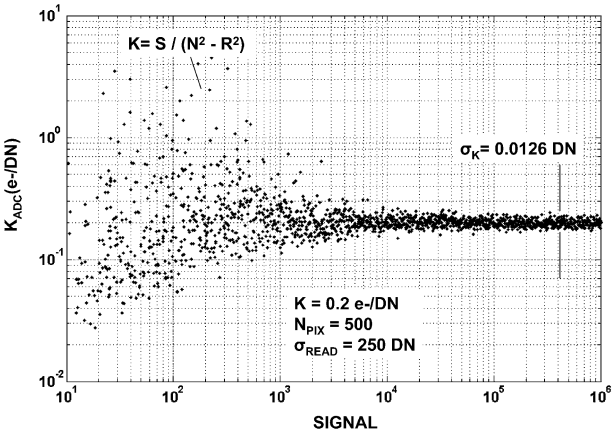

Figure 6.4 $K_{\mathrm{ADC}}(\mathrm{e}^-/\mathrm{DN})$ versus signal showing σ_{K} variation with signal.

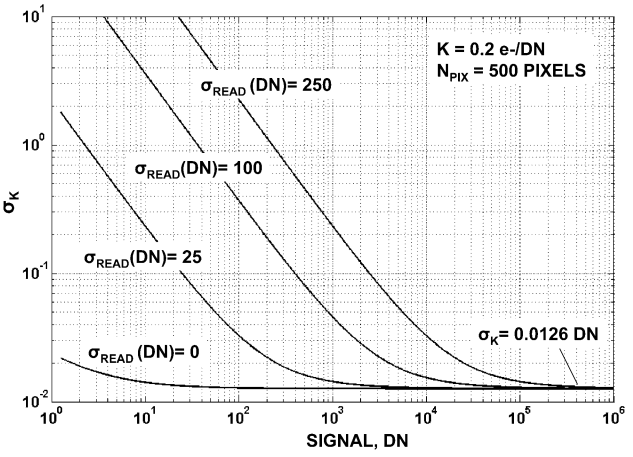

Figure 6.5 $K_{\mathrm{ADC}}(e^-/\mathrm{DN})$ standard deviation with signal and different read noise levels.

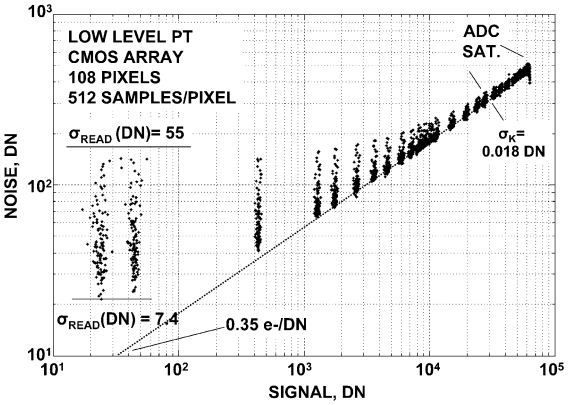

Figure 6.6 Low signal level PTCs for 108 CMOS pixels, each showing a different read noise floor.

uncertainty in K increases as the signal enters the read noise regime. Figures 6.8 and 6.9 are high-level PTCs for the same sensor after the CDS voltage gain is lowered by a factor of 10, which increases K and σ_{K} by the same factor.

Example 6.2

Determine σ_{K} and $\%\sigma_{\mathrm{K}}$ for the PTC data in Figs. 6.7 and 6.9 at a signal level of 2×10^4 DN.

Solution (Fig. 6.7):
From Eq. (6.9):

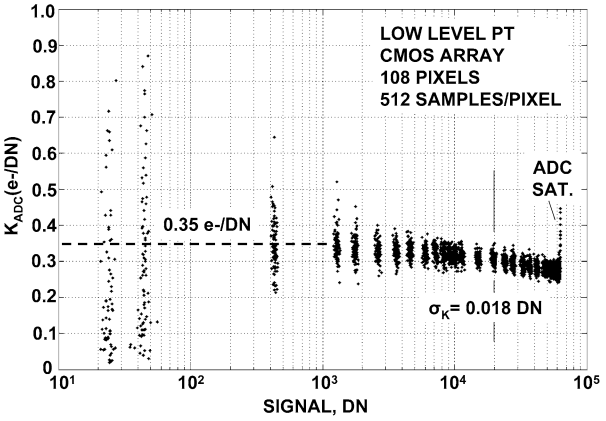

Figure 6.7 $K_{\mathrm{ADC}}(\mathrm{e}^{-}/\mathrm{DN})$ versus signal for Fig. 6.6 showing σ_{K} rms variation.

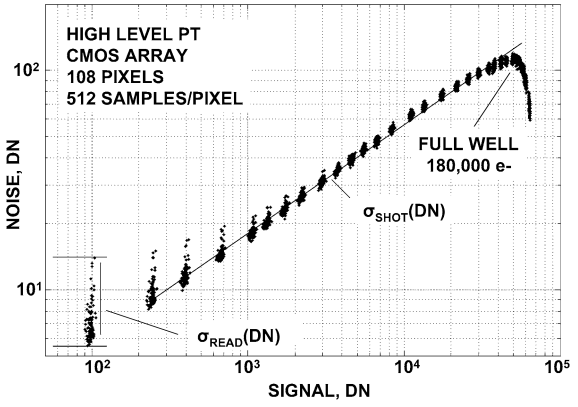

Figure 6.8 High signal level CMOS PTCs.

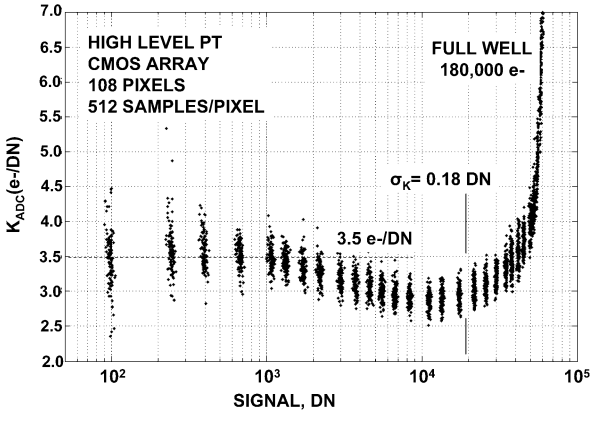

Figure 6.9 $K_{\mathrm{ADC}}(\mathrm{e}^{-}/\mathrm{DN})$ versus signal for Fig. 6.8 showing σ_{K} rms variation.

$$\sigma_K = \left(\frac{2}{512}\right)^{1/2} \times 0.3 = 0.0188 \text{ DN}$$

and [from Eq. (6.12)]

$$\%\sigma_K = \left(\frac{2}{512}\right)^{1/2} \times 100 = 6.25\% \text{ DN}.$$

Solution (Fig. 6.9):
From Eq. (6.9):

$$\sigma_K = \left(\frac{2}{512}\right)^{1/2} \times 3 = 0.188 \text{ DN}$$

and [from Eq. (6.12)]

$$\%\sigma_K = \left(\frac{2}{512}\right)^{1/2} \times 100 = 6.25\% \text{ DN}.$$

It should be mentioned that CMOS detectors exhibit pixel-to-pixel e^-/DN sensitivity variations. This noise source is a different form of FPN compared to the pixel-to-pixel charge-collection deviation. The net FPN (with the e^-/DN variation included) is given by

$$\sigma_{NET} = ({\sigma_K}^2 + {\sigma_{FPN}}^2)^{1/2}. \tag{6.13}$$

Fortunately, σ_K is usually less than σ_{FPN}, and the net FPN is still approximately 1% of the average signal level typically seen for the CCD.

Important Points

1. The measurement accuracy of e^-/DN depends on signal, read noise, and the number of pixels sampled.
2. Signal level has very little influence on e^-/DN variance. However, read noise is critical to measurement accuracy.
3. When read noise is negligible relative to shot noise, e^-/DN variance is equal to $2/N_{PIX}$.

Chapter 7
Nonlinearity

7.1 Introduction

Two fundamental classes of gain nonlinearity exist for CMOS and CCD imagers: V/V nonlinearity and V/e$^-$ nonlinearity. Ideally, V/V nonlinearity for a camera system is dominated by the pixel's source follower amplifier. Nonlinearity characteristics for the amplifier can typically be controlled to less than 1% over a sensor's dynamic range. V/e$^-$ nonlinearity is related to sense node diode capacitance, which increases as charge collects (refer to Fig. 4.3). For CCDs, the sense capacitance change is usually negligible (typically $< 0.2\%$ nonlinearity). However, for CMOS detectors, V/e$^-$ nonlinearity can be significant, exceeding 200% for some pixel architectures (e.g., refer to Sec. 7.3).

7.2 V/V Nonlinearity

Figure 7.1 shows simulated PTCs with V/V nonlinearity characteristics. Note that the shot noise curve does not follow a slope of $1/2$, indicating that K_{ADC}(e$^-$/DN)

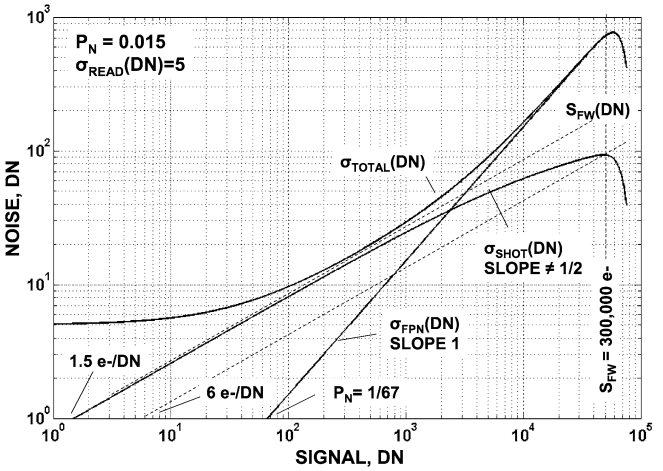

Figure 7.1 PTCs with V/V nonlinearity.

is dependent on signal level and therefore nonlinear. The sensitivity varies from 1.5 e^-/DN in the read noise regime to 6 e^-/DN at full well. Unlike shot noise, the FPN curve remains at a slope of unity because FPN and signal are both proportional to $K_{\mathrm{ADC}}(e^-/\mathrm{DN})$. However, it will be shown in Section 7.3 that the FPN slope changes when V/e^- nonlinearity is present. This characteristic helps distinguish between V/V and V/e^- nonlinearity issues.

The curve in Fig. 7.2 presents a nonlinearity plot of $K_{\mathrm{ADC}}(e^-/\mathrm{DN})$ as a function of signal for Fig. 7.1. The sensitivity varies roughly in a linear fashion from 1.5 to 6 e^-/DN. Nonlinearity is quantified from the plot through the relation

$$\mathrm{NL_K}(\%) = 100\left(\frac{K_{\mathrm{ADC}}(e^-/\mathrm{DN}) - K_{\mathrm{LOW}}(e^-/\mathrm{DN})}{K_{\mathrm{LOW}}(e^-/\mathrm{DN})}\right), \tag{7.1}$$

where $\mathrm{NL_K}(\%)$ is the nonlinearity of $K_{\mathrm{ADC}}(e^-/\mathrm{DN})$, and $K_{\mathrm{LOW}}(e^-/\mathrm{DN})$ is the ADC sensitivity at the lowest signal measured. Figure 7.3 plots $\mathrm{NL_K}(\%)$ for Fig. 7.2, showing a maximum nonlinearity of 300% at full well.

Also included in Fig. 7.2 is a "least squares curve fit" to describe $K_{\mathrm{ADC}}(e^-/\mathrm{DN})$. Figure 7.4 shows the corresponding "nonlinearity residual errors" that are used to compare data to the curve fit. The straight line fit is also used to remove V/V nonlinearity from the PTC in conjunction with the relations

$$S(\mathrm{DN})_{\mathrm{LIN}} = S(\mathrm{DN})\frac{K_{\mathrm{FIT}}(e^-/\mathrm{DN})}{K_{\mathrm{LOW}}(e^-/\mathrm{DN})} \tag{7.2}$$

and

$$\sigma_{\mathrm{SHOT\_LIN}}(\mathrm{DN}) = \sigma_{\mathrm{SHOT}}(\mathrm{DN})\frac{K_{\mathrm{FIT}}(e^-/\mathrm{DN})}{K_{\mathrm{LOW}}(e^-/\mathrm{DN})}, \tag{7.3}$$

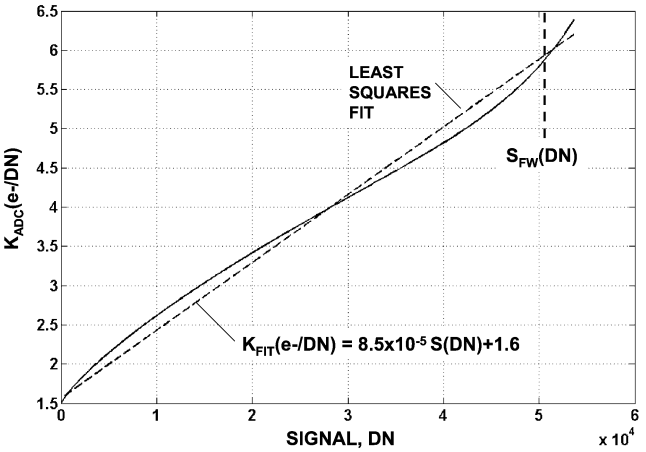

Figure 7.2 $K_{\mathrm{ADC}}(e^-/\mathrm{DN})$ versus signal with least square curve fit.

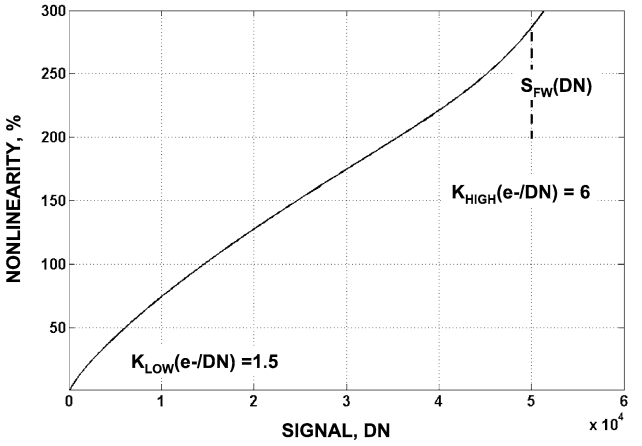

Figure 7.3 Nonlinearity plot for Fig. 7.2.

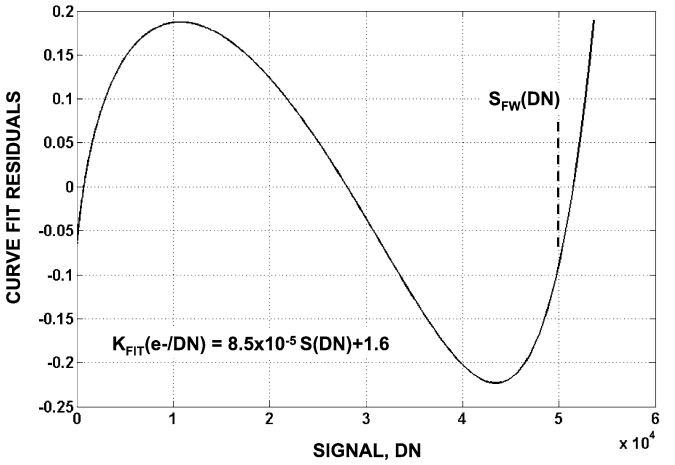

Figure 7.4 Nonlinearity residuals for least squares curve fit shown in Fig. 7.2.

where $S(\mathrm{DN})_{\mathrm{LIN}}$ and $\sigma_{\mathrm{SHOT\_LIN}}(\mathrm{DN})$ are the signal and shot noise levels after linearization, and $K_{\mathrm{FIT}}(\mathrm{e}^{-}/\mathrm{DN})$ is the ADC sensitivity from the least squares curve fit equation. $\sigma_{\mathrm{FPN}}(\mathrm{DN})$ and $\sigma_{\mathrm{TOTAL}}(\mathrm{DN})$ can be made linear in a fashion similar to that of shot noise.

Figure 7.5 shows a new PTC after linearization where the shot noise curve now exhibits an improved slope $1/2$ response (the dotted line in Fig. 7.5 represents a perfect shot noise response for comparison). $K_{\mathrm{ADC}}(\mathrm{e}^{-}/\mathrm{DN})$ remains fixed at approximately 1.5 e^{-}/DN over the sensor's dynamic range. Figure 7.6 plots the new ADC sensitivity, using linearized data through

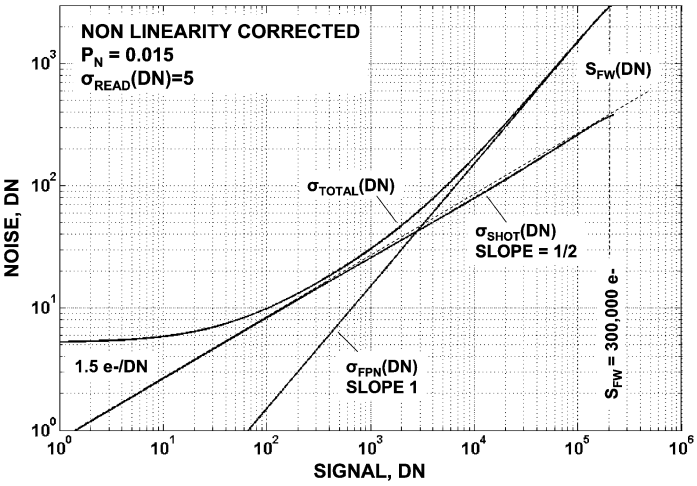

Figure 7.5 PTCs with V/V nonlinearity corrected using least squares curve fit.

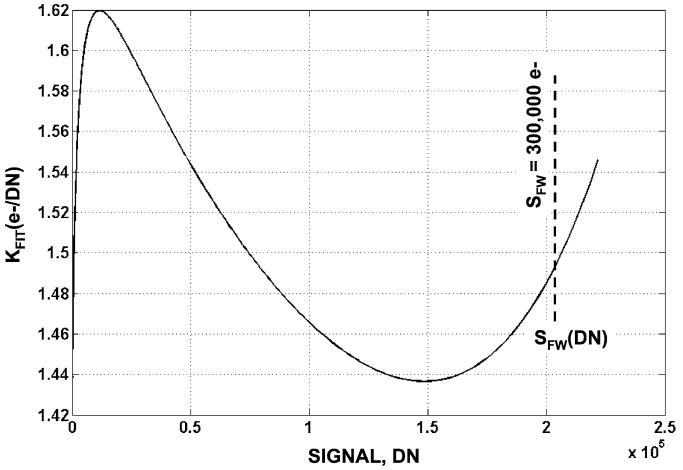

Figure 7.6 $K_{\mathrm{ADC}}(\mathrm{e}^{-}/\mathrm{DN})$ versus signal after V/V nonlinearity is corrected.

$$K_{\mathrm{FIT}}(\mathrm{e}^{-}/\mathrm{DN}) = \frac{S_{\mathrm{LIN}}(\mathrm{DN})}{\sigma_{\mathrm{SHOT\_LIN}}(\mathrm{DN})^2}. \tag{7.4}$$

Figure 7.7 shows two sets of PTCs after Fig. 7.1 is converted to electron units using $K_{\mathrm{ADC}}(\mathrm{e}^{-}/\mathrm{DN})$ and $K_{\mathrm{FIT}}(\mathrm{e}^{-}/\mathrm{DN})$. Note that the discrepancy between the two curves is small, demonstrating that the linearization process has done its job. The Δ shown in the plot represents the difference between the two curves.

It should be mentioned that the nonlinearity plot of Fig. 7.2 produces the same result as the conventional characterization method of measuring nonlinearity by graphing signal as a function of exposure time. However, the exposure period

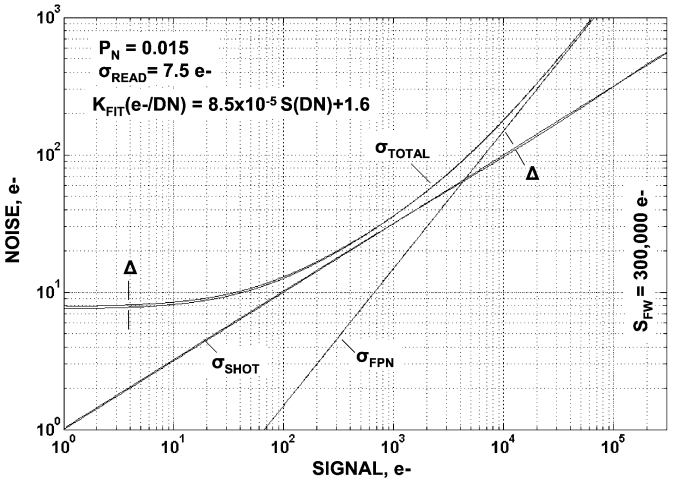

Figure 7.7 PTCs with V/V nonlinearity corrected in electron units.

must be very linear in time to evaluate sensor nonlinearities $< 1\%$. In practice, this requirement may be difficult to realize when covering a large signal dynamic range. For example, a mechanical shutter used to control exposure time usually exhibits nonlinear behavior for short exposure periods. Also, such measurements are sensitive to the stability level of the light source. Measuring nonlinearity by photon transfer through the $K_{\rm ADC}(\rm e^-/DN)$ plot is not dependent on these variables.

Example 7.1

Assume that the ADC sensitivity and signal vary as

$$K_{\rm ADC}(\rm e^-/DN) = 1.5^{(1+0.001t)}$$

and

$$S = t,$$

where t is time (sec). Plot S, $\sigma_{\rm SHOT}$, $\sigma_{\rm FPN}$, S(DN), $\sigma_{\rm SHOT}$(DN), and $\sigma_{\rm FPN}$(DN) as a function of time up to 10^4 sec. On a separate graph, generate PTCs for shot noise and FPN as a function of S(DN). Graphically validate $P_{\rm N}$ and determine the extreme values of $K_{\rm ADC}(\rm e^-/DN)$. Also, plot $K_{\rm ADC}(\rm e^-/DN)$ as functions of S and S(DN). Assume $P_{\rm N} = 0.03$.

Solution:
Figure 7.8 plots the signal and noise sources as a function of time. Figure 7.9 presents photon transfer plots of $\sigma_{\rm SHOT}$(DN) and $\sigma_{\rm FPN}$(DN) as a function of S(DN). The intercept points on the signal axis (noise $=$ 1 DN) indicates that $K_{\rm ADC}(\rm e^-/DN)$

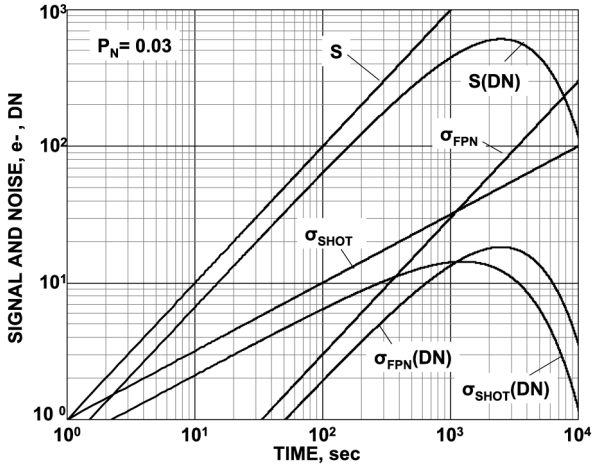

Figure 7.8 V/V nonlinearity example showing individual signal and noise plots with time in electron and DN units.

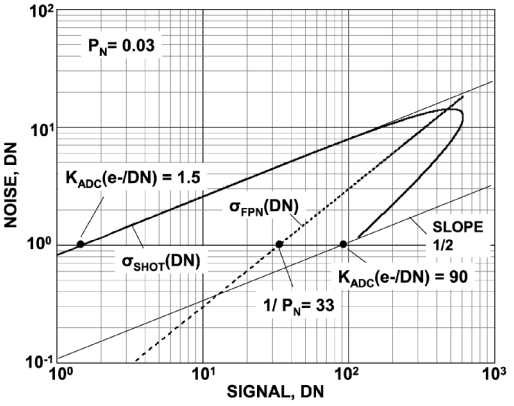

Figure 7.9 PTCs for V/V nonlinearity example showing K_{ADC}(e$^-$/DN) variation.

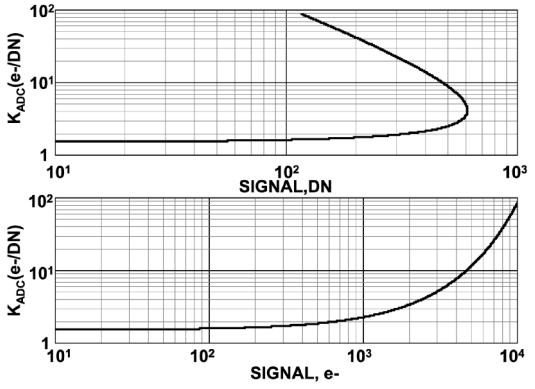

Figure 7.10 K_{ADC}(e$^-$/DN) versus signal for Fig. 7.9 in DN and electron units.

changes from 1.5 to approximately 90 e$^-$/DN. The dotted $\sigma_{\rm FPN}$(DN) curve exhibits a slope of unity with a signal intercept of $P_{\rm N} = 1/33 = 0.03$. Figure 7.10 plots $K_{\rm ADC}$(e$^-$/DN) as functions of S(DN) and S.

Figure 7.11 presents an experimental PTC generated by a CMOS charge transfer pinned photodiode imager. The data points slowly deviate from the ideal slope $1/2$ shot noise curve, which signifies that nonlinearity is present. Figure 7.12 plots $K_{\rm ADC}$(e$^-$/DN), showing a variation of 1.84 to 2.5 e$^-$/DN over the sensor's dynamic range. Figure 7.13 plots nonlinearity using Eq. (7.1) based on a reference

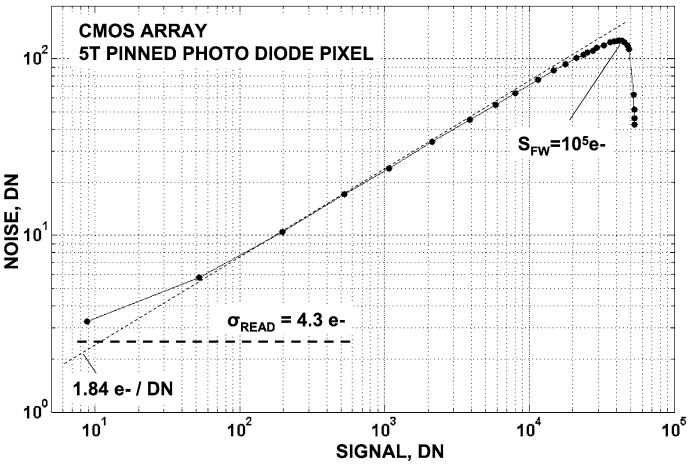

Figure 7.11 PTC generated with a CMOS array with V/V nonlinearity.

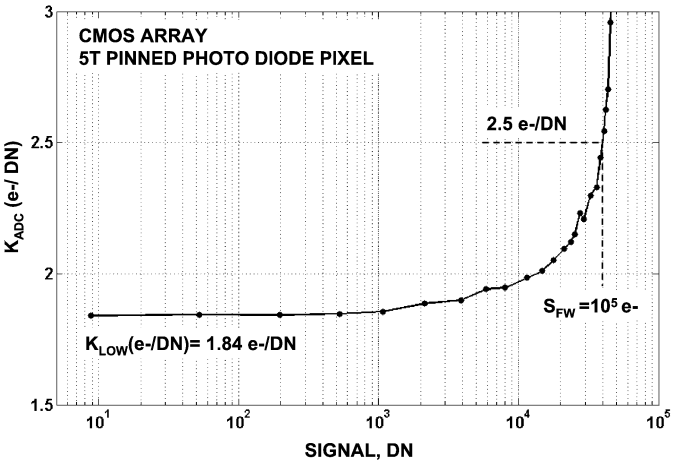

Figure 7.12 $K_{\rm ADC}$(e$^-$/DN) versus signal for Fig. 7.11.

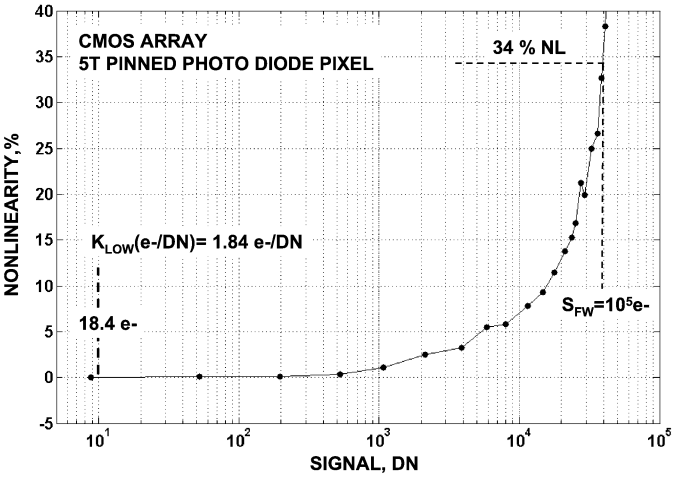

Figure 7.13 Nonlinearity plot for Fig. 7.12.

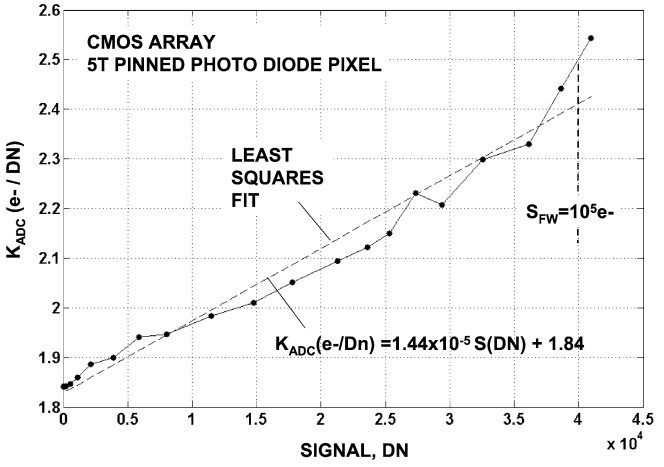

Figure 7.14 K_{ADC}(e$^-$/DN) versus signal with least squares curve fit for Fig. 7.11.

sensitivity of $K_{\mathrm{LOW}}(\mathrm{e}^-/\mathrm{DN}) = 1.84$. Figure 7.14 plots $K_{\mathrm{ADC}}(\mathrm{e}^-/\mathrm{DN})$, along with a curve fit, over the dynamic range of the sensor. Figure 7.15 shows the corresponding nonlinearity residual errors between the data and the straight line fit. Figure 7.16 plots sense node gain (A_{SN}) as a function of signal before and after the data points are linearized.

7.3 V/e$^-$ Nonlinearity

Figure 7.17 presents a photon transfer plot generated by a CMOS imager with V/e$^-$ sense node nonlinearity characteristics. V/e$^-$ nonlinearity is sometimes advanta-

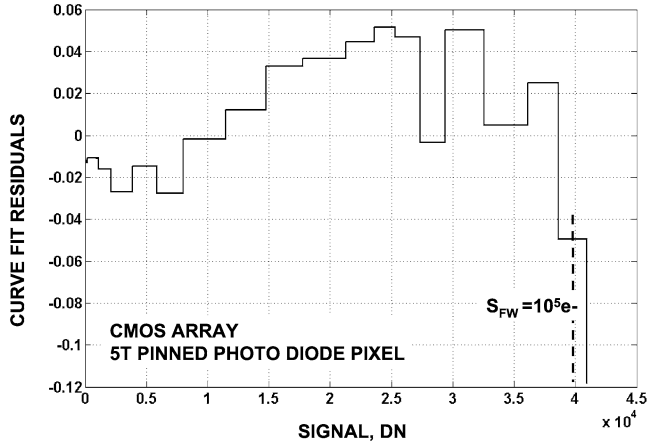

Figure 7.15 Nonlinearity residuals for least squares curve fit shown in Fig. 7.14.

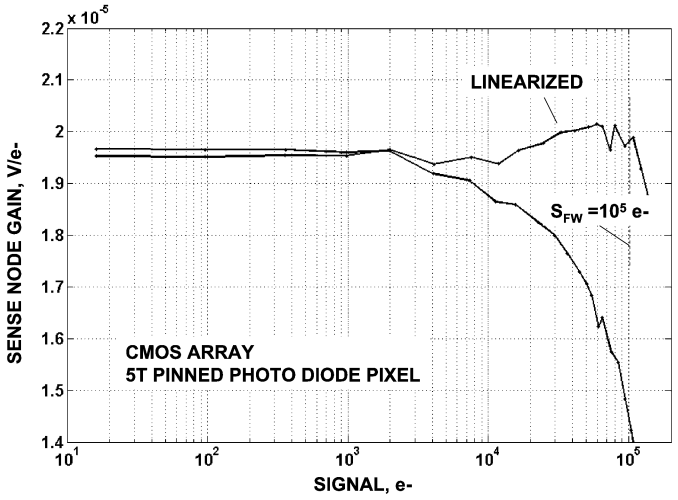

Figure 7.16 Sense node gain (V/e$^-$) for Fig. 7.15 after nonlinearity is corrected.

geous because the gain effect produces a small sense node capacitance for low read noise and a large capacitance for high full-well performance. However, the signal and noise sensitivities vary differently when V/e$^-$ nonlinearity exists. This feature is unlike linear and V/V nonlinear characteristics, whose signal and noise sensitivities are equivalent. The unique behavior associated with V/e$^-$ nonlinearity significantly complicates data reduction algorithms. For example, when converting linear or nonlinear V/V measurements from DN to electron units, the previously used simple formulas are applied:

$$S = S(\mathrm{DN})K_{\mathrm{ADC}}(\mathrm{e}^-/\mathrm{DN}) \tag{7.5}$$

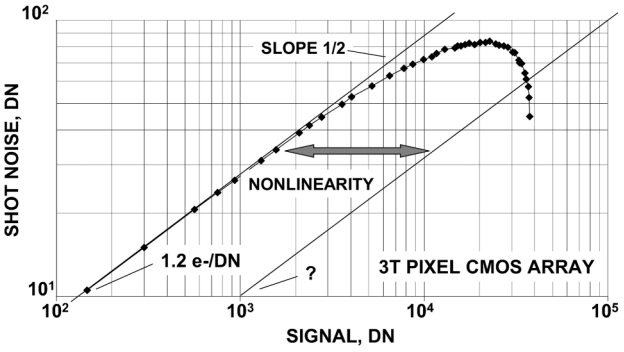

Figure 7.17 CMOS PTC showing V/e$^-$ nonlinearity.

and

$$\sigma_{\mathrm{SHOT}} = \sigma_{\mathrm{SHOT}}(\mathrm{DN})K_{\mathrm{ADC}}(\mathrm{e}^-/\mathrm{DN}). \tag{7.6}$$

However, when V/e$^-$ exists, signal and noise levels must be determined individually through

$$S = S(\mathrm{DN})S_{\mathrm{ADC}}(\mathrm{e}^-/\mathrm{DN}) \tag{7.7}$$

and

$$\sigma_{\mathrm{SHOT}} = \sigma_{\mathrm{SHOT}}(\mathrm{DN})N_{\mathrm{ADC}}(\mathrm{e}^-/\mathrm{DN}), \tag{7.8}$$

where S_{SN}(e$^-$/DN) is referred to as the ADC signal sensitivity, and N_{SN}(e$^-$/DN) is the corresponding ADC noise sensitivity.

In addition, when V/e$^-$ nonlinearity is present, CMOS and CCD performance parameters can not be found by K_{ADC}(e$^-$/DN). Instead, S_{ADC}(e$^-$/DN) is used to determine signal-related performance parameters, such as charge capacity, dark current, quantum efficiency, etc. N_{ADC}(e$^-$/DN) is employed to determine the sense node capacitance and noise related parameters, such as FPN, shot noise, etc.

It should also be pointed out that S_{SN}(e$^-$/DN) and N_{SN}(e$^-$/DN) parameters cannot be determined simply by making mean and rms DN measurements as performed before. Recall that this was the case for linear (and V/V nonlinear) analysis, where K_{ADC}(e$^-$/DN) was found through the standard PT formula S(DN)/ σ_{SHOT}(DN)^2. Fortunately, the photon transfer routine only needs to be slightly modified to measure S_{SN}(e$^-$/DN) and N_{SN}(e$^-$/DN), as discussed at the end of this section.

It is also important to note when C_{SN} is fixed or changes negligibly; K_{ADC}(e$^-$/ DN) = S_{ADC}(e$^-$/DN) = N_{ADC}(e$^-$/DN). This is typically the case when measuring small signals. On the other hand, S_{ADC}(e$^-$/DN) $< N_{\mathrm{ADC}}$(e$^-$/DN) if C_{SN} increases, and K_{ADC}(e$^-$/DN) will produce erroneous measurement results.

A fundamental analysis of the V/e$^-$ nonlinearity problem begins by evaluating the sense node signal sensitivity, $S_{\mathrm{SN}}(\mathrm{e}^-/V_{\mathrm{SN}})$, from the differential equation

$$\frac{dS}{dV_{\mathrm{SN}}} = \frac{C_{\mathrm{SN}}}{q}, \tag{7.9}$$

where C_{SN} is a function of sense node voltage, V_{SN}.

The sense node noise sensitivity, $N_{\mathrm{SN}}(\mathrm{e}^-/V_{\mathrm{SN}})$, is directly governed by the sense node capacitance through

$$N_{\mathrm{SN}}(\mathrm{e}^-/V_{\mathrm{SN}}) = \frac{C_{\mathrm{SN}}}{q}. \tag{7.10}$$

Once C_{SN} is known, $S_{\mathrm{SN}}(V_{\mathrm{SN}}/\mathrm{e}^-)$ and $N_{\mathrm{SN}}(\mathrm{e}^-/V_{\mathrm{SN}})$ are derived from the relations above. From there, other sensitivity parameters are readily determined [e.g., $S_{\mathrm{ADC}}(\mathrm{e}^-/\mathrm{DN})$ or $N_{\mathrm{ADC}}(\mathrm{e}^-/\mathrm{DN})$]. Example 7.2 demonstrates the subtle details behind Eqs. (7.9) and (7.10).

Example 7.2

The photon transfer data shown in Fig. 7.17 is described by a sense node capacitance that varies as

$$C_{\mathrm{SN}} = k1/V_{\mathrm{SN}} \quad \text{and} \quad 0.9 < V_{\mathrm{SN}} < 3.1, \tag{E7.1}$$

where $k1 = 10.909 \times 10^{-15}$.

Using this relationship, generate the following plots by assuming $V_{\mathrm{REF}} = 3.1$ V and a system gain of $A(\mathrm{DN}/V_{\mathrm{SN}}) = A_{\mathrm{SF}}A_{\mathrm{CDS}}A_{\mathrm{ADC}} = 1.76 \times 10^4$ DN/V:

1. C_{SN} versus V_{SN}
2. S and σ_{SHOT} versus V_{SN}
3. $S_{\mathrm{SN}}(\mathrm{e}^-/V_{\mathrm{SN}})$ and $N_{\mathrm{SN}}(\mathrm{e}^-/V_{\mathrm{SN}})$ versus V_{SN}
4. $S(V_{\mathrm{SN}})$ and $\sigma_{\mathrm{SHOT}}(V_{\mathrm{SN}})$ versus V_{SN}
5. $S_{\mathrm{SN}}(\mathrm{e}^-/\mathrm{DN})$, $N_{\mathrm{SN}}(\mathrm{e}^-/\mathrm{DN})$, $K_{\mathrm{ADC}}(\mathrm{e}^-/\mathrm{DN})$ versus S
6. $S_{\mathrm{SN}}(V_{\mathrm{SN}}/\mathrm{e}^-)$ and $N_{\mathrm{SN}}(V_{\mathrm{SN}}/\mathrm{e}^-)$ versus V_{SN}
7. False signal (e^-) based on $K_{\mathrm{ADC}}(\mathrm{e}^-/\mathrm{DN})$ versus true signal (e^-)
8. Nonlinearity for $S_{\mathrm{SN}}(\mathrm{e}^-/\mathrm{DN})$, $N_{\mathrm{SN}}(\mathrm{e}^-/\mathrm{DN})$, $K_{\mathrm{ADC}}(\mathrm{e}^-/\mathrm{DN})$ versus S

Solution:
From Eq. (E7.1), Fig. 7.18 plots C_{SN} as a function of V_{SN}.

The sense node is reset to $V_{\mathrm{REF}} = 3.1$ V. The signal voltage, $S(V_{\mathrm{SN}})$, causes the sense node voltage to discharge following the equation:

$$V_{\mathrm{SN}} = V_{\mathrm{REF}} - S(V_{\mathrm{SN}}). \tag{E7.2}$$

Solving the differential Eq. (7.9) yields

$$S = \frac{k1}{q}\int_{V_{\mathrm{SN}}}^{V_{\mathrm{REF}}} \frac{1}{V_{\mathrm{SN}}} dV_{\mathrm{SN}}. \tag{E7.3}$$

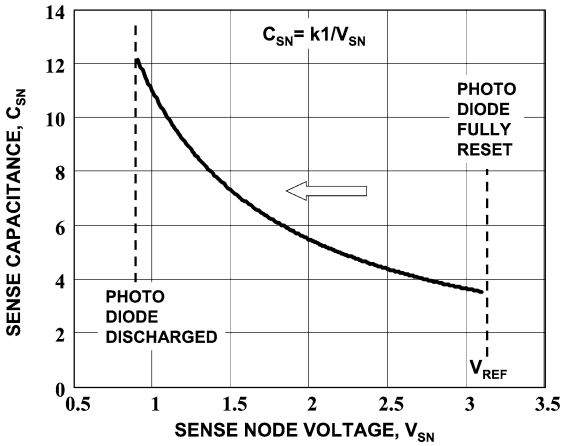

Figure 7.18 Sense node capacitance with sense node voltage.

Integrating Eq. (E7.3) produces the following:

$$S = \frac{k1}{q} \ln\left(\frac{V_{\rm REF}}{V_{\rm SN}}\right) = \frac{k1}{q} \ln\left[\frac{V_{\rm REF}}{V_{\rm REF} - S(V_{\rm SN})}\right]. \tag{E7.4}$$

The corresponding signal shot noise is

$$\sigma_{\rm SHOT} = S^{1/2} = \left\{\frac{k1}{q} \ln\left[\frac{V_{\rm REF}}{V_{\rm REF} - S(V_{\rm SN})}\right]\right\}^{1/2}. \tag{E7.5}$$

Figure 7.19 plots S and $\sigma_{\rm SHOT}$ with $V_{\rm SN}$.

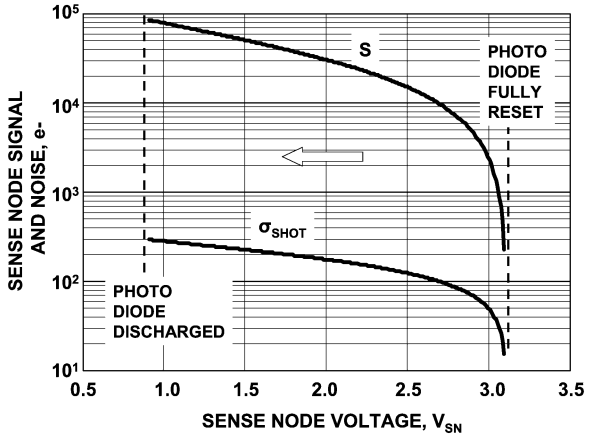

Figure 7.19 Sense node signal and noise (e^-) with sense node voltage.

The signal sensitivity at the sense node is

$$\begin{aligned} S_{\rm SN}({\rm e}^-/V_{\rm SN}) &= \frac{S}{S(V_{\rm SN})} \\ &= \frac{(k1/q)\ln\{V_{\rm REF}/[V_{\rm REF}-S(V_{\rm SN})]\}}{S(V_{\rm SN})}. \end{aligned} \tag{E7.6}$$

The noise sensitivity at the sense node is

$$N_{\rm SN}({\rm e}^-/V_{\rm SN}) = \frac{C_{\rm SN}}{q} = \frac{k1}{q[V_{\rm REF}-S(V_{\rm SN})]}. \tag{E7.7}$$

Figure 7.20 plots $S_{\rm SN}({\rm e}^-/V_{\rm SN})$ and $N_{\rm SN}({\rm e}^-/V_{\rm SN})$ as a function of $V_{\rm SN}$. Note when $S(V_{\rm SN}) = 0$, both equations become equal to $k1/(q \times V_{\rm REF}) = 2.2 \times 10^4$ e$^-$/V. Hence, $K_{\rm ADC}$(e$^-$/DN) $= S_{\rm ADC}$(e$^-$/DN) $= N_{\rm ADC}$(e$^-$/DN), indicating that V/e$^-$ nonlinearity is not significant.

The signal voltage at the sense node is

$$S(V_{\rm SN}) = \frac{S}{S_{\rm SN}({\rm e}^-/V_{\rm SN})}. \tag{E7.8}$$

The noise voltage at the sense node is

$$\sigma_{\rm SHOT}(V_{\rm SN}) = \frac{\sigma_{\rm SHOT}}{N_{\rm SN}({\rm e}^-/V_{\rm SN})} = \frac{S^{1/2}}{N_{\rm SN}({\rm e}^-/V_{\rm SN})}. \tag{E7.9}$$

Figure 7.21 plots $S(V_{\rm SN})$ and $\sigma_{\rm SHOT}(V_{\rm SN})$ as a function of $V_{\rm SN}$ by varying $S(V_{\rm SN})$ in Eqs. (E7.2) and (E7.4). It is interesting to note that the shot noise voltage actually decreases with signal at the upper end of the dynamic range. This is

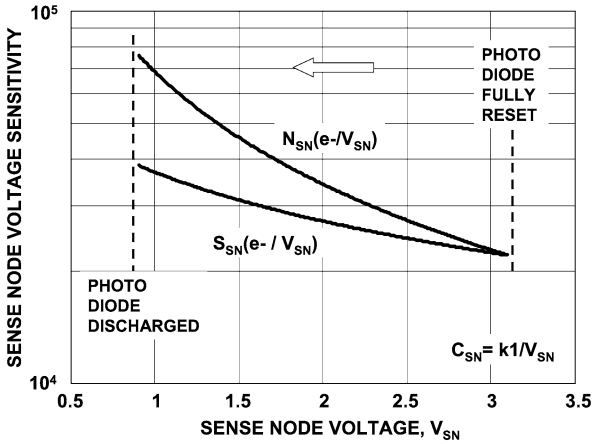

Figure 7.20 Sense node signal and noise sensitivities (e$^-/V_{\rm SN}$) with sense node voltage.

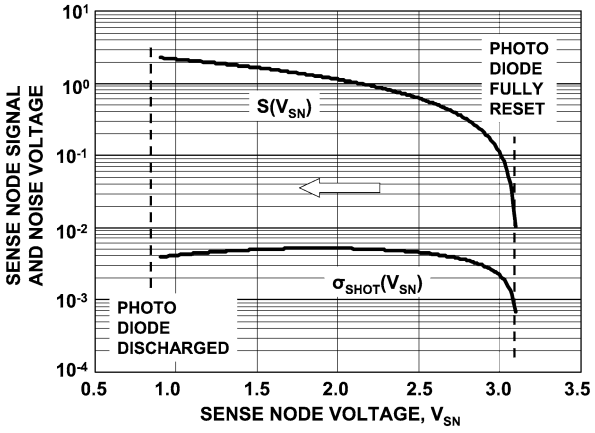

Figure 7.21 Sense node signal and noise voltage with sense node voltage.

because the noise gain (V/e$^-$) is decreasing faster than the signal gain (V/e$^-$). The response is a unique characteristic associated with sense node V/e$^-$ nonlinearity.

The ADC signal sensitivity is

$$S_{\mathrm{ADC}}(\mathrm{e}^-/\mathrm{DN}) = \frac{S_{\mathrm{SN}}(\mathrm{e}^-/V_{\mathrm{SN}})}{A(\mathrm{DN}/V_{\mathrm{SN}})}. \tag{E7.10}$$

The ADC noise sensitivity is

$$N_{\mathrm{SN}}(\mathrm{e}^-/\mathrm{DN}) = \frac{N_{\mathrm{SN}}(\mathrm{e}^-/V_{\mathrm{SN}})}{A(\mathrm{DN}/V_{\mathrm{SN}})}, \tag{E7.11}$$

where $A(\mathrm{DN}/V_{\mathrm{SN}}) = A_{\mathrm{SF}}A_{\mathrm{CDS}}A_{\mathrm{ADC}}$. Figure 7.22 plots the ADC signal and noise sensitivities as a function signal, S.

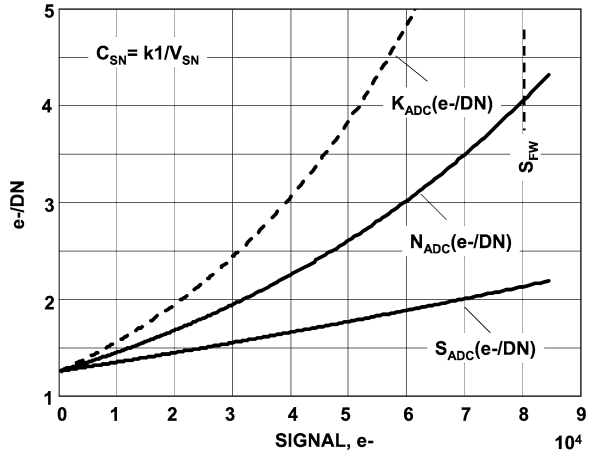

Figure 7.22 ADC sensitivities [S_{ADC}(e$^-$/DN), N_{ADC}(e$^-$/DN), K_{ADC}(e$^-$/DN)] with signal (e$^-$).

When the reciprocals are taken, the sensitivities produce the signal and noise sense node gains. From Eqs. (E7.6) and (E7.7), the node gains, respectively, are

$$S_{\mathrm{SN}}(V_{\mathrm{SN}}/\mathrm{e}^-) = \frac{S(V_{\mathrm{SN}})}{(k1/q)\ln\{V_{\mathrm{REF}}/[V_{\mathrm{REF}} - S(V_{\mathrm{SN}})]\}} \tag{E7.12}$$

and

$$N_{\mathrm{SN}}(V_{\mathrm{SN}}/\mathrm{e}^-) = \frac{q[V_{\mathrm{REF}} - S(V_{\mathrm{SN}})]}{k1}. \tag{E7.13}$$

They are plotted in Fig. 7.23 in μV/e$^-$. Note that when $S(V_{\mathrm{SN}}) = 0$, both equations become $q \times V_{\mathrm{REF}}/k1 = 45 \times 10^{-6}$ V/e$^-$.

S(DN) and σ_{SHOT}(DN) are given as

$$S(\mathrm{DN}) = A_{\mathrm{SF}}A_{\mathrm{CDS}}A_{\mathrm{ADC}}S(V_{\mathrm{SN}}) \tag{E7.14}$$

and

$$\sigma_{\mathrm{SHOT}}(\mathrm{DN}) = A_{\mathrm{SF}}A_{\mathrm{CDS}}A_{\mathrm{ADC}}\sigma_{\mathrm{SHOT}}(V_{\mathrm{SN}}). \tag{E7.15}$$

The linear (and nonlinear V/V) ADC sensitivity is

$$K_{\mathrm{ADC}}(\mathrm{e}^-/\mathrm{DN}) = \frac{S(\mathrm{DN})}{\sigma_{\mathrm{SHOT}}(\mathrm{DN})^2}. \tag{E7.16}$$

The false signal and true signal are given as

$$S_{\mathrm{FALSE}} = S(\mathrm{DN})K_{\mathrm{ADC}}(\mathrm{e}^-/\mathrm{DN}) \tag{E7.17}$$

and

$$S_{\mathrm{TRUE}} = S(\mathrm{DN})S_{\mathrm{ADC}}(\mathrm{e}^-/\mathrm{DN}). \tag{E7.18}$$

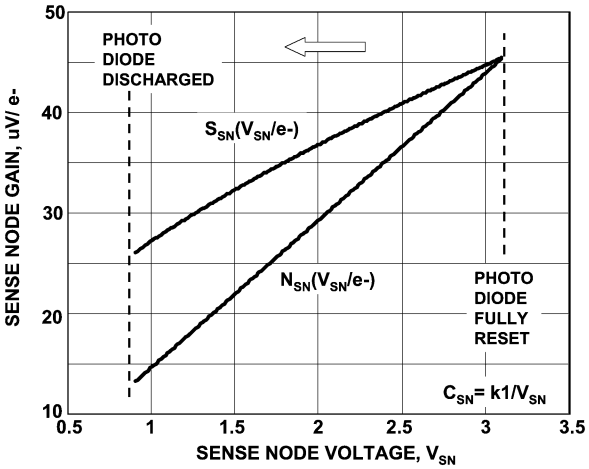

Figure 7.23 Signal and noise sense node gains ($V_{\mathrm{SN}}/\mathrm{e}^-$) with sense node voltage.

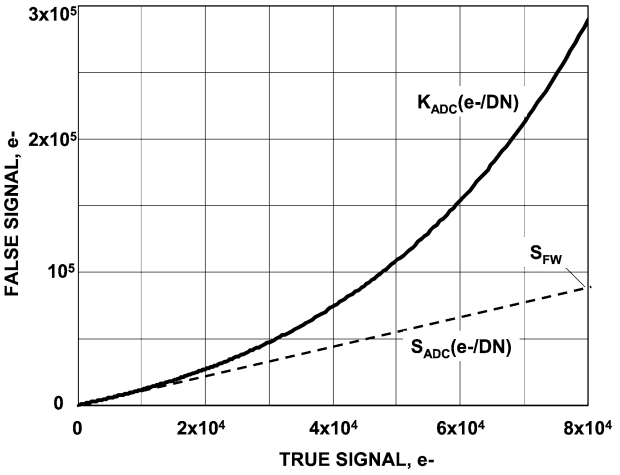

Figure 7.24 False signal based on $K_{\mathrm{ADC}}(\mathrm{e}^-/\mathrm{DN})$ versus true signal based on $S_{\mathrm{ADC}}(\mathrm{e}^-/\mathrm{DN})$.

Figure 7.24 plots the false signal as a function of the true signal. Note for signal levels less than 2×10^4 e^-, both measurements are in fair agreement. The false signal results in an overestimation of charge capacity. The true full well for the sensor is approximately 80,000 e^-, whereas the false measurement, based on $K_{\mathrm{ADC}}(\mathrm{e}^-/\mathrm{DN})$, implies a charge capacity of almost 300,000 e^-.

From Eq. (7.1), the nonlinearities for the three sensitivities are

$$\mathrm{NL_K}(\%) = 100\left[\frac{K_{\mathrm{ADC}}(\mathrm{e}^-/\mathrm{DN}) - K_{\mathrm{LOW}}(\mathrm{e}^-/\mathrm{DN})}{K_{\mathrm{LOW}}(\mathrm{e}^-/\mathrm{DN})}\right], \tag{E7.19}$$

$$\mathrm{NL_S}(\%) = 100\left[\frac{S_{\mathrm{ADC}}(\mathrm{e}^-/\mathrm{DN}) - S_{\mathrm{LOW}}(\mathrm{e}^-/\mathrm{DN})}{S_{\mathrm{LOW}}(\mathrm{e}^-/\mathrm{DN})}\right], \tag{E7.20}$$

and

$$\mathrm{NL_N}(\%) = 100\left[\frac{N_{\mathrm{ADC}}(\mathrm{e}^-/\mathrm{DN}) - N_{\mathrm{LOW}}(\mathrm{e}^-/\mathrm{DN})}{N_{\mathrm{LOW}}(\mathrm{e}^-/\mathrm{DN})}\right]. \tag{E7.21}$$

The above three equations are plotted in Fig. 7.25 as a function of signal. The nonlinearity is 70% and 210% for $S_{\mathrm{ADC}}(\mathrm{e}^-/\mathrm{DN})$ and $N_{\mathrm{ADC}}(\mathrm{e}^-/\mathrm{DN})$, respectively, at full well. The false nonlinearity for $K_{\mathrm{ADC}}(\mathrm{e}^-/\mathrm{DN})$ is 500%.

It should be mentioned that the shot noise level calculated from Eq. (7.8) is at a specific average signal, S(DN). The sense node capacitance is assumed to be fixed at that level for the noise calculation. In reality, noise excursions about S(DN) also cause the sense node capacitance to change slightly. This effect will in turn produce a measured noise that is slightly different from the calculated noise. Example 7.3

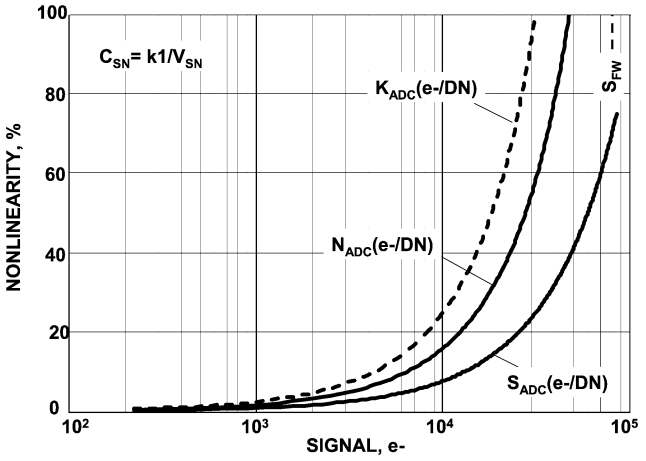

Figure 7.25 Nonlinearity for $S_{\mathrm{ADC}}(\mathrm{e}^-/\mathrm{DN})$, $N_{\mathrm{ADC}}(\mathrm{e}^-/\mathrm{DN})$, $K_{\mathrm{ADC}}(\mathrm{e}^-/\mathrm{DN})$.

will show that the error is negligible, even for noise levels much greater than shot noise and FPN.

Example 7.3

Assume a sense node noise modulation level of $\sigma_{\mathrm{NOISE}}(V_{\mathrm{SN}}) = 0.265$ V for a corresponding signal voltage of $S(V_{\mathrm{SN}}) = 1.5$ V, and assume $A(\mathrm{DN}/V_{\mathrm{SN}}) = 1.76 \times 10^4$ and $V_{\mathrm{REF}} = 3.1$ V. Then, use the parameters and equations derived in Example 7.2 to calculate the following:

1. S
2. $S_{\mathrm{SN}}(\mathrm{e}^-/V_{\mathrm{SN}})$ and $N_{\mathrm{SN}}(\mathrm{e}^-/V_{\mathrm{SN}})$
3. $\sigma_{\mathrm{NOISE}}(V_{\mathrm{SN}})$
4. $S_{\mathrm{ADC}}(\mathrm{e}^-/\mathrm{DN})$ and $N_{\mathrm{SN}}(\mathrm{e}^-/\mathrm{DN})$
5. $S(\mathrm{DN})$ and $\sigma_{\mathrm{NOISE}}(\mathrm{DN})$

Compare the calculated DN noise results to a random number simulator where the sense node capacitance is allowed to vary with the noise modulation.

Solution:
From Eq. (E7.4), the signal on the sense node is

$$S = \frac{k1}{q} \ln\left[\frac{V_{\mathrm{REF}}}{V_{\mathrm{REF}} - S(V_{\mathrm{N}})}\right],$$

and

$$S = \frac{10.909 \times 10^{-15}}{1.6 \times 10^{-19}} \times \ln\left(\frac{3.1}{3.1 - 1.5}\right) = 45{,}095\ \mathrm{e}^-.$$

From Eq. (E7.6), the sense node signal sensitivity is

$$S_{\mathrm{SN}}(\mathrm{e}^-/V_{\mathrm{SN}}) = \frac{S}{S(V_{\mathrm{SN}})} = \frac{45{,}095}{1.5} = 30{,}063.$$

From Eq. (E7.7), the sense node noise sensitivity is

$$N_{\mathrm{SN}}(\mathrm{e}^-/V_{\mathrm{SN}}) = \frac{C_{\mathrm{SN}}}{q} = \frac{k1}{q \times [V_{\mathrm{REF}} - S(V_{\mathrm{SN}})]},$$

$$N_{\mathrm{SN}}(\mathrm{e}^-/V_{\mathrm{SN}}) = \frac{10.909 \times 10^{-15}}{(3.1 - 1.5) \times (1.6 \times 10^{-19})} = 42{,}613.$$

From Eq. (E7.10) and (E7.11), the sense node noise is

$$\begin{aligned} \sigma_{\mathrm{NOISE}} &= \sigma_{\mathrm{NOISE}}(V_{\mathrm{SN}}) \times N_{\mathrm{SN}}(\mathrm{e}^-/V_{\mathrm{SN}}) \\ &= 0.265 \times 42{,}613 = 1.129 \times 10^4 \ \mathrm{e}^- \text{ rms.} \end{aligned}$$

The ADC signal and noise sensitivities are

$$S_{\mathrm{ADC}}(\mathrm{e}^-/\mathrm{DN}) = \frac{S_{\mathrm{SN}}(\mathrm{e}^-/V_{\mathrm{SN}})}{A(\mathrm{DN}/V_{\mathrm{SN}})} = \frac{30{,}063}{1.76 \times 10^4} = 1.71 \ \mathrm{e}^-/\mathrm{DN}$$

and

$$N_{\mathrm{ADC}}(\mathrm{e}^-/\mathrm{DN}) = \frac{N_{\mathrm{SN}}(\mathrm{e}^-/V_{\mathrm{SN}})}{A(\mathrm{DN}/V_{\mathrm{SN}})} = \frac{42{,}613}{1.76 \times 10^4} = 2.42 \ \mathrm{e}^-/\mathrm{DN}.$$

The ADC signal noise and shot noise are

$$S(\mathrm{DN}) = \frac{S}{S_{\mathrm{ADC}}(\mathrm{e}^-/\mathrm{DN})} = \frac{45{,}095}{1.71} = 26{,}400$$

and

$$\sigma_{\mathrm{NOISE}}(\mathrm{DN}) = \frac{\sigma_{\mathrm{NOISE}}}{N_{\mathrm{ADC}}(\mathrm{e}^-/\mathrm{DN})} = \frac{1.129 \times 10^4}{2.42} = 4666.$$

Figure 7.26(a) presents a noise histogram for a sense capacitance that is allowed to vary by noise modulation. Note that the Gaussian distribution is skewed because of a changing sense capacitance. This output represents a measured result. The Fig. 7.26(b) histogram assumes that the noise excursions do not influence the sense capacitance and therefore exhibits a symmetrical response. This output variance represents a calculated result. Note that the calculated and simulated standard deviations are in agreement [i.e., approximately $\sigma_{\mathrm{NOISE}}(\mathrm{DN}) = 4670$].

Although the shapes of the histograms in Fig. 7.26 are different, their standard deviations are nearly identical, showing very little error between calculated and measured results (4672 DN versus 4771 DN, respectively). The error is even

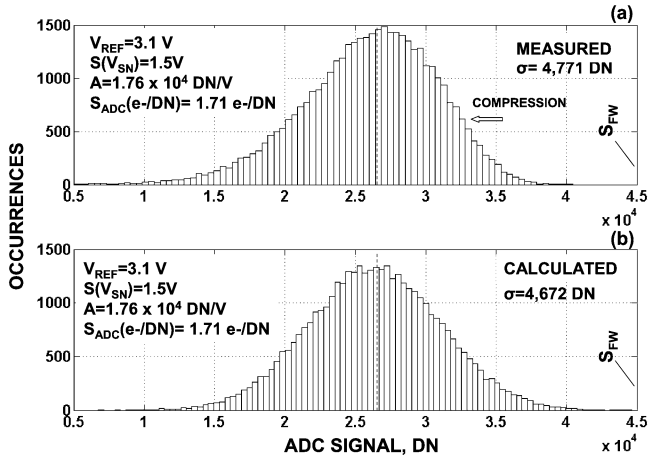

Figure 7.26 Comparison of measured and calculated shot noise levels.

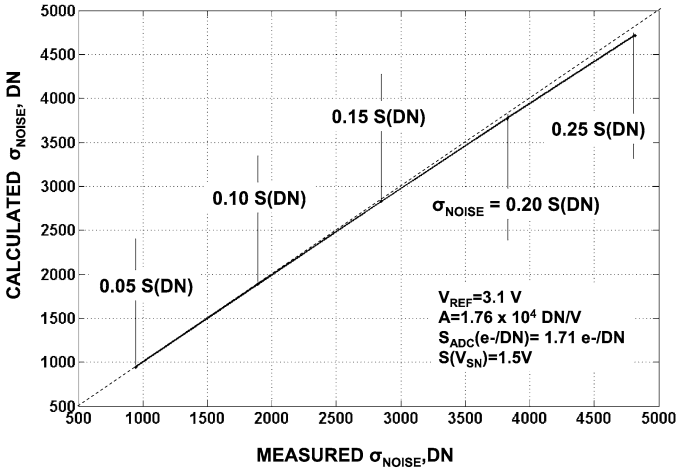

Figure 7.27 Comparison of calculated versus measured noise with signal.

considerably smaller for shot and FPN compared to the noise level analyzed here. For example, the shot noise is only 87.7 DN for a sense node signal of 1.5 V. Figure 7.27 plots the calculated versus the measured noise at the same sense node signal of 1.5 V.

Photon transfer is employed to differentiate between V/V and V/e^- nonlinearity problems. For example, Figs. 7.28 and 7.29 are PTCs that plot shot noise and FPN on log and linear scales. For the log plot, the shot noise curve does not follow the slope $1/2$ line, which is a sign that either V/V and/or V/e^- nonlinearity exists.

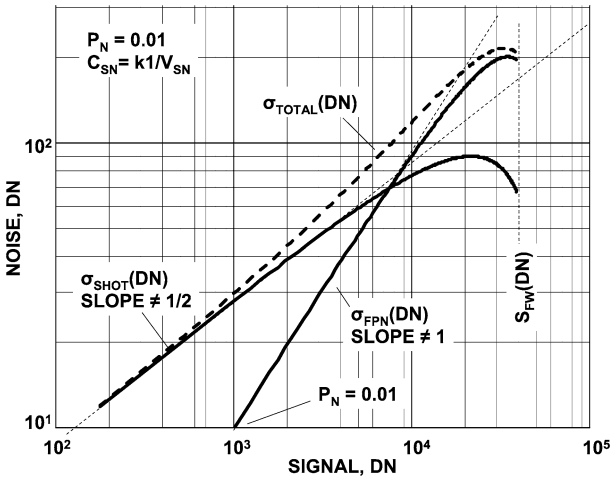

Figure 7.28 PTCs showing that FPN does not follow a slope 1 curve when V/e$^-$ is present.

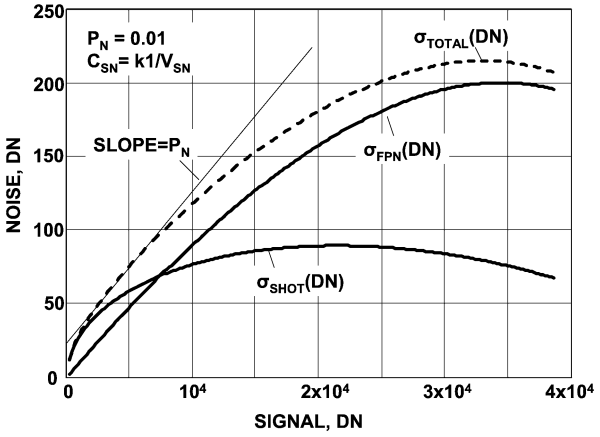

Figure 7.29 Linear PTCs for Fig. 28.

However, also note that FPN does not follow the slope 1 curve, which indicates that V/e$^-$ is definitely present (recall from Fig. 7.1 that FPN follows a unity slope when V/V nonlinearity exists). Therefore, the onset of V/e$^-$ nonlinearity takes place when FPN deviates from the slope 1 curve.

V/V and V/e$^-$ nonlinearity can also be distinguished by plotting $S_{\rm SN}$(e$^-$/DN) and $N_{\rm SN}$(e$^-$/DN) with signal. For example, Fig. 7.30 shows such a plot generated by a CMOS imager with both V/V and V/e$^-$ nonlinearity issues. Note that the signal and noise sensitivities initially change together for low signal levels, indicating that V/V nonlinearity is present. However, at a signal level of 15,000 DN (56,000 e$^-$), the two parameters separate, signifying that V/e$^-$ nonlinearity is also at play.

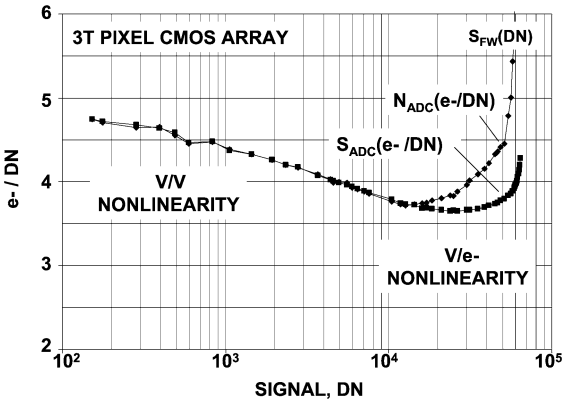

Figure 7.30 CMOS array with both V/e$^-$ and V/V nonlinearity.

The PTC shot noise curve shown in Fig. 7.28 can be made linear by the relations

$$S(\text{DN})_{\text{LIN}} = S(\text{DN})\frac{S_{\text{FIT}}(\text{e}^-/\text{DN})}{S_{\text{LOW}}(\text{e}^-/\text{DN})} \tag{7.11}$$

and

$$\sigma_{\text{SHOT\_LIN}}(\text{DN}) = \sigma_{\text{SHOT}}(\text{DN})\frac{N_{\text{FIT}}(\text{e}^-/\text{DN})}{N_{\text{LOW}}(\text{e}^-/\text{DN})}, \tag{7.12}$$

where $S(\text{DN})_{\text{LIN}}$ and $\sigma_{\text{SHOT\_LIN}}(\text{DN})$ are the signal and shot noise levels after linearization, and $S_{\text{FIT}}(\text{e}^-/\text{DN})$ and $N_{\text{FIT}}(\text{e}^-/\text{DN})$ are the ADC signal and noise sensitivities from a curve fit to $S_{\text{ADC}}(\text{e}^-/\text{DN})$ and $N_{\text{ADC}}(\text{e}^-/\text{DN})$ data. $\sigma_{\text{FPN}}(\text{DN})$ and $\sigma_{\text{TOTAL}}(\text{DN})$ are made linear in a similar fashion as shot noise. Note that for low signal levels,

$$S_{\text{LOW}}(\text{e}^-/\text{DN}) = N_{\text{LOW}}(\text{e}^-/\text{DN}) = K_{\text{LOW}}(\text{e}^-/\text{DN}). \tag{7.13}$$

Figure 7.31 shows PTCs after Fig. 7.28 is made linear using Eqs. (7.11) and (7.12). Absolute linearization is shown in Fig. 7.32, where the DN units in Fig. 7.28 have been converted to electron units, using $S_{\text{ADC}}(\text{e}^-/\text{DN})$ and $N_{\text{ADC}}(\text{e}^-/\text{DN})$ directly.

As a side note, when V/e$^-$ is present it is more difficult to determine the FPN nonuniformity factor, P_{N}, from the total noise [$\sigma_{\text{TOTAL}}(\text{DN})$] curve. The problem is demonstrated in Figs. 7.28 and 7.29. However, by converting DN data to electron units [using Eqs. (7.7) and (7.8)], the data are forced into a slope 1 curve (as shown in Fig. 7.32). The FPN and the shot noise curves exhibit slopes of 1 and $1/2$ up to full well without nonlinearity. The FPN noise factor, P_{N}, can then be determined from the total noise curve, which is $P_{\text{N}} = 0.01$ in this case.

Fortunately, the photon transfer technique discussed for linear and V/V nonlinear systems only needs to be slightly modified to deal with V/e$^-$ nonlinearity and experimentally determine $S_{\text{ADC}}(\text{e}^-/\text{DN})$ and $N_{\text{ADC}}(\text{e}^-/\text{DN})$ in a straightforward

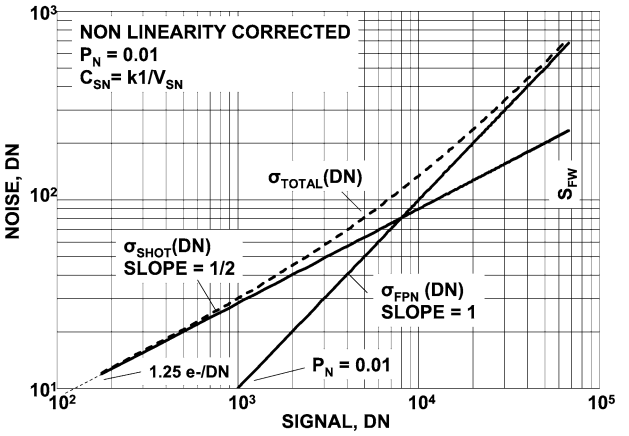

Figure 7.31 V/e$^-$ nonlinearity corrected for Fig. 7.17 in DN units.

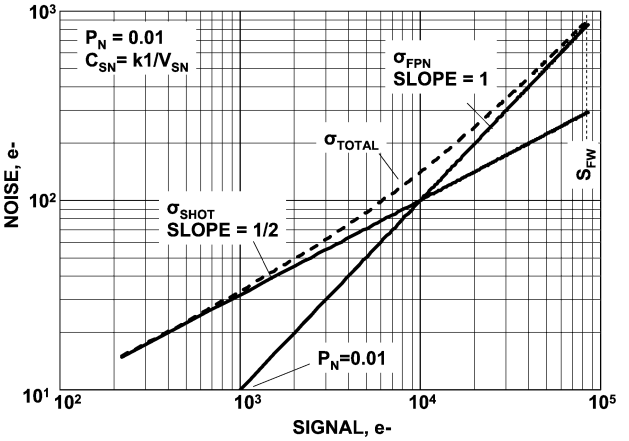

Figure 7.32 V/e$^-$ nonlinearity corrected for Fig. 7.31 in electron units.

fashion. First, S is found at a low S(DN) level using the traditional photon transfer relation [i.e., $K_{\mathrm{ADC}}(\mathrm{e}^-/\mathrm{DN}) = \mathrm{S(DN)}/\sigma^2_{\mathrm{SHOT}}(\mathrm{DN})$] and Eq. (7.5). This can be assumed because $K_{\mathrm{ADC}}(\mathrm{e}^-/\mathrm{DN}) = S_{\mathrm{ADC}}(\mathrm{e}^-/\mathrm{DN})$ at low signal levels. As C_{SN} begins to vary for higher signal levels, the light level (or exposure time) is precisely tracked. This permits one to also follow S because the number of electrons generated is proportional to the relative light level measured. The data collected for S and S(DN) give the signal sensitivity as a function of signal for all light levels measured through

$$S_{\mathrm{ADC}}(\mathrm{e}^-/\mathrm{DN}) = \frac{S}{S(\mathrm{DN})}. \tag{7.14}$$

After S is known, $N_{\mathrm{ADC}}(\mathrm{e}^-/\mathrm{DN})$ is readily determined by measuring $\sigma_{\mathrm{SHOT}}(\mathrm{DN})$ and using the relation

$$N_{\mathrm{ADC}}(\mathrm{e}^-/\mathrm{DN}) = \frac{S^{1/2}}{\sigma_{\mathrm{SHOT}}(\mathrm{DN})}. \tag{7.15}$$

The sense node signal and noise sensitivities are found through

$$S_{\mathrm{SN}}(\mathrm{e}^-/V_{\mathrm{SN}}) = S_{\mathrm{ADC}}(\mathrm{e}^-/\mathrm{DN}) A_{\mathrm{SF}} A_{\mathrm{CDS}} A_{\mathrm{ADC}} \tag{7.16}$$

and

$$N_{\mathrm{SN}}(\mathrm{e}^-/V_{\mathrm{SN}}) = N_{\mathrm{ADC}}(\mathrm{e}^-/\mathrm{DN}) A_{\mathrm{SF}} A_{\mathrm{CDS}} A_{\mathrm{ADC}}. \tag{7.17}$$

Once $N_{\mathrm{SN}}(\mathrm{e}^-/V_{\mathrm{SN}})$ is known, the sense node capacitance is determined through Eq. (7.10), i.e.,

$$C_{\mathrm{SN}} = qN_{\mathrm{SN}}(\mathrm{e}^-/V_{\mathrm{SN}}). \tag{7.18}$$

Appendix A provides a step-by-step procedure that uses experimental data to generate PTCs and related data products for a camera system that exhibits V/e$^-$ nonlinearity.

Important Points

1. Two fundamental classes of gain nonlinearity exist for CMOS and CCD imagers: V/V nonlinearity and V/e$^-$ nonlinearity.
2. The $K(\mathrm{e}^-/\mathrm{DN})$ nonlinearity plot is insensitive to exposure nonlinearity and light source instability.
3. Nonlinear PTCs can be made linear through e$^-$/DN.
4. Absolute linearization is achieved by converting DN units to electron units.
5. V/V nonlinearity influences the PTC shot noise curve, whereas the FPN curve is not affected. Shot noise and FPN curves are both influenced when V/e$^-$ nonlinearity exists.
6. Conventional linear or V/V nonlinear photon transfer analysis is not applicable when V/e$^-$ nonlinearity is present.
7. Signal and noise sensitivity are equal when V/V nonlinearity is present but not equal when V/e$^-$ exists.

Chapter 8
Flat Fielding

8.1 Theory

Fixed pattern noise is removed from images by a technique called *flat fielding*, where a computer adjusts pixel sensitivities to be equal. Fixed pattern noise severely limits S/N performance for CCD and CMOS imagers, which will be discussed in Chapter 10. Fortunately, simple computer algorithms can remove FPN and achieve the shot noise limit, thereby significantly improving S/N performance. The image processing routine is based on the following linear equation:

$$S_{i\mathrm{COR}} = \mu_{\mathrm{FF}} \frac{S_{i\mathrm{RAW}}}{S_{i\mathrm{FF}}}, \tag{8.1}$$

where $\mathrm{S}_{i\mathrm{COR}}$ is the signal level of the corrected ith pixel without FPN (e^-), $S_{i\mathrm{RAW}}$ is the signal level of the ith raw uncorrected pixel (e^-), $S_{i\mathrm{FF}}$ is the signal level of the ith flat-field pixel used to remove FPN (e^-), and μ_{FF} is the average flat-field signal level (e^-). Equation (8.1) also can be applied directly to DN camera units as

$$S_{i\mathrm{COR}}(\mathrm{DN}) = \mu_{\mathrm{FF}}(\mathrm{DN}) \frac{S_{i\mathrm{RAW}}(\mathrm{DN})}{S_{i\mathrm{FF}}(\mathrm{DN})}. \tag{8.2}$$

For PT work, it should be mentioned that flat fielding can be substituted for the frame differencing technique illustrated in Fig. 5.3 to remove FPN. In doing so, the number of frames required to generate PTCs is reduced, and the flat-fielding process is verified for theoretical shot noise limited performance.

The flat-fielding technique demonstrated in Fig. 8.1 shows two raw sinusoidal video traces that are FPN limited (labeled as S_{RAW}). Also presented is a flat-field trace used to remove FPN (labeled as S_{FF}). The solid dark curves shown are the corrected traces after the raw traces are divided (pixel-by-pixel) by the flat-field level and the result multiplied by μ_{FF} according to Eq. (8.1). Note that S/N performance improves significantly after flat fielding. Figure 8.2 presents images for the lowest-contrast sinusoidal shown in Fig. 8.1 before and after flat fielding is performed. The improvement in image quality is obvious.

After flat fielding is performed, the corrected image contains "remnant shot noise" from the flat field itself. Ideally, only shot noise from the raw signal should

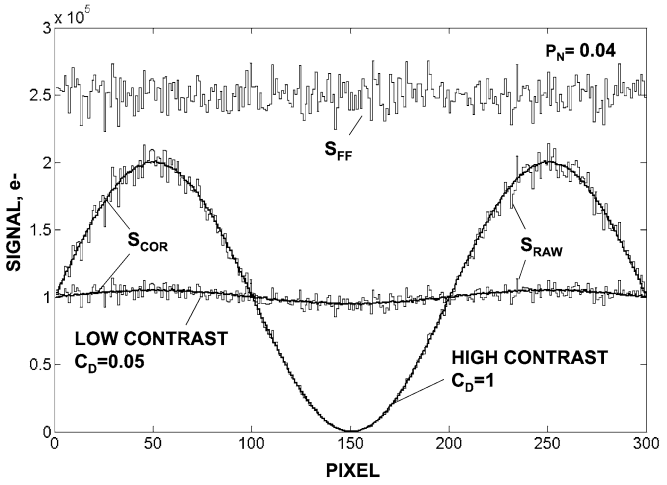

Figure 8.1 High- and low-contrast sinusoidal responses before and after flat fielding.

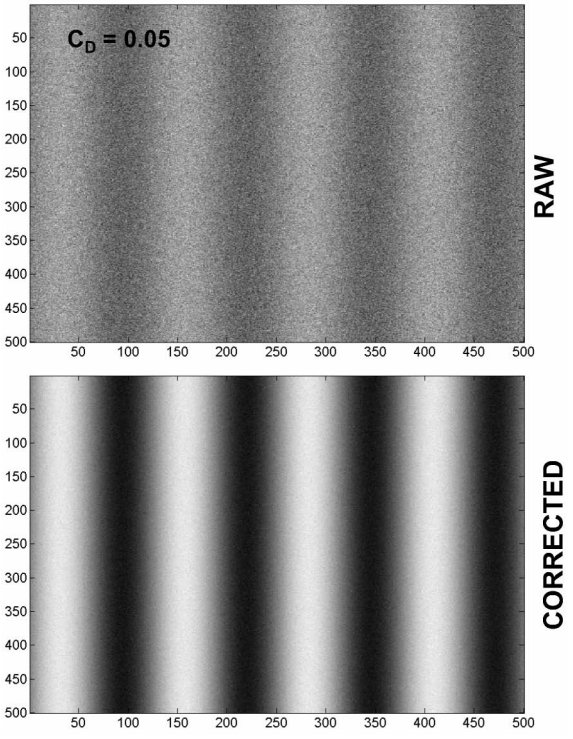

Figure 8.2 Images for Fig. 8.1 before and after flat fielding for the low-contrast sinusoid.

be present. The amount of noise contained in the corrected image can be found by the propagation of errors formula when applied to Eq. (8.1) as follows:

$$\sigma_{\mathrm{COR}}^2 = \left[\frac{\partial S_{\mathrm{COR}}}{\partial S_{\mathrm{FF}}}\right]^2 \sigma_{\mathrm{SHOT\_FF}}^2 + \left[\frac{\partial S_{\mathrm{COR}}}{\partial S_{\mathrm{RAW}}}\right]^2 \sigma_{\mathrm{SHOT\_RAW}}^2 + \sigma_{\mathrm{READ}}^2, \quad (8.3)$$

where σ_{COR} is the noise of the corrected image, and $\sigma_{\mathrm{SHOT\_FF}}$ and $\sigma_{\mathrm{SHOT\_RAW}}$ are the shot noise levels of the flat field and raw image, respectively. The analysis assumes that the raw image itself is generated by a uniform source of illumination (i.e., flat field).

Differentiating Eq. (8.3) yields

$$\sigma_{\mathrm{COR}}^2 = \left[\frac{-\mu_{\mathrm{FF}} S_{\mathrm{RAW}}}{S_{\mathrm{FF}}^2}\right]^2 \sigma_{\mathrm{SHOT\_FF}}^2 + \left[\frac{\mu_{\mathrm{FF}}}{S_{\mathrm{FF}}}\right]^2 \sigma_{\mathrm{SHOT\_RAW}}^2 + \sigma_{\mathrm{READ}}^2. \quad (8.4)$$

After noting that $\mu_{\mathrm{FF}} = S_{\mathrm{FF}}$, Eq. (8.4) is simplified to

$$\sigma_{\mathrm{COR}} = \left[\sigma_{\mathrm{READ}}^2 + \sigma_{\mathrm{SHOT\_RAW}}^2 + \left(\frac{S_{\mathrm{RAW}}}{S_{\mathrm{FF}}}\sigma_{\mathrm{SHOT\_FF}}\right)^2\right]^{1/2}. \quad (8.5)$$

Note that the ideal shot noise limited response could be achieved if $S_{\mathrm{FF}} \gg S_{\mathrm{RAW}}$. Unfortunately, this requirement can't be met if S_{RAW} is near full-well conditions. However, the shot-noise contribution from the flat-field frame can be reduced to a negligible level if several flat fields are averaged together before Eq. (8.1) is applied. The resultant noise of the corrected image when the flat fields are averaged is

$$\sigma_{\mathrm{COR}} = \left[\sigma_{\mathrm{READ}}^2 + \sigma_{\mathrm{SHOT\_RAW}}^2 + \left(\frac{S_{\mathrm{RAW}}}{S_{\mathrm{FF}} N_{\mathrm{FF}}^{1/2}}\sigma_{\mathrm{SHOT\_FF}}\right)^2\right]^{1/2}, \quad (8.6)$$

where N_{FF} is the number of flat fields taken and averaged.

Noting that $\sigma_{\mathrm{SHOT\_RAW}}^2 = S_{\mathrm{RAW}}$ and $\sigma_{\mathrm{SHOT\_FF}}^2 = S_{\mathrm{FF}}$, Eq. (8.6) reduces to

$$\sigma_{\mathrm{COR}} = \left\{\sigma_{\mathrm{READ}}^2 + \left[S_{\mathrm{RAW}}\left(1 + \frac{S_{\mathrm{RAW}}}{Q_{\mathrm{FF}}}\right)\right]\right\}^{1/2}, \quad (8.7)$$

where

$$Q_{\mathrm{FF}} = S_{\mathrm{FF}} N_{\mathrm{FF}}. \quad (8.8)$$

Q_{FF} is defined as the "flat field quality factor."

Note that when $S_{\mathrm{RAW}}/Q_{\mathrm{FF}} \ll 1$, and read noise is negligible, Eq. (8.7) reduces to

$$\sigma_{\mathrm{COR}} = S_{\mathrm{RAW}}^{1/2}, \quad (8.9)$$

producing the ideal shot noise limit. On a log-log plot, σ_{COR} will exhibit a slope of $1/2$ as a function of signal.

When $S_{\mathrm{RAW}}/Q_{\mathrm{FF}} \gg 1$, Eq. (8.7) simplifies to

$$\sigma_{\mathrm{COR}} = \frac{S_{\mathrm{RAW}}}{Q_{\mathrm{FF}}^{1/2}}, \tag{8.10}$$

and the corrected noise increases linearly with signal, thus exhibiting a slope of unity on a log-log plot and a slope of $Q_{\mathrm{FF}}^{-1/2}$ on linear coordinates.

For the special case when $Q_{\mathrm{FF}} = S_{\mathrm{FF}} = S_{\mathrm{RAW}}$, Eq. (8.7) becomes

$$\sigma_{\mathrm{COR}} = (2S_{\mathrm{RAW}})^{1/2} = 2^{1/2}\sigma_{\mathrm{SHOT\_RAW}}; \tag{8.11}$$

i.e., when a flat field flattens another flat field at the same signal level, the resultant shot noise is the square root of two times higher than the original shot noise level.

Example 8.1

Determine the noise level after flat fielding given that $S_{\mathrm{RAW}} = 10^5$ e$^-$, and $S_{\mathrm{FF}} = 10^5$ e$^-$ for $N_{\mathrm{FF}} = 1$, 10, and 100. Compare the results to the ideal shot noise level. Assume σ_{READ} is negligible.

Solution:
The ideal shot noise limited response after flat fielding is $(10^5)^{1/2} = 316$ e$^-$.
From Eq. (8.7),

$$\sigma_{\mathrm{COR}} = \left\{10^5\left[1 + \frac{10^5}{(10^5 \times 1)}\right]\right\}^{1/2} = 2^{1/2} \times 316 = 447 \text{ e}^-$$

when $N_{\mathrm{FF}} = 1$;

$\sigma_{\mathrm{COR}} = 331$ e$^-$ when $N_{\mathrm{FF}} = 10$;

and

$\sigma_{\mathrm{COR}} = 317$ e$^-$ when $N_{\mathrm{FF}} = 100$.

Equating the corrected and raw noise levels reveals an interesting connection between P_{N} and Q_{FF}:

$$\left\{\sigma_{\mathrm{READ}}^2 + \left[S_{\mathrm{RAW}}\left(1 + \frac{S_{\mathrm{RAW}}}{Q_{\mathrm{FF}}}\right)\right]\right\}^{1/2} = \left[\sigma_{\mathrm{READ}}^2 + S_{\mathrm{RAW}} + (S_{\mathrm{RAW}}P_{\mathrm{N}})\right]^{1/2}. \tag{8.12}$$

Simplifying and solving for Q_{FF} yields

$$Q_{\mathrm{FF}} = \frac{1}{P_{\mathrm{N}}^2}. \tag{8.13}$$

Note that when $Q_{\mathrm{FF}} < 1/P_{\mathrm{N}}^2$, the corrected noise floor is actually greater than the raw noise floor, which totally defeats the purpose of flat fielding.

8.2 Photon Transfer Verification

Photon transfer is a powerful tool to confirm that FPN is being properly removed through the flat-fielding technique. If the flat-fielding process is performed correctly, the ideal shot noise PTC will be obtained. Figure 8.3 presents PTCs of $\sigma_{\mathrm{TOTAL}}(\mathrm{DN})$, $\sigma_{\mathrm{SHOT+READ}}(\mathrm{DN})$, and $\sigma_{\mathrm{COR}}(\mathrm{DN})$, assuming $Q_{\mathrm{FF}}(\mathrm{DN}) = 15{,}000$. Note that the noise of the corrected curve is greater than the ideal shot noise curve by $2^{1/2}$ at 15,000 DN, as Eq. (8.11) predicts. Also, the corrected response approaches a slope of unity when $S_{\mathrm{RAW}} > S_{\mathrm{FF}}$, as indicated by Eq. (8.10). To achieve the shot noise limit over the sensor's entire dynamic range, $Q_{\mathrm{FF}}(\mathrm{DN})$ must be increased.

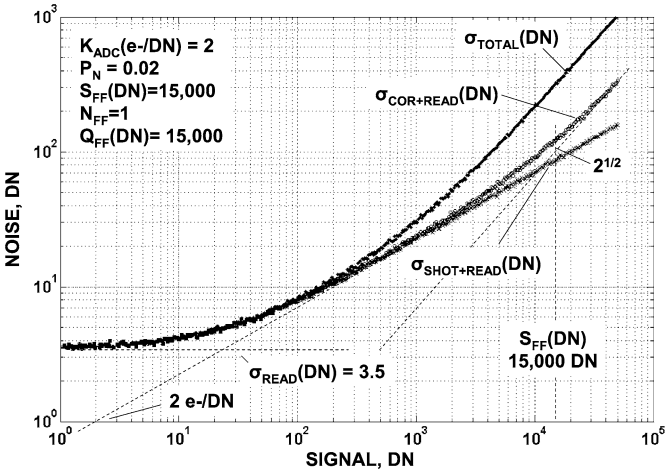

Figure 8.3 PTC verification if flat fielding is performed properly.

Example 8.2

Generate a set of PTCs after flat fielding for the PTCs in Example 5.1. Assume $Q_{\mathrm{FF}} = 10^2$, 10^3, 10^4, 10^5, and 10^6 e^-, and $N_{\mathrm{FF}} = 1$. Calculate the flat-field level where the corrected noise is greater than the raw noise. Assume $P_{\mathrm{N}} = 0.02$.

Solution:
Figure 8.4 shows the desired PTCs. A flat-field quality factor $> 10^6$ e^- is required for shot noise limited performance over the full dynamic range. From Eq. (8.13), the noise contained in the corrected image is greater than the raw frame noise when

$$Q_{\mathrm{FF}} < \frac{1}{0.02^2} < 2500\ \mathrm{e}^-.$$

Note from Fig. 8.4 that the corrected PTC lays on top of the raw FPN curve when Eq. (8.13) applies.

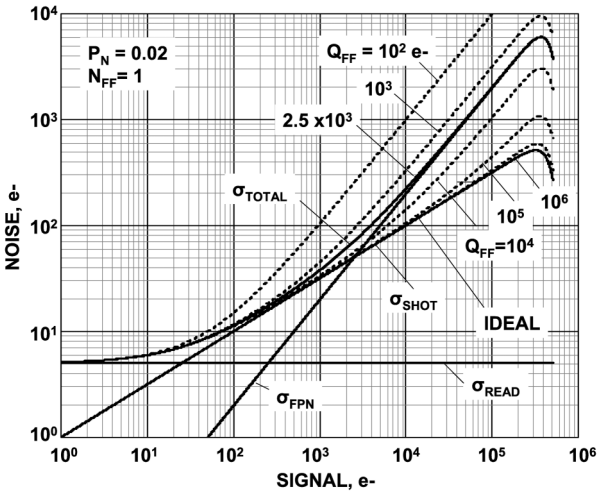

Figure 8.4 PTC response with different flat-fielding quality factors compared to the ideal shot noise response.

Figure 8.5 presents a random number simulation that further demonstrates the flat-fielding process. The noise associated with the linearly increasing raw signal shown is primarily dominated by FPN. The plot also includes four flat-field levels with quality factors of $Q_{\rm FF} = 50{,}000$; 10,000; 2000; and 500 e^-. The simulation then divides the raw pixel values by the flat-field pixels as defined by Eq. (8.1). Figure 8.6 shows the corrected response for a quality factor of $Q_{\rm FF} = 50{,}000$ that leaves behind only shot noise. Figure 8.7 plots the shot noise contained in the

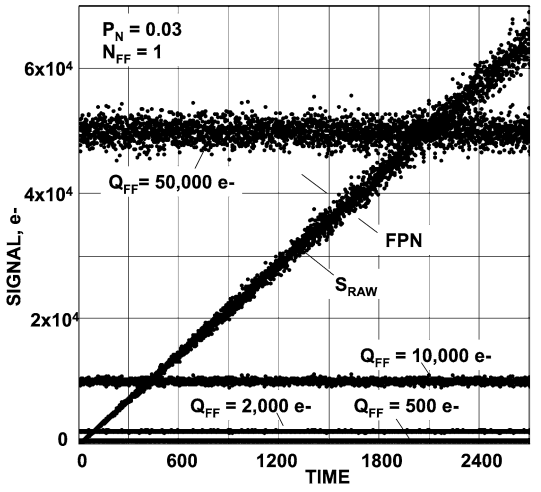

Figure 8.5 Raw signal response showing FPN build up along with four flat field levels with different $Q_{\rm FF}$.

corrected response for each quality factor. Note that the noise level for $Q_{\mathrm{FF}} = 50{,}000$ is slightly noisier than the ideal shot noise response also included in the plot. As Q_{FF} is reduced, the corrected noise dramatically increases and surpasses the FPN contained in the raw signal. Figure 8.8 shows the corrected noise responses when N_{FF} is increased from 1 to 10. Results show an improved response relative to Fig. 8.7 by a factor of $10^{1/2}$.

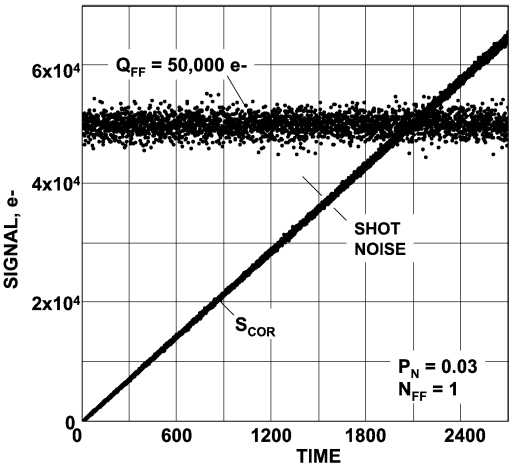

Figure 8.6 FPN removal after flat fielding is applied to the raw response shown in Fig. 8.5.

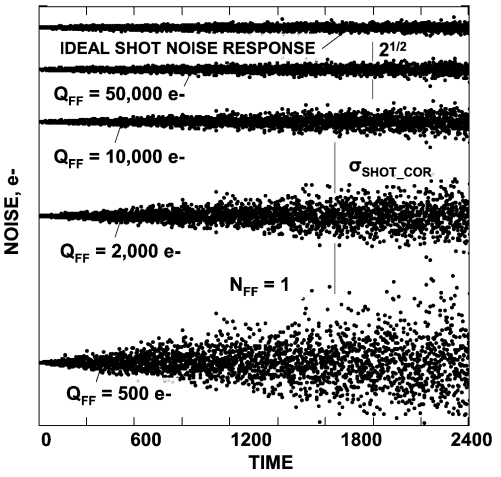

Figure 8.7 Noise level after flat fielding for each Q_{FF} level compared to the ideal shot noise response.

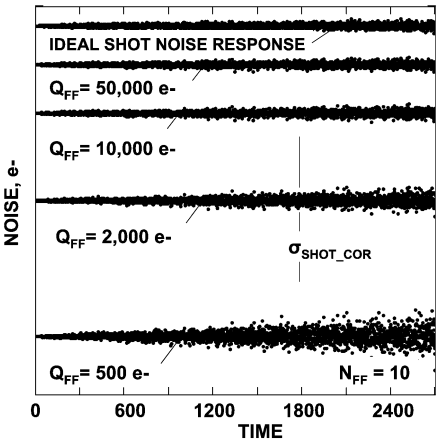

Figure 8.8 Noise reduction when 10 flat fields are averaged compared to the ideal shot noise response.

8.3 Nonlinearity

Flat fielding is also applicable when V/V nonlinearity is present, as demonstrated in the next example.

Example 8.3

Perform the same simulation exercise as Fig. 8.5 but assume the signal and ADC sensitivity vary as

$$S = 10t$$

and

$$K_{\mathrm{ADC}}(\mathrm{e}^{-}/\mathrm{DN}) = 0.1 + 0.004S^{0.5},$$

where t is the exposure time (sec). Perform the simulation in DN units.

Solution:
The signal and noise relations in DN units are

$$S(\mathrm{DN}) = \frac{S}{K_{\mathrm{ADC}}(\mathrm{e}^{-}/\mathrm{DN})},$$

$$\sigma_{\mathrm{SHOT}}(\mathrm{DN}) = \frac{S^{1/2}}{K_{\mathrm{ADC}}(\mathrm{e}^{-}/\mathrm{DN})},$$

and

$$\sigma_{\mathrm{FPN}}(\mathrm{DN}) = \frac{SP_{\mathrm{N}}}{K_{\mathrm{ADC}}(\mathrm{e}^{-}/\mathrm{DN})}.$$

Figure 8.9 shows the PTCs of the above relations. The total noise curve with unity slope indicates a FPN of 3%. As seen from the shot noise curve, the nonlinearity causes $K_{\mathrm{ADC}}(\mathrm{e}^-/\mathrm{DN})$ to vary from 0.11 to 1.37 e^-/DN.

Figure 8.10 presents noise simulation results where the raw signal and the four flat-field levels are plotted as a function of exposure time. Figure 8.11 shows the corrected response after flat fielding for $Q_{\mathrm{FF}} = 50{,}000$ DN. Figure 8.12 plots the shot noise for each quality factor, including the ideal shot noise level (assuming $N_{\mathrm{FF}} = 1$).

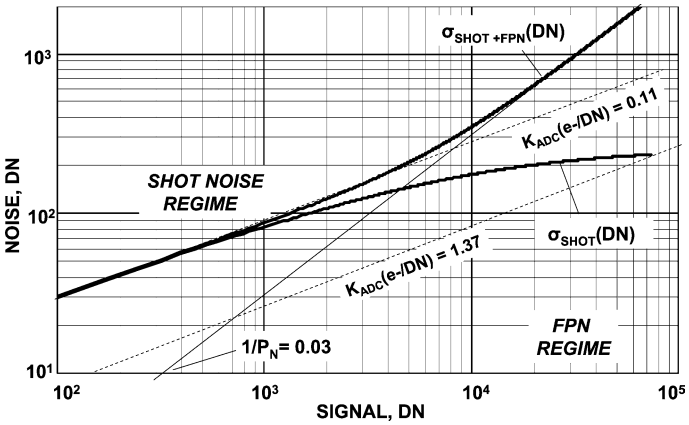

Figure 8.9 PTC responses with V/V nonlinearity present.

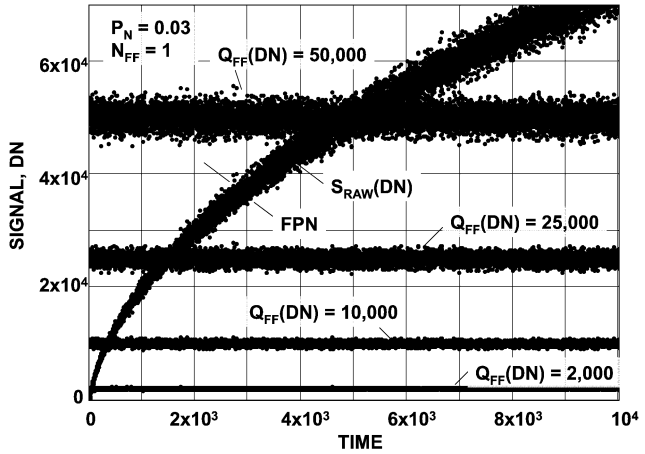

Figure 8.10 Raw signal response with time showing V/V nonlinearity and four flat-field levels.

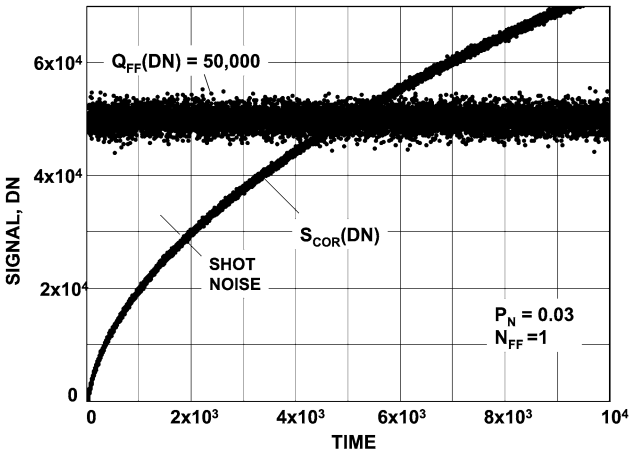

Figure 8.11 FPN removed from raw response by flat fielding for Fig. 8.10.

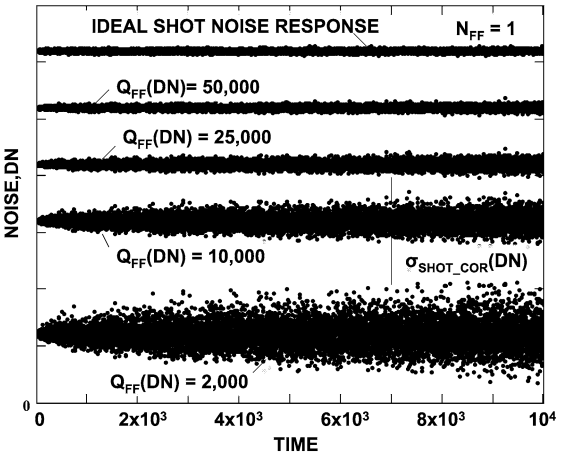

Figure 8.12 Noise level after flat fielding for each Q_{FF} compared to the ideal shot noise response.

Although flat fielding produces theoretical performance for linear and V/V nonlinear detectors, FPN cannot be entirely removed when V/e$^-$ nonlinearity is present. Example 8.4 provides insight behind the severity of the problem.

Example 8.4

Refer back to Example 7.2, which introduced V/e$^-$ nonlinearity, and perform the same simulation exercise as in Fig. 8.10 by assuming the same sense node capacitance change as

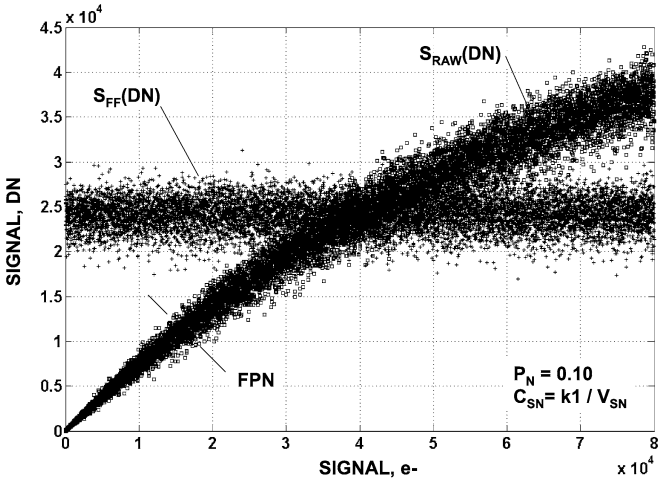

Figure 8.13 Raw response and flat field level for a sensor with V/e$^-$ nonlinearity measured in Fig. 7.17.

$$C_{\mathrm{SN}} = \frac{k1}{V_{\mathrm{SN}}}, \quad 0.9 < V_{\mathrm{SN}} < 3.1,$$

where $k1 = 10.909 \times 10^{-15}$.

To emphasize the V/e$^-$ nonlinearity problem on flat fielding, assume the shot noise of the flat field is negligible (i.e., $Q_{\mathrm{FF}} = \infty$) and use an abnormally large FPN quality factor of $P_{\mathrm{N}} = 0.1$. Also, generate PTCs when $S_{\mathrm{FF}}(\mathrm{DN}) = 24{,}200$ and $P_{\mathrm{N}} = 0$, 0.01, 0.03, and 0.10. Then keep P_{N} fixed at 0.03 and make a different set of PTCs for these flat-field levels: $S_{\mathrm{FF}}(\mathrm{DN}) = 794$; 7442; 24,200; and 37,670.

Solution:
Figure 8.13 shows the flat-fielding simulation plot. $S_{\mathrm{RAW}}(\mathrm{DN})$ and the related noise increase nonlinearly with S because of a changing sense node capacitance. Also shown is a flat-field level of $S_{\mathrm{FF}}(\mathrm{DN}) = 24{,}200$, which is used to flatten the raw signal. Figure 8.14 shows the corrected response. Although most of the FPN is removed, a small amount of "remnant FPN" remains (as indicated). It is only when $S_{\mathrm{FF}}(\mathrm{DN}) = S_{\mathrm{RAW}}(\mathrm{DN})$ that FPN is entirely eliminated, and the result equals the ideal shot noise limit. Figure 8.15 plots the corrected noise levels for different $P_{\mathrm{N}} = 0$, 0.01, 0.03, and 0.1. Note that the shot noise at the flat-field level remains fixed, whereas the remnant FPN increases on either side of $S_{\mathrm{FF}}(\mathrm{DN})$ and becomes larger with P_{N}.

Figures 8.16 and 8.17 show the corresponding PTCs plotted on linear and log coordinates for $P_{\mathrm{N}} = 0$, 0.01, 0.03, and 0.10, with $S_{\mathrm{FF}}(\mathrm{DN}) = 24{,}200$. Both the raw and corrected responses are shown. Similar to the behavior seen in Fig. 8.14, remnant FPN first increases, then decreases to the shot noise level at $S_{\mathrm{FF}}(\mathrm{DN}) = 24{,}200$. Beyond that level, the noise level continually increases until full well is

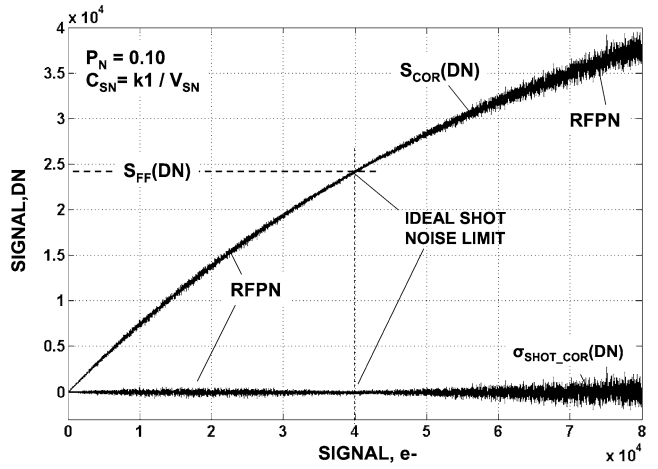

Figure 8.14 FPN removed by flat fielding for Fig. 8.13 showing remnant FPN due to V/e$^-$ nonlinearity.

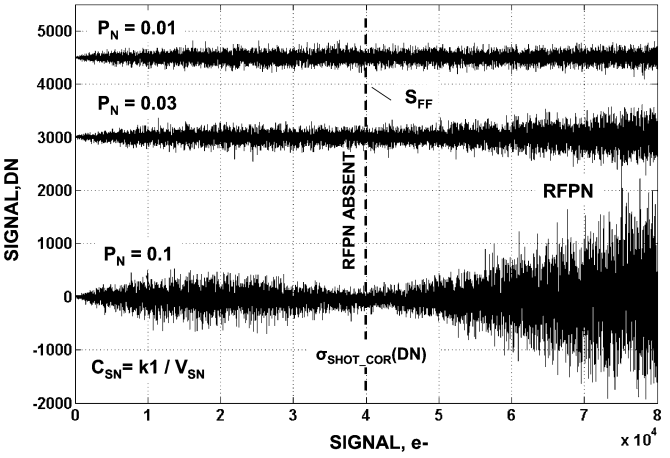

Figure 8.15 Noise responses showing remnant FPN becoming negligible when the FPN quality factor P_{N} approaches 0.01.

reached. Also shown in the figures are curves without FPN (i.e., $P_{\mathrm{N}} = 0$), which represent the ideal response. Figure 8.18 shows a PTC on linear coordinates with P_{N} fixed at 0.03 for $S_{\mathrm{FF}}(\mathrm{DN}) = 794$; 7,442; 24,200; and 37,670 DN (the signal levels are indicated as dots in the figure). Note that the responses become closer to the ideal shot noise response (shown in Fig. 8.16) as the flat-field signal level increases. However, remnant FPN prevents the curve from exhibiting the perfect response; only the indicated dots achieve that response.

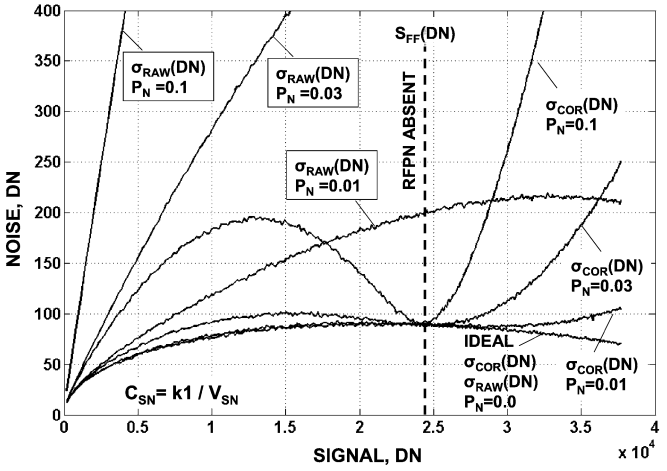

Figure 8.16 PTC responses before and after flat fielding showing remnant FPN for different P_{N} compared to the ideal shot noise response.

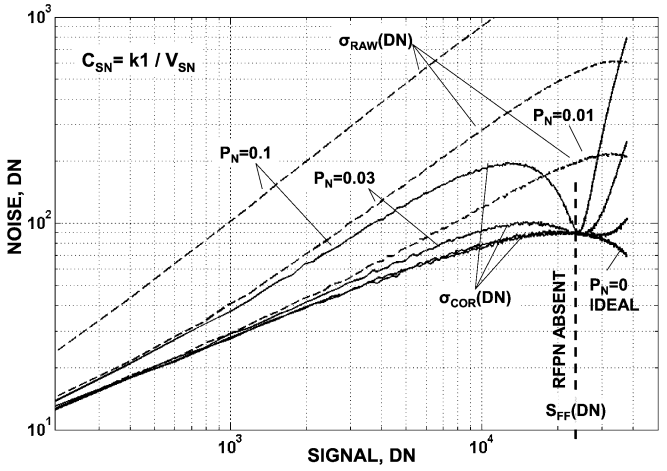

Figure 8.17 Log PTC responses for Fig. 8.16.

The CMOS detector analyzed in Example 8.4 is highly nonlinear. However, the assumed FPN noise of 10% was highly exaggerated to show the V/e$^-$ nonlinearity flat-fielding problem. Fortunately, the level of remnant FPN is negligible when the FPN is 1%, which is typical of CCD and CMOS detectors (as demonstrated in Fig 8.15). However, other camera-related FPN sources, such as vignetting, shading, and interference fringing, which are often greater than pixel-to-pixel FPN, can lead to flattening issues. For example, Fig. 8.19 shows a response to a uniform light stimulus where 10% shading across the pixels is present. Note that the flattened response is the reverse of the raw trace because the modulation gain is greater

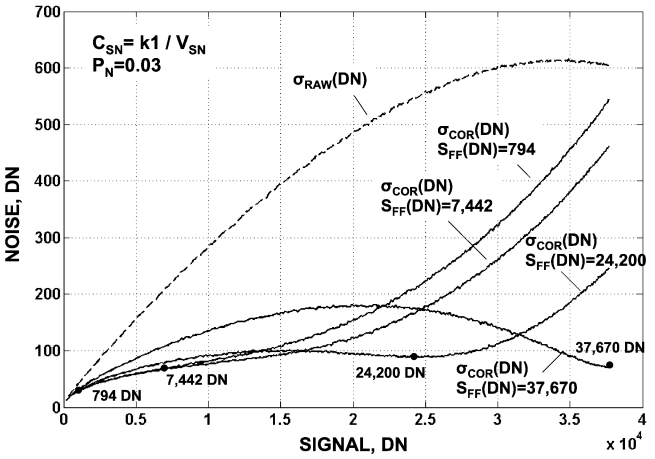

Figure 8.18 PTC responses before and after flat fielding using different flat field levels to remove FPN.

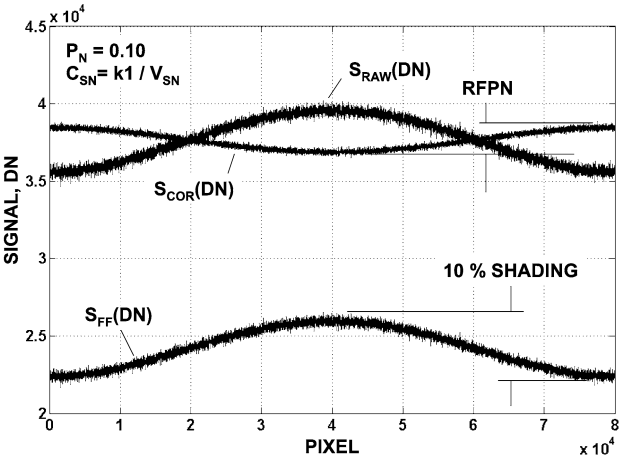

Figure 8.19 Raw and corrected responses showing remnant FPN due to image shading.

for the flat field than the raw trace [i.e., $N_{\mathrm{FF}}(\mathrm{DN/e^-}) > N_{\mathrm{RAW}}(\mathrm{DN/e^-})$]. The opposite effect occurs when $N_{\mathrm{FF}}(\mathrm{DN/e^-}) < N_{\mathrm{RAW}}(\mathrm{DN/e^-})$, as shown in Fig. 8.20. As before, remnant FPN is not present only when $S_{\mathrm{FF}}(\mathrm{DN}) = S_{\mathrm{RAW}}(\mathrm{DN})$. PTCs can be generated to quantify the problem.

Important Points

1. Shot noise limited performance can be achieved by removing FPN through the flat-fielding technique.
2. The amount of FPN removal is proportional to the square root of the number of flat fields averaged and their signal level.

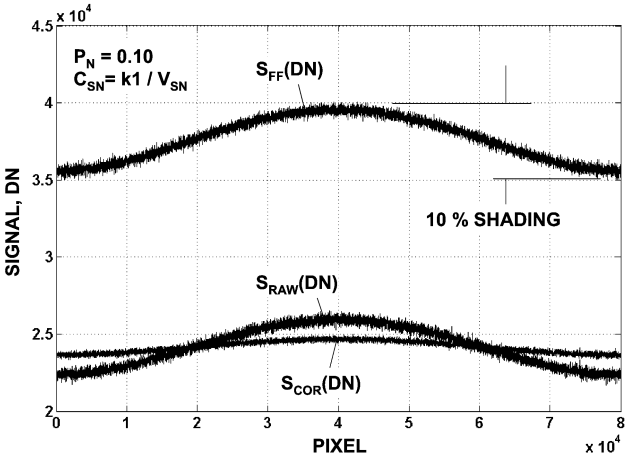

Figure 8.20 Raw and corrected responses showing remnant FPN due to shading.

3. Flat fielding is totally effective in eliminating FPN for linear and V/V nonlinear detectors.
4. FPN cannot be completely removed when V/e^- nonlinearity exists.
5. Remnant FPN generated by V/e^- nonlinear detectors is usually negligible relative to shot noise. However, camera-related FPN sources can lead to significant remnant FPN.

Chapter 9
Modulation Photon Transfer

9.1 Introduction

Discussions to this point have assumed that a flat-field light source is used to stimulate the detector. This chapter develops PT relations for nonuniform light sources, such as a sinusoidal stimulus. Results derived in this chapter provide significant insight and quantification of S/N performance for images in general, which is discussed in Chapter 10.

9.2 Sinusoidal Signal

Nonuniform light analysis begins by assuming that the detector's output response to a sinusoidal photon input source is described by

$$\mathrm{SIN} = P\mathrm{QE_I}\left\{1 + C_\mathrm{P}\mathrm{MTF_D}\sin\left[\pi\left(\frac{f_\mathrm{S}n_\mathrm{ix}}{f_\mathrm{N}} + 0.5\right)\right]\right\}, \tag{9.1}$$

where SIN is the pixel signal ($\mathrm{e^-}$), n_ix is the number of pixels across the array (i.e., $n_\mathrm{ix} = 1, 2, 3$, etc.), and C_P is the incident "photon contrast" defined by

$$C_\mathrm{P} = \frac{S_\mathrm{MAX}(P) - S_\mathrm{MIN}(P)}{S_\mathrm{MAX}(P) + S_\mathrm{MIN}(P)}, \tag{9.2}$$

where $S_\mathrm{MAX}(P)$ and $S_\mathrm{MIN}(P)$ are the maximum and minimum number of incident photons per pixel. In Eq. (9.1), $\mathrm{MTF_D}$ is the pixel's modulation transfer function (MTF) given by

$$\mathrm{MTF_D} = \frac{\sin\left(\dfrac{\pi f_\mathrm{S}p_\mathrm{f}}{2f_\mathrm{N}}\right)}{\dfrac{\pi f_\mathrm{S}p_\mathrm{f}}{2f_\mathrm{N}}}, \tag{9.3}$$

where f_S is the spatial frequency of the sinusoidal input (cycles/cm), p_f is the normalized pixel aperture opening (the ratio of the active pixel opening to the pixel pitch), and f_N is the Nyquist spatial frequency defined by

$$f_\mathrm{N} = \frac{1}{2p_\mathrm{ix}}, \tag{9.4}$$

where p_ix is the pixel pitch (cm).

Equation (9.1) can be simplified to

$$\mathrm{SIN} = P\mathrm{QE_I}\{1 + C_\mathrm{D}\sin[\pi(fn_\mathrm{ix} + 0.5)]\}, \tag{9.5}$$

where the normalized spatial frequency, f, is defined as

$$f = \frac{f_\mathrm{S}}{f_\mathrm{N}}. \tag{9.6}$$

C_D is the "detector's contrast" defined as

$$C_\mathrm{D} = C_\mathrm{I}\mathrm{MTF_D} = \frac{S_\mathrm{MAX} - S_\mathrm{MIN}}{S_\mathrm{MAX} + S_\mathrm{MIN}}, \tag{9.7}$$

where the detector's maximum and minimum signal excursions are

$$S_\mathrm{MAX} = P\mathrm{QE_I}(1 + C_\mathrm{D}) \tag{9.8}$$

and

$$S_\mathrm{MIN} = P\mathrm{QE_I}(1 - C_\mathrm{D}). \tag{9.9}$$

Example 9.1

Plot Eqs. (9.1) and (9.5) by assuming $P = 20{,}000$ photons/pixel, $\mathrm{QE_I} = 0.5$, $C_\mathrm{P} = 1$, and $\mathrm{MTF_D} = 0.5$ for $f = 1$ and $f = 0.6$.

Solution:
From Eq. 9.1, Figure 9.1 plots the input photon flux as a function of pixel distance across the detector for the two spatial frequencies given. The discrete data points shown represent the number of interacting photons per pixel.

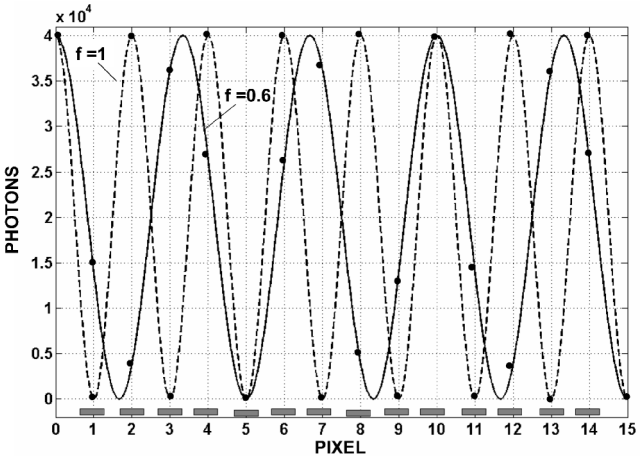

Figure 9.1 Sinusoidal input light stimulus to the detector.

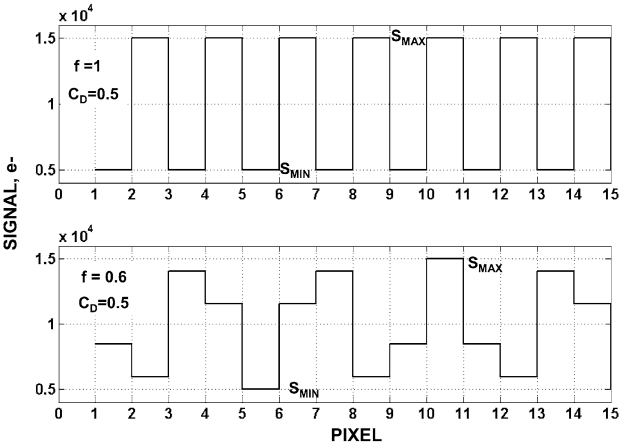

Figure 9.2 Pixel output response (e^-) to the photon input shown in Fig. 9.1.

Figure 9.2 plots the detector's output signal given by Eq. (9.5) as a function of the pixel for each spatial frequency.

Applying the general averaging relation

$$x_{\mathrm{m}} = \frac{1}{n}\sum_{i=1}^{n} x_i \tag{9.10}$$

to Eq. (9.5) produces the mean signal level for the detector,

$$S_{\mathrm{SIN}} = \frac{P\mathrm{QE_I}}{n_{\mathrm{ix}}}\sum_{1}^{n_{\mathrm{ix}}} 1 + C_{\mathrm{D}}\sin[\pi(fn_{\mathrm{ix}} + 0.5)]. \tag{9.11}$$

If the number of sinusoidal cycles sampled by the pixels is large (i.e., $n_{\mathrm{ix}} \gg 2/f$), Eq. (9.11) reduces to

$$S_{\mathrm{SIN}} = P\mathrm{QE_I} = \frac{S_{\mathrm{MAX}} + S_{\mathrm{MIN}}}{2}. \tag{9.12}$$

Applying the general standard deviation relation

$$\sigma = \left[\frac{1}{n}\sum_{i}^{N}(x_i - x_{\mathrm{m}})^2\right]^{1/2} \tag{9.13}$$

to Eq. (9.5) produces the standard deviation (rms) level for the detector:

$$\delta_{\mathrm{SIN}} = \left[\frac{1}{n_{\mathrm{ix}}}\sum_{1}^{n_{\mathrm{ix}}} P\mathrm{QE_I}\{1 + C_{\mathrm{D}}\sin[\pi(fn_{\mathrm{ix}} + 0.5)] - S_{\mathrm{SIN}}\}^2\right]^{1/2}. \tag{9.14}$$

If the number of sinusoidal cycles sampled by the pixels is large (i.e., $n_{\mathrm{ix}} \gg 2/f$), Eq. (9.14) reduces to

$$\delta_{\mathrm{SIN}} = 0.707 S_{\mathrm{SIN}} C_{\mathrm{D}}. \tag{9.15}$$

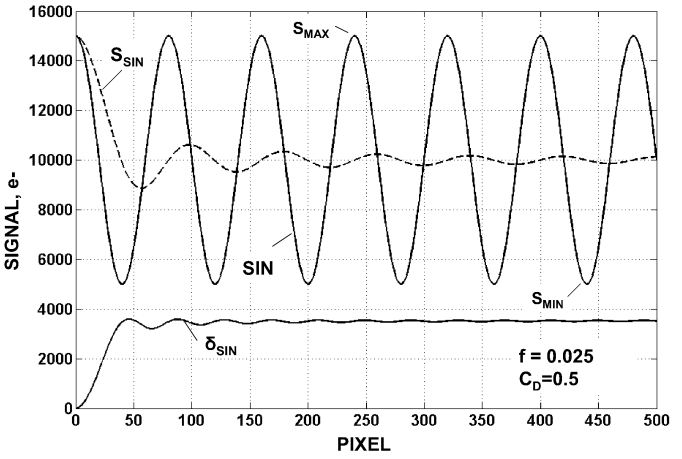

Figure 9.3 Output (SIN), average signal ($S_{\rm SIN}$), and rms modulation ($\delta_{\rm SIN}$) responses as a function of pixel count.

From Eqs. (9.11) and (9.14), the mean and standard deviation are plotted in Fig. 9.3, assuming $f = 0.025$, $C_{\rm D} = 0.5$, and $S_{\rm SIN} = 10{,}000$ e$^-$. Note that the average signal and corresponding standard deviation approach the constant level given by Eqs. (9.12) and (9.15) for a large $n_{\rm ix}$. Figure 9.4 shows similar plots for the spatial frequency $f = 0.91$.

Example 9.2

Determine $S_{\rm MAX}$, $S_{\rm MIN}$, $S_{\rm SIN}$, and $\delta_{\rm SIN}$ under steady-state conditions for Fig. 9.3. Assume $PQE_{\rm I} = 10{,}000$ e$^-$, $C_{\rm D} = 0.5$, and $f = 0.025$.

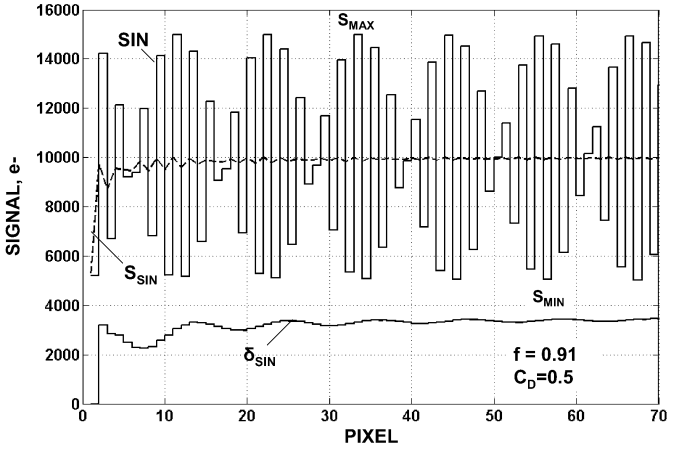

Figure 9.4 Similar responses as Fig. 9.3 at a higher spatial frequency.

Solution:
From Eq. (9.5), the charge generated by the detector is

$$\text{SIN} = 10{,}000\{1 + 0.5\sin[\pi(0.025 \times n_{\text{ix}} + 0.5)]\}.$$

From Eq. (9.8), the maximum signal level is

$$S_{\text{MAX}} = 10{,}000 \times (1 + 0.5) = 15{,}000\ \text{e}^{-}.$$

From Eq. (9.9), the minimum signal level is

$$S_{\text{MIN}} = 10{,}000 \times (1 - 0.5) = 5000\ \text{e}^{-}.$$

From Eq. (9.12), the average signal is

$$S_{\text{SIN}} = \frac{10{,}000 + 5000}{2} = 10{,}000\ \text{e}^{-}.$$

From Eq. (9.15), the standard deviation is

$$\delta_{\text{SIN}} = 10{,}000 \times \frac{0.5}{2^{1/2}} = 3536\ \text{e}^{-}.$$

9.3 Sinusoidal Noise

Shot noise and FPN vary sinusoidally with the signal described by Eq. (9.5). For example, Figs. 9.5 and 9.6 plot shot noise and FPN generated for $S_{\text{SIN}} = 10{,}000\ \text{e}^{-}$

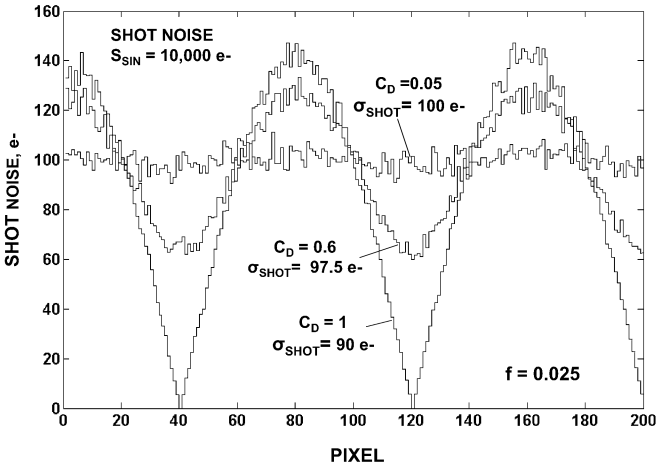

Figure 9.5 Sinusoidal shot noise for different contrast levels.

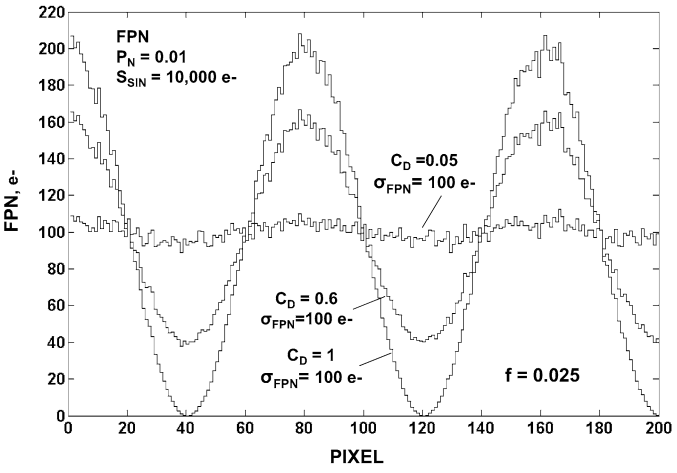

Figure 9.6 Sinusoidal FPN for different contrast levels.

at different contrast levels ($C_{\mathrm{D}} = 1$, 0.6, and 0.05). Each figure labels the average noise level for each contrast level. Figure 9.7 plots the average noise for both sources as a function of contrast, assuming several cycles are sampled (i.e., $n_{\mathrm{ix}} \gg 2/f$). Note that the FPN level is constant with contrast as

$$\sigma_{\mathrm{SIN\_FPN}} = P_{\mathrm{N}} S_{\mathrm{SIN}}. \tag{9.16}$$

However, the shot noise is slightly dependent on contrast. For low-contrast signals, the average rms shot noise can be approximated by

$$\sigma_{\mathrm{SIN\_SHOT}} \approx S_{\mathrm{SIN}}^{1/2}. \tag{9.17}$$

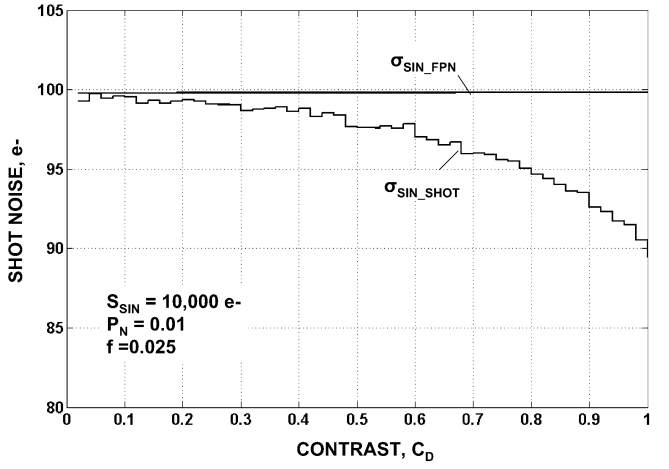

Figure 9.7 Average sinusoidal shot noise and FPN as a function of contrast.

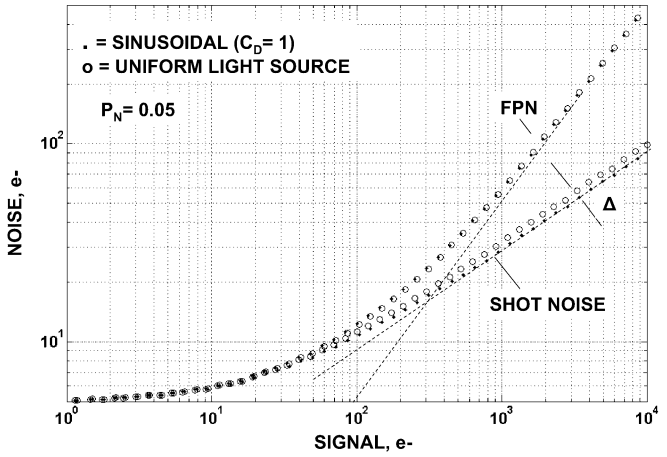

Figure 9.8 Sinusoidal and uniform PTCs showing slightly different shot noise responses.

Note that Eq. (9.17) can be in error by as much as 10% for a 100% contrast level as compared to a measured result. Discussions in this book will primarily focus on low-contrast images where S/N performance is most critical. Therefore, it will be assumed that Eq. (9.17) applies to the upcoming discussions. With this assumption, the total noise associated with a sine wave response is simply

$$\sigma_{\mathrm{SIN\_TOTAL}} = \left[\sigma^2_{\mathrm{READ}} + S_{\mathrm{SIN}} + (P_{\mathrm{N}} S_{\mathrm{SIN}})^2\right]^{1/2}. \tag{9.18}$$

It is also important to note that sinusoidal noise is approximately equal to the noise generated by a uniform light source when the average signal levels are the same (i.e., $S_{\mathrm{SIN}} = S$). Therefore, we can equate flat field and sinusoidal noise through

$$\sigma_{\mathrm{SIN\_TOTAL}} = \left[\sigma^2_{\mathrm{READ}} + S + (P_{\mathrm{N}} S)^2\right]^{1/2}, \quad S_{\mathrm{SIN}} = S, \tag{9.19}$$

where S is the average flat-field level.

Figure 9.8 displays simulated PTCs generated by a sinusoidal source with 100% contrast (i.e., $C_{\mathrm{D}} = 1$) and a flat-field source. Shot noise and FPN are plotted as a function of the signal level, assuming $S = S_{\mathrm{SIN}}$. Note that the FPN curves for both stimuli sources are identical. However, the shot noise curves differ slightly (10%) for reasons that were explained in Fig. 9.7.

Example 9.3

Determine the average signal and shot noise, given that the signal varies as

$$\mathrm{SIN} = 10{,}000 e^{-n_{\mathrm{ix}}/200}\{1 + C_{\mathrm{D}} \sin[\pi(f n_{\mathrm{ix}} + 0.5)]\} \tag{E9.1}$$

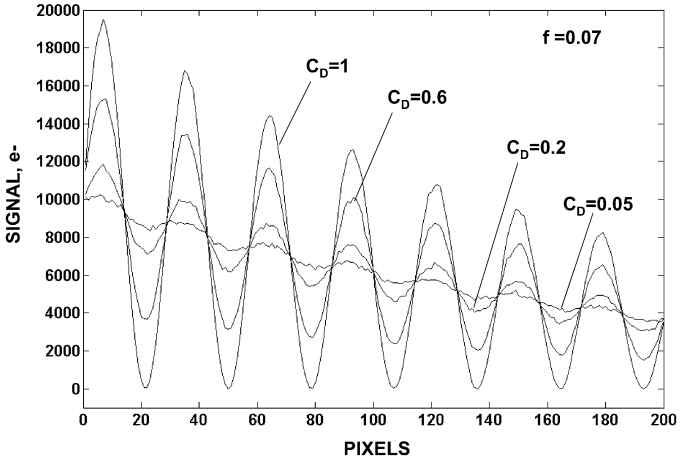

Figure 9.9 Decaying sinusoidal responses with the contrast levels defined in Example 9.3.

Table 9.1 Measured and calculated results for average signal and corresponding shot noise.

	$C_{\mathrm{D}} = 1$	$C_{\mathrm{D}} = 0.6$	$C_{\mathrm{D}} = 0.2$	$C_{\mathrm{D}} = 0.05$
Measured signal (e^-)	6448	6392	6334	6313
Measured shot noise (e^-)	71	76	78	78
Eq. (9.17), shot noise (e^-)	80	80	79	79

Compare the simulated measured results to Eq. (9.17). Assume $C_{\mathrm{D}} = 1$, 0.6, 0.2, 0.05, and $n_{\mathrm{ix}} = 200$ pixels.

Solution:
Figure 9.9 plots Eq. (E9.1) for the four contrast levels given. Table 9.1 provides measured results for the average signal and corresponding shot noise. Equation (9.17) calculates the shot noise and is also tabulated. Note that Eq. (9.17) is in agreement with measured results when the contrast is relatively low.

9.4 Modulation PTC

In Chapter 10 it will be shown that PTCs generated by an image quantify the image's S/N performance. The plots are referred to as modulation PTCs (MPTCs) and are generated experimentally in the same fashion as flat-field PTCs. For example, Fig. 9.10 shows a MPTC where rms modulation contained in the image is plotted as a function of average signal. Also included are shot noise and FPN PTCs produced by a uniform light stimulus.

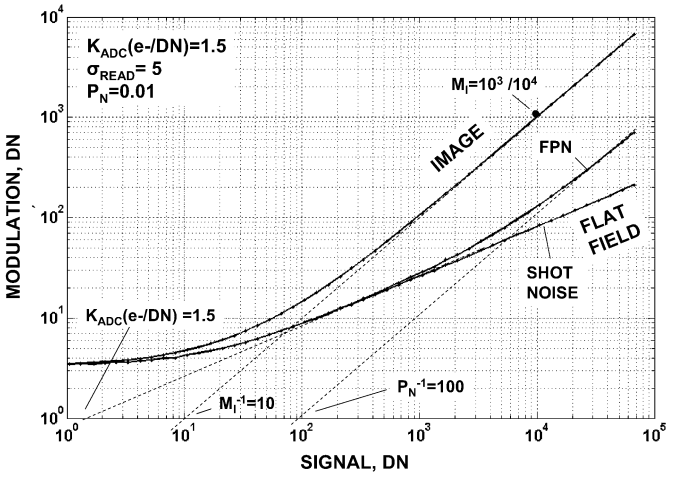

Figure 9.10 Uniform and image modulation PTC responses.

The total modulation contained in an image is composed of read noise, image shot noise, and image FPN as well as the useful signal modulation. In equation form, this is

$$\sigma_{\mathrm{I\_M}} = \left(\sigma^2_{\mathrm{READ}} + \sigma^2_{\mathrm{I\_SHOT}} + \sigma^2_{\mathrm{I\_FPN}} + \delta^2_{\mathrm{I}}\right)^{1/2}, \tag{9.20}$$

where $\sigma_{\mathrm{I\_M}}$ is the total image modulation, $\sigma_{\mathrm{I\_SHOT}}$ and $\sigma_{\mathrm{I\_FPN}}$ are the average shot noise and FPN for the image, and δ_{I} is the rms signal modulation. All noise sources, except the read noise, are generated by the image. The signal modulation is derived from the useful contrast information contained in the image.

Equation (9.20) can be described in terms of signal as

$$\sigma_{\mathrm{I\_M}} = \left[\sigma^2_{\mathrm{READ}} + S_{\mathrm{I}} + (P_{\mathrm{N}}S_{\mathrm{I}})^2 + (M_{\mathrm{I}}S_{\mathrm{I}})^2\right]^{1/2}, \tag{9.21}$$

where S_{I} is the average signal level of the image. M_{I} is referred to as the "image modulation constant" that varies with image contrast. The parameter is defined as

$$M_{\mathrm{I}} = \frac{\delta_{\mathrm{I}}}{S_{\mathrm{I}}} = \frac{[\sigma^2_{\mathrm{I\_M}} - \sigma^2_{\mathrm{READ}} - S_{\mathrm{I}} - (P_{\mathrm{N}}S_{\mathrm{I}})^2]^{1/2}}{S_{\mathrm{I}}}. \tag{9.22}$$

When the image noise sources are small relative to signal modulation, Eq. (9.22) reduces to

$$M_{\mathrm{I}} = \frac{\delta_{\mathrm{I}}}{S_{\mathrm{I}}} = \frac{\sigma_{\mathrm{I\_M}}}{S_{\mathrm{I}}}, \tag{9.23}$$

which exhibits a slope 1 response for large signal on a MPTC (as shown in Fig. 9.10).

Example 9.4

Determine the image modulation constant, M_{I}, for the MPTC shown in Fig. 9.10.

Solution:
The MPTC shows an example data point on the slope 1 curve used to calculate M_{I}. From Eq. (9.23),

$$M_{\mathrm{I}} = \frac{10^3}{10^4} = 0.1 \quad \text{(i.e., 10\% modulation or contrast)}.$$

Note that the image modulation is 10 times greater than the average image FPN (i.e., $M_{\mathrm{I}} = 10P_{\mathrm{N}}$); therefore, Eq. (9.23) applies.

Example 9.5

Determine the image modulation constant, M_{SIN}, for a sinusoidal stimulus. Assume several cycles of the sinusoid are sampled such that Eq. (9.15) applies.

Solution:
From Eq. (9.15), the rms modulation for a sine wave response is

$$\delta_{\mathrm{SIN}} = 0.707 \times C_{\mathrm{D}} \times S_{\mathrm{SIN}}. \tag{E9.2}$$

From Eq. (9.23),

$$M_{\mathrm{SIN}} = 0.707 C_{\mathrm{D}} \frac{S_{\mathrm{SIN}}}{S_{\mathrm{SIN}}} = 0.707 C_{\mathrm{D}} = 0.707 \times C_{\mathrm{P}} \times \mathrm{MTF}_{\mathrm{D}}. \tag{E9.3}$$

Example 9.6

Generate MPTCs in DN units for the sinusoidal image shown in Fig. 9.11 using the following parameters:

$C_{\mathrm{D}} = 1,\ 0.25,\ 0.0625,$ and 0.0313
$\sigma_{\mathrm{READ}} = 5\ \mathrm{e}^-$
$K_{\mathrm{ADC}}(\mathrm{e}^-/\mathrm{DN}) = 2.5$
$P_{\mathrm{N}} = 0.01$

Also include shot noise and FPN flat-field PTCs. Calculate M_{SIN} for the $C_{\mathrm{D}} = 0.0313$ contrast case and compare the result to the measured results from the MPTC.

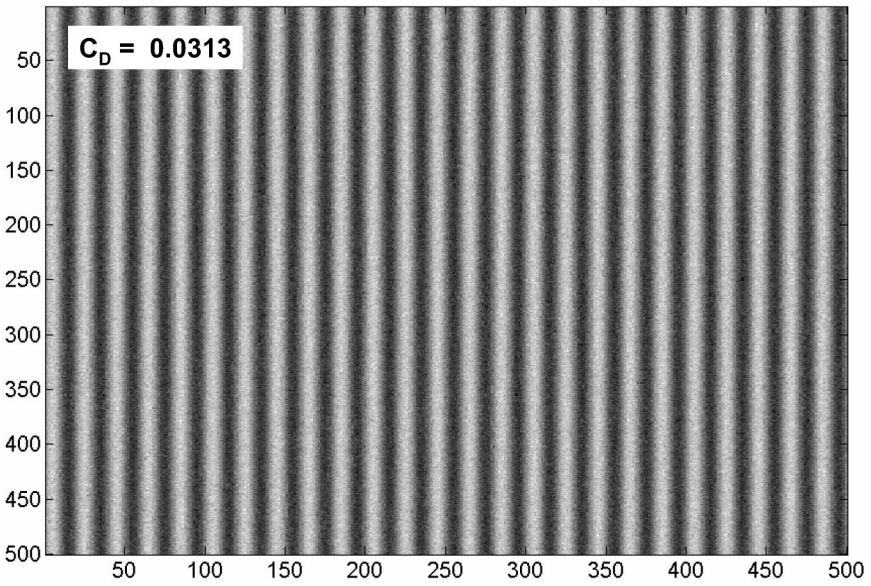

Figure 9.11 Sinusoidal image.

Solution:
Substituting Eq. (E9.3) into Eq. (9.21) yields the total sinusoidal modulation. In electron units, this total is

$$\sigma_{\mathrm{SIN\_M}} = \left[\sigma^2_{\mathrm{READ}} + S_{\mathrm{SIN}} + (P_{\mathrm{N}} S_{\mathrm{SIN}})^2 + (0.707 C_{\mathrm{D}} S_{\mathrm{SIN}})^2\right]^{1/2}. \quad \text{(E9.4)}$$

And in DN units, the total sinusoidal modulation is

$$\sigma_{\mathrm{SIN\_M}}(\mathrm{DN}) = \frac{[\sigma^2_{\mathrm{READ}} + S_{\mathrm{SIN}} + (P_{\mathrm{N}} S_{\mathrm{SIN}})^2 + (0.707 C_{\mathrm{D}} S_{\mathrm{SIN}})^2]^{1/2}}{K_{\mathrm{ADC}}(\mathrm{e^-/DN})}. \quad \text{(E9.5)}$$

Figure 9.12 simulates Eq. (E9.5) using random number generators for the noise sources to produce MPTCs for each contrast case. Also included for comparision are the shot noise and FPN flat-field PTCs.

From Eq. (E9.3), the theoretical sinusoidal modulation factor is calculated for $C_{\mathrm{D}} = 0.0313$ as

$$M_{\mathrm{SIN}} = 0.707 \times C_{\mathrm{D}} = 0.707 \times 0.0313 = 0.0221.$$

M_{SIN} is measured from the MPTC shown in Fig. 9.12 using Eq. (9.22).

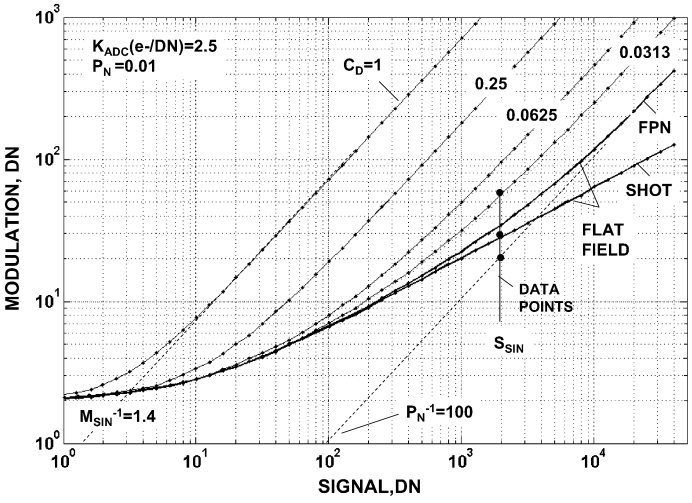

Figure 9.12 Modulation PTCs for the image shown in Fig. 9.11 in comparison to flat field PTC responses.

For example, Fig. 9.12 shows the following set of data points at $S_{\mathrm{SIN}}(\mathrm{DN}) = 2000$:

$$\sigma_{\mathrm{SIN\_M}} = 56 \text{ DN } (C_{\mathrm{D}} = 0.0313)$$
$$\sigma_{\mathrm{READ}} = 2 \text{ DN}$$
$$\sigma_{\mathrm{SIN\_SHOT}} = 29 \text{ DN}$$
$$\sigma_{\mathrm{SIN\_FPN}} = 20 \text{ DN}$$

Substituting these quantities into Eq. (9.22) yields

$$M_{\mathrm{SIN}} = \frac{(56^2 - 2^2 - 29^2 - 20^2)^{1/2}}{2000} = \frac{2061^{1/2}}{2000} = 0.022,$$

which is in agreement with the theoretical result from Eq. (E9.3).

Note that, as M_{SIN} decreases, the MPTC curve approaches the flat-field FPN responses, indicating that the quality of the image is degrading. When the contrast becomes zero (i.e., $M_{\mathrm{SIN}} = \delta_{\mathrm{I}} = 0$), the image becomes equivalent to a flat field. Figure 9.13 reduces the contrast factors relative to those applied in Fig. 9.12 to show the transition that takes place (i.e., $C_{\mathrm{D}} = 0.0313$, 0.0156, 0.0078, and 0.0031). Note that the lowest-contrast ($C_{\mathrm{D}} = 0.0031$, $M_{\mathrm{SIN}} = 0.0022$) curve essentially lies on top of the FPN flat-field response, indicating that the image would be completely lost in FPN. Figure 9.14 presents a similar set of curves with FPN removed; they show that the two curves separate, indicating that the contrast would still be seen. S/N performance for these imaging situations is discussed in Chapter 10.

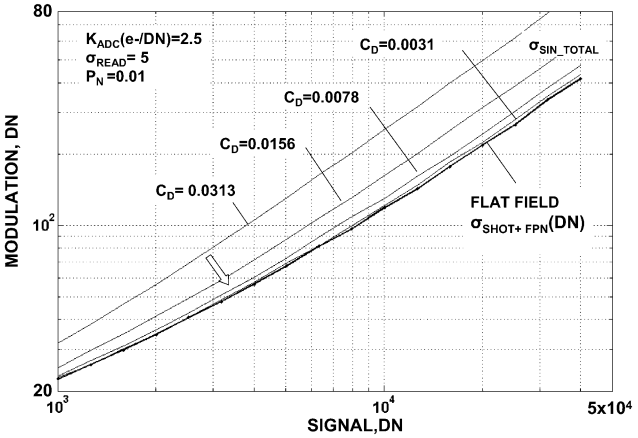

Figure 9.13 PTC responses with FPN and reduced contrast relative to Fig. 9.12.

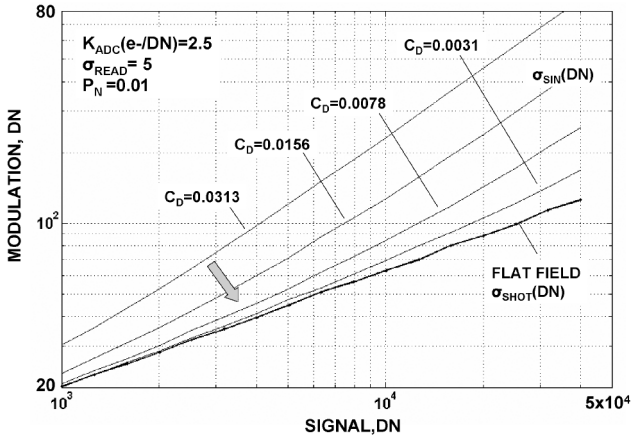

Figure 9.14 PTC responses without FPN and with reduced contrast relative to Fig. 9.12.

Example 9.7

Plot the sinusoidal image modulation factor, M_{SIN}, as a function of spatial frequency for different normalized pixel fill factors ($p_{\mathrm{f}} = 1$, 0.5, 0.2, and 0.02). Assume for this plot that incident photon contrast is $C_{\mathrm{P}} = 1$ (i.e., 100% input photon contrast).

Solution:
From Eq. (9.3),

$$M_{\mathrm{SIN}} = 0.707 \frac{\sin\left(\dfrac{\pi f p_{\mathrm{f}}}{2}\right)}{\dfrac{\pi f p_{\mathrm{f}}}{2}}. \tag{E9.6}$$

Figure 9.15 plots M_{SIN} as a function of spatial frequency for the desired pixel fill factors indicated. Note that for very small pixel fill factors, the modulation constant is invariant with spatial frequency and fixed at $M_{\mathrm{SIN}} = 0.707$.

Figure 9.16 presents a collection of MPTCs derived from different regions contained in the image of Fig. 9.17. Figure 9.18 shows the partial images characterized and labeled 2 through 5. Each image exhibits a different modulation factor depending on its contrast level. For example, the "rose" exhibits a modulation factor of $M_{\mathrm{I}} = 0.18$. This signal modulation is only 3.6 times greater than the 5% FPN

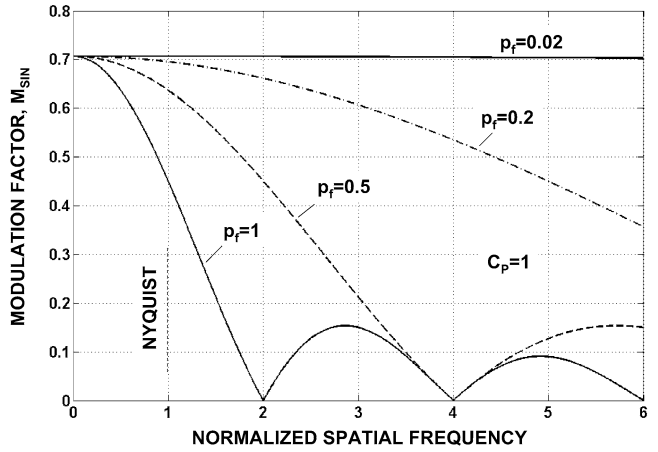

Figure 9.15 Modulation factor as a function of spatial frequency for different pixel fill factors.

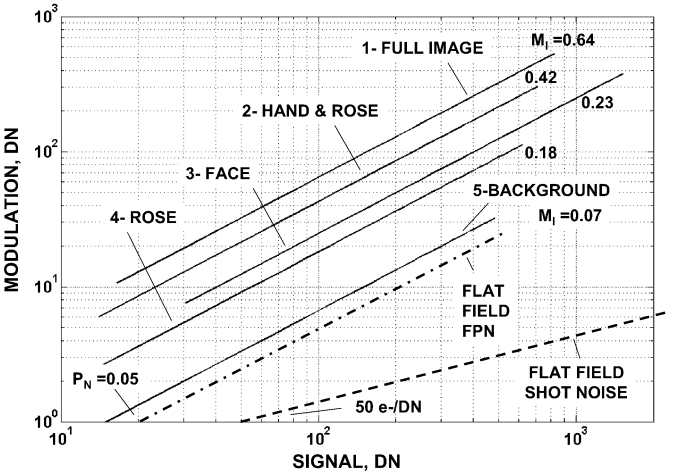

Figure 9.16 Modulation PTC responses for the images shown in Figs. 9.17–9.18.

Figure 9.17 Image used to generate modulation PTC response shown in Fig. 9.16.

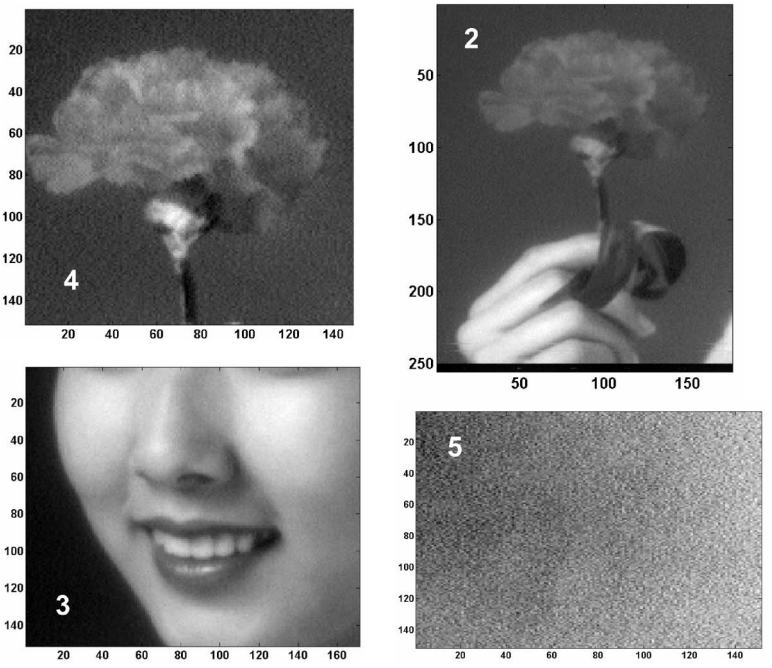

Figure 9.18 Images used to generate modulation PTC responses shown in Fig. 9.16.

measured from a flat-field exposure and therefore exhibits poor image quality. The background in image 5 shows FPN with a slight amount of shading in light. Hence, the image modulation factor is only slightly greater than FPN ($M_{\mathrm{I}} = 0.07$ versus $P_{\mathrm{N}} = 0.05$). FPN is greater than normal (i.e., $P_{\mathrm{N}} = 0.01$) for this sensor because of pixel color filters.

Important Points

1. For a nonuniform light source, FPN is proportional to the average signal level. Shot noise is equal to the square root of the average signal level, assuming that the contrast of the image is relatively low.
2. The amount of useful signal modulation for an image is derived from the contrast contained in the image.
3. The total modulation contained in an image is composed of signal modulation and noise sources (i.e., read noise, image shot, and FPN).
4. Image noise becomes equivalent to the noise contained in a flat-field image for very low-contrast scenes, assuming the average signal levels are the same.
5. Modulation photon transfer curves (MPTCs) are used to quantify the S/N performance for images (refer to Chapter 10).
6. The modulation constant derived by a MPTC specifies the amount of useful signal modulation contained in an image. The parameter is proportional to the incoming photon scene contrast and the pixel MTF.

Chapter 10
Signal-to-noise Performance

10.1 Uniform Stimulus

Data from a PTC provides signal-to-noise (S/N) performance directly (i.e., no further data taking is necessary). S/N is determined by dividing signal by noise for each PTC data point taken. The result is plotted as a function of signal in either DN or electron units.

In equation form, S/N for a uniform flat-field stimulus input is given by

$$\left[\frac{\mathrm{S}}{\mathrm{N}}\right]_{\mathrm{FF}} = \frac{S}{\sigma_{\mathrm{TOTAL}}} = \frac{S}{[\sigma^2_{\mathrm{READ}} + \eta_{\mathrm{i}} S + (P_{\mathrm{N}} S)^2]^{1/2}}. \tag{10.1}$$

Three different noise regimes exist over an S/N plot: read noise, shot noise, and FPN. S/N for the read noise regime is

$$\left[\frac{\mathrm{S}}{\mathrm{N}}\right]_{\mathrm{FF\_READ}} = \frac{S}{\sigma_{\mathrm{READ}}}, \tag{10.2}$$

which is proportional to signal and produces a slope 1 curve when plotted on log-log coordinates.

The S/N within the shot noise regime is

$$\left[\frac{\mathrm{S}}{\mathrm{N}}\right]_{\mathrm{FF\_SHOT}} = \frac{S}{\sigma_{\mathrm{SHOT}}} = \frac{S}{(\eta_{\mathrm{i}} S)^{1/2}} = \left(\frac{S}{\eta_{\mathrm{i}}}\right)^{1/2} \tag{10.3}$$

and increases by the square root of signal with a slope of $1/2$.

The S/N within the FPN regime is

$$\left[\frac{\mathrm{S}}{\mathrm{N}}\right]_{\mathrm{FF\_FPN}} = \frac{S}{\sigma_{\mathrm{FPN}}} = \frac{1}{P_{\mathrm{N}}} \tag{10.4}$$

and is independent of signal, producing a slope of 0. The FPN regime begins at a signal level of $1/P_{\mathrm{N}}^2$ of approximately 10,000 e^- for CCD and CMOS imagers. Beyond this signal level, S/N performance is fixed at about $1/P_{\mathrm{N}} = 100$.

Example 10.1

For the PTCs shown in Fig. 5.4, plot $[S/N]_{FF}$ as a function of signal. Assume these FPN quality factors: $P_N = 0.005$, 0.01, 0.02, 0.04, and 0.08.

Solution:
Figure 10.1 shows the desired plots and S/N regimes. For high signals, $[S/N]_{FF}$ asymptotically approaches $1/P_N$ [Eq. (10.4)] at a signal level of $1/P_N^2$ e^- [Eq. (3.14)]. Note that $[S/N]_{FF}$ appears to increase at full well. This behavior is only a full-well saturation artifact where pixel crosstalk reduces noise modulation. In reality, $[S/N]_{FF}$ actually dramatically decreases.

Example 10.2

For the flat-field quantum yield PTCs shown in Fig. 3.13, plot $[S/N]_{FF}$ as a function of signal.

Solution:
Figure 10.2 presents the desired plots. For a given signal level, $[S/N]_{FF}$ decreases by the square root of quantum yield [i.e., (Eq. 10.3)].

Signal-to-noise for x-ray imaging applications is severely limited by its shot noise. For example, $[S/N]_{FF} = 10$, given $\eta_i = 1000$ e^- (i.e., 3.65 keV x-ray photons) at a full-well level of 10^5 e^-. In comparison, visible photons exhibit a $[S/N]_{FF}$ of 316 for the same signal level.

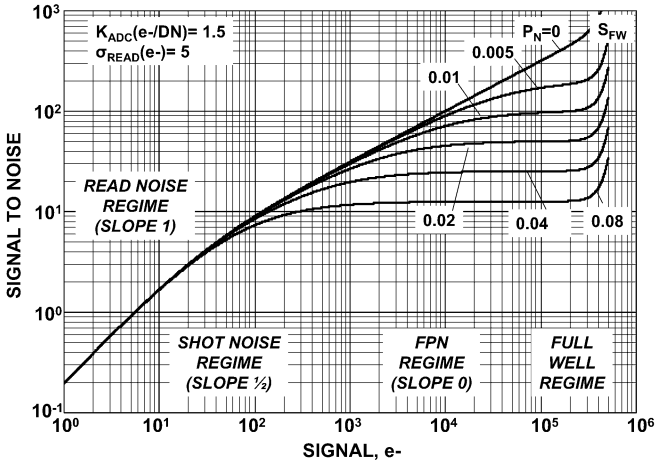

Figure 10.1 Signal-to-noise as a function of signal and different FPN quality factors (P_N) for the PTC data presented in Fig. 5.5 showing four S/N regimes.

Signal-to-noise degradation due to quantum yield is demonstrated in Fig 10.3, which shows sinusoidal images at two different quantum yields. Signal-to-noise is 10 times lower for the $\eta_i = 100$ x-ray image compared to the $\eta_i = 1$ visible image.

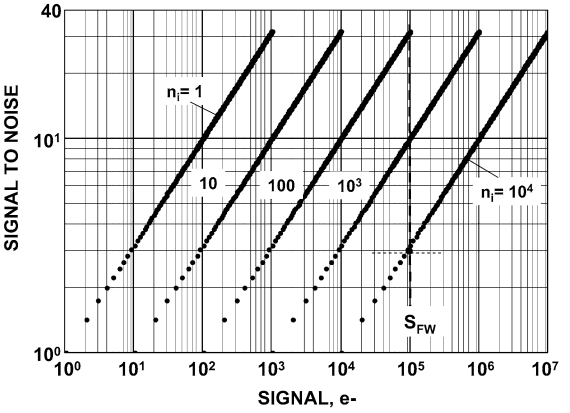

Figure 10.2 Signal-to-noise with signal and quantum yield.

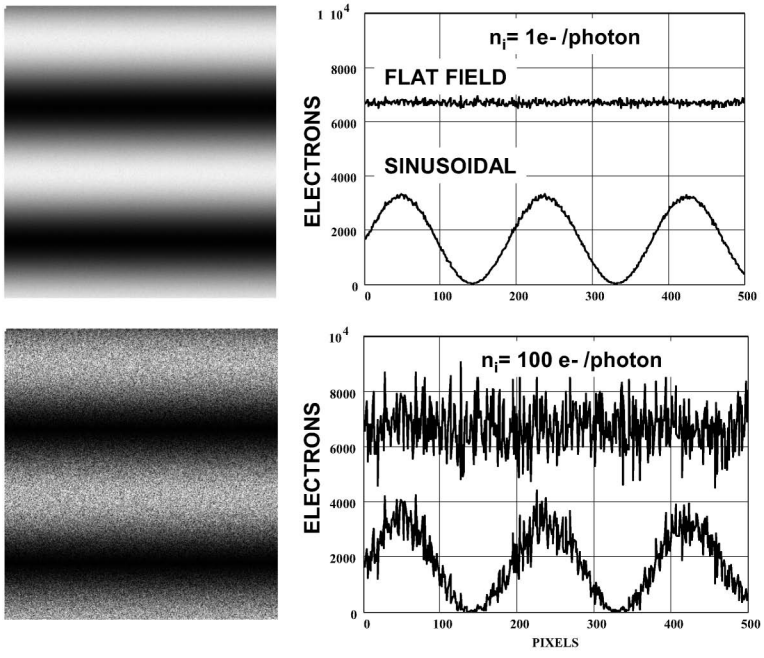

Figure 10.3 Images with corresponding video traces for visible ($\eta_i = 1$) and x-rays ($\eta_i = 100$).

10.2 Image S/N Performance

The general S/N relation for an image is defined as

$$\left[\frac{\mathrm{S}}{\mathrm{N}}\right]_{\mathrm{I}} = \frac{\delta_{\mathrm{I}}}{\sigma_{\mathrm{I\_TOTAL}}} = \frac{M_{\mathrm{I}} S_{\mathrm{I}}}{[\sigma^2_{\mathrm{READ}} + S_{\mathrm{I}} + (P_{\mathrm{N}} S_{\mathrm{I}})^2]^{1/2}}. \tag{10.5}$$

Discussions in Chapter 9 showed that the noise level was equivalent for a low-contrast image and a flat-field image when their average signal levels were the same (i.e., $S_{\mathrm{I}} = S$). Therefore, letting $S_{\mathrm{I}} = S$ in Eq. (10.5) produces

$$\left[\frac{\mathrm{S}}{\mathrm{N}}\right]_{\mathrm{I}} = M_{\mathrm{I}} \left[\frac{\mathrm{S}}{\mathrm{N}}\right]_{\mathrm{FF}}. \tag{10.6}$$

This important relation shows that optimizing flat-field S/N produces the highest S/N for an image. Note that $[\mathrm{S/N}]_{\mathrm{I}}$ is always less than $[\mathrm{S/N}]_{\mathrm{FF}}$ by the image modulation factor M_{I}.

Example 10.3

Assuming $S = S_{\mathrm{I}}$, determine $[\mathrm{S/N}]_{\mathrm{SIN}}$ for a sinusoidal image given the following parameters:

$$[\mathrm{S/N}]_{\mathrm{FF}} = 500$$
$$C_{\mathrm{P}} = 0.01$$
$$\mathrm{MTF}_{\mathrm{D}} = 0.5$$

Solution:
From Eqs. (10.6) and (E9.3),

$$\left[\frac{\mathrm{S}}{\mathrm{N}}\right]_{\mathrm{SIN}} = 0.707 C_{\mathrm{P}} \mathrm{MTF}_{\mathrm{D}} \left[\frac{\mathrm{S}}{\mathrm{N}}\right]_{\mathrm{FF}}. \tag{E10.1}$$

When the given parameters are substituted,

$$[\mathrm{S/N}]_{\mathrm{SIN}} = 0.707 \times 0.01 \times 0.5 \times 500 = 1.76.$$

Figure 10.4 plots $[\mathrm{S/N}]_{\mathrm{SIN}}$ and $[\mathrm{S/N}]_{\mathrm{FF}}$ for different C_{D} (with and without FPN) for sinusoidal and flat-field illumination. $[\mathrm{S/N}]_{\mathrm{FF}}$ represents a standard for the highest S/N that can be achieved (as observed in the figure). Quality images require S/N > 10, a level indicated by the dotted line in Fig. 10.4. As demonstrated in Fig. 10.4, for very low-contrast scenes, it is crucial to remove FPN. For example, Fig. 10.5 presents a sinusoidal image with and without FPN removal for $C_{\mathrm{D}} = 0.03125$. A S/N improvement of 3.5 is achieved when FPN is eliminated at full well (10^5 e^-).

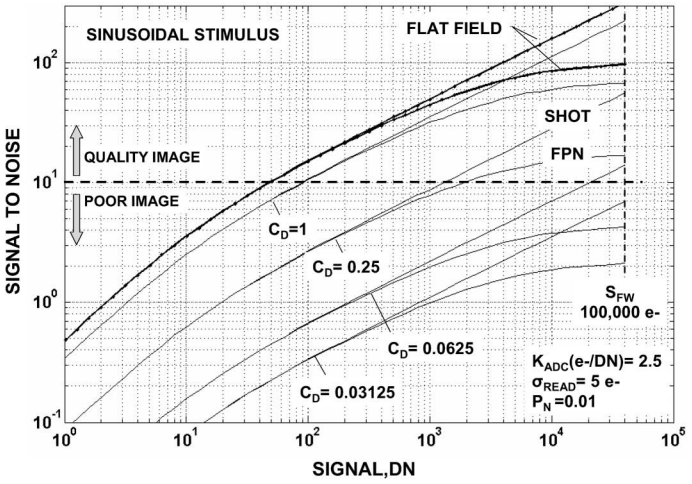

Figure 10.4 Sinusoidal S/N for different contrasts with and without FPN in comparison to flat-field responses.

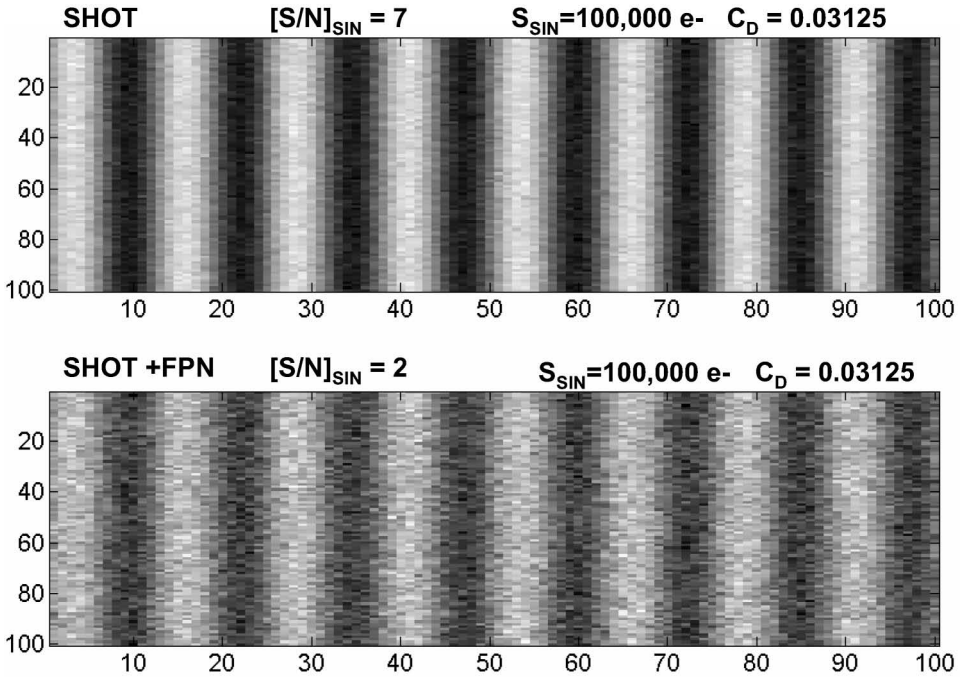

Figure 10.5 Images taken from Fig. 10.4 showing S/N improvement when FPN is removed.

Example 10.4

Derive the read noise, shot noise, and FPN S/N regimes for an image and a

sinusoidal stimulus. Also plot $[\mathrm{S/N}]_{\mathrm{SIN}}$, given $C_{\mathrm{D}} = 1$, 0.25, and 0.0625. Assume $P_{\mathrm{N}} = 0.02$ and $\sigma_{\mathrm{READ}} = 5$.

Solution:
The S/N regimes for an image are given by

$$\left[\frac{\mathrm{S}}{\mathrm{N}}\right]_{\mathrm{I\_READ}} = \frac{M_{\mathrm{I}} S_{\mathrm{I}}}{\sigma_{\mathrm{READ}}} = M_{\mathrm{I}}\left[\frac{\mathrm{S}}{\mathrm{N}}\right]_{\mathrm{FF\_READ}}, \tag{E10.2}$$

$$\left[\frac{\mathrm{S}}{\mathrm{N}}\right]_{\mathrm{I\_SHOT}} = M_{\mathrm{I}} S_{\mathrm{I}}^{1/2} = M_{\mathrm{I}}\left[\frac{\mathrm{S}}{\mathrm{N}}\right]_{\mathrm{FF\_SHOT}}, \tag{E10.3}$$

and

$$\left[\frac{\mathrm{S}}{\mathrm{N}}\right]_{\mathrm{I\_FPN}} = \frac{M_{\mathrm{I}}}{P_{\mathrm{N}}} = M_{\mathrm{I}}\left[\frac{\mathrm{S}}{\mathrm{N}}\right]_{\mathrm{FF\_FPN}}. \tag{E10.4}$$

Assuming $M_{\mathrm{I}} = 0.707 C_{\mathrm{D}} S_{\mathrm{SIN}}$, the corresponding S/N regimes for a sinusoidal image are

$$\left[\frac{\mathrm{S}}{\mathrm{N}}\right]_{\mathrm{SIN\_READ}} = 0.707 C_{\mathrm{D}} \frac{S_{\mathrm{SIN}}}{\sigma_{\mathrm{READ}}} = 0.707 C_{\mathrm{D}}\left[\frac{\mathrm{S}}{\mathrm{N}}\right]_{\mathrm{FF\_READ}}, \tag{E10.5}$$

$$\left[\frac{\mathrm{S}}{\mathrm{N}}\right]_{\mathrm{SIN\_SHOT}} = 0.707 C_{\mathrm{D}} S_{\mathrm{SIN}}^{1/2} = 0.707 C_{\mathrm{D}}\left[\frac{\mathrm{S}}{\mathrm{N}}\right]_{\mathrm{FF\_SHOT}}, \tag{E10.6}$$

and

$$\left[\frac{\mathrm{S}}{\mathrm{N}}\right]_{\mathrm{SIN\_FPN}} = 0.707 \frac{C_{\mathrm{D}}}{P_{\mathrm{N}}} = 0.707 C_{\mathrm{D}}\left[\frac{\mathrm{S}}{\mathrm{N}}\right]_{\mathrm{FF\_FPN}}. \tag{E10.7}$$

Figure 10.6 plots $[\mathrm{S/N}]_{\mathrm{SIN}}$ as a function of S_{SIN}. Each noise regime is labeled. $[\mathrm{S/N}]_{\mathrm{SIN}}$ reaches a maximum given by Eq. (E10.7), as indicated on the plot. For example, for $C_{\mathrm{D}} = 0.0625$, the S/N performance is only

$$[\mathrm{S/N}]_{\mathrm{SIN}} = 0.707 \times \frac{0.0625}{0.02} = 2.2.$$

The sinusoidal image in Fig. 10.7 demonstrates improved image quality as $[\mathrm{S/N}]_{\mathrm{SIN}}$ varies from 1 to 7. Although image quality is subjective, noticeably better imagery occurs when $[\mathrm{S/N}]_{\mathrm{SIN}} > 10$, where the "salt and pepper" noise is inconspicuous.

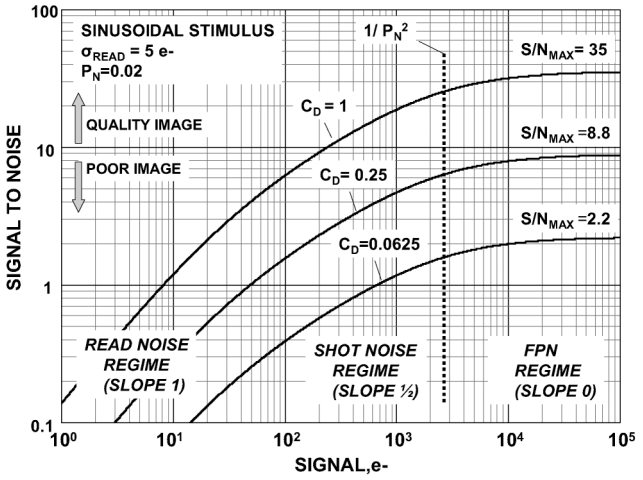

Figure 10.6 Sinusoidal S/N plots for Example 10.4.

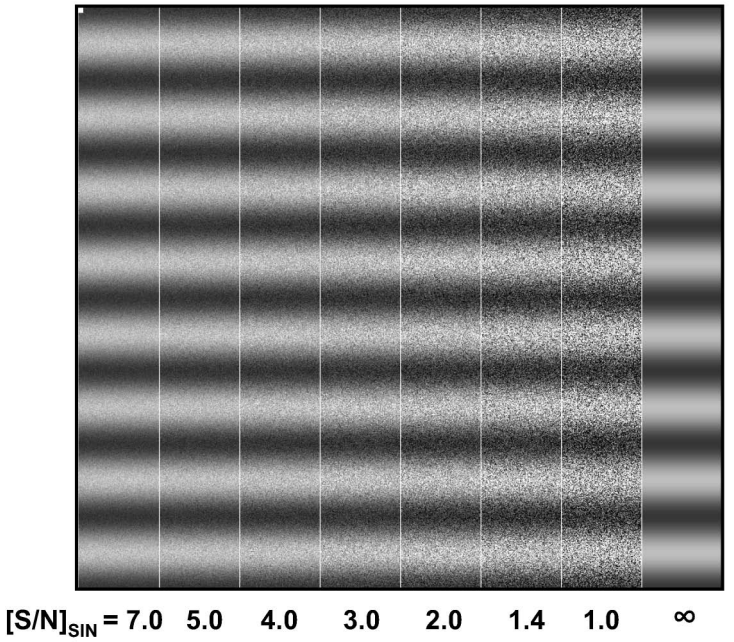

Figure 10.7 Sinusoidal image quality as a function of S/N compared to the ideal.

Example 10.5

Plot $[\mathrm{S/N}]_{\mathrm{I}}$ for the five images analyzed in Figs. 9.16–9.18 (given $M_{\mathrm{I}} = 0.64, 0.42,$

0.23, 0.18, and 0.07). Generate individual S/N plots, with and without FPN. Also show flat-field responses. Also calculate $[S/N]_I$ for image 4 (the "rose" image) with and without FPN at a signal level of 1000 DN (50,000 e^-). Assume $P_N = 0.05$, $\sigma_{READ} = 15\ e^-$, and $K_{ADC}(e^-/DN) = 50$.

Solution:
From Eq. (10.5), the $[S/N]_I$ is given by

$$\left[\frac{S}{N}\right]_I = M_I \frac{S_I}{[15^2 + S_I + (0.05S_I)^2]^{1/2}}. \tag{E10.8}$$

Figure 10.8 plots Eq. (E10.8) with and without FPN for the images, along with flat field S/N curves. Note that images 2–5 fall below the criteria S/N > 10 for a quality image because of FPN. When FPN is removed, the images are all acceptable for a signal level of >100 DN (5000 e^-). From Eq. (E10.8), the $[S/N]_I$ for image 4 with FPN is

$$[S/N]_I = 0.18 \times \frac{50,000}{[15^2 + 50,000 + (0.05 \times 50,000)^2]^{1/2}}$$

$$[S/N]_I = 3.59.$$

From Eq. (E10.8), the $[S/N]_I$ for image 4 without FPN is

$$[S/N]_I = 0.18 \times \frac{50,000}{(15^2 + 50,000)^{1/2}}$$

$$[S/N]_I = 40.3.$$

Note that the images shown in Fig. 9.18 are printed with FPN.

10.3 Flat Fielding

The S/N for a uniform illumination after FPN is removed by flat fielding is given as

$$\left[\frac{S}{N}\right]_{FF\_COR} = \frac{S}{\left[\sigma_{READ}^2 + S\left(1 + \frac{S}{Q_{FF}}\right)\right]^{1/2}}. \tag{10.7}$$

Assuming read noise is negligible, three special conditions apply to Eq. (10.7):

$$\left[\frac{S}{N}\right]_{FF\_COR} = Q_{FF}^{1/2} \quad \frac{S}{Q_{FF}} \gg 1, \tag{10.8}$$

$$\left[\frac{S}{N}\right]_{FF\_COR} = S^{1/2} \quad \frac{S}{Q_{FF}} \ll 1, \tag{10.9}$$

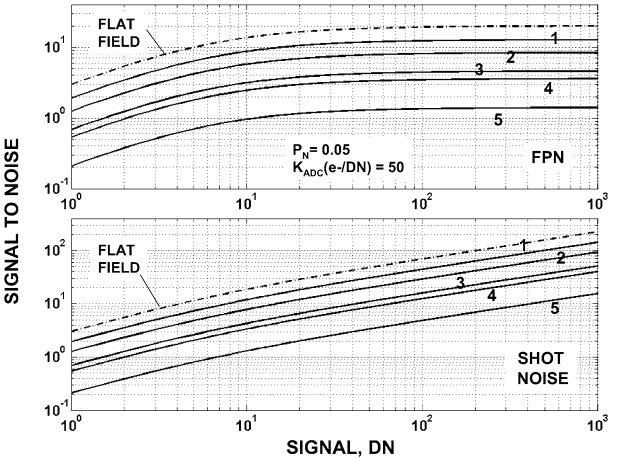

Figure 10.8 Signal-to-noise performance for the images presented in Figs. 9.17–9.18 compared to flat-field S/N with and without FPN.

and

$$\left[\frac{\mathrm{S}}{\mathrm{N}}\right]_{\mathrm{FF\_COR}} = \left(\frac{S}{2}\right)^{1/2} \quad S = Q_{\mathrm{FF}}. \tag{10.10}$$

Equation (10.8) suggests that S/N is limitless by making Q_{FF} as large as desired. However, the condition $S/Q_{\mathrm{FF}} \gg 1$ is limited by the sensor's full-well performance. Equation (10.9) is the best performance that can be achieved (i.e., shot noise limited).

Example 10.6

For the PTC in Fig. 5.4, plot the $[\mathrm{S/N}]_{\mathrm{FF\_COR}}$. Assume these flat-field quality factors: $Q_{\mathrm{FF}} = 2 \times 10^1$, 2×10^2, 2×10^3, 2×10^4, and 2×10^5 e^-.

Solution:
Figure 10.9 presents the desired curves. $[\mathrm{S/N}]_{\mathrm{FF\_COR}}$ nearly reaches the ideal shot noise limited response when $Q_{\mathrm{FF}} = 2 \times 10^5$ (e.g., $N_{\mathrm{FF}} = 1$ and S_{FW}). Further improvement is achieved by increasing N_{FF}.

Assuming that read noise is negligible, the S/N improvement achieved by flat fielding is

$$\left[\frac{\mathrm{S}}{\mathrm{N}}\right]_{\mathrm{FF\_IM}} = \frac{[\mathrm{S/N}]_{\mathrm{FF\_COR}}}{[\mathrm{S/N}]_{\mathrm{FF}}} = \left[\frac{1 + SP_{\mathrm{N}}^2}{1 + \dfrac{S}{Q_{\mathrm{FF}}}}\right]^{1/2}. \tag{10.11}$$

Note that when $Q_{\mathrm{FF}} = 1/P_{\mathrm{N}}^2$, then $[\mathrm{S/N}]_{\mathrm{FF\_IM}} = 1$ and is independent of signal. Also, when $S/Q_{\mathrm{FF}} \ll 1$ and $SP_{\mathrm{N}} \gg 1$, then $[\mathrm{S/N}]_{\mathrm{FF\_IM}} = P_{\mathrm{N}} S^{1/2}$.

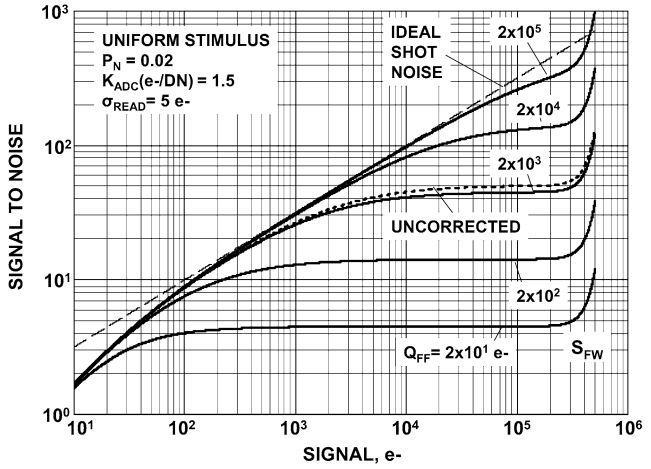

Figure 10.9 Signal-to-noise for a uniform stimulus after flat fielding for different $Q_{\rm FF}$ compared to the ideal shot noise response.

Example 10.7

Plot $[\mathrm{S/N}]_{\rm FF\_IM}$ as a function of signal. Assume $P_{\rm N} = 0.01$, and $Q_{\rm FF} = 10^2$, 10^3, 10^4, 10^5, 10^6, and 10^7 e^-.

Solution:
The desired plots, from Eq. (10.11), are presented in Fig. 10.10. For signals less

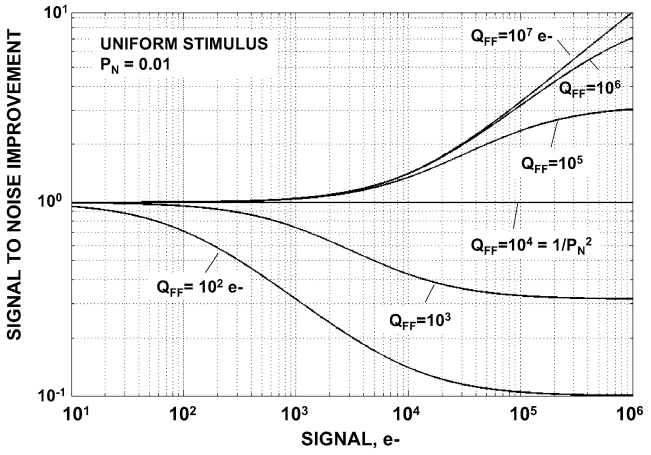

Figure 10.10 Signal-to-noise improvement with signal and different flat-fielding quality factors.

than 1000 e^-, flat fielding serves no purpose because shot noise is greater than FPN. In fact, if $Q_{\mathrm{FF}} < 1/P_{\mathrm{N}}^2$, the process will actually degrade S/N.

The S/N that is achieved for a corrected image is given by

$$\left[\frac{\mathrm{S}}{\mathrm{N}}\right]_{\mathrm{I\_COR}} = \frac{M_{\mathrm{I}} S_{\mathrm{I}}}{\left[\sigma_{\mathrm{READ}}^2 + S_{\mathrm{I}}\left(1 + \dfrac{S_{\mathrm{I}}}{Q_{\mathrm{FF}}}\right)\right]^{1/2}}, \tag{10.12}$$

which, for low-contrast images, is equivalent to

$$\left[\frac{\mathrm{S}}{\mathrm{N}}\right]_{\mathrm{I\_COR}} = M_{\mathrm{I}}\left[\frac{\mathrm{S}}{\mathrm{N}}\right]_{\mathrm{FF\_COR}}. \tag{10.13}$$

Also, from Eqs. (10.5) and (10.12), the improvement for a low-contrast image after flat fielding is

$$\left[\frac{\mathrm{S}}{\mathrm{N}}\right]_{\mathrm{I\_IM}} = \frac{[\mathrm{S/N}]_{\mathrm{I\_COR}}}{[\mathrm{S/N}]_{\mathrm{I}}} = \frac{1 + P_{\mathrm{N}}^2 S_{\mathrm{I}}}{1 + \dfrac{S_{\mathrm{I}}}{Q_{\mathrm{FF}}}} = \left[\frac{\mathrm{S}}{\mathrm{N}}\right]_{\mathrm{FF}}. \tag{10.14}$$

The maximum S/N that can be achieved for an image when FPN is optimally ($S_{\mathrm{I}}/Q_{\mathrm{FF}} \ll 1$) removed is given by

$$\left[\frac{\mathrm{S}}{\mathrm{N}}\right]_{\mathrm{I\_MAX}} = M_{\mathrm{I}}(S_{\mathrm{FW}})^{1/2}. \tag{10.15}$$

Figure 10.11 presents a low-contrast sinusoidal image used to demonstrate S/N improvement by flat fielding. Figure 10.12 shows the assumed photon input and electron output responses for the parameters indicated. Q_{FF} varies from 1 to 10^4 e^-, as indicated in Fig. 10.11. The S/N surpasses the raw S/N response when $Q_{\mathrm{FF}} = 1/P_{\mathrm{N}}^2 = 2500$ e^-. The raw and ideal shot noise responses are also shown on the right-hand side of the plot.

Example 10.8

Derive the sinusoidal $[\mathrm{S/N}]_{\mathrm{SIN\_COR}}$ after FPN is removed by flat fielding.

Solution:
From Eq. (E9.3), the sinusoidal modulation factor is given by

$$M_{\mathrm{SIN}} = 0.707 \times C_{\mathrm{D}}.$$

Substituting M_{SIN} into Eq. (10.12) produces

$$\left[\frac{\mathrm{S}}{\mathrm{N}}\right]_{\mathrm{SIN\_COR}} = \frac{0.707 C_{\mathrm{D}} S_{\mathrm{SIN}}}{\left[\sigma_{\mathrm{READ}}^2 + S_{\mathrm{SIN}}\left(1 + \dfrac{S_{\mathrm{SIN}}}{Q_{\mathrm{FF}}}\right)\right]^{1/2}}, \tag{E10.9}$$

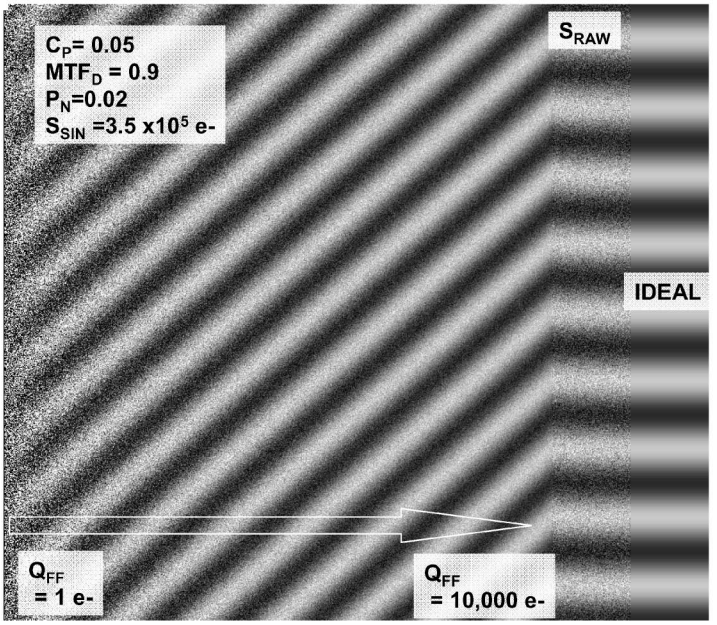

Figure 10.11 Image S/N improvement versus Q_{FF} compared to a raw response with FPN and the ideal response without noise.

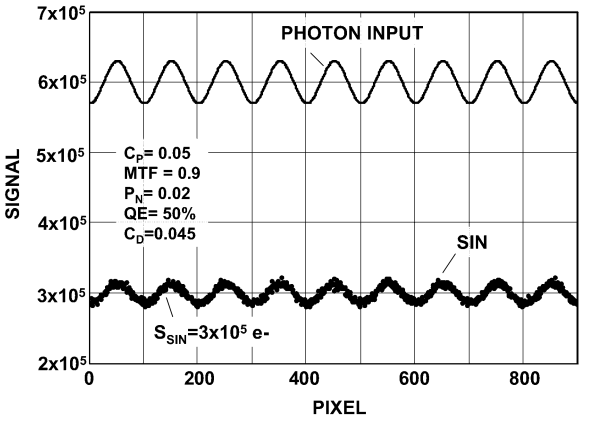

Figure 10.12 Photon and detector signals assumed for Fig. 10.11.

which is equivalent to

$$\left[\frac{\mathrm{S}}{\mathrm{N}}\right]_{\mathrm{SIN\_COR}} = 0.707 C_{\mathrm{D}} \left[\frac{\mathrm{S}}{\mathrm{N}}\right]_{\mathrm{FF\_COR}}. \tag{E10.10}$$

The three special conditions noted above also apply to Eq. (E10.9) and yield

$$\left[\frac{\mathrm{S}}{\mathrm{N}}\right]_{\mathrm{SIN\_COR}} = 0.707 C_{\mathrm{D}} Q_{\mathrm{FF}}^{1/2}, \quad S_{\mathrm{SIN}}/Q_{\mathrm{FF}} \gg 1; \tag{E10.11}$$

$$\left[\frac{\mathrm{S}}{\mathrm{N}}\right]_{\mathrm{SIN\_COR}} = 0.707 C_{\mathrm{D}} S_{\mathrm{SIN}}^{1/2}, \quad S_{\mathrm{SIN}}/Q_{\mathrm{FF}} \ll 1; \tag{E10.12}$$

and

$$\left[\frac{\mathrm{S}}{\mathrm{N}}\right]_{\mathrm{SIN\_COR}} = 0.707 C_{\mathrm{D}} \left(\frac{S_{\mathrm{SIN}}}{2}\right)^{1/2}, \quad S_{\mathrm{SIN}} = Q_{\mathrm{FF}}. \tag{E10.13}$$

Example 10.9

For the image in Fig. 10.11, plot $[\mathrm{S/N}]_{\mathrm{SIN\_COR}}$ as a function of S_{SIN} for the following flat-field quality factors: $Q_{\mathrm{FF}} = 10$; 100; 1,000; and 10,000 e^-. Also plot the uncorrected S/N. Assume $P_{\mathrm{N}} = 0.02$.

Solution:
From Eq. (E10.9), Figure 10.13 shows the desired curves, including the ideal shot noise curve and uncorrected responses.

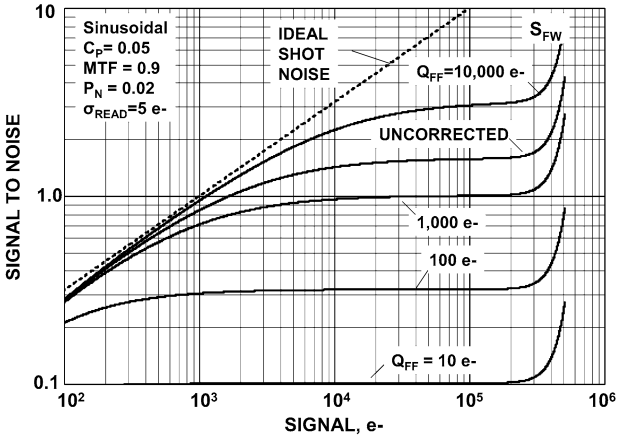

Figure 10.13 S/N versus signal (S_{SIN}) for Fig. 10.11.

Example 10.10

Plot $[\mathrm{S/N}]_{\mathrm{SIN\_MAX}}$ as a function of full well, given $C_{\mathrm{DET}} = 1.0$, 0.1, 0.01, and 0.001. Assume that FPN has been removed from the image.

Solution:
From Eq. (E9.3), the sinusoidal modulation factor is given by

$$M_{\mathrm{SIN}} = 0.707 \times C_{\mathrm{D}}.$$

From Eq. (10.15),

$$\left[\frac{\mathrm{S}}{\mathrm{N}}\right]_{\mathrm{SIN\_MAX}} = 0.707 C_{\mathrm{DET}} (S_{\mathrm{FW}})^{1/2}.$$

Figure 10.14 presents the desired plots. Note that a detector contrast of 1% requires a full well of 2×10^6 e^- for good S/N performance (>10).

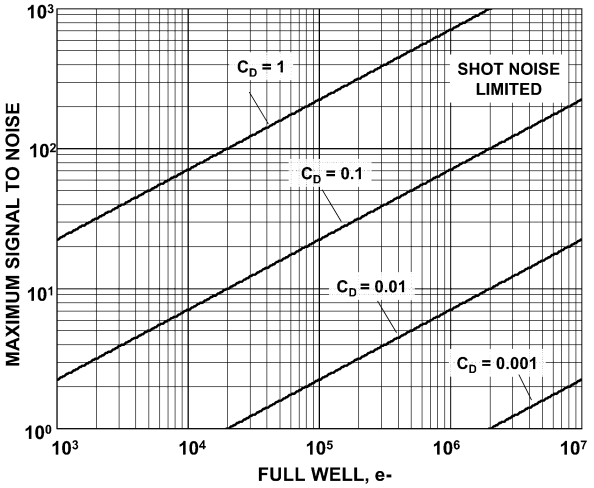

Figure 10.14 Maximum S/N versus full well for different detector contrasts.

10.4 Image Averaging

Multiple frames can be averaged to improve S/N performance beyond the standard shot noise limit. The technique works as long as the images remain stationary during the data-taking process.

For uniform illumination, the S/N for frame averaging is given by

$$\left[\frac{\mathrm{S}}{\mathrm{N}}\right]_{\mathrm{FF\_AV}} = \frac{S}{\left[\dfrac{\sigma^2_{\mathrm{READ}} + S}{N_{\mathrm{AV}}} + (P_{\mathrm{N}}S)^2\right]^{1/2}}, \tag{10.16}$$

where N_{AV} is the number of frames averaged. Note that random noise sources (shot noise and read noise) are reduced by $N_{\mathrm{AV}}^{1/2}$. However, frame averaging does not improve S/N when FPN is present, unless the signal is smaller than $<1/{P_{\mathrm{N}}}^2$.

When flat fielding is employed to remove FPN, Eq. (10.16) simplifies to

$$\left[\frac{\mathrm{S}}{\mathrm{N}}\right]_{\mathrm{FF\_AV}} = \frac{SN_{\mathrm{AV}}^{1/2}}{(\sigma^2_{\mathrm{READ}} + S)^{1/2}} = N_{\mathrm{AV}}^{1/2}\left[\frac{\mathrm{S}}{\mathrm{N}}\right]_{\mathrm{FF}}. \tag{10.17}$$

And when read noise is negligible, Eq. (10.17) reduces to

$$\left[\frac{\mathrm{S}}{\mathrm{N}}\right]_{\mathrm{FF\_AV}} = (SN_{\mathrm{AV}})^{1/2}. \tag{10.18}$$

Figure 10.15 plots Eqs. (10.16) and (10.17) for different N_{AV}. S/N is limited to 50 when FPN is present (i.e., $1/P_{\mathrm{N}} = 1/0.02$). In comparison, S/N can be improved by more than an order of magnitude when FPN is removed and 10 images are averaged at a signal level of 10^5 e^-.

The S/N when multiple images are averaged is given by

$$\left[\frac{\mathrm{S}}{\mathrm{N}}\right]_{\mathrm{I\_AV}} = \frac{M_{\mathrm{I}}S_{\mathrm{I}}}{\left[\dfrac{\sigma^2_{\mathrm{READ}} + S_{\mathrm{I}}}{N_{\mathrm{AV}}} + (P_{\mathrm{N}}S_{\mathrm{I}})^2\right]^{1/2}} = M_{\mathrm{I}}\left[\frac{\mathrm{S}}{\mathrm{N}}\right]_{\mathrm{FF\_AV}}, \tag{10.19}$$

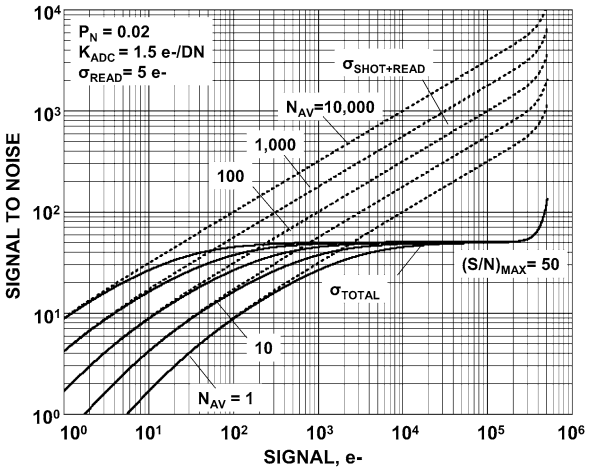

Figure 10.15 S/N versus signal for different frame averages with and without FPN.

and after flat fielding,

$$\left[\frac{\mathrm{S}}{\mathrm{N}}\right]_{\mathrm{I\_AV}} = \frac{M_{\mathrm{I}} S_{\mathrm{I}} N_{\mathrm{AV}}^{1/2}}{(\sigma_{\mathrm{READ}}^2 + S_{\mathrm{I}})^{1/2}} = M_{\mathrm{I}} \left[\frac{\mathrm{S}}{\mathrm{N}}\right]_{\mathrm{FF\_AV}} = M_{\mathrm{I}} N_{\mathrm{AV}}^{1/2} \left[\frac{\mathrm{S}}{\mathrm{N}}\right]_{\mathrm{FF}}. \quad (10.20)$$

Figure 10.16 presents simulated images that demonstrate the benefits of flat fielding and frame averaging when applied together on a very low-contrast scene. Figure 10.16(a) shows a sinusoidal image of low contrast ($C_{\mathrm{D}} = 0.0025$, $S_{\mathrm{SIN}} = 10^5$ e$^-$). Signal modulation is barely visible because FPN is present ($P_{\mathrm{N}} = 0.01$). Figure 10.16(b) is produced after FPN is removed, showing an improved response. Figure 10.16(c) is the product after 100 images are averaged, thereby increasing the S/N by a factor of 10. For comparison, Fig. 10.16(d) shows the response without noise.

Example 10.11

For each image shown in Fig. 10.16, determine $[\mathrm{S/N}]_{\mathrm{SIN\_AV}}$. As used in Fig. 10.16, assume the following parameters: $C_{\mathrm{D}} = 0.0025$, $S_{\mathrm{SIN}} = 10^5$ e$^-$, $P_{\mathrm{N}} = 0.01$, $N_{\mathrm{AV}} = 100$, and $\sigma_{\mathrm{READ}} =$ negligible.

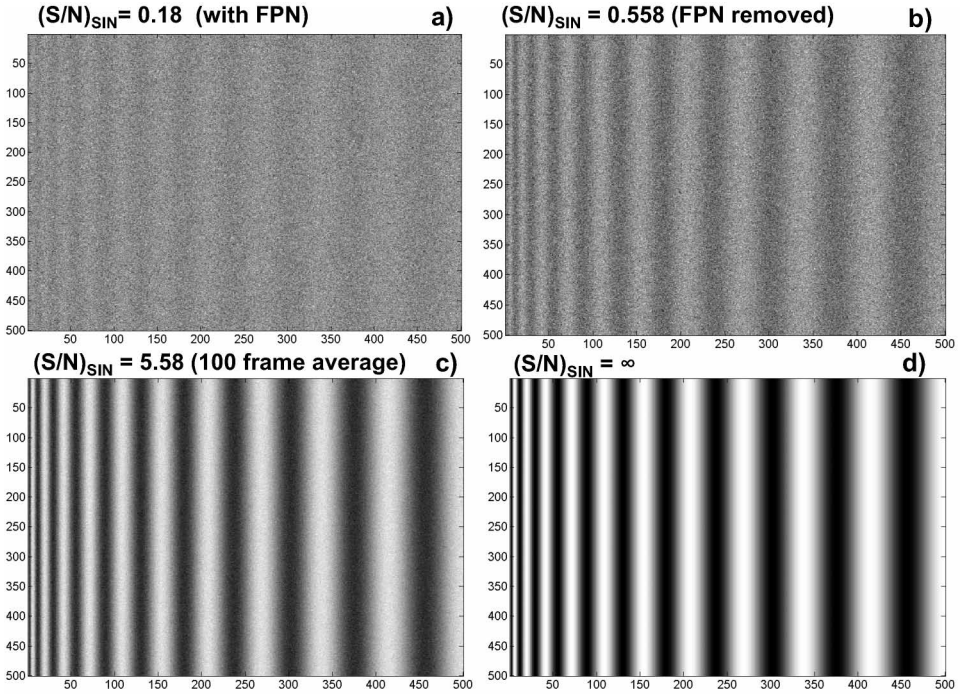

Figure 10.16 Raw, FPN removed, frame-averaged, and ideal sinusoidal responses.

Solution:
From Eq. (10.19), the sinusoidal S/N with frame averaging is given by

$$\left[\frac{\mathrm{S}}{\mathrm{N}}\right]_{\mathrm{SIN\_AV}} = \frac{0.707 C_{\mathrm{D}} S_{\mathrm{SIN}}}{\left[\dfrac{\sigma^2_{\mathrm{READ}} + S_{\mathrm{SIN}}}{N_{\mathrm{AV}}} + (P_{\mathrm{N}} S_{\mathrm{SIN}})^2\right]^{1/2}}; \tag{E10.14}$$

and after flat fielding [Eq. (10.20)],

$$\left[\frac{\mathrm{S}}{\mathrm{N}}\right]_{\mathrm{SIN\_AV}} = \frac{0.707 C_{\mathrm{D}} S_{\mathrm{SIN}} N_{\mathrm{AV}}^{1/2}}{(\sigma^2_{\mathrm{READ}} + S_{\mathrm{SIN}})^{1/2}}. \tag{E10.15}$$

Figure 10.16(a) with FPN:

From Eq. (E10.14) and $N_{\mathrm{AV}} = 1$,

$$[\mathrm{S/N}]_{\mathrm{SIN\_AV}} = \frac{0.707 \times 0.0025 \times 10^5}{[10^5 + (0.01 \times 10^5)^2]^{1/2}} = 0.178.$$

Figure 10.16(b) without FPN:

From Eq. (E10.15) and $N_{\mathrm{AV}} = 1$,

$$[\mathrm{S/N}]_{\mathrm{SIN\_AV}} = \frac{0.707 \times 0.0025 \times 10^5}{(10^5)^{1/2}} = 0.558.$$

Figure 10.16(c) when averaging is applied:

From Eq. (E10.15) and $N_{\mathrm{AV}} = 100$,

$$[\mathrm{S/N}]_{\mathrm{SIN\_AV}} = \frac{0.707 \times 0.0025 \times 10^5}{(10^5/100)^{1/2}} = 5.58.$$

Figure 10.16(d) exhibits a S/N of infinity without noise.

10.5 On-Chip Averaging

CCDs offer the feature of *on-chip averaging*, where a specified number of rows and/or columns are summed and then read out. For example, a $1k \times 1k$ CCD imager can be formatted into a 500×500 imager by a 2 column $\times$ 2 row summation. The general flat-field S/N relation for on-chip summation is

$$\left[\frac{\mathrm{S}}{\mathrm{N}}\right]_{\mathrm{FF\_SUM}} = \frac{N_{\mathrm{X}} N_{\mathrm{Y}} S}{[\sigma^2_{\mathrm{READ}} + N_{\mathrm{X}} N_{\mathrm{Y}} S(S P_{\mathrm{N}}^2 + 1)]^{1/2}}, \tag{10.21}$$

where N_{X} and N_{Y} are the number of pixels summed in the column and the row directions, respectively.

The S/N for the three noise regimes are

$$\left[\frac{\mathrm{S}}{\mathrm{N}}\right]_{\mathrm{FF\_SUM\_READ}} = \frac{N_{\mathrm{X}}N_{\mathrm{Y}}S}{\sigma_{\mathrm{READ}}} = N_{\mathrm{X}}N_{\mathrm{Y}}\left[\frac{\mathrm{S}}{\mathrm{N}}\right]_{\mathrm{FF}}, \tag{10.22}$$

$$\left[\frac{\mathrm{S}}{\mathrm{N}}\right]_{\mathrm{FF\_SUM\_SHOT}} = (N_{\mathrm{X}}N_{\mathrm{Y}}S)^{1/2} = (N_{\mathrm{X}}N_{\mathrm{Y}})^{1/2}\left[\frac{\mathrm{S}}{\mathrm{N}}\right]_{\mathrm{FF}}, \tag{10.23}$$

and

$$\left[\frac{\mathrm{S}}{\mathrm{N}}\right]_{\mathrm{FF\_SUM\_FPN}} = \frac{(N_{\mathrm{X}}N_{\mathrm{Y}})^{1/2}}{P_{\mathrm{N}}} = (N_{\mathrm{X}}N_{\mathrm{Y}})^{1/2}\left[\frac{\mathrm{S}}{\mathrm{N}}\right]_{\mathrm{FF}}. \tag{10.24}$$

The S/N for an image when pixel summing is employed is

$$\left[\frac{\mathrm{S}}{\mathrm{N}}\right]_{\mathrm{I\_SUM}} = \frac{N_{\mathrm{X}}N_{\mathrm{Y}}M_{\mathrm{I}}S_{\mathrm{I}}}{[\sigma^2_{\mathrm{READ}} + N_{\mathrm{X}}N_{\mathrm{Y}}S_{\mathrm{I}}(S_{\mathrm{I}}P^2_{\mathrm{N}} + 1)]^{1/2}} = M_{\mathrm{I}}\left[\frac{\mathrm{S}}{\mathrm{N}}\right]_{\mathrm{FF\_SUM}}. \tag{10.25}$$

Example 10.12

Plot the flat-field S/N with and without FPN when on-chip summation is applied. Assume $P_{\mathrm{N}} = 0.01$, $\sigma_{\mathrm{READ}} = 10\ \mathrm{e}^-$, and use the following summing formats:

$$N_{\mathrm{X}} = 1 \quad N_{\mathrm{Y}} = 1$$
$$N_{\mathrm{X}} = 2 \quad N_{\mathrm{Y}} = 2$$
$$N_{\mathrm{X}} = 5 \quad N_{\mathrm{Y}} = 5$$

Solution:
From Eq. (10.21), Figs. 10.17 and 10.18 present the desired plots.

Important Points

1. Flat-field S/N is limited to approximately 100 $(1/P_{\mathrm{N}})$ for CCD and CMOS imagers. FPN dominates S/N performance for signals greater than about 10,000 e^- $(1/P^2_{\mathrm{N}})$.
2. Shot noise limited performance is the best S/N performance that can be achieved. Maximum S/N performance is equal to the square root of full well.
3. Flat-field S/N performance decreases by the square root of quantum yield. Visible and near-IR photons $(\eta_{\mathrm{i}} = 1)$ produce the highest S/N performance.
4. A uniform flat field produces the highest S/N. Image S/N is always less than flat-field S/N by the modulation constant, M_{I}.
5. S/N performance for low-contrast images is proportional to flat-field S/N.
6. Quality images require S/N > 10.

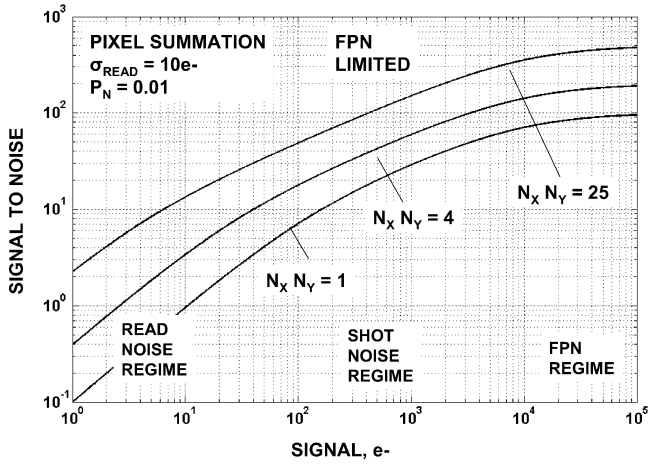

Figure 10.17 S/N with signal for different on-chip summing formats with FPN.

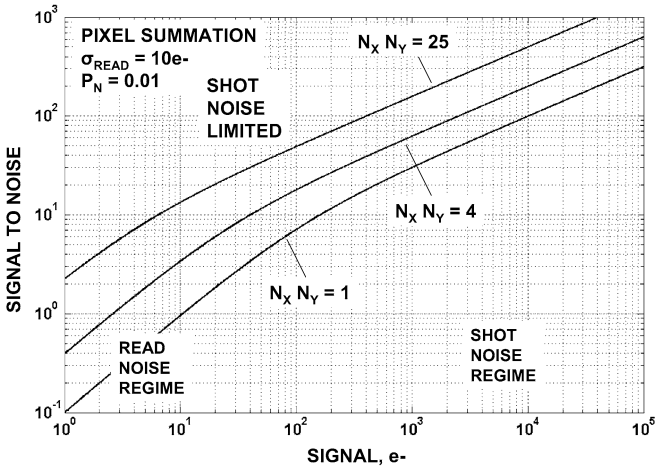

Figure 10.18 S/N with signal for different on-chip summing formats without FPN.

7. Averaging images increases S/N by the square root of the number of frames averaged, assuming FPN is removed. Averaging images does not improve S/N when FPN dominates.
8. Pixel summing increases S/N by the square root of the number of pixels summed, including images that are FPN limited.

Chapter 11
Read Noise

11.1 Introduction

The first data points collected by a PTC typically measure the read noise floor. This chapter reviews common CCD and CMOS read noise sources and their unique influence on PTCs. Table 11.1 lists the noise types in the order they will be presented. The general read noise equation is given by

$$\sigma_{\mathrm{READ}} = (\sigma_{\mathrm{SF}}^2 + \sigma_{\mathrm{RESET}}^2 + \sigma_{\mathrm{D\_SHOT}}^2 + \sigma_{\mathrm{D\_FPN}}^2 + \sigma_{\mathrm{ADC}}^2 + \sigma_{\mathrm{OFF\_FPN}}^2 + \sigma_{\mathrm{SY}}^2)^{1/2}. \tag{11.1}$$

It is important to point out that Eq. (11.1) is applied to all equations in the previous chapters that contain the term σ_{READ}.

11.2 Pixel Source Follower Noise

Ultimately, a pixel's source follower MOSFET, shown in Fig. 4.3, limits the read noise floor. Fortunately, other noise sources can usually be reduced to negligible levels relative to source follower noise. For example, dark current noise is removed by cooling the sensor to a low operating temperature. Remarkably, source follower noise for high-performance CMOS and CCD cameras have been driven down to approximately one noise electron rms.

To provide the reader some insight to the variables behind source follower read noise, we present a general formula that theoretically determines its amplitude. In

Table 11.1 Types of noise.

Noise Source	Symbol
Pixel source follower noise	σ_{SF}
Sense node reset noise	σ_{RESET}
Thermal dark current shot noise	$\sigma_{\mathrm{D\_SHOT}}$
Dark current FPN	$\sigma_{\mathrm{D\_FPN}}$
ADC quantizing noise	σ_{ADC}
Offset FPN	σ_{OFF}
System noise	σ_{SY}

electron units, the noise source is given by

$$\sigma_{\mathrm{SF}} = \frac{1}{\mathrm{A_{SN}A_{SF}}(1 - e^{-t_{\mathrm{s}}/\tau_{\mathrm{D}}})} \left[\int_0^{\infty} S_{\mathrm{DET}}(f) H_{\mathrm{CDS}}(f) df \right]^{1/2}, \tag{11.2}$$

where σ_{SF} is the source follower noise (e^- rms), f is electrical frequency (Hz), t_{s} is the correlated double sampling (CDS) sample-to-sample time (sec), and τ_{D} is the CDS dominant time constant.[1] $H_{\mathrm{CDS}}(f)$ is the CDS transfer function, expressed as

$$H_{\mathrm{CDS}}(f) = \left[\frac{1}{1 + (2\pi f \tau_{\mathrm{D}})^2} \right] [2 - 2\cos(2\pi f t_{\mathrm{s}})]. \tag{11.3}$$

The second term of Eq. (11.3) describes the frequency response of the CDS processor. The first term sets the CDS bandwidth for white noise rejection before sampling takes place through

$$B = \frac{1}{4\tau_{\mathrm{D}}}, \tag{11.4}$$

where B is defined as the equivalent noise bandwidth (Hz). The dominant time constant is nominally set to $\tau_{\mathrm{D}} = 0.5 t_{\mathrm{s}}$ for high-performance camera systems.

Pixel source follower MOSFET noise is composed of three components: white noise, flicker noise, and random telegraph signal (RTS) noise. In the frequency domain, the source follower's output noise power spectrum, $S_{\mathrm{DET}}(f)$, is given by

$$S_{\mathrm{DET}}(f) = W(f)^2 \left(1 + \frac{f_{\mathrm{c}}}{f} \right) + S_{\mathrm{RTS}}(f), \tag{11.5}$$

where $W(f)$ is the thermal white noise (V/Hz$^{1/2}$), f_{c} is the flicker noise corner frequency (i.e., the frequency where white and flicker noise are equal), and $S_{\mathrm{RTS}}(f)$ is the RTS noise power given by

$$S_{\mathrm{RTS}}(f) = \frac{2\Delta I^2 \tau_{\mathrm{RTS}}}{4 + (2\pi f \tau_{\mathrm{RTS}})^2}, \tag{11.6}$$

where τ_{RTS} is the RTS characteristic time constant (sec), and ΔI is the source follower current modulation induced by RTS (A). For CCD imagers, source follower noise is typically limited by flicker noise, whereas CMOS detectors are limited by RTS.[5]

Example 11.1

Plot the source follower read noise as a function of CDS sample-to-sample time, given the following parameters:

$W(f) = 15$ nV/Hz$^{1/2}$
$A_{\mathrm{SF}} = 0.9$ V/V

$$\tau_{\mathrm{D}} = 0.5t_{\mathrm{s}}$$
$$A_{\mathrm{SN}} = 6\ \mu\mathrm{V/e}^{-}$$
$$S_{\mathrm{RTS}}(f) = 0$$

Assume $f_{\mathrm{c}} = 10^3$, 10^4, 10^5, and 10^6 Hz.

Solution:
Applying Eq. (11.2), Fig. 11.1 shows the desired noise plots. Note that read noise decreases by the square root of t_{s} (or $2\tau_{\mathrm{D}}$) and levels out when the $1/f$ corner frequency is encountered (approximately at $t_{\mathrm{s}} = 1/f_{\mathrm{c}}$).

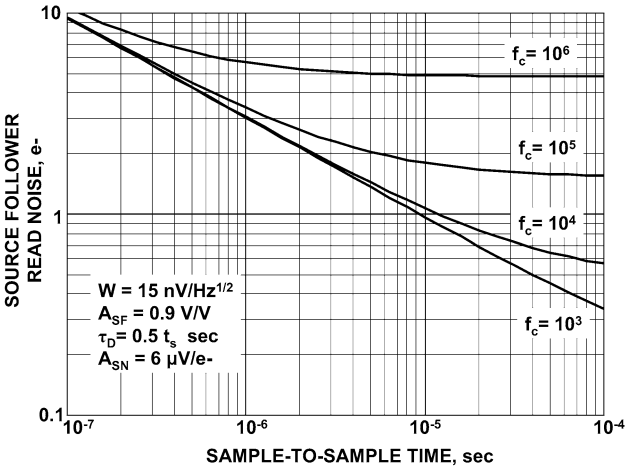

Figure 11.1 Source follower noise (rms e^{-}) with sample time for different $1/f$ corner frequencies.

11.3 Sense Node Reset Noise

Reset noise voltage is thermally generated by the channel resistance associated with the reset MOSFET induced on the sense node capacitor (refer to Fig. 4.3).[1] As a result, the sense node reference voltage is different each time a pixel is reset. Reset noise voltage is given by

$$\sigma_{\mathrm{RESET}}(V_{\mathrm{SN}}) = (4kTBR)^{1/2}, \tag{11.8}$$

where $\sigma_{\mathrm{RESET}}(V_{\mathrm{SN}})$ is the reset noise voltage (rms V), R is the MOSFET channel resistance (ohms), k is Boltzmann's constant (1.38×10^{-23} J/K), and T is the operating temperature (K).

Substituting $B = 1/4\tau$ into Eq. (11.8) yields

$$\sigma_{\mathrm{RESET}}(V_{\mathrm{SN}}) = \left(\frac{kTR}{\tau}\right)^{1/2}. \tag{11.9}$$

Noting that $\tau = RC_{\rm SN}$, Eq. (11.9) can be simplified to

$$\sigma_{\rm RESET}(V_{\rm SN}) = \left(\frac{kT}{C_{\rm SN}}\right)^{1/2}. \tag{11.10}$$

And since $C_{\rm SN} = q/V_{\rm SN}$, reset noise in terms of noise electrons is

$$\sigma_{\rm RESET} = \left(\frac{kTC_{\rm SN}}{q}\right)^{1/2}. \tag{11.11}$$

Note that Eqs. (11.10) and (11.11) appear to be in conflict. According to Eq. (11.10), reset noise voltage is lowered by increasing the sense node capacitance. On the other hand, Eq. (11.11) indicates that decreasing the capacitance is the best strategy. Obviously, for high S/N performance, it is desirable to have the number of noise electrons as low as possible because a photo-generated signal is composed of electrons. Therefore, Eq. (11.10) can be misleading. Together these equations serve as a good example for why noise (and other) measurements need to be made in the absolute units provided by photon transfer.

Assuming $C_{\rm SN} = q/A_{\rm SN}$, reset noise also can be expressed in terms of sense node gain as

$$\sigma_{\rm RESET} = \left(\frac{kT}{qA_{\rm SN}}\right)^{1/2}, \tag{11.12}$$

and

$$\sigma_{\rm RESET}(V_{\rm SN}) = \left(\frac{kTA_{\rm SN}}{q}\right)^{1/2}. \tag{11.13}$$

Note that low reset noise is achieved by making sense node gain as high as possible in terms of noise electrons.

Example 11.2

Determine the reset noise for a sense node gain of 1 μV/e$^-$. Express in electron and voltage units. Assume $T = 300$ K.

Solution:
From Eqs. (11.12) and (11.13), the reset noise on the sense node is

$$\sigma_{\rm RESET} = \left\{(1.38\times10^{-23})\times\frac{300}{[(1.6\times10^{-19})\times10^{-6}]}\right\}^{1/2} = 160\ {\rm e}^-\ {\rm rms},$$

and

$$\sigma_{\rm RESET}(V_{\rm SN}) = \left[(1.38\times10^{-23})\times\frac{300\times10^{-6}}{(1.6\times10^{-19})}\right]^{1/2} = 1.6\times10^{-4}\ {\rm V\ rms}.$$

For CCDs, reset noise is entirely removed by CDS signal processing, and therefore it is not an issue. However, it is difficult to remove reset noise for specific CMOS pixel architectures even if CDS processing is employed. For these pixels, reset noise increases by $2^{1/2}$ after CDS processing is applied because two samples are differenced. Two popular CMOS readout modes that exhibit this difficulty are referred to as "rolling shutter" and "snap."[6,7] Figure 11.2 presents a family of PTCs for these modes showing reset noise levels before and after CDS processing. The PTCs demonstrate that reset noise is significantly greater than the 5 e^- source follower noise that was assumed in the simulation. For example, a state-of-the-art sense node gain of 50 $\mu V/e^-$ generates 24 e^- of reset noise before CDS processing (as shown). A gain of 1000 $\mu V/e^-$ would be required to reduce reset noise to 5 e^-, which corresponds to a sense node capacitance of only 0.15 fF (this is not possible through design). Eliminating reset noise for CMOS imagers is briefly discussed in Sec. 11.6.

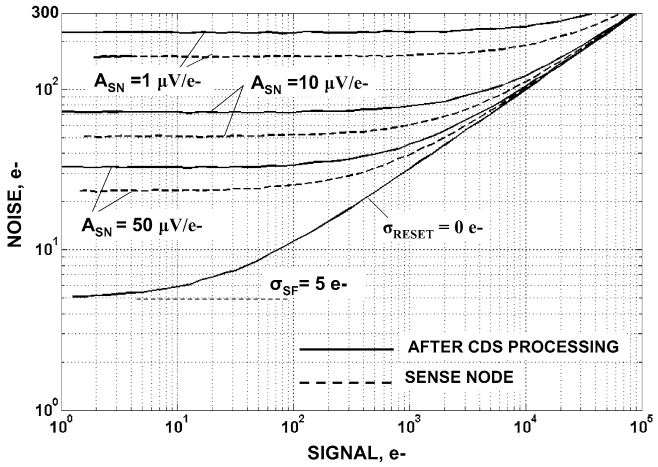

Figure 11.2 PTC responses for different sense node gains (V/e^-) compared to the ideal source follower noise without reset noise.

11.4 Dark Current Noise

All pixels naturally generate an unwanted source of charge, referred to as dark current. Although many kinds of dark current sources exist, thermally generated dark current is the most common source. The amount of dark charge produced varies from pixel to pixel, which contributes to the read noise floor. Two forms of thermal dark current noise exist: dark shot noise and dark FPN. The shot noise component is given by

$$\sigma_{\mathrm{D\_SHOT}} = (D)^{1/2}, \tag{11.14}$$

where D is the average dark current (e^-) given as

$$D = t_I D_R, \tag{11.15}$$

where t_I is the integration time allowed to collect dark charge (sec). D_R is the average dark current rate (e^-/sec/pixel) given by[1]

$$D_R = 2.55 \times 10^{15} P_A D_{FM} T^{1.5} e^{-E_g/(2kT)}, \tag{11.16}$$

where P_A is the pixel area (cm^{-2}); D_{FM} is the dark current figure-of-merit at 300 K (nA/cm^2), which varies significantly depending on the sensor manufacturer; k is Boltzmann's constant (8.62×10^{-5} eV/K); and E_g is the silicon bandgap energy given as

$$E_g = 1.1557 - \frac{7.021 \times 10^{-4} T^2}{1108 + T}. \tag{11.17}$$

Dark current FPN is expressed as

$$\sigma_{D\_FPN} = D D_N, \tag{11.18}$$

where D_N is the dark current FPN quality factor. This parameter typically varies between 10% and 40% for CCD and CMOS imagers. Note that "dark" FPN (D_N) is much greater than "light" FPN (P_N) by approximately 10–40 times.

Example 11.3

Find the average dark current rate, and related shot noise and FPN, given the following parameters:

$t_I = 0.08$ sec

$D_{FM} = 0.5$ nA/cm^2

$D_N = 0.3$

$T = 0$ C (273 K)

$P_A = (8 \times 10^{-4})^2$ cm^2

Solution:
From Eq. (11.17), the bandgap energy is

$$E_g = 1.1557 - \frac{(7.021 \times 10^{-4}) \times 273^2}{1108 + 273} = 1.120278 \text{ eV}.$$

From Eq. (11.16), the average dark current rate is

$$D_R = (2.55 \times 10^{15}) \times (8 \times 10^{-4})^2 \times 0.5 \times 273^{1.5} \times \exp\left[-\frac{1.120278}{2 \times (8.62 \times 10^{-5}) \times 273}\right];$$

$$D_{\mathrm{R}} = 178.3 \text{ e}^{-}/\text{sec}.$$

From Eq. (11.15), the dark current signal is

$$D = t_{\mathrm{I}} D_{\mathrm{R}} = 0.08 \times 178 = 14.2 \text{ e}^{-}.$$

From Eq. (11.14), the dark shot noise is

$$\sigma_{\mathrm{D\_SHOT}} = (14.2)^{1/2} = 3.77 \text{ e}^{-} \text{ rms}.$$

From Eq. (11.18), the dark FPN is

$$\sigma_{\mathrm{D\_FPN}} = 14.2 \times 0.3 = 4.26 \text{ e}^{-} \text{ rms}.$$

Example 11.4

Generate a PTC where the read noise is composed of dark and source follower noise. Assume the following:

$$K_{\mathrm{ADC}}(\text{e}^{-}/\text{DN}) = 1.5$$
$$\sigma_{\mathrm{SF}}(\text{DN}) = 3.33$$
$$D_{\mathrm{FM}} = 0.5 \text{ nA/cm}^2$$
$$D_{\mathrm{N}} = 0.3$$
$$P_{\mathrm{A}} = (8 \times 10^{-4})^2 \text{ cm}^2$$
$$t_{\mathrm{I}} = .08 \text{ sec}$$
$$T = 50,\ 40,\ 30,\ 20,\ 10,\ 0,\ -10,\ -20 \text{ C}$$

Make separate plots, with and without dark current FPN.

Solution:
The read noise and signal shot noise together are

$$\sigma_{\mathrm{READ+SHOT}} = [\sigma_{\mathrm{SF}}^2 + D + (DD_{\mathrm{N}})^2 + \sigma_{\mathrm{SHOT}}^2]^{1/2}. \tag{E11.1}$$

The read noise and signal shot noise without dark FPN is

$$\sigma_{\mathrm{READ+SHOT}} = (\sigma_{\mathrm{SF}}^2 + D + \sigma_{\mathrm{SHOT}}^2)^{1/2}. \tag{E11.2}$$

Equations (E11.1) and (E11.2) are plotted in Figs. 11.3 and 11.4, respectively. Note that the operating temperature must be less than -10 deg C for the dark current noise to be negligible compared to source follower noise. In comparing figures, it can be seen that dark FPN completely dominates dark shot noise.

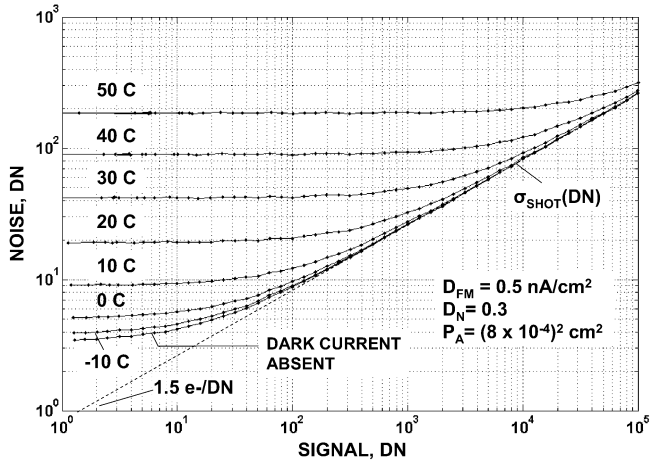

Figure 11.3 PTC responses with thermal dark current FPN at different operating temperatures.

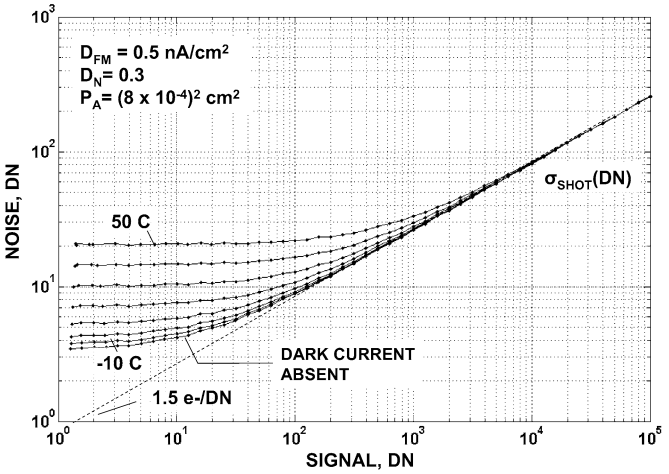

Figure 11.4 PTC responses with thermal dark current FPN removed.

Dark current parameters D_{N} and D_{FM} are found by plotting dark current shot noise and FPN as a function of dark current signal. A PTC generated like this, without a light source, is referred to as a "dark transfer curve" (DTC). Dark signal is varied by changing either the integration time or the operating temperature. The parameters $K_{\mathrm{ADC}}(\mathrm{e}^{-}/\mathrm{DN})$, D, D_{R}, D_{FM}, and D_{N} all can be determined from a DTC. Working equations to find these parameters are

$$K_{\mathrm{ADC}}(\mathrm{e}^{-}/\mathrm{DN}) = \frac{D(\mathrm{DN})}{\sigma_{\mathrm{D\_SHOT}}(\mathrm{DN})^2}, \tag{11.19}$$

where $D(\mathrm{DN})$ is the average dark current signal given by

$$D(\mathrm{DN}) = \frac{D}{K_{\mathrm{ADC}}(\mathrm{e}^{-}/\mathrm{DN})}. \tag{11.20}$$

The dark current figure of merit is found by substituting Eq. (11.16) into Eq. (11.15) and solving for D_{FM}, which yields

$$D_{\mathrm{FM}} = \frac{D_{\mathrm{R}}}{2.55 \times 10^{15} P_{\mathrm{A}} T^{1.5} e^{-E_{\mathrm{g}}/(2kT)}}. \tag{11.21}$$

The dark current FPN quality factor is defined by

$$D_{\mathrm{N}} = \frac{\sigma_{\mathrm{D\_FPN}}(\mathrm{DN})}{D(\mathrm{DN})}. \tag{11.22}$$

Note that the dark current signal level, where the dark shot noise and dark FPN are equal, is

$$D_{\mathrm{SHOT=FPN}} = \frac{1}{D_{\mathrm{N}}^2}. \tag{11.23}$$

Example 11.5

Figure 11.5 shows DTCs with and without dark current FPN based on these parameters:

$$K_{\mathrm{ADC}}(\mathrm{e}^{-}/\mathrm{DN}) = 1.5$$
$$\sigma_{\mathrm{SF}}(\mathrm{DN}) = 3.33$$

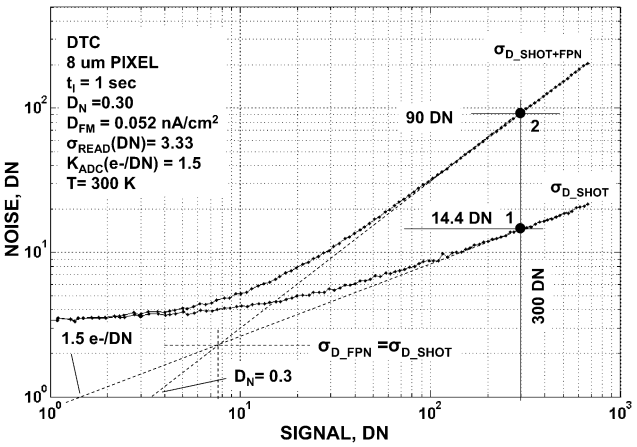

Figure 11.5 Dark transfer curve generated without light.

$$D_{\mathrm{FM}} = \text{nA/cm}^2$$
$$D_{\mathrm{N}} = 0.3$$
$$P_{\mathrm{A}} = (8 \times 10^{-4})^2 \text{ cm}^2$$
$$t_{\mathrm{I}} = 1 \text{ sec}$$
$$T = 300 \text{ K}$$

From the DTC curve presented, confirm $K_{\mathrm{ADC}}(\mathrm{e}^-/\mathrm{DN})$, D, D_{R}, D_{FM}, and D_{N}. Find the dark signal level where dark FPN begins to dominate dark shot noise.

Solution:
From Eq. (11.19) and data point 1 on the dark shot noise curve,

$$K_{\mathrm{ADC}}(\mathrm{e}^-/\mathrm{DN}) = \frac{300}{14.4^2} = 1.5.$$

From Eq. (11.20), the signal level at data point 1 is

$$D = 300 \times 1.5 = 450 \text{ e}^-.$$

From Eq. (11.15), the dark current rate is

$$D_{\mathrm{R}} = \frac{450}{1} = 450 \text{ e}^-/\text{sec}.$$

From Eq. (11.17), the silicon bandgap at 300 K is

$$E_{\mathrm{g}} = 1.1157 - \frac{7.021 \times 10^{-4} \times 300^2}{1108 + 300} = 1.071.$$

From Eq. (11.21), the dark current figure of merit is

$$\begin{aligned} D_{\mathrm{FM}} &= \frac{450}{\left\{(2.55 \times 10^{15}) \times (8 \times 10^{-4})^2 \times 300^{1.5} \exp\left[-\dfrac{1.071}{2 \times (8.62 \times 10^{-5}) \times 300}\right]\right\}} \\ &= 0.052 \text{ nA/cm}^2. \end{aligned}$$

From Eq. (11.22) and data point 2 on the FPN curve,

$$D_{\mathrm{N}} = \frac{90}{300} = 0.3.$$

From Eq. (11.23), the dark signal level where dark FPN starts to dominate dark shot noise is

$$D_{\mathrm{SHOT=FPN}} = \frac{1}{(0.3)^2} = 11 \text{ e}^-.$$

Figure 11.6 shows the buildup of dark current for 150 CMOS pixels as a function of time. The data are used to generate the DTCs presented in Fig. 11.7 with and without dark FPN. Note from Fig. 11.6 that dark current increases nonlinearly with time, indicating that D_{FM} is not a constant. Also note from Fig. 11.7 that the dark FPN slope 1 curve shifts toward the right, which signifies that D_{N} is decreasing with the signal level. Figure 11.8 plots dark current nonlinearity using the relation

$$\mathrm{NL_D} = 1 - \frac{D(\mathrm{DN})_{\mathrm{m}}/t_{\mathrm{m}}}{D(\mathrm{DN})/t_{\mathrm{I}}}, \tag{11.24}$$

where $\mathrm{NL_D}$ is the dark current nonlinearity, and $D(\mathrm{DN})_{\mathrm{m}}$ is the dark signal at some arbitrary time t_{m} (shown in Fig. 11.8 at 2.6 sec).

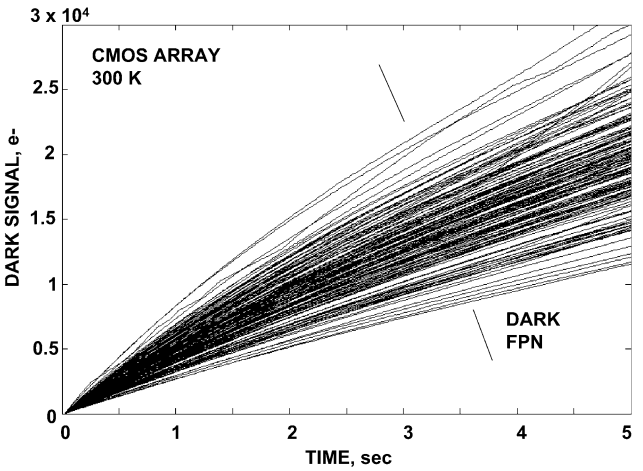

Figure 11.6 Nonlinear dark current build-up for 256 CMOS pixels showing dark FPN.

Example 11.6

For Fig. 11.7, determine the variation of dark FPN over the signal range measured.

Solution:
From Eq. (11.22) and the two data points [at $D(\mathrm{DN}) = 1000$)] shown in Fig. 11.7,

$$D_{\mathrm{N}} = \frac{300}{1000} = 0.3\ (30\%),$$

and

$$D_{\mathrm{N}} = \frac{200}{1000} = 0.2\ (20\%).$$

Nonlinearity characteristics shown in Figs. 11.6 to 11.8 are common to specific types of CMOS and CCD imagers, where dark current is influenced by electric

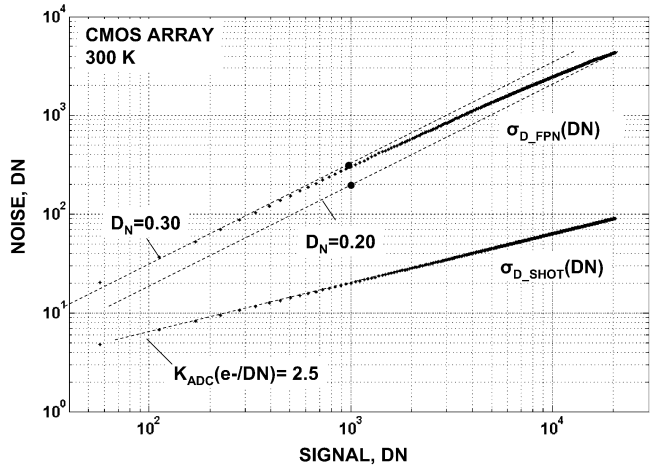

Figure 11.7 Dark transfer curves measuring dark current FPN nonlinearity with signal.

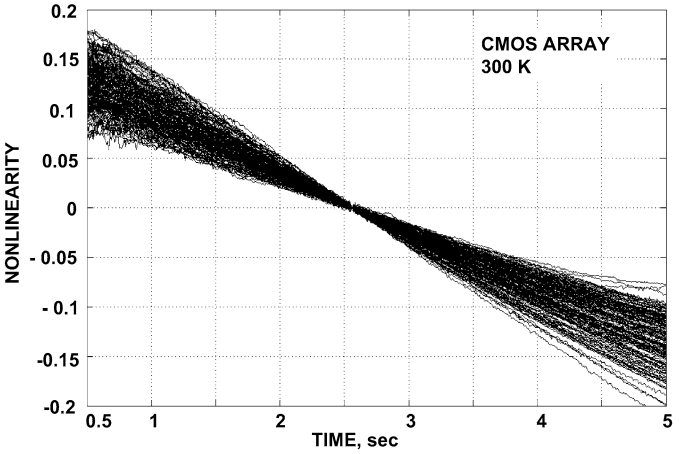

Figure 11.8 Dark current nonlinearity versus time for Fig. 11.6.

fields internal to a pixel. The fields decrease as signal charge collects, which in turn reduces the dark current rate. Dark current analysis is complex for these sensors, so DTC helps identify and quantify the problems like this. Fortunately, the majority of imagers (especially CCDs) behave according to the dark current relations given above.

PTC and DTC can be generated together on a single graph. For example, Fig. 11.9 shows a PTC/DTC combination plot. The DTC is generated by changing the integration time, yielding information for $K_{\mathrm{ADC}}(\mathrm{e}^{-}/\mathrm{DN})$, D_{N}, and D_{FM} para-

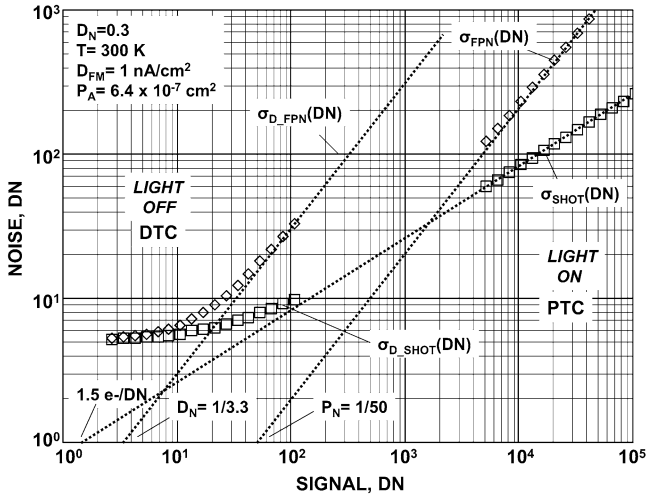

Figure 11.9 DTC and PTC responses generated on the same plot.

meters. For high signals, the integration time is fixed and the light level is varied to generate PTCs. The plot provides information for $K_{\mathrm{ADC}}(\mathrm{e}^{-}/\mathrm{DN})$ and P_{N}. Note that the dark and light shot noise curves merge on the slope $1/2$ line, whereas the two slope 1 curves are different and produce D_{N} and P_{N}.

11.5 ADC Quantizing Noise

11.5.1 Linear encoding

Figure 11.10 shows transfer characteristics for a linear ADC. As indicated, when a pixel signal is digitized it introduces an uncertainty, which can add to the read noise floor. The rms error about the perfect ramp response shown is called "ADC quantizing noise." For an ideal ADC, this noise amounts to

$$\sigma_{\mathrm{ADC}}(\mathrm{DN}) = \left(\frac{1}{12}\right)^{1/2} = 0.2887. \tag{11.25}$$

In terms of rms noise electrons,

$$\sigma_{\mathrm{ADC}} = 0.2887 K_{\mathrm{ADC}}(\mathrm{e}^{-}/\mathrm{DN}). \tag{11.26}$$

Equation (11.26) shows that quantizing noise is dependent on the ADC sensitivity, $K_{\mathrm{ADC}}(\mathrm{e}^{-}/\mathrm{DN})$. This connection is demonstrated in Fig. 11.11, which presents three 2 e^{-} read noise images at different sensitivities (2, 10, and 100 e^{-}/DN). As $K_{\mathrm{ADC}}(\mathrm{e}^{-}/\mathrm{DN})$ increases, the quantizing noise becomes apparent until it dominates the read noise floor. Figure 11.12 presents "stacked" column traces through each image shown in Fig. 11.11. The quantizing noise "steps" become more apparent as

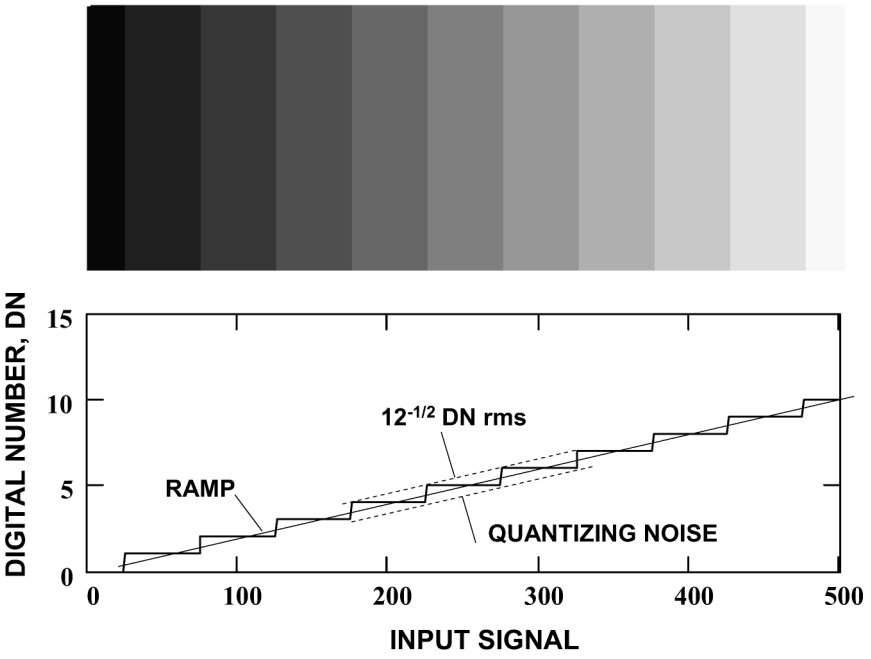

Figure 11.10 ADC quantizing noise image and transfer curve.

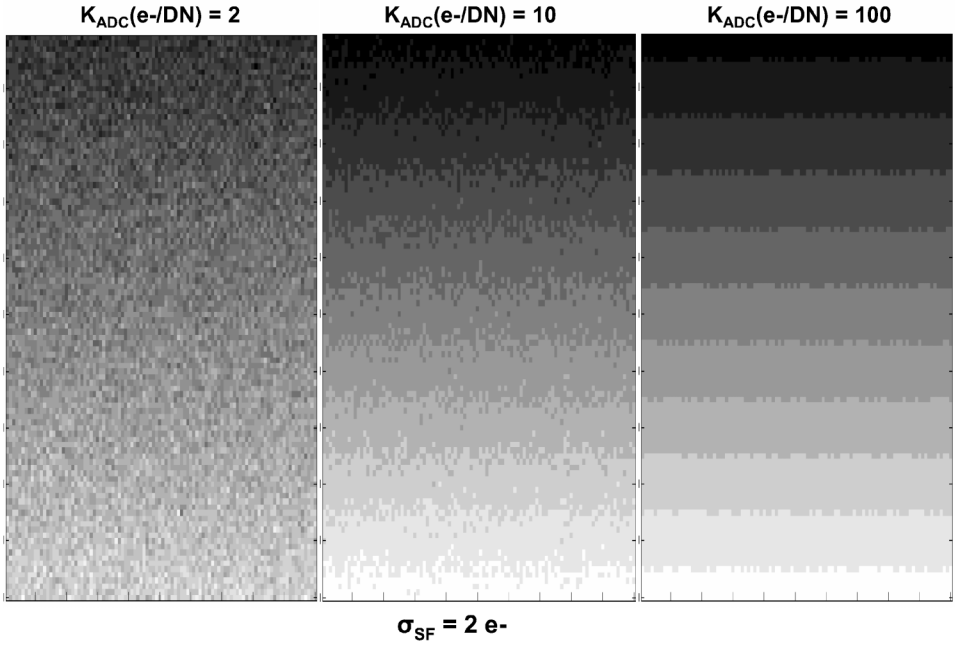

Figure 11.11 ADC quantizing noise images being hidden by random source follower noise by different K_{ADC}(e^{-}/DN).

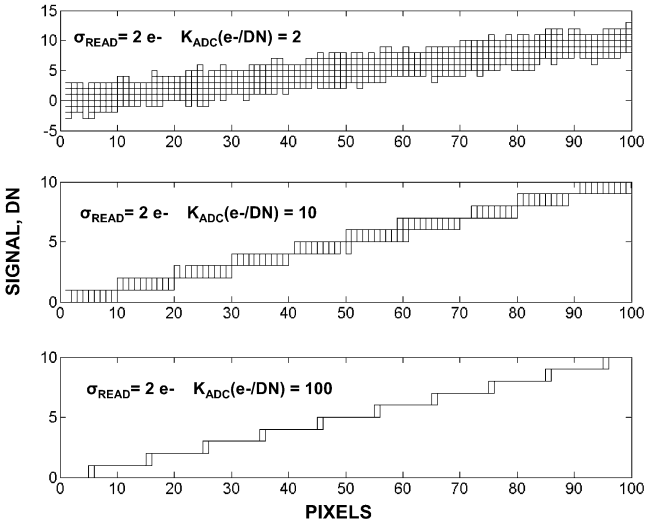

Figure 11.12 Video column traces of Fig. 11.10.

the ADC sensitivity increases. Note that quantizing noise becomes completely hidden when $K_{\mathrm{ADC}}(\mathrm{e}^-/\mathrm{DN})$ is approximately equal to the random noise level. Therefore, for proper noise encoding, we simply let

$$K_{\mathrm{ADC}}(\mathrm{e}^-/\mathrm{DN}) = \sigma_{\mathrm{READ}}. \tag{11.27}$$

This relation forces read noise to 1 DN rms, without quantizing noise issues.

Figure 11.13 shows similar images where signal shot noise is introduced along with the 2 e^- read noise floor. Comparing Figs. 11.11 and 11.13 shows that shot noise further hides the quantizing noise, which allows for a higher $K_{\mathrm{ADC}}(\mathrm{e}^-/\mathrm{DN})$. In fact, the ADC sensitivity required for a camera system depends on the lowest noise expected to be digitized, i.e.,

$$K_{\mathrm{ADC}}(\mathrm{e}^-/\mathrm{DN}) = \sigma_{\mathrm{LOW}}, \tag{11.28}$$

where σ_{LOW} is the lowest noise level encountered by a camera system (which includes FPN sources).

Example 11.7

Determine the read and shot noise for each DN step shown in Fig. 11.13 without ADC quantizing noise. Assume $\sigma_{\mathrm{SF}} = 2\,\mathrm{e}^-$.

Solution:
The random noise for each DN level is composed of source follower and shot noise, i.e.,

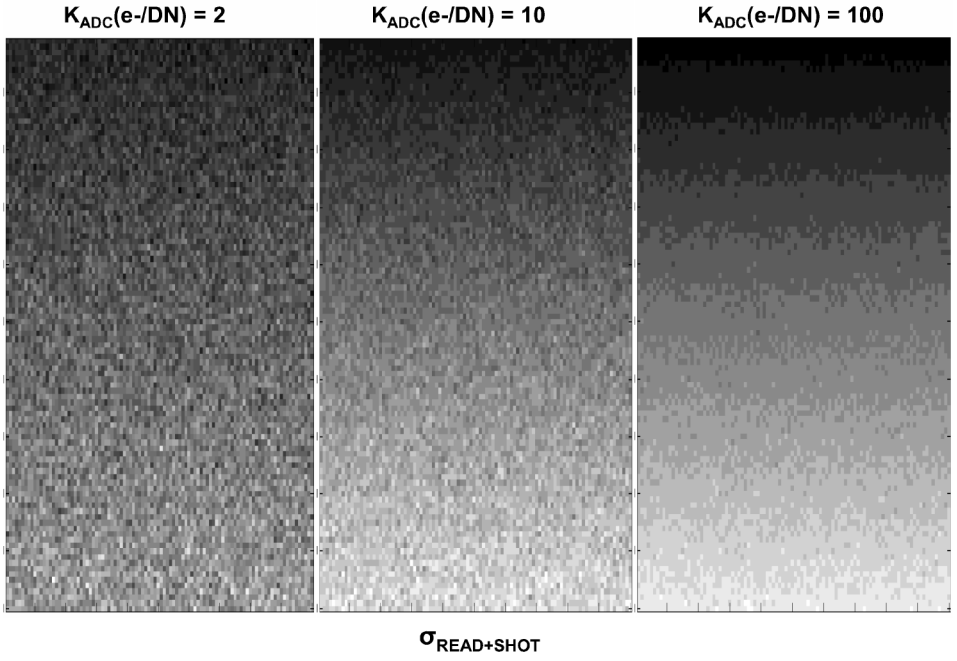

Figure 11.13 ADC quantizing noise images being hidden by random source follower and shot noise with different $K_{\mathrm{ADC}}(\mathrm{e}^{-}/\mathrm{DN})$.

$$\sigma_{\mathrm{READ+SHOT}}(\mathrm{DN}) = \left\{ [\sigma_{\mathrm{READ}}(\mathrm{DN})]^2 + \frac{S(\mathrm{DN})}{K_{\mathrm{ADC}}(\mathrm{e}^{-}/\mathrm{DN})} \right\}^{1/2}. \qquad \text{(E11.3)}$$

Table 11.2 tabulates the noise level as calculated by Eq. (E11.3).

Table 11.2 and Fig. 11.13 can be compared. The noise levels tabulated should be greater than $\sigma_{\mathrm{ADC}}(\mathrm{DN})$ if proper encoding is to take place [i.e., greater than 0.2887 DN, as defined by Eq. (11.25)]. This is not the condition for the third column. The second column is marginal, whereas the first column is satisfactory.

Besides encoding read noise properly, it is also important to encode the maximum signal level expected, which is typically the charge capacity of the sensor. The full-well encoding required is determined by

$$N_{\mathrm{ADC}} = \frac{S_{\mathrm{FW}}}{K_{\mathrm{ADC}}(\mathrm{e}^{-}/\mathrm{DN})}, \qquad (11.29)$$

where N_{ADC} is the number of DN levels required from the ADC. Substituting Eq. (11.27), which is the requirement to encode read noise properly into Eq. (11.29), yields

$$N_{\mathrm{ADC}} = \frac{S_{\mathrm{FW}}}{\sigma_{\mathrm{READ}}}, \qquad (11.30)$$

Table 11.2 Read and shot noise levels for Fig. 11.13.

DN Level	$\sigma_{\mathrm{READ+SHOT}}(\mathrm{DN})$ $K_{\mathrm{ADC}}(\mathrm{e^-/DN}) = 2\ \mathrm{e^-/DN}$ $\sigma_{\mathrm{READ}}(\mathrm{DN}) = 1\ \mathrm{DN}$	$\sigma_{\mathrm{READ+SHOT}}(\mathrm{DN})$ $K_{\mathrm{ADC}}(\mathrm{e^-/DN}) = 10\ \mathrm{e^-/DN}$ $\sigma_{\mathrm{READ}}(\mathrm{DN}) = 0.2\ \mathrm{DN}$	$\sigma_{\mathrm{READ+SHOT}}(\mathrm{DN})$ $K_{\mathrm{ADC}}(\mathrm{e^-/DN}) = 100\ \mathrm{e^-/DN}$ $\sigma_{\mathrm{READ}}(\mathrm{DN}) = 0.02\ \mathrm{DN}$
0	1	0.2000	0.0200
1	1.2247	0.3742	0.1020
2	1.4142	0.4899	0.1428
3	1.5811	0.5831	0.1744
4	1.7321	0.6633	0.2010
5	1.8708	0.7348	0.2245
6	2	0.8000	0.2458
7	2.1213	0.8602	0.2653
8	2.2361	0.9165	0.2835
9	2.3452	0.9695	0.3007
10	2.4495	1.0198	0.3169

which is simply the dynamic range for a camera system (a good rule of thumb to remember).

The number of bits required from an ADC is

$$N_{\mathrm{BITS}} = \frac{\log(N_{\mathrm{ADC}})}{\log(2)}. \tag{11.31}$$

Example 11.8

Plot the number of ADC bits required as a function of the lowest noise level to be encoded for different full-well levels (10^4, 5×10^4, 10^5, 5×10^5, and 10^6 e^-).

Solution:
From Eqs. (11.28) and (11.30), the number of DN levels required is

$$N_{\mathrm{ADC}} = \frac{S_{\mathrm{FW}}}{\sigma_{\mathrm{LOW}}}. \tag{E11.4}$$

Figure 11.14 plots Eq. (E11.4). For example, 16 bits is required to encode an 8 e^- noise level and a 5×10^5 full-well signal.

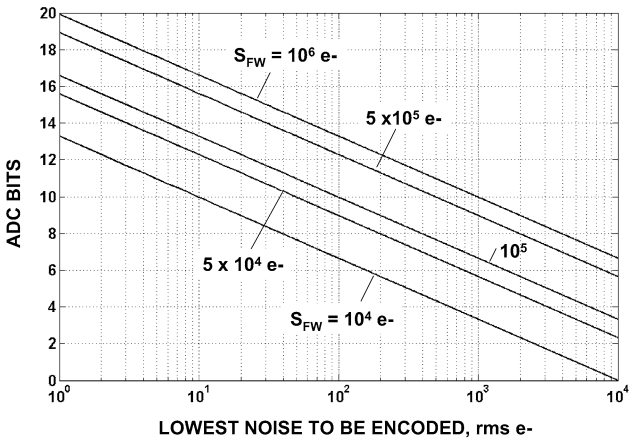

Figure 11.14 Number of ADC bits required to encode specific noise and full-well levels.

Example 11.9

Assume a camera system will be taking pictures that are always FPN limited. Determine the number of ADC bits required, given that the full well is 10^5 e^- and $P_{\mathrm{N}} = 0.01$.

Solution:
From Eqs. (11.28) and (11.30), the onset of FPN is

$$\frac{1}{P_{\mathrm{N}}^2} = \frac{1}{(0.01)^2} = 10{,}000\ \mathrm{e}^-.$$

Therefore, the lowest FPN to be encoded is

$$\sigma_{\mathrm{FPN}} = 0.01 \times 10{,}000 = 100\ \mathrm{e}^-.$$

From Fig. 11.14, the number of bits required is

$$N_{\mathrm{BITS}} = 10.$$

Figure 11.15 shows $\sigma_{\mathrm{READ+SHOT}}(\mathrm{DN})$ PTC responses, with and without ADC quantizing noise, at different read noise levels (100 e^-, 60 e^-, and 2 e^-). The plots assume a fixed ADC sensitivity of $K_{\mathrm{ADC}}(\mathrm{e}^-/\mathrm{DN}) = 100$ and an 8-bit ADC. When $\sigma_{\mathrm{READ}} < K_{\mathrm{ADC}}(\mathrm{e}^-/\mathrm{DN})$, quantizing error becomes appreciable. Note that quantizing noise is cyclic with a signal period of 1 DN for the 2 e^- noise case. The cyclic signature is quenched when the noise level is above 0.5 DN. The dotted line shown assumes a fixed quantizing noise of 0.2887 DN [i.e., Eq. (11.25)], which is only valid when the cyclic pattern is not present. Figure 11.16 presents noise variance PTCs using the same data set as Fig. 11.15, with and without quantizing noise. $K_{\mathrm{ADC}}(\mathrm{e}^-/\mathrm{DN})^{-1}$ is equal to the slope of all curves (i.e., $1/100$).

Figure 11.17 shows PTC data taken from a CMOS sensor that incorporates an on-chip 10-bit ADC. The ADC exhibits a bit weighting problem: the noise

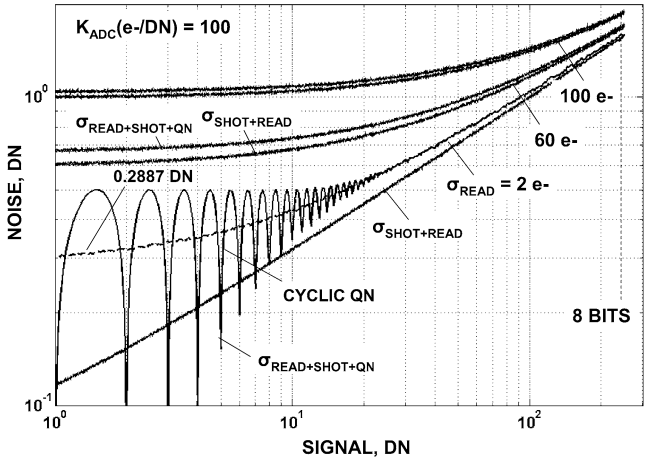

Figure 11.15 PTC responses showing how ADC quantizing noise becomes increasingly dominant as random read noise decreases.

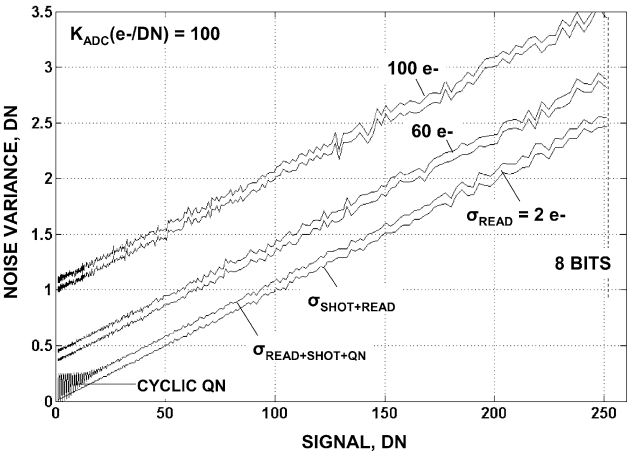

Figure 11.16 Corresponding variance PTCs for Fig. 11.15.

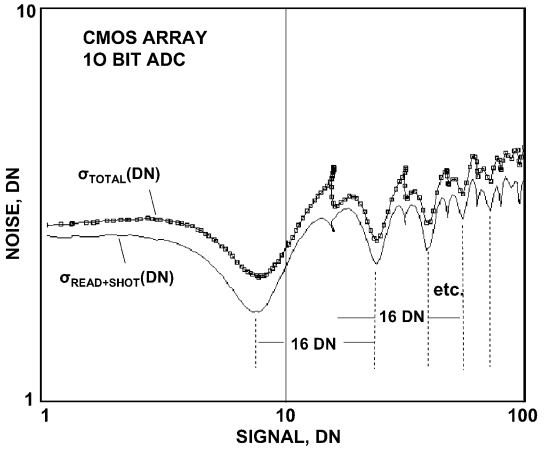

Figure 11.17 PTC responses demonstrating an ADC bit weighting problem.

varies cyclically every 16 bits in the signal. The source of the difficulty is seen in Fig. 11.18, where output DN is plotted against input signal. The staircase is interrupted every 16 bits, which reflects each "kink" in the PTC. Assuming additional ADC bits are available for full-well encoding, one can hide quantizing problems like this by increasing the voltage gain before the ADC, but this is not desirable.

11.5.2 Nonlinear encoding

All PTCs presented previously show that linear encoding excessively encodes shot noise and FPN. For example, a read noise of 10 e^- is equivalent to 1 DN, assuming $K_{\mathrm{ADC}}(\mathrm{e}^-/\mathrm{DN}) = \sigma_{\mathrm{READ}}$. However, a shot noise of 1000 e^- is encoded to

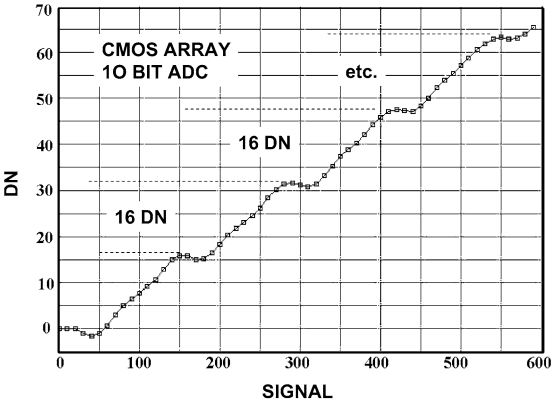

Figure 11.18 ADC transfer function showing the bit weighting problem characterized in Fig. 11.17.

100 DN, which is a hundred times greater encoding power than is necessary. For optimum shot noise digitization, $K_{\mathrm{ADC}}(\mathrm{e}^{-}/\mathrm{DN})$ should increase by the square root of the signal (i.e., $S^{1/2}$). Changing the ADC sensitivity in this manner will encode the shot noise to a fixed 1 DN level over the sensor's dynamic range. This encoding processor is called a "square-rooter"—a powerful compression technique applied to shot-noise-limited detectors.[1]

Figure 11.19 shows three PTCs that demonstrate the encoding compression technique. The first labeled curve, $K_{\mathrm{ADC}}(\mathrm{e}^{-}/\mathrm{DN}) = 2$, produces the standard, linearly encoded total noise PTC. FPN is encoded to 500 DN at full well [$S_{\mathrm{FW}}(\mathrm{DN}) = 50{,}000$]. The second plot assumes that $K_{\mathrm{ADC}}(\mathrm{e}^{-}/\mathrm{DN}) = S^{1/2}$, which optimally

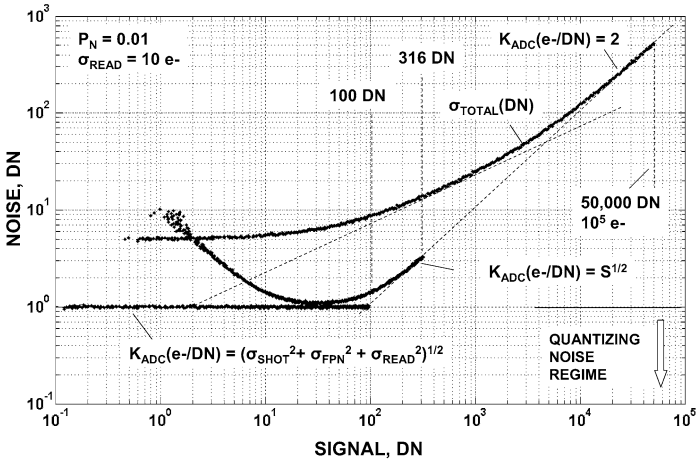

Figure 11.19 Square-rooter PTC responses showing optimum encoding for different $K_{\mathrm{ADC}}(\mathrm{e}^{-}/\mathrm{DN})$.

encodes shot noise to 1 DN. However, this sensitivity setting still over-encodes the read noise and FPN, which is seen in Fig. 11.19 when the curve deviates from the 1 DN noise level. In order to compress all three noise sources optimally to 1 DN, we let the ADC sensitivity vary as

$$K_{\mathrm{ADC}}(\mathrm{e^-/DN}) = \left[\sigma_{\mathrm{READ}}^2 + \eta_{\mathrm{i}} S + (P_{\mathrm{N}} S)^2\right]^{1/2}. \tag{11.32}$$

A PTC that assumes Eq. (11.32) is also shown in Fig. 11.19 as a flat-line response of 1 DN. Note that only 100 DN is required to cover the detector's dynamic range compared to 50,000 DN for linear encoding. This represents a compression ratio of 500 without information loss.

Substituting Eq. (11.32) into Eq. (11.29) determines the number of DN levels required for optimum nonlinear encoding:

$$N_{\mathrm{ADC}} = \frac{S_{\mathrm{FW}}}{[\sigma_{\mathrm{READ}}^2 + \eta_{\mathrm{i}} S + (P_{\mathrm{N}} S)^2]^{1/2}}. \tag{11.33}$$

If FPN dominates read and shot noise at full well, Eq. (11.33) simply reduces to

$$N_{\mathrm{ADC}} = \frac{1}{P_{\mathrm{N}}}. \tag{11.34}$$

Example 11.10

For Fig. 11.19, determine the number of DN levels and ADC bits required, given the following ADC sensitivities:

$$K_{\mathrm{ADC}}(\mathrm{e^-/DN}) = 2$$
$$K_{\mathrm{ADC}}(\mathrm{e^-/DN}) = \mathrm{S}^{1/2}$$
$$K_{\mathrm{ADC}}(\mathrm{e^-/DN}) = \left[\sigma_{\mathrm{READ}}^2 + S + (P_{\mathrm{N}} S)^2\right]^{1/2}$$

Assume a full well of $S_{\mathrm{FW}} = 10^5$ e$^-$, $\sigma_{\mathrm{READ}} = 10$ e$^-$, and $P_{\mathrm{N}} = 0.01$.

Solution:

1. $K_{\mathrm{ADC}}(\mathrm{e^-/DN}) = 2$
   From Eqs. (11.29) and (11.31):

$$N_{\mathrm{ADC}} = \frac{10^5}{2} = 50{,}000 \text{ DN}$$
$$N_{\mathrm{BITS}} = \frac{\log(50{,}000)}{\log 2} = 15.6 \text{ (or 16 bits)}$$

2. $K_{\mathrm{ADC}}(\mathrm{e}^{-}/\mathrm{DN}) = S^{1/2}$
   From Eqs. (11.29) and (11.31):

$$N_{\mathrm{ADC}} = \frac{10^5}{(10^5)^{1/2}} = 316 \text{ DN}$$

$$N_{\mathrm{BITS}} = \frac{\log(316)}{\log 2} = 8.3 \text{ (or 9 bits)}$$

3. $K_{\mathrm{ADC}}(\mathrm{e}^{-}/\mathrm{DN}) = [\sigma^2_{\mathrm{READ}} + S + (P_{\mathrm{N}}S)^2]^{1/2}$
   From Eqs. (11.34) and (11.31):

$$N_{\mathrm{ADC}} = \frac{1}{0.01} = 100 \text{ DN}$$

$$N_{\mathrm{BITS}} = \frac{\log(100)}{\log 2} = 6.6 \text{ (or 7 bits)}$$

These results are shown in Fig. 11.19.

Figure 11.20 shows two PTCs that assume $K_{\mathrm{ADC}}(\mathrm{e}^{-}/\mathrm{DN}) = S^{1/2}$ and $K_{\mathrm{ADC}}(\mathrm{e}^{-}/\mathrm{DN}) = 4 \times S^{1/2}$. The latter curve produces noise levels less than 1 DN, taking the sensor into the quantizing noise regime. Although further compression does take place (from 320 DN to 80 DN), the cyclic quantizing noise pattern also emerges. As long as the noise level is >1 DN, quantizing noise is controlled, which is the case when $K_{\mathrm{ADC}}(\mathrm{e}^{-}/\mathrm{DN}) = S^{1/2}$.

Figure 11.21 presents images showing full 10-bit encoding with the signal compressed to 6, 5, and 4 bits. Note that the 4-bit image has insufficient encoding and

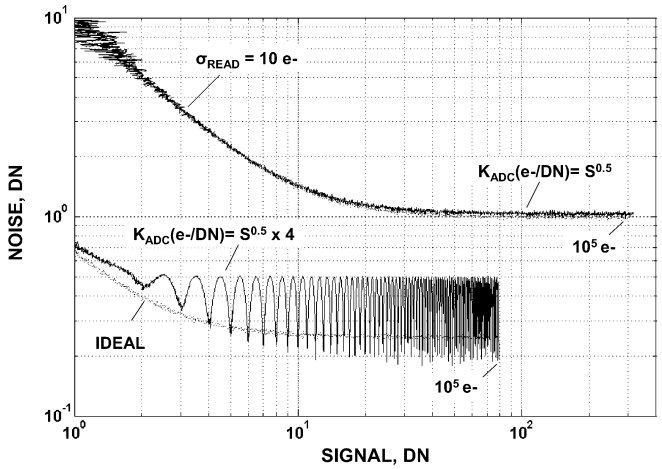

Figure 11.20 Square-rooter PTC responses showing ADC quantizing noise when the read noise level drops below 1 DN rms.

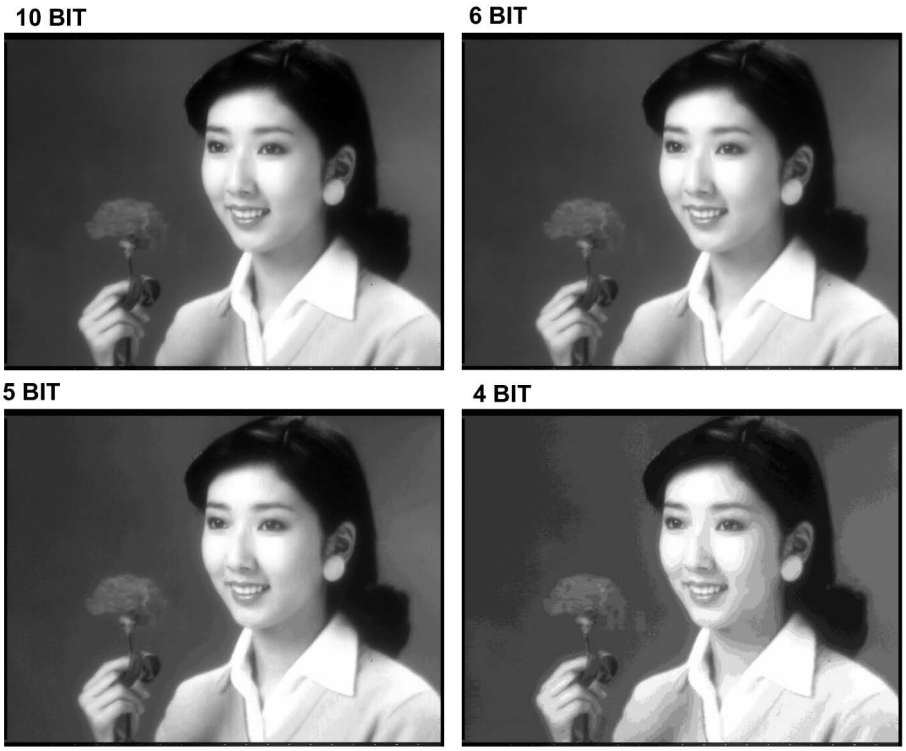

Figure 11.21 Square-rooter images showing 6-, 5- and 4-bit compressions from 10 bits.

shows ADC quantizing noise. Additional square-root discussions, including hardware implementation, are given in Ref. 1.

11.6 Offset Fixed Pattern Noise

Figures 5.9 and 5.10 demonstrated the importance of precisely knowing the offset level for accurate signal measurement. For CCD imagers, the offset level needs to be tracked for each amplifier port. For CMOS imagers, all pixels must be monitored because each pixel exhibits a different offset level. For example, Fig. 11.22 presents a single row of CMOS pixels showing 1000 e^- rms of offset FPN.

CMOS offset FPN noise is significantly greater than reset noise, which itself is greater than pixel source follower noise. For example, Fig. 11.23 compares offset, reset, and source follower noise for a CMOS imager (250 e^-, 28 e^-, and 2.5 e^- rms, respectively). Also shown for reference are three 5.9 keV, 1620 e^- x-ray events contained in the row of pixels. Figure 11.24 is a magnified view showing how much larger reset noise is to source follower noise.

For certain CMOS readout modes (rolling shutter and snap), "digital CDS" (DCDS) is employed to remove offset FPN and reset noise (e.g., Figs. 11.23 and 11.24 were processed in this manner).[8] DCDS processing first quickly reads

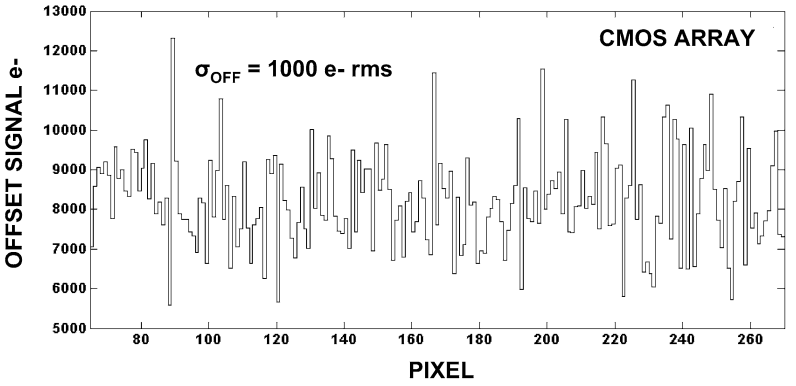

Figure 11.22 CMOS pixel offset FPN.

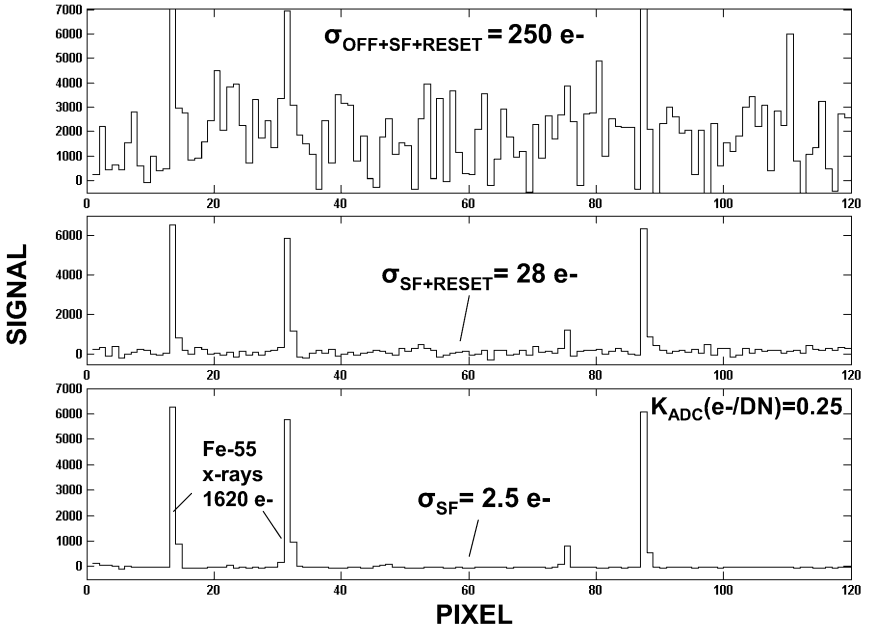

Figure 11.23 CMOS array video traces that compare offset FPN, reset and source follower noise levels.

all pixels after being globally reset. The offset/reset levels samples are stored in a computer. Then the signal charge is integrated for a specified period of time. The pixels are then read again, and their video levels are stored in the computer. Lastly, the video and offset/reset levels are differenced by the computer, thus performing DCDS. For example, Fig. 11.25 shows a video stream where four frames were taken by a 128×128 CMOS array. First, the sequence shows the offset/reset noise samples collected for the first frame. The noise level is approximately 250 e^-,

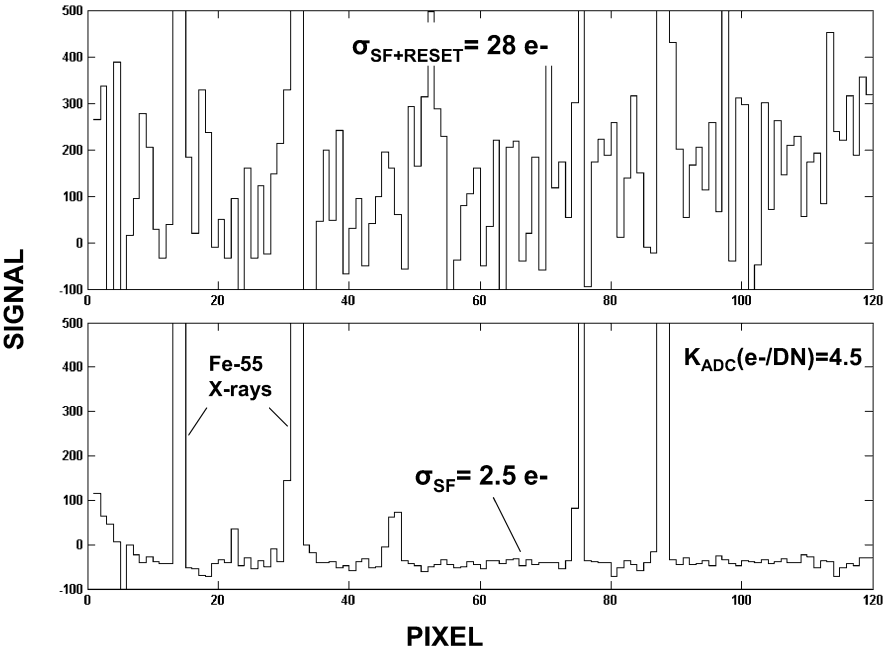

Figure 11.24 Magnified view of Fig. 11.23 showing 1620 e^- x-ray events imbedded in reset and source follower noise.

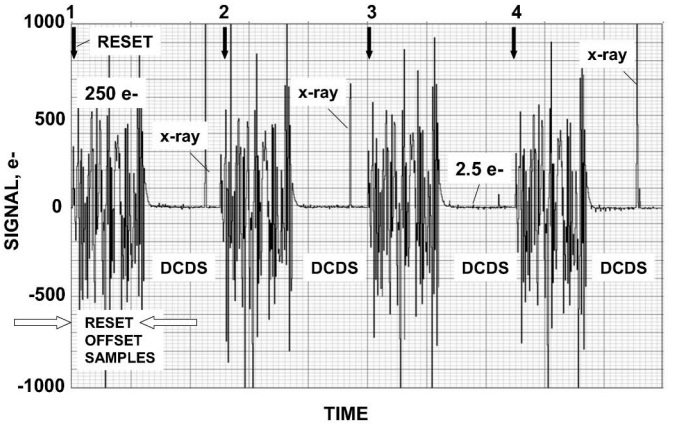

Figure 11.25 Video trace comparing noise level before and after digital CDS processing.

consisting primarily of offset FPN. After collecting offset/reset levels, the device integrates signal charge for 0.65 sec (not shown in the figure). The quiet region shown is the processed video after the two samples are subtracted by computer (i.e., DCDS). Offset and reset noise are removed entirely, reducing the read noise level to 2.5 e^-. The sequence is repeated three more times as shown. Note that

some 1620 e^- x-ray events are seen in the quiet processed regions. Figure 11.26 shows a full image of the x-ray events after DCDS is performed for the same imager and processing conditions. For comparison, Fig. 11.27 shows the raw video before DCDS processing, where offset/reset noise is present. Some x-ray events are circled but are difficult to see in the 250 e^- noise floor.

Offset FPN sources can enter downstream of the CDS processor. For example, Fig. 11.28 is a dark image taken from a single addressed CMOS pixel that shows an offset level that is systematically changing as it is read out. As the image shows, the offset variance is the same from row to row. The top of Fig. 11.29 presents a raw video trace taken before the offset pattern can be clearly seen. The second trace is derived from a 100 frame average. The offset FPN can now be seen because the averaging process reduces the random noise generated by source follower noise by a factor of 10 (the image in Fig. 11.28 is derived from this data). The first and second traces are then subtracted to remove the offset pattern. The bottom trace of Fig. 11.29 is the result after subtraction. Note that the video only contains random noise without offset FPN.

Figure 11.30 presents PTC data generated by a CMOS imager with CDS signal processing applied. As indicated, the total noise curve, $\sigma_{\mathrm{TOTAL}}(\mathrm{DN})$, exhibits some offset FPN created downstream of the CDS. This offset is removed by taking two back-to-back frames for each data point and subtracting them (pixel by pixel).

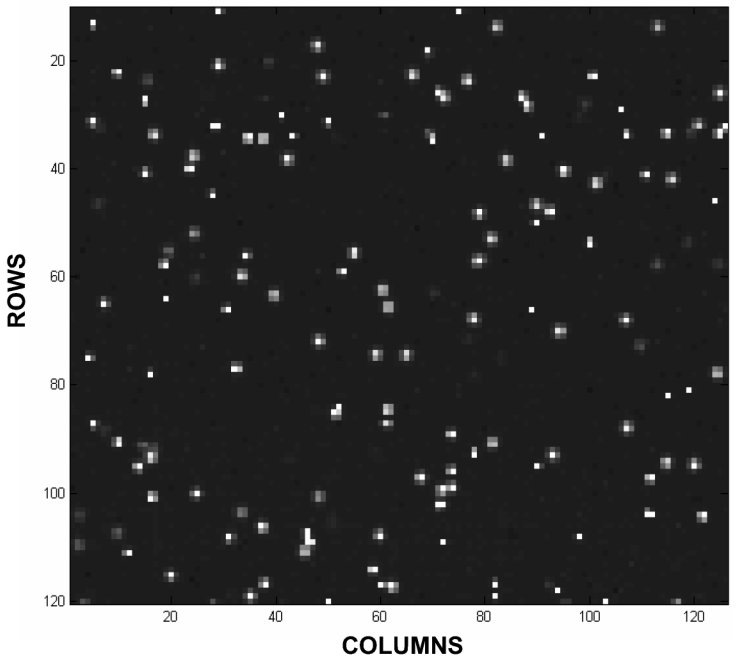

Figure 11.26 Fe-55 1620 e^- x-ray events after DCDS.

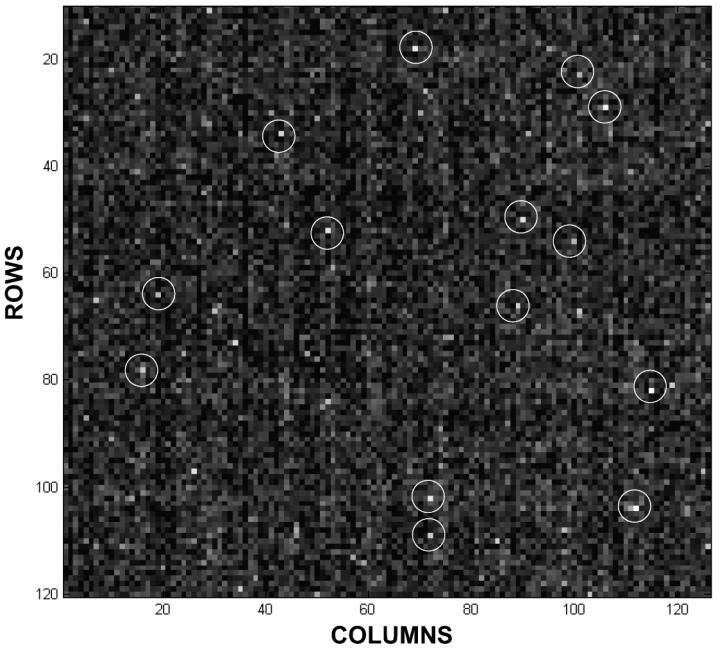

Figure 11.27 Fe-55 1620 e^- x-ray events before DCDS.

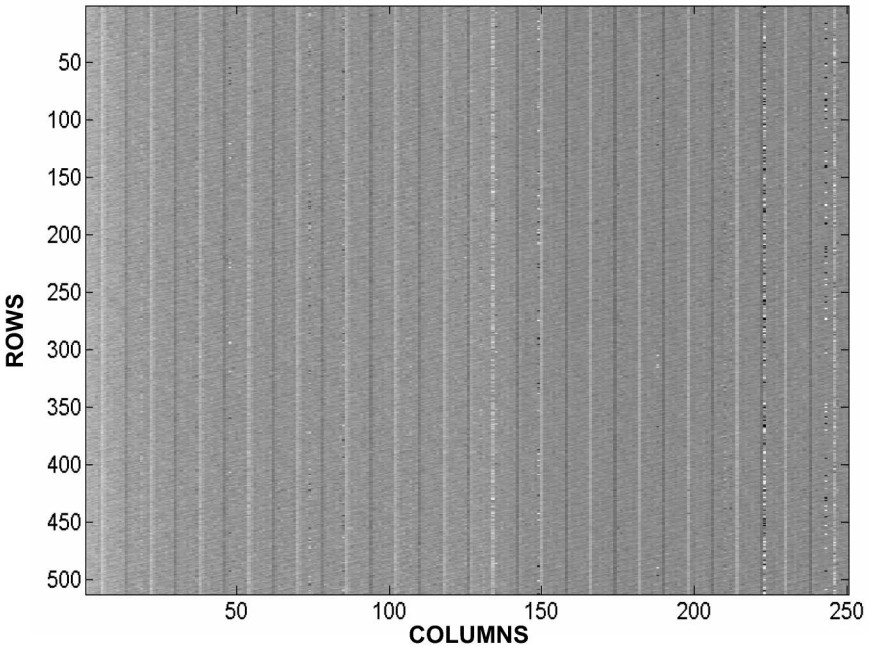

Figure 11.28 Systematic offset FPN.

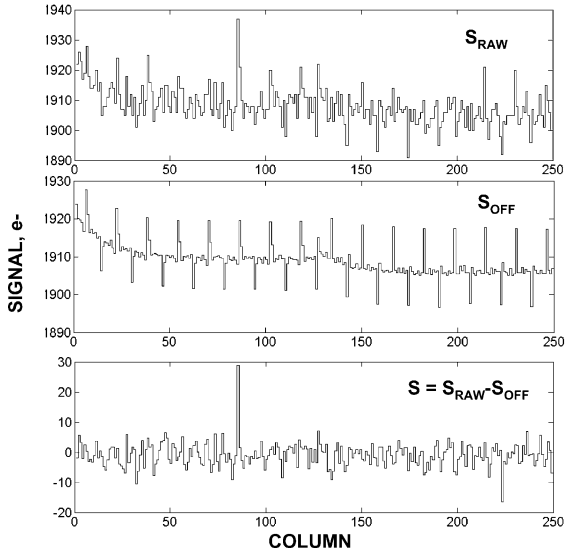

Figure 11.29 Raw signal, frame averaged offset FPN and differenced noise.

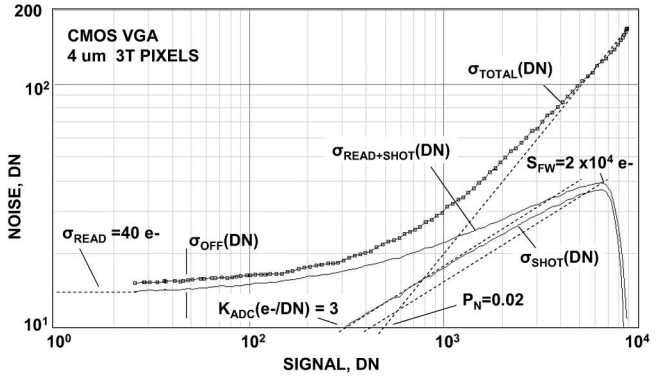

Figure 11.30 CMOS array PTC responses showing offset FPN after on-chip CDS processing and removal through frame differencing.

The process removes both offset and pixel FPN, leaving only read and shot noise. The result is plotted along with the shot noise curve.

11.7 System Noise

Dozens of system noise problems can potentially degrade the read noise floor, including preamp noise, transient noise, synchronous and nonsynchronous logic noise, settling and ringing noise, ground bounce noise, luminescence, clock phase jitter noise, ADC feedback noise, power supply noise, circuit crosstalk noise, oscillation noise, and electromagnetic noise, to name just a few. The majority of these

sources are dynamic as the noise level changes from frame to frame. For example, Fig. 11.31 shows two dark CMOS images taken at two different rates (2.25 and 5.0 Mpixels/sec). Although the system noise appears to be well behaved for the slower rate, it increases significantly when the readout frequency is doubled. The noise source is also nonsynchronous (i.e., not fixed from frame to frame), making it difficult to remove by computer. For purposes of analysis, all system noise sources are lumped together into one term called σ_{SY}. Ideally, the noise sources should not be present.

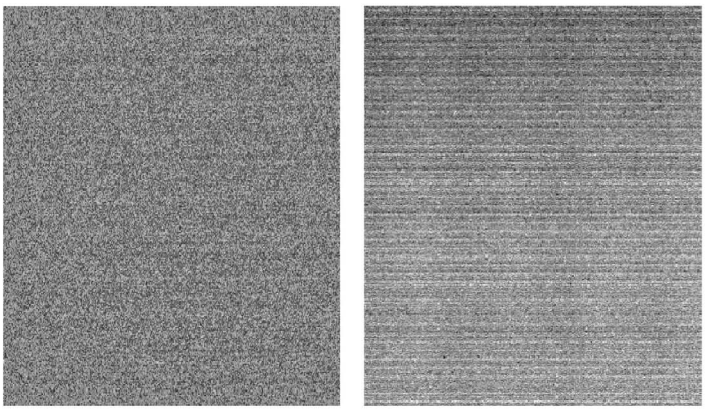

Figure 11.31 System noise compared at two pixel rates.

Important Points

1. The pixel source follower amplifier ultimately limits the read noise floor for CCD and CMOS imagers. PTC determines if the ideal noise floor has been achieved.
2. Reset and offset FPN noise are removed by CDS/DCDS signal processing.
3. A dark transfer curve (DTC) is generated without a light source to determine various dark current performance parameters, including the PT conversion constant $K_{\mathrm{ADC}}(\mathrm{e}^-/\mathrm{DN})$.
4. Thermal dark current FPN dominates dark shot noise at all signal levels.
5. ADC quantizing noise is made negligible by hiding the noise in random noise, such as pixel source follower noise. For proper noise encoding, $K_{\mathrm{ADC}}(\mathrm{e}^-/\mathrm{DN})$ is made equal to the read noise level in electron units.
6. The number of DN levels required to encode both read noise and full well optimally is equal to the sensor's dynamic range.
7. Linear ADC encoding excessively digitizes the noise source, such as shot noise and FPN. Optimal encoding is achieved when $K_{\mathrm{ADC}}(\mathrm{e}^-/\mathrm{DN})$ is made equal to the noise level in electron units.

Chapter 12
Lux Transfer

12.1 Introduction

A lux transfer curve (LTC) is a powerful extension of PTC, whereas a PTC is generated with an uncalibrated light source, and a LTC utilizes an absolute light source.[9] Therefore, LTC characterizes a camera system in absolute terms. For example, commercial camera sensitivity is often quoted in terms of "minimum detection limit" at an illumination level typically specified in units of lux. LTC will produce this figure-of-merit parameter in addition to other absolute performance parameters.

A LTC is based on the relation

$$\left[\frac{\mathrm{S}}{\mathrm{N}}\right]_{\mathrm{A\_FF}} = \frac{S_{\mathrm{A}}}{[\sigma^2_{\mathrm{READ}} + S_{\mathrm{A}} + (S_{\mathrm{A}}P_{\mathrm{N}})^2]^{1/2}}, \tag{12.1}$$

where $[\mathrm{S/N}]_{\mathrm{A\_FF}}$ is the absolute flat-field S/N performance, and

$$S_{\mathrm{A}} = LN_{\mathrm{L}}t_{\mathrm{I}}\mathrm{QE}_{\mathrm{I}}P_{\mathrm{A}}T_{\mathrm{L}}[4f\#^2(1+m)^2]^{-1}, \tag{12.2}$$

which is the absolute signal (e^-), where $f\#$ and m are the f number and magnification of a lens above the imager, T_{L} is the transmission of the lens, L is the luminance light level emitted from a Lambertian diffuse surface that overfills the collection lens (or detector if a lens is not used) given in lux, and N_{L} is the number of photons/cm^2-sec for one lux. For example, the number of photons at a 0.550-μm wavelength (green) for one lux is 4.02×10^{11} photons/cm^2-sec. Discussions below assume this wavelength to be a standard.

Signal can also be expressed in radiometric units as

$$S_{\mathrm{A}} = N_{\mathrm{P}}t_{\mathrm{I}}\mathrm{QE}_{\mathrm{I}}P_{\mathrm{A}}T_{\mathrm{L}}[4f\#^2(1+m)^2]^{-1}, \tag{12.3}$$

where N_{P} is photons/cm^2/sec at a specific wavelength.

The following examples demonstrate how LTCs are generated and applied using the relations above. A simulation computer program used to create LTCs is presented in Appendix C as a reference.

Example 12.1

Generate a standard flat-field LTC, with and without pixel FPN, for the following camera parameters:

$$T_{\mathrm{L}} = 1$$

$$f\# = 30$$

$$m = 0.001$$

$$\mathrm{QE}_{\mathrm{I}} = 0.8$$

$$P_{\mathrm{A}} = (8 \times 10^{-4})^2 = 6.4 \times 10^{-7}\ \mathrm{cm}^2$$

$$S_{\mathrm{FW}} = 2 \times 10^5\ \mathrm{e}^-$$

$$\sigma_{\mathrm{SF}} = 5\ \mathrm{e}^-$$

$$P_{\mathrm{N}} = 0.01$$

$$\lambda = 0.550\ \mu\mathrm{m}$$

$$t_{\mathrm{I}} = 1000, 10, \text{ and } 0.1\ \mathrm{sec}$$

Assume dark current is negligible (i.e., $D_{\mathrm{FM}} = 0$). Also, generate a LTC without a lens for the same parameters.

Solution:
From Eqs. (12.1) and (12.2), Fig. 12.1 presents the desired LTCs. The read noise, shot noise, and FPN regimes are labeled for the 0.1-sec curve. S/N performance for

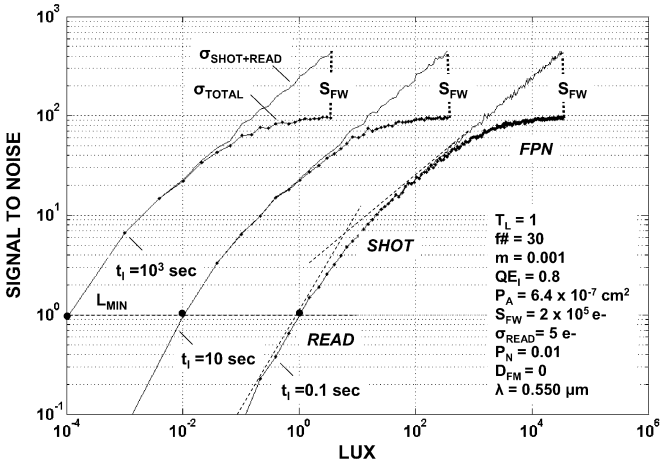

Figure 12.1 Classical LTC as a function of lux light level showing three noise regimes.

each exposure asymptotically approaches 100 (i.e., $1/P_{\mathrm{N}}$) when FPN is present, whereas the shot noise limited curves exhibit an S/N of 447 (i.e., $S_{\mathrm{FW}}^{1/2}$) at full well. The curves are used to predict the amount of light required to reach a specified S/N level. For example, it takes 36 k lux to achieve S/N $= 447$ for a 0.1-sec exposure.

Figure 12.2 presents LTCs without a lens. Note in comparison to Fig. 12.1 that the lens reduces the light level to the detector by 3600$\times$ because of the $4f\#^2$ term in Eq. (12.2) (i.e., 4×30^2). For a 0.1-sec exposure, it takes only 10 lux to achieve maximum S/N (i.e., 447 without FPN).

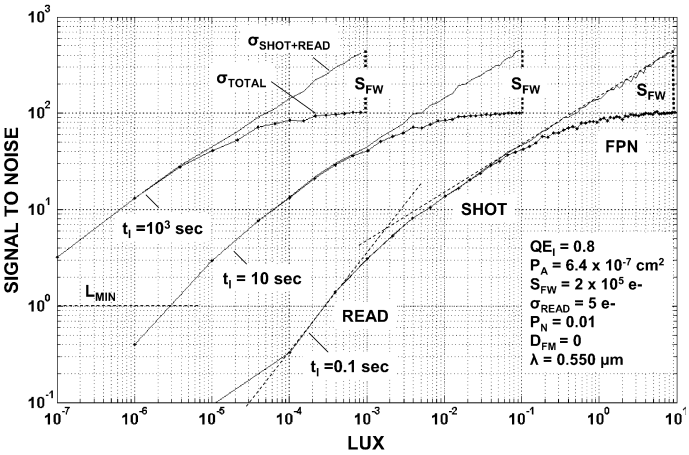

Figure 12.2 Corresponding LTC for Fig. 12.1 without a lens.

Example 12.2

For the same camera parameters specified in Example 12.1, generate LTCs by varying the integration time for the family of light levels: $L = 0.1$, 10, and 1000.

Solution:
From Eqs. (12.1) and (12.2), Fig. 12.3 presents the desired LTCs.

Example 12.3

This LTC example includes dark current noise, which makes S/N performance dependent on operating temperature. Generate a flat-field LTC, given the

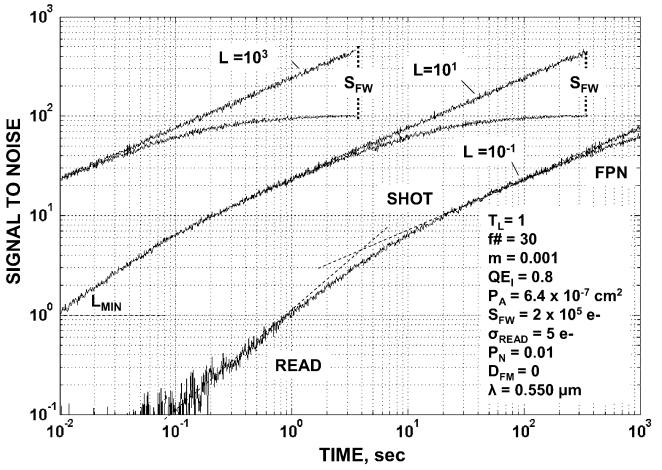

Figure 12.3 Corresponding LTC as a function of exposure time for Fig. 12.1.

following parameters:

$$D_{\mathrm{FM}} = 0.3 \text{ nA/cm}^2$$
$$D_{\mathrm{N}} = 0.30$$
$$T = 358 \text{ K}$$
$$T_{\mathrm{L}} = 1$$
$$f\# = 3$$
$$m = 0.001$$
$$\mathrm{QE_I} = 0.2$$
$$P_{\mathrm{A}} = (2 \times 10^{-4})^2 = 4 \times 10^{-8} \text{ cm}^2$$
$$S_{\mathrm{FW}} = 10^4 \text{ e}^-$$
$$\sigma_{\mathrm{SF}} = 10 \text{ e}^-$$
$$P_{\mathrm{N}} = 0.01$$
$$\lambda = 0.550 \text{ µm}$$
$$t_{\mathrm{I}} = 0.001, 0.01, \text{ and } 0.1 \text{ sec}$$

For comparison, also provide a LTC without dark current FPN.

Solution:
The read noise is composed of source follower and dark noise, i.e.,

$$\sigma_{\mathrm{READ}} = (\sigma^2_{\mathrm{SF}} + \sigma^2_{\mathrm{D\_SHOT}} + \sigma^2_{\mathrm{D\_FPN}})^{1/2}, \tag{E12.1}$$

where the dark shot noise and FPN sources are described in Sec. 11.4. Substituting this relation into Eq. (12.1) produces the LTC shown in Fig. 12.4. Dark current and related noise generated for each exposure are indicated in the figure. For example, for a 0.1 exposure, the dark current FPN totals 123 e^- (i.e., $\sigma_{D\_FPN} = 413 \times D_N$) and thus degrades S/N significantly. In Fig. 12.5, dark current FPN is removed. In this case, the dark current shot noise of 20 e^- degrades S/N only slightly (i.e., $\sigma_{D\_SHOT} = 413^{1/2}$).

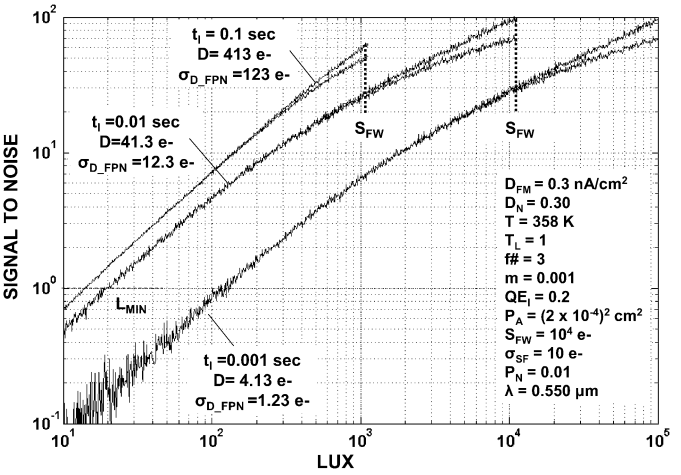

Figure 12.4 LTC with thermal dark current with dark FPN.

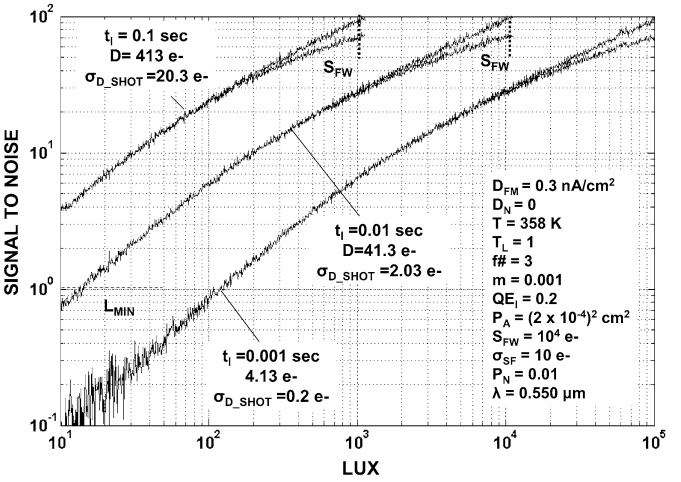

Figure 12.5 Corresponding LTC for Fig. 12.4 without dark FPN.

12.2 Minimum Detection Limit

Minimum detectable sensitivity is defined when S/N = 1, i.e., from Eq. (12.1):

$$1 = \frac{S_{\mathrm{A}}}{[\sigma^2_{\mathrm{READ}} + S_{\mathrm{A}} + (S_{\mathrm{A}}P_{\mathrm{N}})^2]^{1/2}}. \tag{12.4}$$

The illumination level for this condition is derived by first writing Eq. (12.4) into quadratic form as

$$1 = (P^2_{\mathrm{N}} - 1)S^2_{\mathrm{A}} + S_{\mathrm{A}} + \sigma^2_{\mathrm{READ}}. \tag{12.5}$$

Since $P^2_{\mathrm{N}} \ll 1$, Eq. (12.5) simplifies to

$$S^2_{\mathrm{A}} - S_{\mathrm{A}} - \sigma^2_{\mathrm{READ}} = 0. \tag{12.6}$$

Solving for a positive signal yields

$$S_{\mathrm{A\_MIN}} = \frac{1 + (1 + 4\sigma^2_{\mathrm{READ}})^{1/2}}{2}, \quad \mathrm{S/N} = 1, \tag{12.7}$$

where $S_{\mathrm{A\_MIN}}$ is the absolute signal level for S/N $= 1$.

Substituting $S_{\mathrm{A\_MIN}}$ into Eq. (12.2) and solving for the amount of lux yields

$$L_{\mathrm{MIN}} = \frac{S_{\mathrm{A\_MIN}}}{N_{\mathrm{L}}t_{\mathrm{I}}\mathrm{QE}_{\mathrm{I}}P_{\mathrm{A}}T_{\mathrm{L}}[4f\#^2(1+m)^2]^{-1}}, \tag{12.8}$$

where L_{MIN} is the light level that produces S/N $= 1$.

Equation (12.8) represents an important performance camera figure of merit. Note that the detection limits are indicated for the LTCs shown in Figs. 12.1–12.5. For example, the limits for Fig. 12.1 are 10^{-4}, 10^{-2}, and 10^{0} lux for the three exposures analyzed.

High-performance, cooled, backside-illuminated imagers exhibit impressive low-light sensitivity performance. For example, Fig. 12.6 analyzes an imager with

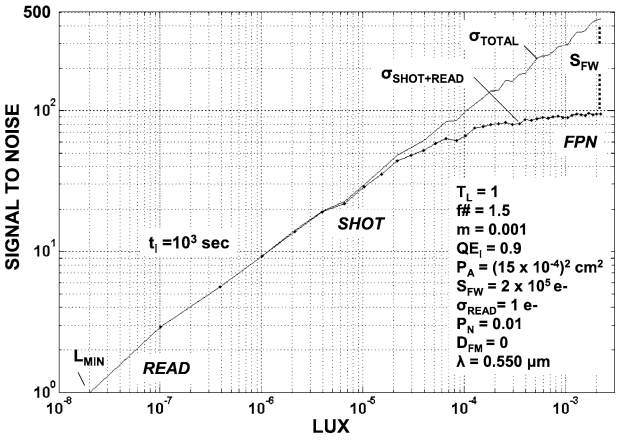

Figure 12.6 LTC generated for an ultra-sensitive astronomical camera system.

a detection limit of 2×10^{-8} lux for the parameters indicated. A camera system like this is typically found at astronomical observatories.

Example 12.4

Plot the detection limit as a function of read noise for different pixel sizes ($p_{\mathrm{ix}} = 2$, 3, 4, 6, 10, and 15 μm). Assume these parameters:

$$
\begin{aligned}
&T_{\mathrm{L}} = 1 \\
&f\# = 3 \\
&m = 0.001 \\
&\mathrm{QE}_{\mathrm{I}} = 0.25 \\
&S_{\mathrm{FW}} = 4 \times 10^4 \ \mathrm{e}^- \\
&P_{\mathrm{N}} = 0.01 \\
&\lambda = 0.550 \ \mu\mathrm{m} \\
&t_{\mathrm{I}} = 0.03 \ \mathrm{sec}
\end{aligned}
$$

Also plot the minimum illumination required for different f numbers ($f\# = 3$, 5, 6, 8, 11, and 16). Assume $p_{\mathrm{ix}} = 4$ μm.

Solution:
From Eq. (12.8), Figs. 12.7 and 12.8 present the desired plots. It is interesting to compare these curves to small pixel–commercial camera data sheets that show similar characteristics.

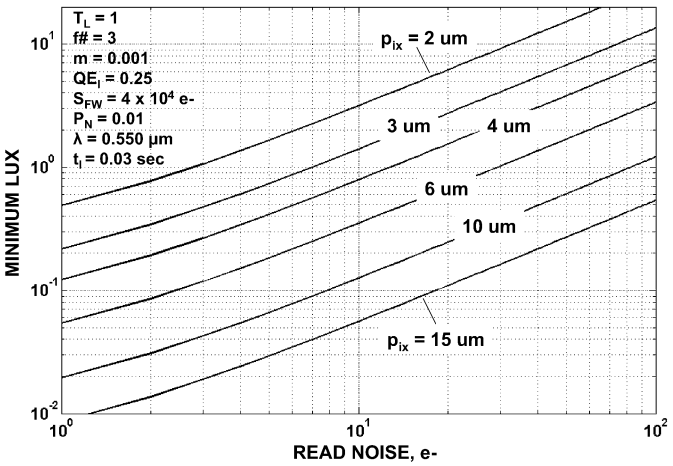

Figure 12.7 Minimum detectable light level as a function of read noise and pixel size.

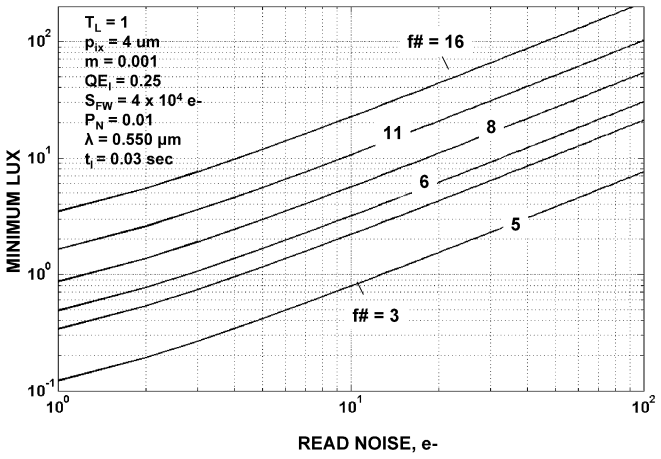

Figure 12.8 Minimum detectable light level as a function of read noise and lens f-number.

12.3 Responsivity

Responsivity is a common performance parameter used to specify a camera's overall sensitivity. This figure of merit is defined as

$$R_{\mathrm{e}}(V_{\mathrm{SN}}) = A_{\mathrm{SN}} N_{\mathrm{L}} \mathrm{QE}_{\mathrm{I}} P_{\mathrm{A}}, \tag{12.9}$$

where $R_{\mathrm{e}}(V_{\mathrm{SN}})$ is the pixel responsivity at the pixel's sense node (V/lux-sec), and A_{SN} is the pixel's sense node gain (V/e$^-$).

Note that V/lux-sec is a relative unit and can be misleading, depending on what point within the camera the voltage is measured. For example, responsivity may also be specified downstream of the sense node where the voltage gain is different. This problem is circumvented by specifying responsivity in absolute terms of e$^-$/lux-sec as

$$R_{\mathrm{e}} = N_{\mathrm{L}} \mathrm{QE}_{\mathrm{I}} P_{\mathrm{A}}. \tag{12.10}$$

In this case, responsivity is only dependent on the pixel size and quantum efficiency, and it is independent of voltage gain. It is assumed that the interacting QE applies to the entire pixel and not just the pixel's active fill factor.

Example 12.5

Plot pixel responsivity in units of V/lux-sec and e$^-$/lux-sec, given the following parameters:

$$\mathrm{QE_I} = 0.25$$
$$P_\mathrm{A} = (4 \times 10^{-4})^2 = 1.6 \times 10^{-7}\ \mathrm{cm}^2$$
$$\lambda = 0.550\ \mu\mathrm{m}\ (N_\mathrm{L} = 4.02 \times 10^{11}\ \text{photons/cm}^2\text{-sec})$$
$$A_\mathrm{SN} = 10, 20, 30, 40, 50, \text{ and } 60\ \mu\mathrm{V/e}^-$$

Solution:
Figure 12.9 plots relative responsivity as defined by Eq. (12.9). The responsivity

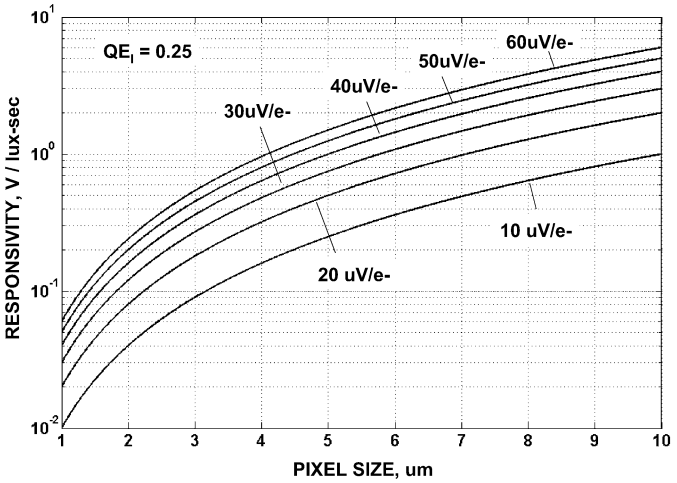

Figure 12.9 Relative responsivity as function of pixel size and sense node gain (V/e^-).

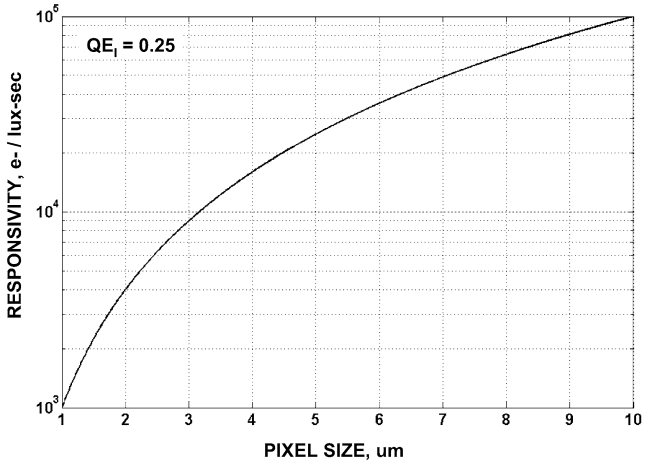

Figure 12.10 Absolute responsivity as a function of pixel size.

is different depending on A_{SN}. Figure 12.10 plots absolute responsivity using Eq. (12.10), producing a single plot.

12.4 Modulation LTC

Assuming the contrast is relatively low (refer to Chapter 9), LTC also can be applied to images through the relation

$$\left[\frac{\mathrm{S}}{\mathrm{N}}\right]_{\mathrm{A\_I}} = \frac{M_{\mathrm{I}} S_{\mathrm{I}}}{[\sigma^2_{\mathrm{READ}} + S_{\mathrm{I}} + (S_{\mathrm{I}} P_{\mathrm{N}})^2]^{1/2}}, \tag{12.11}$$

where $[\mathrm{S/N}]_{\mathrm{A\_I}}$ is the absolute S/N of the image, M_{I} is the image modulation factor, and S_{I} is the absolute average signal level of the image given either by Eq. (12.2) or Eq. (12.3).

From Chapter 10 discussions, $[\mathrm{S/N}]_{\mathrm{I}}$ can be expressed in terms of $[\mathrm{S/N}]_{\mathrm{FF}}$ through

$$\left[\frac{\mathrm{S}}{\mathrm{N}}\right]_{\mathrm{A\_I}} = \left[\frac{\mathrm{S}}{\mathrm{N}}\right]_{\mathrm{A\_FF}} M_{\mathrm{I}}. \tag{12.12}$$

This process produces a modulation LTC (MLTC). As discussed in Chapter 10, optimum S/N for an image is achieved when flat-field S/N is maximized.

Example 12.6

Generate MLTCs, given that the image exhibits a modulation factor of $M_{\mathrm{I}} = 0.0318$. Assume the following parameters:

$T_{\mathrm{L}} = 1$

$f\# = 30$

$m = 0.001$

$\mathrm{QE}_{\mathrm{I}} = 0.8$

$P_{\mathrm{A}} = (8 \times 10^{-4})^2 = 6.4 \times 10^{-7}\ \mathrm{cm}^2$

$S_{\mathrm{FW}} = 2 \times 10^5\ \mathrm{e}^-$

$\sigma_{\mathrm{SF}} = 5\ \mathrm{e}^-$

$P_{\mathrm{N}} = 0.01$

$\lambda = 0.550\ \mu\mathrm{m}$

$t_{\mathrm{I}} = 1000, 10,$ and 0.1 sec

Solution:
From Eq. (12.11), Fig. 12.11 presents the desired modulation LTCs. Note that pixel FPN must be removed before quality images can be obtained (i.e., S/N > 10). The

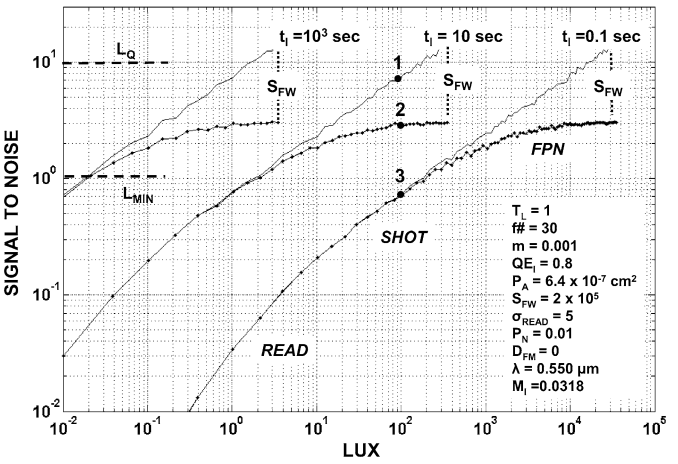

Figure 12.11 Modulation LTC showing minimum detection limit (L_{MIN}) and quality image level (L_{Q}).

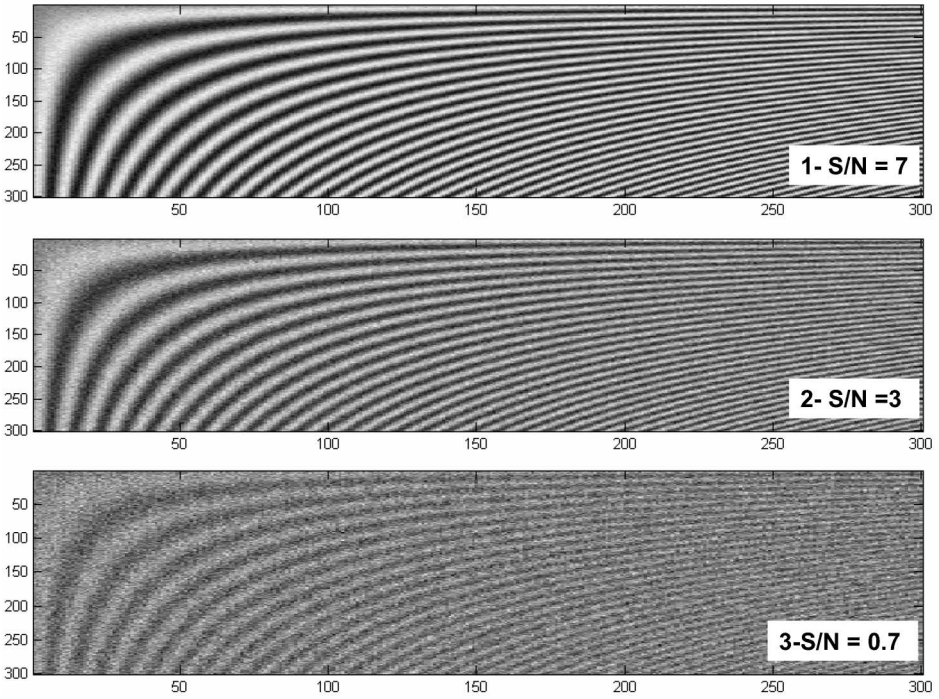

Figure 12.12 Corresponding images for the three data points shown in Fig. 12.11.

horizontal line at S/N $= 1$ indicates the minimum detection limit for the camera. Figure 12.12 shows simulated sinusoidal images with $M_{\mathrm{I}} = 0.0318$ for three data

points shown in Fig. 12.11 (labeled 1, 2, and 3). The corresponding S/N performance for each image is also indicated.

The signal level required to achieve a specified S/N is derived by first writing Eq. (12.11) in quadratic form for S_{I} as

$$S_{\mathrm{I}}^2\left(\left[\frac{\mathrm{S}}{\mathrm{N}}\right]_{\mathrm{A\_I}}^2 - M_{\mathrm{I}}^2\right) + S_{\mathrm{I}}\left[\frac{\mathrm{S}}{\mathrm{N}}\right]_{\mathrm{A\_I}}^2 + \sigma_{\mathrm{READ}}^2\left[\frac{\mathrm{S}}{\mathrm{N}}\right]_{\mathrm{A\_I}}^2 = 0. \tag{12.13}$$

From this equation, the signal S_{I} is then solved for a specified S/N and read noise level. Once the signal is known, the lux light level is determined through

$$\mathrm{L_{UX}} = \frac{S_{\mathrm{I}}}{N_{\mathrm{LUX}} t_{\mathrm{I}} \mathrm{QE_I} P_{\mathrm{A}} T_{\mathrm{L}} [4f\#^2(1+m)^2]^{-1}}. \tag{12.14}$$

Example 12.7

Plot light level as a function of the image modulation constant for $[\mathrm{S/N}]_{\mathrm{A\_I}} = 1$, 2, 5, 10, 20, 30, 50, and 70. Assume the following parameters:

$T_{\mathrm{L}} = 1$

$f\# = 3$

$m = 0.001$

$\mathrm{QE_I} = 0.8$

$P_{\mathrm{A}} = (8 \times 10^{-4})^2 = 6.4 \times 10^{-7}$ cm^2

$P_{\mathrm{N}} = 0.01$

$\lambda = 0.550$ μm

$t_{\mathrm{I}} = 1$ sec

$\sigma_{\mathrm{SF}} = 10\ \mathrm{e}^-$

$S_{\mathrm{FW}} = 10^5\ \mathrm{e}^-$

Vary the image modulation from 0 to 0.25. Make separate plots with and without FPN.

Solution:
Figure 12.13 shows the desired plots without FPN. Note that full well limits S/N performance to 70 for the highest modulation level (i.e., $M_{\mathrm{I}} = 0.25$). Figure 12.14 assumes that pixel FPN is present, limiting S/N to only 23 for the same modulation level.

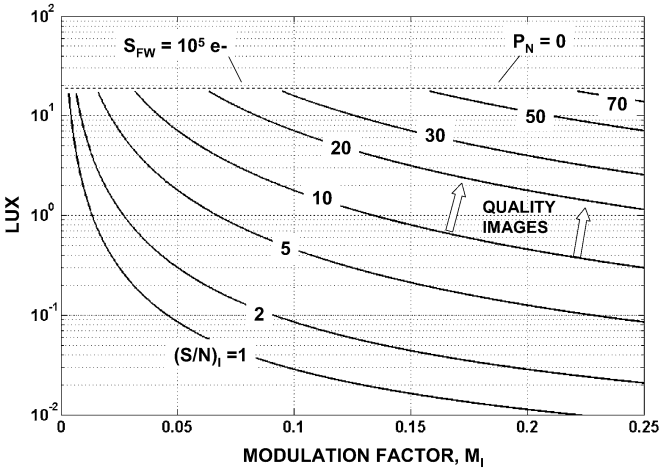

Figure 12.13 Lux light level required to reach a specified S/N performance level with modulation factor (without FPN).

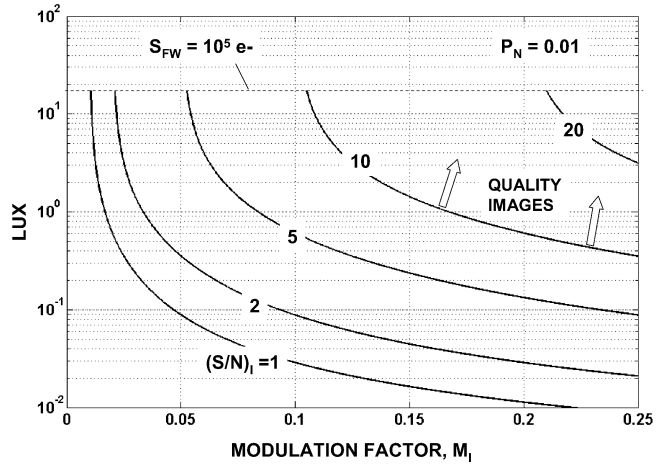

Figure 12.14 Lux light level required to reach a specified S/N performance level with modulation factor (with FPN).

12.5 Acceptable Image

A quality image is generated when S/N > 10 (i.e., the first acceptable image as defined by the ISO12232 standard). In equation form, this is

$$10 = \frac{M_{\mathrm{I}} S_{\mathrm{I}}}{[\sigma^2_{\mathrm{READ}} + S_{\mathrm{I}} + (S_{\mathrm{I}} P_{\mathrm{N}})^2]^{1/2}}. \tag{12.15}$$

The illumination level required to meet this condition is found by writing Eq. (12.15) in quadratic form as

$$10 = (100P_{\mathrm{N}}^2 - M_{\mathrm{I}}^2)S_{\mathrm{I}}^2 + 100S_{\mathrm{I}} + 100\sigma_{\mathrm{READ}}^2. \tag{12.16}$$

Solving for signal and substituting into

$$L_{\mathrm{Q}} = \frac{S_{\mathrm{Q}}}{N_{\mathrm{L}}t_{\mathrm{I}}\mathrm{QE}_{\mathrm{I}}P_{\mathrm{A}}T_{\mathrm{L}}[4f\#^2(1+m)^2]^{-1}} \tag{12.17}$$

yields the average lux level required to achieve S/N $= 10$.

Example 12.8

Use the same parameters as Example 12.7 and plot the light level required to achieve $[\mathrm{S/N}]_{\mathrm{I}} = 10$ for an image modulation of $M_{\mathrm{I}} = 0.2$ as a function of an operating temperature that ranges from 200 to 400 K. Assume these dark current parameters:

$$D_{\mathrm{FM}} = 0.3 \text{ nA/cm}^2$$

$$D_{\mathrm{N}} = 0.3$$

$$t_{\mathrm{I}} = 0.001, 0.01, 0.1, 1, \text{ and } 10 \text{ sec}$$

Plot the results with and without dark FPN.

Solution:
The read noise is composed of source follower and dark noise as defined by Eq. (E12.1). From Eq. (12.17), Fig. 12.15 presents the desired plots. Note that

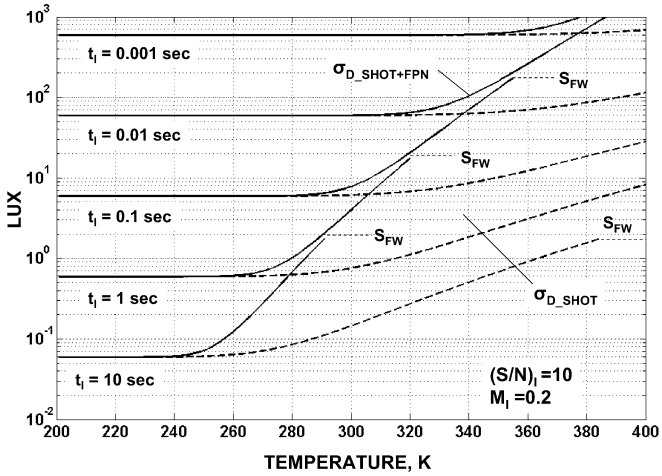

Figure 12.15 Lux light level to achieve a $[\mathrm{S/N}]_{\mathrm{I}} = 10$ as a function of operating temperature.

the light level must be increased as the temperature (and dark current) increases. Full well eventually limits performance for all exposures. Removing dark FPN extends performance to higher operating temperatures, as shown.

12.6 LTC Ratio

LTCs can be compared through their ratio as

$$\left[\frac{\mathrm{S}}{\mathrm{N}}\right]_{\mathrm{R}} = \frac{\left[\frac{\mathrm{S}}{\mathrm{N}}\right]_{\mathrm{A\_FF1}}}{\left[\frac{\mathrm{S}}{\mathrm{N}}\right]_{\mathrm{A\_FF2}}}, \tag{12.18}$$

where $(\mathrm{S/N})_{\mathrm{A\_FF1}}$ and $(\mathrm{S/N})_{\mathrm{A\_FF2}}$ are the two LTC sets. Typically, one performance parameter is varied to show performance tradeoffs as demonstrated in the next example.

Example 12.9

Compare a flat-field LTC generated at an operating temperature of 300 K to other LTCs taken at 260, 280, 300, 320, 340, 360, and 380 K. Assume the following parameters:

$T_{\mathrm{L}} = 1$

$f\# = 3$

$m = 0.001$

$\mathrm{QE_I} = 0.8$

$P_{\mathrm{A}} = 6.4 \times 10^{-7}$ cm^2

$S_{\mathrm{FW}} = 2 \times 10^5$

$\sigma_{\mathrm{SF}} = 5$ e$^-$

$P_{\mathrm{N}} = 0.01$

$D_{\mathrm{FM}} = 0.1$ nA/cm^2

$D_{\mathrm{N}} = 0$ (assume dark current FPN is removed through subtraction)

$\lambda = 0.550$ μm

$t_{\mathrm{I}} = 1$ sec

On a separate plot, also generate individual LTCs for each operating temperature.

Solution:
Figure 12.16 shows LTCs at each operating temperature. Note that S/N performance does not improve as the operating temperature approaches 260 K because dark current shot noise becomes negligible. From Eq. (12.18), Fig. 12.17 shows LTC comparisons. For example, S/N performance at an operating temperature of 300 K is approximately 10 times better than 380 K operation for a 10^{-1} lux light level.

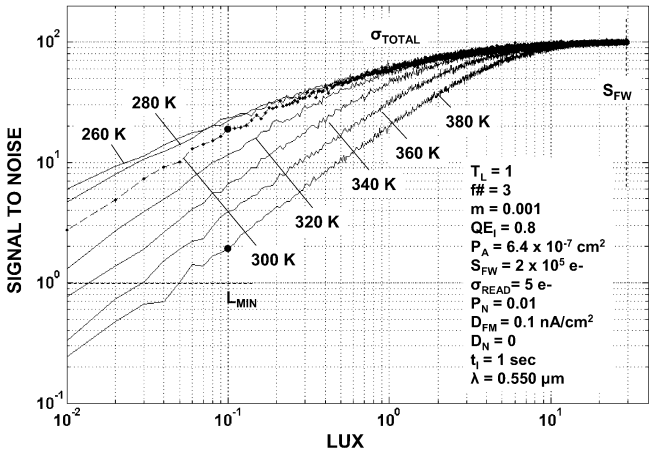

Figure 12.16 LTC at different operating temperatures.

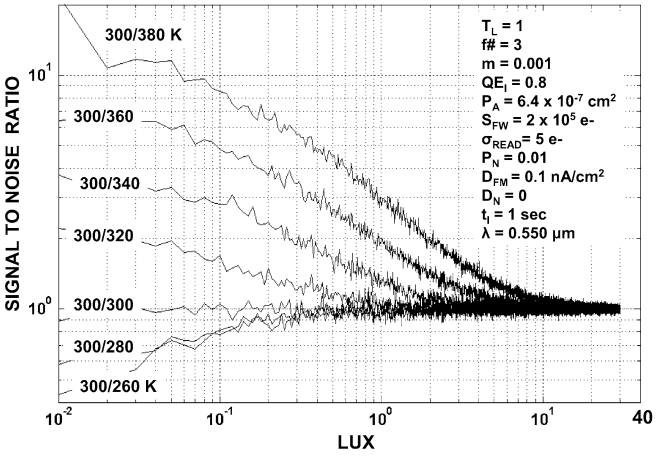

Figure 12.17 Comparison LTC for Fig. 12.16 showing S/N at different operating temperatures relative to 300 K.

12.7 LTC Data Sequence

Before a LTC is generated, dark and light PTCs are usually produced to determine individual detector performance parameters (S_{FW}, σ_{READ}, P_{N}, D_{N}, D_{FM}, etc.). For example, Fig. 12.18 shows a flat-field PTC taken by a CMOS VGA imager listing the parameters that were found, including a $\mathrm{QE} = 0.25$. Theoretically, a LTC is then generated by substituting PTC parameters into Eqs. (12.1) and (12.2). This plot is shown in Fig. 12.19. Next, an absolute light source is used to generate an experimental LTC curve. Figure 12.20 shows this response. Modeling and experimental data are in good agreement for the imager.

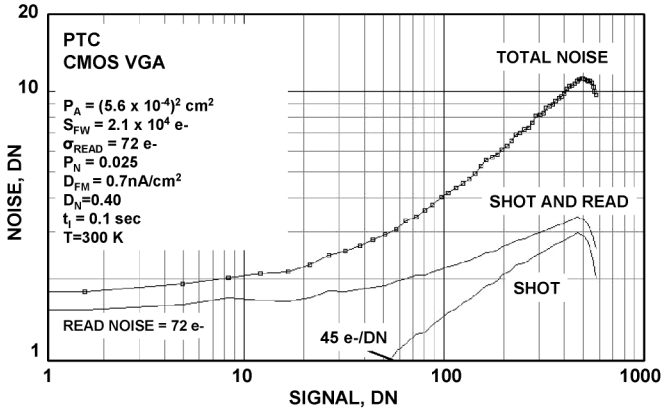

Figure 12.18 PTC responses for a CMOS imager.

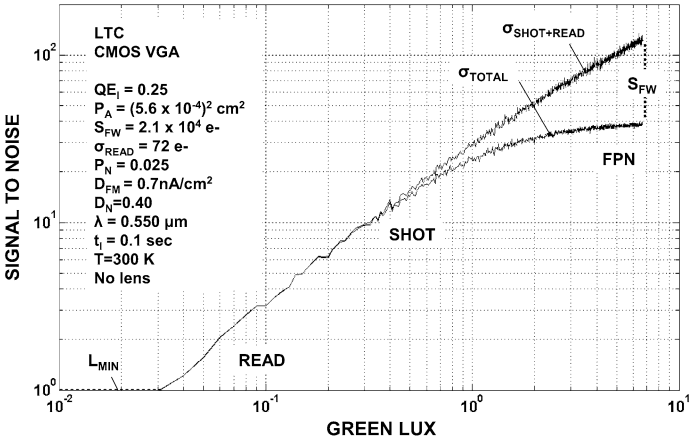

Figure 12.19 Corresponding LTC for the CMOS array characterized in Fig. 12.18.

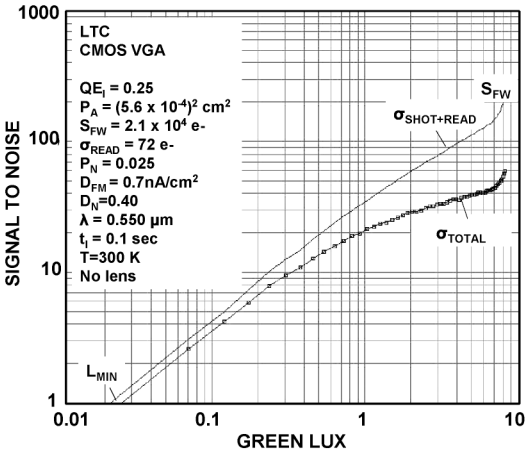

Figure 12.20 Corresponding experimental LTC for the CMOS array characterized in Fig. 12.18.

Example 12.10

For the LTC data shown in Fig. 12.20, determine the following:

1. Minimum detection limit, $L_{\rm MIN}$
2. Minimum detection limit, $L_{\rm MIN}$ for a $f\# = 3$ lens system
3. Relative responsivity, $R(V_{\rm SN})$
4. Absolute responsitivity, R

Assume a sense node sensitivity of 40 μV/e$^-$.

Solution:
From Fig. 12.20, the minimum detection limit for the imager is approximately 0.025 lux. A $f\# = 3$ lens reduces the light by $(4f\#^2) = 4 \times 3^2 = 36$. Hence, the minimum detectable light level is 0.9 lux.

From Eq. (12.9), the relative responsivity is

$$R_{\rm e}(V_{\rm SN}) = (40 \times 10^{-6}) \times (4.02 \times 10^{11}) \times 0.25 \times (5.6 \times 10^{-4})^2$$
$$= 1.26 \text{ V/lux-sec.}$$

From Eq. (12.10), the absolute responsivity is

$$R = (4.02 \times 10^{11}) \times 0.25 \times (5.6 \times 10^{-4})^2 = 3.15 \times 10^4 \text{ e}^-\text{/lux-sec.}$$

Important Points

1. A LTC is an extension of a PTC where data is generated by an absolute light source.

2. A LTC plots S/N performance as a function of absolute light level in photometric (lux) or radiometric (photons/cm^2-sec) units.
3. A LTC shows the minimum detectable light level for a camera system when S/N $= 0$.
4. MLTCs show the light level required to produce a quality image when S/N $= 10$.

Appendix A
PTC Data Reduction Example

This appendix demonstrates how various photon transfer products are generated from an experimental data set generated by a CMOS imager with V/e$^-$ nonlinearity.

Example A.1

Plot the following curves from the raw data set given in Table A.1:

Figure A.1 S(DN), σ_{TOTAL}(DN), $\sigma_{\mathrm{SHOT+READ}}$(DN) versus L
Figure A.2 σ_{TOTAL}(DN), σ_{SHOT}(DN), σ_{FPN}(DN) versus S(DN)
Figure A.3 V_{SF} versus V_{SN}
Figure A.4 $S(V_{\mathrm{SN}})$, $\sigma_{\mathrm{SHOT}}(V_{\mathrm{SN}})$ versus V_{SN}
Figure A.5 K_{ADC}(e$^-$/DN), S_{ADC}(e$^-$/DN), N_{ADC}(e$^-$/DN) versus S
Figure A.6 K_{ADC}(e$^-$/DN), S_{ADC}(e$^-$/DN), N_{ADC}(e$^-$/DN) nonlinearity (%) versus S
Figure A.7 $\sigma_{\mathrm{SHOT+FPN}}$, σ_{SHOT}, σ_{FPN} versus S
Figure A.8 False S versus True S
Figure A.9 P_{N} versus S
Figure A.10 $S_{\mathrm{SN}}(\mathrm{e}^-/V_{\mathrm{SN}})$, $N_{\mathrm{SN}}(\mathrm{e}^-/V_{\mathrm{SN}})$ versus S
Figure A.11 $S_{\mathrm{SN}}(\mu V_{\mathrm{SN}}/\mathrm{e}^-)$, $N_{\mathrm{SN}}(\mu V_{\mathrm{SN}}/\mathrm{e}^-)$ versus S
Figure A.12 Sense node S/N sensitivity ratio $\dfrac{S_{\mathrm{SN}}(\mathrm{e}^-/V_{\mathrm{SN}})}{N_{\mathrm{SN}}(\mathrm{e}^-/V_{\mathrm{SN}})}$ versus S
Figure A.13 C_{SN} versus V_{SN}
Figure A.14 C_{SN} versus S
Figure A.15 S/N($\sigma_{\mathrm{SHOT+FPN}}$, σ_{SHOT}) versus S

Table A.1 Raw experimental data.

COL A:	Raw ADC signal, $\mathrm{DN}_{\mathrm{ADC}}$
COL B:	Total noise, σ_{TOTAL}(DN)
COL C:	Shot and read noise, $\sigma_{\mathrm{SHOT+READ}}$(DN)
COL D:	Relative light level, L
COL E:	Light level gain, A_{L}

Note that **COL C** is generated by differencing two identical frames taken back to back, pixel by pixel, to remove FPN.

Table A.1 Raw experimental data.

	A	B	C	D	E
Data Points	Raw Signal (DN)	Total Noise (rms DN)	Shot+ Read Noise (rms DN)	Light Level	Light Gain
1	1.16E+03	1.22E+01	1.22E+01	3.10E−02	1.00E+00
2	1.31E+03	1.63E+01	1.62E+01	6.20E−02	2.00E+00
3	1.57E+03	2.19E+01	2.15E+01	1.17E−01	3.77E+00
4	1.76E+03	2.52E+01	2.45E+01	1.57E−01	5.06E+00
5	1.94E+03	2.79E+01	2.70E+01	1.93E−01	6.23E+00
6	2.31E+03	3.32E+01	3.16E+01	2.70E−01	8.71E+00
7	2.57E+03	3.65E+01	3.45E+01	3.24E−01	1.05E+01
8	3.11E+03	4.27E+01	3.95E+01	4.36E−01	1.41E+01
9	3.38E+03	4.57E+01	4.20E+01	4.93E−01	1.59E+01
10	3.77E+03	4.99E+01	4.49E+01	5.75E−01	1.85E+01
11	4.58E+03	5.71E+01	5.00E+01	7.47E−01	2.41E+01
12	5.06E+03	6.14E+01	5.30E+01	8.49E−01	2.74E+01
13	6.22E+03	6.99E+01	5.82E+01	1.10E+00	3.55E+01
14	7.51E+03	7.84E+01	6.30E+01	1.40E+00	4.50E+01
15	8.78E+03	8.67E+01	6.70E+01	1.67E+00	5.39E+01
16	9.68E+03	9.20E+01	6.95E+01	1.89E+00	6.10E+01
17	1.10E+04	9.88E+01	7.24E+01	2.20E+00	7.10E+01
18	1.20E+04	1.03E+02	7.40E+01	2.46E+00	7.94E+01
19	1.27E+04	1.08E+02	7.60E+01	2.64E+00	8.52E+01
20	1.40E+04	1.15E+02	7.85E+01	2.97E+00	9.58E+01
21	1.57E+04	1.22E+02	7.95E+01	3.45E+00	1.11E+02
22	1.62E+04	1.26E+02	8.10E+01	3.59E+00	1.16E+02
23	1.69E+04	1.27E+02	8.09E+01	3.78E+00	1.22E+02
24	1.77E+04	1.31E+02	8.19E+01	4.03E+00	1.30E+02
25	1.86E+04	1.36E+02	8.27E+01	4.28E+00	1.38E+02
26	1.98E+04	1.39E+02	8.20E+01	4.65E+00	1.50E+02
27	2.12E+04	1.44E+02	8.30E+01	5.09E+00	1.64E+02
28	2.26E+04	1.51E+02	8.34E+01	5.56E+00	1.79E+02
29	2.36E+04	1.55E+02	8.43E+01	5.90E+00	1.90E+02
30	2.55E+04	1.54E+02	8.25E+01	6.57E+00	2.12E+02
31	2.65E+04	1.58E+02	8.15E+01	6.92E+00	2.23E+02
32	2.82E+04	1.63E+02	8.07E+01	7.56E+00	2.44E+02
33	2.97E+04	1.64E+02	8.00E+01	8.16E+00	2.63E+02
34	3.12E+04	1.64E+02	7.70E+01	8.82E+00	2.85E+02
35	3.20E+04	1.66E+02	7.63E+01	9.17E+00	2.96E+02

Table A.1 (Continued.)

	A	**B**	**C**	**D**	**E**
Data Points	Raw Signal (DN)	Total Noise (rms DN)	Shot+ Read Noise (rms DN)	Light Level	Light Gain
36	3.37E+04	1.60E+02	7.20E+01	9.94E+00	3.21E+02
37	3.41E+04	1.59E+02	7.04E+01	1.02E+01	3.28E+02
38	3.50E+04	1.61E+02	7.00E+01	1.06E+01	3.43E+02
39	3.64E+04	1.51E+02	6.45E+01	1.14E+01	3.67E+02
40	3.71E+04	1.49E+02	6.15E+01	1.19E+01	3.83E+02
41	3.78E+04	1.38E+02	5.78E+01	1.24E+01	3.98E+02
42	3.83E+04	1.30E+02	5.28E+01	1.26E+01	4.07E+02
43	3.87E+04	1.11E+02	4.51E+01	1.29E+01	4.17E+02

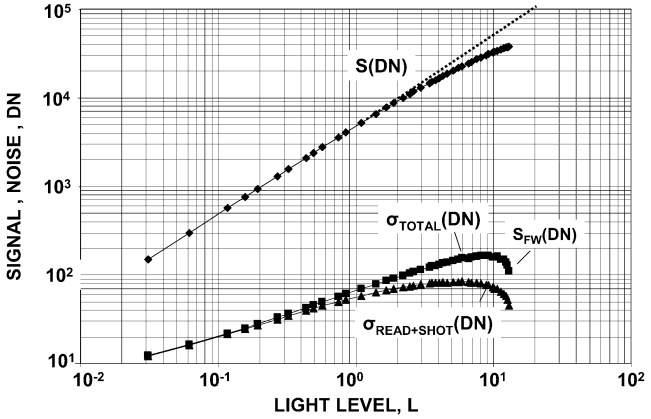

Figure A.1 Signal and noise as a function of light level.

Assume the following parameters for the detector and camera system:

Source follower gain: $A_{\mathrm{SF}} = 0.9$ V/V
CDS gain: $A_{\mathrm{CDS}} = 6$ V/V
ADC gain: $A_{\mathrm{ADC}} = 3250$ DN/V
Sense node reference voltage: $V_{\mathrm{REF}} = 3.1$ V
Source follower offset voltage: $V_{\mathrm{SF\_OFF}} = 1.9$ V
ADC offset level: $S_{\mathrm{ADC\_OFF}}(\mathrm{DN}) = 1007$
Read noise: $\sigma_{\mathrm{READ}}(\mathrm{DN}) = 5.93$

Solution:

Figure A.1

$S(\mathrm{DN})$, $\sigma_{\mathrm{TOTAL}}(\mathrm{DN})$, $\sigma_{\mathrm{SHOT+READ}}(\mathrm{DN})$ versus L.

Table A.2 Calculated results.

COL F: Signal in DN units

$$S(\mathrm{DN}) = \mathrm{DN}_{\mathrm{ADC}} - S_{\mathrm{ADC\_OFF}}(\mathrm{DN})$$

COL G: Signal shot noise

$$\sigma_{\mathrm{SHOT}}(\mathrm{DN}) = [\sigma_{\mathrm{SHOT+READ}}(\mathrm{DN})^2 - \sigma_{\mathrm{READ}}(\mathrm{DN})^2]^{1/2}$$

COL H: Pixel FPN

$$\sigma_{\mathrm{FPN}}(\mathrm{DN}) = [\sigma_{\mathrm{TOTAL}}(\mathrm{DN})^2 - \sigma_{\mathrm{SHOT+READ}}(\mathrm{DN})^2]^{1/2}$$

COL I: Shot and FPN

$$\sigma_{\mathrm{FPN+SHOT}}(\mathrm{DN}) = [\sigma_{\mathrm{FPN}}(\mathrm{DN})^2 + \sigma_{\mathrm{SHOT}}(\mathrm{DN})^2]^{1/2}$$

COL J: Source follower signal voltage

$$S(V_{\mathrm{SF}}) = \frac{S(\mathrm{DN})}{A_{\mathrm{CDS}} \times A_{\mathrm{ADC}}}$$

Figure A.2
S(DN), σ_{TOTAL}(DN), σ_{SHOT}(DN), σ_{FPN}(DN) versus S(DN)

Table A.3 Calculated results.

COL K: Source follower voltage

$$V_{\mathrm{SF}} = V_{\mathrm{SF\_OFF}} - S(V_{\mathrm{SF}})$$

COL L: Source follower noise voltage

$$\sigma_{\mathrm{SHOT}}(V_{\mathrm{SF}}) = \frac{\sigma_{\mathrm{SHOT}}(\mathrm{DN})}{A_{\mathrm{CDS}} A_{\mathrm{ADC}}}$$

COL M: Sense node signal voltage

$$S(V_{\mathrm{SN}}) = \frac{S(V_{\mathrm{SF}})}{A_{\mathrm{SF}}}$$

COL N: Raw sense node voltage

$$V_{\mathrm{SN}} = V_{\mathrm{REF}} - S(V_{\mathrm{SN}})$$

COL O: Sense node shot noise voltage

$$\sigma_{\mathrm{SHOT}}(V_{\mathrm{SN}}) = \frac{\sigma_{\mathrm{SHOT}}(V_{\mathrm{SF}})}{A_{\mathrm{SF}}}$$

Table A.2 Calculated results.

	F	**G**	**H**	**I**	**J**
Data Points	Signal (DN)	Shot Noise (rms DN)	FPN (rms DN)	FPN+ Shot Noise (rms DN)	SF Signal Voltage (V)
1	1.49E+02	1.07E+01	1.09E+00	1.07E+01	7.64E−03
2	2.99E+02	1.50E+01	2.27E+00	1.52E+01	1.53E−02
3	5.65E+02	2.07E+01	4.34E+00	2.11E+01	2.90E−02
4	7.57E+02	2.38E+01	5.87E+00	2.45E+01	3.88E−02
5	9.29E+02	2.63E+01	7.13E+00	2.73E+01	4.76E−02
6	1.30E+03	3.10E+01	1.00E+01	3.26E+01	6.68E−02
7	1.56E+03	3.40E+01	1.20E+01	3.60E+01	8.02E−02
8	2.10E+03	3.91E+01	1.62E+01	4.23E+01	1.08E−01
9	2.37E+03	4.16E+01	1.80E+01	4.53E+01	1.22E−01
10	2.76E+03	4.45E+01	2.18E+01	4.96E+01	1.42E−01
11	3.57E+03	4.96E+01	2.76E+01	5.68E+01	1.83E−01
12	4.05E+03	5.26E+01	3.10E+01	6.11E+01	2.08E−01
13	5.21E+03	5.79E+01	3.86E+01	6.96E+01	2.67E−01
14	6.51E+03	6.27E+01	4.67E+01	7.82E+01	3.34E−01
15	7.77E+03	6.67E+01	5.50E+01	8.65E+01	3.98E−01
16	8.67E+03	6.92E+01	6.03E+01	9.18E+01	4.45E−01
17	9.95E+03	7.22E+01	6.72E+01	9.86E+01	5.10E−01
18	1.10E+04	7.38E+01	7.23E+01	1.03E+02	5.64E−01
19	1.17E+04	7.58E+01	7.63E+01	1.08E+02	6.00E−01
20	1.30E+04	7.83E+01	8.46E+01	1.15E+02	6.64E−01
21	1.47E+04	7.92E+01	9.26E+01	1.22E+02	7.54E−01
22	1.52E+04	8.08E+01	9.60E+01	1.25E+02	7.79E−01
23	1.59E+04	8.06E+01	9.83E+01	1.27E+02	8.14E−01
24	1.67E+04	8.17E+01	1.03E+02	1.31E+02	8.58E−01
25	1.76E+04	8.25E+01	1.08E+02	1.36E+02	9.01E−01
26	1.88E+04	8.18E+01	1.12E+02	1.39E+02	9.64E−01
27	2.02E+04	8.28E+01	1.18E+02	1.44E+02	1.04E+00
28	2.16E+04	8.32E+01	1.26E+02	1.51E+02	1.11E+00
29	2.26E+04	8.41E+01	1.30E+02	1.55E+02	1.16E+00
30	2.45E+04	8.22E+01	1.30E+02	1.54E+02	1.26E+00
31	2.55E+04	8.13E+01	1.35E+02	1.57E+02	1.31E+00
32	2.72E+04	8.05E+01	1.42E+02	1.63E+02	1.39E+00
33	2.87E+04	7.98E+01	1.43E+02	1.64E+02	1.47E+00
34	3.02E+04	7.68E+01	1.45E+02	1.64E+02	1.55E+00
35	3.10E+04	7.61E+01	1.47E+02	1.66E+02	1.59E+00

Table A.2 (Continued.)

	F	G	H	I	J
Data Points	Signal (DN)	Shot Noise (rms DN)	FPN (rms DN)	FPN+ Shot Noise (rms DN)	SF Signal Voltage (V)
36	3.26E+04	7.18E+01	1.43E+02	1.60E+02	1.67E+00
37	3.31E+04	7.01E+01	1.42E+02	1.59E+02	1.70E+00
38	3.40E+04	6.97E+01	1.45E+02	1.61E+02	1.75E+00
39	3.53E+04	6.42E+01	1.37E+02	1.51E+02	1.81E+00
40	3.61E+04	6.12E+01	1.36E+02	1.49E+02	1.85E+00
41	3.68E+04	5.75E+01	1.25E+02	1.38E+02	1.89E+00
42	3.73E+04	5.25E+01	1.18E+02	1.29E+02	1.91E+00
43	3.77E+04	4.47E+01	1.02E+02	1.11E+02	1.93E+00

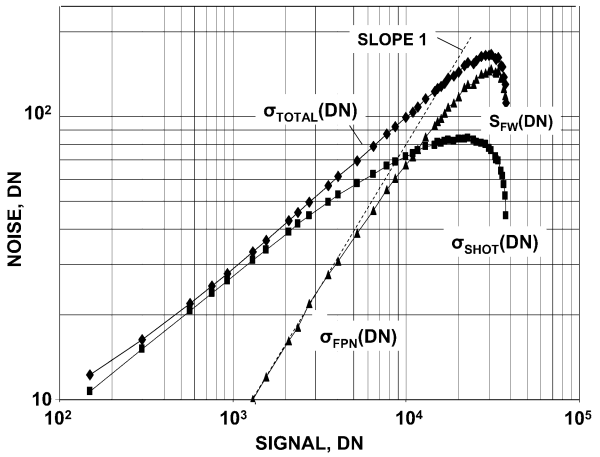

Figure A.2 Classical PTC responses showing FPN does not follow a slope 1 curve indicating V/e$^-$ nonlinearity is present.

Figure A.3

V_{SF} versus V_{SN}

The slope of this curve is the source follower gain, A_{SF}.

Figure A.4

$S(V_{\mathrm{SN}})$, $\sigma_{\mathrm{SHOT}}(V_{\mathrm{SN}})$ versus V_{SN}

For small signals, it can be assumed that

$$S_{\mathrm{ADC}}(\mathrm{e}^-/\mathrm{DN}) = N_{\mathrm{ADC}}(\mathrm{e}^-/\mathrm{DN}) = K_{\mathrm{ADC}}(\mathrm{e}^-/\mathrm{DN}) = \frac{S(\mathrm{DN})}{\sigma_{\mathrm{SHOT}}(\mathrm{DN})^2}.$$

Table A.3 Calculated results.

	K	**L**	**M**	**N**	**O**
Data Points	SF Voltage (V)	SF Shot Noise (rms V)	Sense Node Signal (V)	Sense Node Voltage (V)	Sense Node Shot Noise (rms V)
1	1.89E+00	5.47E−04	8.49E−03	3.09E+00	6.08E−04
2	1.88E+00	7.71E−04	1.70E−02	3.08E+00	8.57E−04
3	1.87E+00	1.06E−03	3.22E−02	3.07E+00	1.18E−03
4	1.86E+00	1.22E−03	4.31E−02	3.06E+00	1.35E−03
5	1.85E+00	1.35E−03	5.29E−02	3.05E+00	1.50E−03
6	1.83E+00	1.59E−03	7.42E−02	3.03E+00	1.77E−03
7	1.82E+00	1.74E−03	8.91E−02	3.01E+00	1.93E−03
8	1.79E+00	2.00E−03	1.20E−01	2.98E+00	2.23E−03
9	1.78E+00	2.13E−03	1.35E−01	2.96E+00	2.37E−03
10	1.76E+00	2.28E−03	1.57E−01	2.94E+00	2.54E−03
11	1.72E+00	2.55E−03	2.03E−01	2.90E+00	2.83E−03
12	1.69E+00	2.70E−03	2.31E−01	2.87E+00	3.00E−03
13	1.63E+00	2.97E−03	2.97E−01	2.80E+00	3.30E−03
14	1.57E+00	3.22E−03	3.71E−01	2.73E+00	3.57E−03
15	1.50E+00	3.42E−03	4.43E−01	2.66E+00	3.80E−03
16	1.46E+00	3.55E−03	4.94E−01	2.61E+00	3.95E−03
17	1.39E+00	3.70E−03	5.67E−01	2.53E+00	4.11E−03
18	1.34E+00	3.78E−03	6.26E−01	2.47E+00	4.20E−03
19	1.30E+00	3.89E−03	6.67E−01	2.43E+00	4.32E−03
20	1.24E+00	4.01E−03	7.38E−01	2.36E+00	4.46E−03
21	1.15E+00	4.06E−03	8.37E−01	2.26E+00	4.52E−03
22	1.12E+00	4.14E−03	8.66E−01	2.23E+00	4.60E−03
23	1.09E+00	4.14E−03	9.05E−01	2.20E+00	4.60E−03
24	1.04E+00	4.19E−03	9.53E−01	2.15E+00	4.65E−03
25	9.99E−01	4.23E−03	1.00E+00	2.10E+00	4.70E−03
26	9.36E−01	4.19E−03	1.07E+00	2.03E+00	4.66E−03
27	8.64E−01	4.25E−03	1.15E+00	1.95E+00	4.72E−03
28	7.91E−01	4.27E−03	1.23E+00	1.87E+00	4.74E−03
29	7.39E−01	4.31E−03	1.29E+00	1.81E+00	4.79E−03
30	6.42E−01	4.22E−03	1.40E+00	1.70E+00	4.69E−03
31	5.93E−01	4.17E−03	1.45E+00	1.65E+00	4.63E−03
32	5.06E−01	4.13E−03	1.55E+00	1.55E+00	4.59E−03
33	4.29E−01	4.09E−03	1.63E+00	1.47E+00	4.55E−03
34	3.49E−01	3.94E−03	1.72E+00	1.38E+00	4.37E−03

Table A.3 (Continued.)

Data Points	K SF Voltage (V)	L SF Shot Noise (rms V)	M Sense Node Signal (V)	N Sense Node Voltage (V)	O Sense Node Shot Noise (rms V)
35	3.10E−01	3.90E−03	1.77E+00	1.33E+00	4.33E−03
36	2.26E−01	3.68E−03	1.86E+00	1.24E+00	4.09E−03
37	2.01E−01	3.60E−03	1.89E+00	1.21E+00	4.00E−03
38	1.54E−01	3.58E−03	1.94E+00	1.16E+00	3.97E−03
39	8.73E−02	3.29E−03	2.01E+00	1.09E+00	3.66E−03
40	4.94E−02	3.14E−03	2.06E+00	1.04E+00	3.49E−03
41	1.22E−02	2.95E−03	2.10E+00	1.00E+00	3.28E−03
42	−1.08E−02	2.69E−03	2.12E+00	9.77E−01	2.99E−03
43	−3.24E−02	2.29E−03	2.15E+00	9.53E−01	2.55E−03

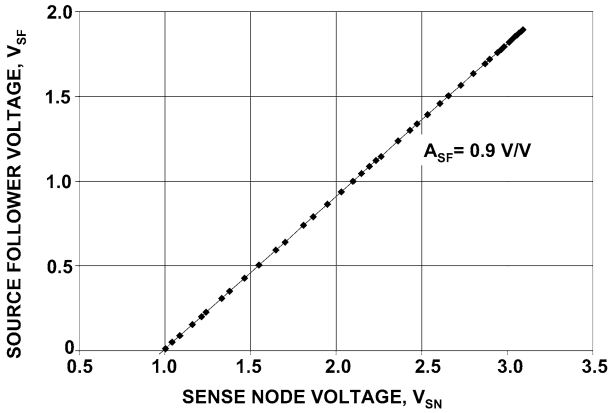

Figure A.3 Source follower output voltage versus sense node voltage.

Therefore,

$$K_{\mathrm{ADC}}(\mathrm{e^-/DN}) = \frac{S(\mathrm{DN})}{\sigma_{\mathrm{SHOT}}(\mathrm{DN})^2} = \frac{149}{10.7^2} = 1.3\ \mathrm{e^-/DN}.$$

From this result, the first light level generates a charge level of

$$S1 = S1(\mathrm{DN}) \times K_{\mathrm{ADC}}(\mathrm{e^-/DN}) = 149 \times 1.3 = 195\ \mathrm{e^-}.$$

From this reference level, the charge generated for subsequent light levels are

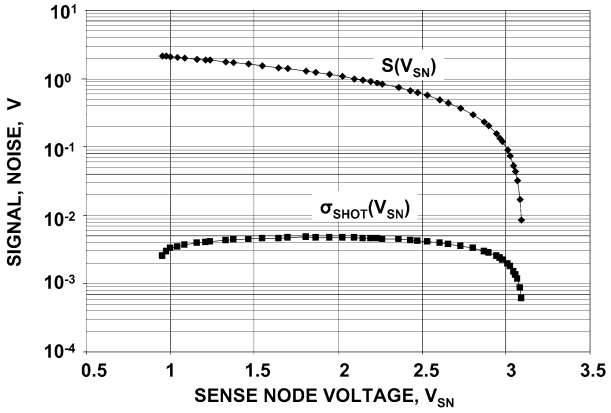

Figure A.4 Sense node signal and noise voltage as a function of sense node voltage.

$$S = A_{\mathrm{L}} \times 195\ \mathrm{e}^{-},$$

where A_{L} is the light gain tabulated in **COL E**.

Table A.4: Calculated results.

COL P: Signal in electron units

$$S = A_{\mathrm{L}} \times 195$$

COL Q: ADC signal sensitivity

$$S_{\mathrm{ADC}}(\mathrm{e}^{-}/\mathrm{DN}) = \frac{S}{S(\mathrm{DN})}$$

COL R: ADC signal sensitivity nonlinearity

$$S_{\mathrm{ADC}}(\mathrm{e}^{-}/\mathrm{DN})\ \text{nonlinearity}\ (\%) = 100 \times \frac{S_{\mathrm{ADC}}(\mathrm{e}^{-}/\mathrm{DN}) - 1.31}{1.31}$$

COL S: Signal shot noise in electron units

$$\sigma_{\mathrm{SHOT}} = S^{1/2}$$

COL T: ADC noise sensitivity

$$N_{\mathrm{ADC}}(\mathrm{e}^{-}/\mathrm{DN}) = \frac{\sigma_{\mathrm{SHOT}}}{\sigma_{\mathrm{SHOT}}(\mathrm{DN})}$$

Table A.5: Calculated results.

COL U: ADC noise sensitivity nonlinearity

$$\text{Assuming } N_{\mathrm{ADC}}(\mathrm{e}^{-}/\mathrm{DN})_{\mathrm{LOW}} = S_{\mathrm{ADC}}(\mathrm{e}^{-}/\mathrm{DN})_{\mathrm{LOW}} = 1.31$$

$$N_{\mathrm{ADC}}(\mathrm{e}^{-}/\mathrm{DN})\ \text{nonlinearity}\ (\%) = 100 \times \frac{N_{\mathrm{ADC}}(\mathrm{e}^{-}/\mathrm{DN}) - 1.31}{1.31}$$

Table A.4 Calculated results.

	P	**Q**	**R**	**S**	**T**
Data Points	Signal e^-	ADC Signal Sensitivity (e^-/DN)	ADC Signal Linearity (%)	Shot Noise (rms e^-)	ADC Noise Sensitivity (e^-/DN)
1	1.95E+02	1.31E+00	−9.73E−02	1.40E+01	1.31E+00
2	3.90E+02	1.30E+00	−4.31E−01	1.97E+01	1.31E+00
3	7.36E+02	1.30E+00	−5.65E−01	2.71E+01	1.31E+00
4	9.88E+02	1.30E+00	−4.12E−01	3.14E+01	1.32E+00
5	1.21E+03	1.31E+00	−2.43E−01	3.48E+01	1.32E+00
6	1.70E+03	1.30E+00	−5.00E−01	4.12E+01	1.33E+00
7	2.04E+03	1.30E+00	−5.26E−01	4.51E+01	1.33E+00
8	2.74E+03	1.31E+00	−3.53E−01	5.24E+01	1.34E+00
9	3.10E+03	1.31E+00	−1.99E−01	5.57E+01	1.34E+00
10	3.62E+03	1.31E+00	3.69E−02	6.01E+01	1.35E+00
11	4.70E+03	1.32E+00	5.02E−01	6.85E+01	1.38E+00
12	5.34E+03	1.32E+00	7.09E−01	7.31E+01	1.39E+00
13	6.93E+03	1.33E+00	1.57E+00	8.33E+01	1.44E+00
14	8.78E+03	1.35E+00	2.96E+00	9.37E+01	1.49E+00
15	1.05E+04	1.35E+00	3.23E+00	1.02E+02	1.54E+00
16	1.19E+04	1.37E+00	4.65E+00	1.09E+02	1.57E+00
17	1.38E+04	1.39E+00	6.16E+00	1.18E+02	1.63E+00
18	1.55E+04	1.41E+00	7.48E+00	1.24E+02	1.69E+00
19	1.66E+04	1.42E+00	8.28E+00	1.29E+02	1.70E+00
20	1.87E+04	1.44E+00	1.01E+01	1.37E+02	1.75E+00
21	2.17E+04	1.48E+00	1.27E+01	1.47E+02	1.86E+00
22	2.26E+04	1.49E+00	1.35E+01	1.50E+02	1.86E+00
23	2.38E+04	1.50E+00	1.43E+01	1.54E+02	1.91E+00
24	2.54E+04	1.52E+00	1.57E+01	1.59E+02	1.95E+00
25	2.69E+04	1.53E+00	1.69E+01	1.64E+02	1.99E+00
26	2.93E+04	1.56E+00	1.88E+01	1.71E+02	2.09E+00
27	3.20E+04	1.59E+00	2.10E+01	1.79E+02	2.16E+00
28	3.50E+04	1.62E+00	2.35E+01	1.87E+02	2.25E+00
29	3.71E+04	1.64E+00	2.52E+01	1.93E+02	2.29E+00
30	4.13E+04	1.68E+00	2.86E+01	2.03E+02	2.47E+00
31	4.35E+04	1.71E+00	3.03E+01	2.09E+02	2.57E+00
32	4.76E+04	1.75E+00	3.35E+01	2.18E+02	2.71E+00
33	5.13E+04	1.79E+00	3.66E+01	2.27E+02	2.84E+00
34	5.55E+04	1.83E+00	4.01E+01	2.36E+02	3.07E+00
35	5.77E+04	1.86E+00	4.20E+01	2.40E+02	3.16E+00

Table A.4 (Continued.)

	P	**Q**	**R**	**S**	**T**
Data Points	Signal e^-	ADC Signal Sensitivity (e^-/DN)	ADC Signal Linearity (%)	Shot Noise (rms e^-)	ADC Noise Sensitivity (e^-/DN)
36	6.25E+04	1.92E+00	4.62E+01	2.50E+02	3.48E+00
37	6.40E+04	1.93E+00	4.74E+01	2.53E+02	3.61E+00
38	6.69E+04	1.97E+00	5.01E+01	2.59E+02	3.71E+00
39	7.16E+04	2.03E+00	5.47E+01	2.68E+02	4.17E+00
40	7.47E+04	2.07E+00	5.81E+01	2.73E+02	4.47E+00
41	7.77E+04	2.11E+00	6.11E+01	2.79E+02	4.85E+00
42	7.94E+04	2.13E+00	6.28E+01	2.82E+02	5.37E+00
43	8.13E+04	2.16E+00	6.48E+01	2.85E+02	6.37E+00

COL V: ADC Sensitivity

$$K_{\mathrm{ADC}}(\mathrm{e^-/DN}) = \frac{S(\mathrm{DN})}{\sigma_{\mathrm{SHOT}}(\mathrm{DN})^2}\ (false)$$

COL W: ADC Sensitivity nonlinearity

$$K_{\mathrm{ADC}}(\mathrm{e^-/DN})\ \text{nonlinearity}\ (\%) = 100 \times \frac{K_{\mathrm{ADC}}(\mathrm{e^-/DN}) - 1.31}{1.31}\ (false)$$

COL X: Signal electron units

$$S = S(\mathrm{DN}) \times K_{\mathrm{ADC}}(\mathrm{e^-/DN})\ (false)$$

COL Y: Signal shot noise electron units

$$\sigma_{\mathrm{SHOT}} = [S(\mathrm{DN}) \times K_{\mathrm{ADC}}(\mathrm{e^-/DN})]^{1/2}\ (false)$$

Columns V–Y determine certain "false" quantities that assume $K_{\mathrm{ADC}}(\mathrm{e^-/DN}) = S_{\mathrm{ADC}}(\mathrm{e^-/DN}) = N_{\mathrm{ADC}}(\mathrm{e^-/DN})$ over the full dynamic range of the sensor. This assumption results in serious errors for most performance parameters. The false result shows why it is necessary to separately track $S_{\mathrm{ADC}}(\mathrm{e^-/DN})$ and $N_{\mathrm{ADC}}(\mathrm{e^-/DN})$ when V/e^- nonlinearity is present.

Figure A.5:
$S_{\mathrm{ADC}}(\mathrm{e^-/DN})$, $N_{\mathrm{ADC}}(\mathrm{e^-/DN})$, $K_{\mathrm{ADC}}(\mathrm{e^-/DN})$ versus S

Figure A.6:
$S_{\mathrm{ADC}}(\mathrm{e^-/DN})$, $N_{\mathrm{ADC}}(\mathrm{e^-/DN})$, $K_{\mathrm{ADC}}(\mathrm{e^-/DN})$ nonlinearity (%) versus S

Table A.5 Calculated results.

	U	**V**	**W**	**X**	**Y**
Data Points	ADC Noise Linearity (%)	*False* ADC Sensitivity (e^-/DN)	*False* ADC Linearity (%)	*False* Signal	*False* Shot Noise
1	−2.00E−02	1.31E+00	5.75E−02	1.95E+02	1.40E+01
2	2.11E−01	1.32E+00	8.57E−01	3.95E+02	1.99E+01
3	2.08E−01	1.32E+00	9.86E−01	7.47E+02	2.73E+01
4	9.16E−01	1.34E+00	2.26E+00	1.01E+03	3.18E+01
5	9.75E−01	1.34E+00	2.21E+00	1.24E+03	3.53E+01
6	1.35E+00	1.35E+00	3.24E+00	1.76E+03	4.20E+01
7	1.49E+00	1.36E+00	3.55E+00	2.12E+03	4.61E+01
8	2.37E+00	1.38E+00	5.16E+00	2.89E+03	5.38E+01
9	2.24E+00	1.37E+00	4.73E+00	3.25E+03	5.70E+01
10	3.15E+00	1.39E+00	6.36E+00	3.85E+03	6.20E+01
11	5.40E+00	1.45E+00	1.05E+01	5.17E+03	7.19E+01
12	5.98E+00	1.46E+00	1.15E+01	5.91E+03	7.69E+01
13	9.77E+00	1.55E+00	1.86E+01	8.10E+03	9.00E+01
14	1.40E+01	1.65E+00	2.62E+01	1.08E+04	1.04E+02
15	1.72E+01	1.74E+00	3.31E+01	1.35E+04	1.16E+02
16	2.02E+01	1.81E+00	3.81E+01	1.57E+04	1.25E+02
17	2.45E+01	1.91E+00	4.59E+01	1.90E+04	1.38E+02
18	2.87E+01	2.02E+00	5.42E+01	2.22E+04	1.49E+02
19	2.98E+01	2.04E+00	5.57E+01	2.39E+04	1.55E+02
20	3.33E+01	2.12E+00	6.15E+01	2.74E+04	1.66E+02
21	4.19E+01	2.34E+00	7.87E+01	3.44E+04	1.85E+02
22	4.20E+01	2.33E+00	7.77E+01	3.54E+04	1.88E+02
23	4.60E+01	2.44E+00	8.64E+01	3.88E+04	1.97E+02
24	4.88E+01	2.51E+00	9.15E+01	4.19E+04	2.05E+02
25	5.18E+01	2.58E+00	9.72E+01	4.54E+04	2.13E+02
26	5.96E+01	2.81E+00	1.15E+02	5.29E+04	2.30E+02
27	6.50E+01	2.95E+00	1.25E+02	5.95E+04	2.44E+02
28	7.16E+01	3.12E+00	1.39E+02	6.76E+04	2.60E+02
29	7.49E+01	3.20E+00	1.44E+02	7.25E+04	2.69E+02
30	8.87E+01	3.63E+00	1.77E+02	8.90E+04	2.98E+02
31	9.59E+01	3.86E+00	1.95E+02	9.84E+04	3.14E+02
32	1.07E+02	4.20E+00	2.20E+02	1.14E+05	3.38E+02
33	1.17E+02	4.51E+00	2.44E+02	1.29E+05	3.59E+02
34	1.34E+02	5.13E+00	2.92E+02	1.55E+05	3.94E+02
35	1.41E+02	5.36E+00	3.09E+02	1.66E+05	4.08E+02

Table A.5 (Continued.)

Data Points	**U** ADC Noise Linearity (%)	**V** *False* ADC Sensitivity (e^-/DN)	**W** *False* ADC Linearity (%)	**X** *False* Signal	**Y** *False* Shot Noise
36	1.66E+02	6.34E+00	3.84E+02	2.07E+05	4.55E+02
37	1.75E+02	6.73E+00	4.14E+02	2.23E+05	4.72E+02
38	1.83E+02	7.00E+00	4.34E+02	2.38E+05	4.88E+02
39	2.18E+02	8.57E+00	5.54E+02	3.03E+05	5.50E+02
40	2.41E+02	9.64E+00	6.36E+02	3.48E+05	5.90E+02
41	2.70E+02	1.11E+01	7.50E+02	4.10E+05	6.40E+02
42	3.10E+02	1.35E+01	9.32E+02	5.04E+05	7.10E+02
43	3.87E+02	1.88E+01	1.34E+03	7.09E+05	8.42E+02

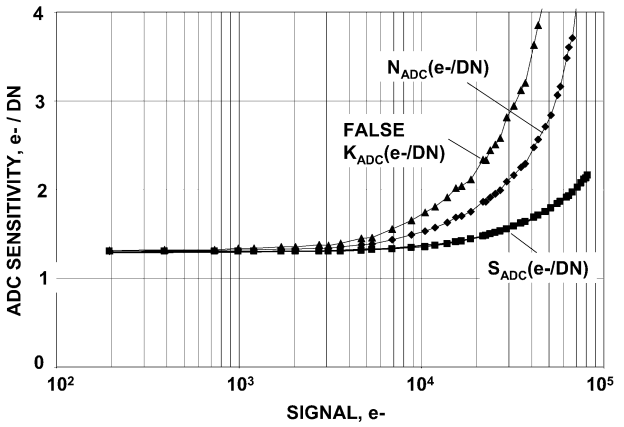

Figure A.5 Signal and noise ADC sensitivities (e^-/DN) as a function of signal.

Table A.6: Calculated results.

COL Z: FPN electron units

$$\sigma_{\mathrm{FPN}} = \sigma_{\mathrm{FPN}}(\mathrm{DN}) \times N_{\mathrm{ADC}}(\mathrm{e^-/DN})$$

COL AA: Shot and FPN electron units

$$\sigma_{\mathrm{SHOT+FPN}} = (\sigma^2_{\mathrm{SHOT}} + \sigma^2_{\mathrm{FPN}})^{1/2}$$

COL AB: Total noise electron units

$$\sigma_{\mathrm{TOTAL}} = (\sigma^2_{\mathrm{READ}} + \sigma^2_{\mathrm{SHOT}} + \sigma^2_{\mathrm{FPN}})^{1/2}$$

Table A.6 Calculated results.

	Z	**AA**	**AB**	**AC**	**AD**
Data Points	FPN (rms e^-)	FPN+ Shot Noise (rms e^-)	FPN+ Shot+ Read Noise (rms e^-)	P_N (%)	*False* P_N (%)
1	1.43E+00	1.40E+01	1.60E+01	7.35E−01	7.35E−01
2	2.98E+00	2.00E+01	2.14E+01	7.63E−01	7.58E−01
3	5.69E+00	2.77E+01	2.88E+01	7.73E−01	7.67E−01
4	7.76E+00	3.24E+01	3.33E+01	7.86E−01	7.76E−01
5	9.44E+00	3.61E+01	3.69E+01	7.77E−01	7.68E−01
6	1.33E+01	4.33E+01	4.40E+01	7.84E−01	7.69E−01
7	1.60E+01	4.79E+01	4.85E+01	7.83E−01	7.68E−01
8	2.17E+01	5.67E+01	5.72E+01	7.90E−01	7.69E−01
9	2.42E+01	6.07E+01	6.12E+01	7.79E−01	7.61E−01
10	2.95E+01	6.70E+01	6.74E+01	8.16E−01	7.91E−01
11	3.81E+01	7.84E+01	7.88E+01	8.10E−01	7.73E−01
12	4.30E+01	8.48E+01	8.51E+01	8.05E−01	7.65E−01
13	5.56E+01	1.00E+02	1.00E+02	8.02E−01	7.42E−01
14	6.97E+01	1.17E+02	1.17E+02	7.94E−01	7.17E−01
15	8.44E+01	1.33E+02	1.33E+02	8.03E−01	7.07E−01
16	9.50E+01	1.45E+02	1.45E+02	7.99E−01	6.96E−01
17	1.10E+02	1.61E+02	1.61E+02	7.92E−01	6.75E−01
18	1.22E+02	1.74E+02	1.74E+02	7.88E−01	6.58E−01
19	1.30E+02	1.83E+02	1.83E+02	7.82E−01	6.52E−01
20	1.48E+02	2.01E+02	2.01E+02	7.91E−01	6.53E−01
21	1.72E+02	2.26E+02	2.27E+02	7.93E−01	6.30E−01
22	1.79E+02	2.33E+02	2.33E+02	7.91E−01	6.32E−01
23	1.88E+02	2.43E+02	2.43E+02	7.90E−01	6.19E−01
24	2.00E+02	2.56E+02	2.56E+02	7.89E−01	6.13E−01
25	2.15E+02	2.71E+02	2.71E+02	8.00E−01	6.16E−01
26	2.34E+02	2.90E+02	2.90E+02	8.00E−01	5.95E−01
27	2.55E+02	3.11E+02	3.11E+02	7.95E−01	5.83E−01
28	2.83E+02	3.39E+02	3.40E+02	8.10E−01	5.83E−01
29	2.98E+02	3.55E+02	3.55E+02	8.02E−01	5.74E−01
30	3.21E+02	3.80E+02	3.80E+02	7.77E−01	5.30E−01
31	3.46E+02	4.04E+02	4.04E+02	7.95E−01	5.29E−01
32	3.84E+02	4.42E+02	4.42E+02	8.07E−01	5.21E−01
33	4.06E+02	4.65E+02	4.65E+02	7.90E−01	4.98E−01
34	4.44E+02	5.02E+02	5.02E+02	8.00E−01	4.78E−01

Table A.6 (Continued.)

	Z	**AA**	**AB**	**AC**	**AD**
Data Points	FPN (rms e$^-$)	FPN+ Shot Noise (rms e$^-$)	FPN+ Shot+ Read Noise (rms e$^-$)	P_{N} (%)	*False* P_{N} (%)
35	4.64E+02	5.23E+02	5.23E+02	8.05E−01	4.74E−01
36	4.99E+02	5.58E+02	5.58E+02	7.98E−01	4.38E−01
37	5.14E+02	5.73E+02	5.73E+02	8.03E−01	4.30E−01
38	5.39E+02	5.98E+02	5.98E+02	8.05E−01	4.27E−01
39	5.69E+02	6.29E+02	6.29E+02	7.94E−01	3.86E−01
40	6.08E+02	6.67E+02	6.67E+02	8.14E−01	3.77E−01
41	6.07E+02	6.68E+02	6.68E+02	7.81E−01	3.40E−01
42	6.35E+02	6.95E+02	6.95E+02	8.00E−01	3.18E−01
43	6.50E+02	7.09E+02	7.09E+02	7.99E−01	2.70E−01

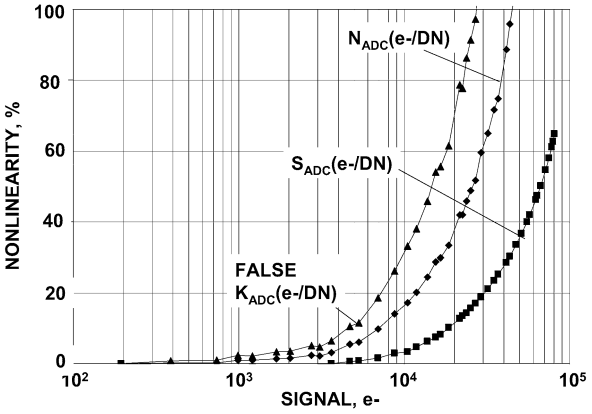

Figure A.6 Signal and noise nonlinearity as a function of signal.

COL AC: FPN quality factor

$$P_{\mathrm{N}} = \frac{\sigma_{\mathrm{FPN}}}{S}$$

COL AD: FPN quality factor

$$P_{\mathrm{N}} = \frac{\sigma_{\mathrm{FPN}}(\mathrm{DN})}{S(\mathrm{DN})}\ (false)$$

Figure A.7:

σ_{TOTAL}, σ_{SHOT}, σ_{FPN} versus S

Figure A.8:
False S versus true S

Figure A.9:
True $P_{\rm N}$ and *false* $P_{\rm N}$ versus S

Table A.7: Calculated results.

COL AE: Signal sense node sensitivity

$$S_{\rm SN}({\rm e}^-/V_{\rm SN}) = \frac{S}{S(V_{\rm SN})}$$

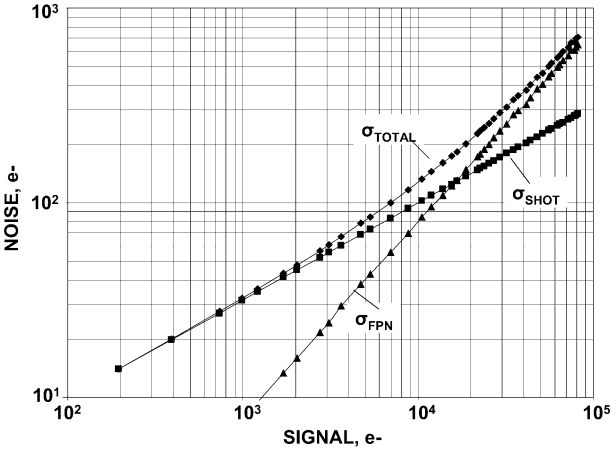

Figure A.7 Corresponding PTC responses for Fig. A1.2 in electron units.

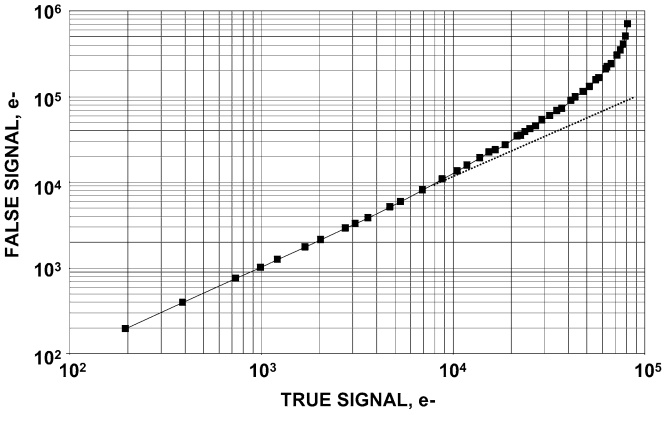

Figure A.8 False versus true signal based on $K_{\rm ADC}$(e$^-$/DN) and $S_{\rm ADC}$(e$^-$/DN), respectively.

Table A.7 Calculated results.

	AE	**AF**	**AG**	**AH**	**AI**
Data Points	Sense Node Signal Sensitivity (e^-/V)	Sense Node Noise Sensitivity (e^-/V)	Sense Node Signal Gain ($\mu V/e^-$)	Sense Node Noise Gain ($\mu V/e^-$)	*False* Sense Node Gain ($\mu V/e^-$)
1	2.30E+04	2.30E+04	4.35E+01	4.35E+01	4.35E+01
2	2.29E+04	2.30E+04	4.37E+01	4.34E+01	4.31E+01
3	2.29E+04	2.30E+04	4.37E+01	4.34E+01	4.31E+01
4	2.29E+04	2.32E+04	4.37E+01	4.31E+01	4.25E+01
5	2.29E+04	2.32E+04	4.36E+01	4.31E+01	4.26E+01
6	2.29E+04	2.33E+04	4.37E+01	4.29E+01	4.21E+01
7	2.29E+04	2.33E+04	4.37E+01	4.29E+01	4.20E+01
8	2.29E+04	2.35E+04	4.37E+01	4.25E+01	4.14E+01
9	2.29E+04	2.35E+04	4.36E+01	4.25E+01	4.15E+01
10	2.30E+04	2.37E+04	4.35E+01	4.22E+01	4.09E+01
11	2.31E+04	2.42E+04	4.33E+01	4.13E+01	3.94E+01
12	2.32E+04	2.44E+04	4.32E+01	4.10E+01	3.90E+01
13	2.34E+04	2.52E+04	4.28E+01	3.96E+01	3.67E+01
14	2.37E+04	2.62E+04	4.22E+01	3.82E+01	3.45E+01
15	2.37E+04	2.70E+04	4.21E+01	3.71E+01	3.27E+01
16	2.41E+04	2.76E+04	4.16E+01	3.62E+01	3.15E+01
17	2.44E+04	2.86E+04	4.10E+01	3.50E+01	2.98E+01
18	2.47E+04	2.96E+04	4.05E+01	3.38E+01	2.82E+01
19	2.49E+04	2.98E+04	4.02E+01	3.35E+01	2.79E+01
20	2.53E+04	3.07E+04	3.95E+01	3.26E+01	2.69E+01
21	2.59E+04	3.26E+04	3.86E+01	3.07E+01	2.43E+01
22	2.61E+04	3.26E+04	3.83E+01	3.06E+01	2.45E+01
23	2.63E+04	3.36E+04	3.81E+01	2.98E+01	2.33E+01
24	2.66E+04	3.42E+04	3.76E+01	2.92E+01	2.27E+01
25	2.69E+04	3.49E+04	3.72E+01	2.86E+01	2.21E+01
26	2.73E+04	3.67E+04	3.66E+01	2.72E+01	2.03E+01
27	2.78E+04	3.79E+04	3.59E+01	2.64E+01	1.93E+01
28	2.84E+04	3.95E+04	3.52E+01	2.53E+01	1.82E+01
29	2.88E+04	4.02E+04	3.48E+01	2.49E+01	1.78E+01
30	2.96E+04	4.34E+04	3.38E+01	2.30E+01	1.57E+01
31	3.00E+04	4.50E+04	3.34E+01	2.22E+01	1.48E+01
32	3.07E+04	4.76E+04	3.26E+01	2.10E+01	1.36E+01
33	3.14E+04	4.98E+04	3.18E+01	2.01E+01	1.26E+01
34	3.22E+04	5.38E+04	3.11E+01	1.86E+01	1.11E+01

Table A.7 (Continued.)

Data Points	**AE** Sense Node Signal Sensitivity (e^-/V)	**AF** Sense Node Noise Sensitivity (e^-/V)	**AG** Sense Node Signal Gain ($\mu V/e^-$)	**AH** Sense Node Noise Gain ($\mu V/e^-$)	**AI** *False* Sense Node Gain ($\mu V/e^-$)
35	3.26E+04	5.54E+04	3.06E+01	1.80E+01	1.06E+01
36	3.36E+04	6.12E+04	2.98E+01	1.64E+01	8.99E+00
37	3.39E+04	6.33E+04	2.95E+01	1.58E+01	8.46E+00
38	3.45E+04	6.51E+04	2.90E+01	1.54E+01	8.14E+00
39	3.56E+04	7.31E+04	2.81E+01	1.37E+01	6.65E+00
40	3.63E+04	7.84E+04	2.75E+01	1.28E+01	5.91E+00
41	3.70E+04	8.51E+04	2.70E+01	1.18E+01	5.12E+00
42	3.74E+04	9.42E+04	2.67E+01	1.06E+01	4.22E+00
43	3.79E+04	1.12E+05	2.64E+01	8.94E+00	3.03E+00

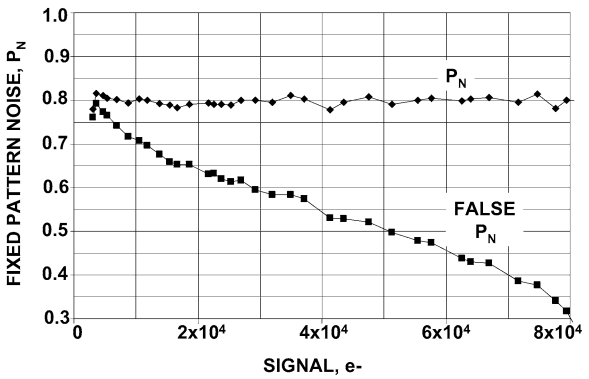

Figure A.9 False and true FPN with signal based on $K_{\mathrm{ADC}}(e^-/DN)$ and $N_{\mathrm{ADC}}(e^-/DN)$, respectively.

COL AF: Sense node noise sensitivity

$$N_{\mathrm{SN}}(e^-/V_{\mathrm{SN}}) = \frac{\sigma_{\mathrm{SHOT}}}{\sigma_{\mathrm{SHOT}}(V_{\mathrm{SN}})}$$

COL AG: Signal sense node gain

$$S_{\mathrm{SN}}(V_{\mathrm{SN}}/e^-) = \left[\frac{S}{S(V_{\mathrm{SN}})}\right]^{-1}$$

COL AH: Noise sense node gain

$$N_{\mathrm{SN}}(V_{\mathrm{SN}}/e^-) = \left[\frac{\sigma_{\mathrm{SHOT}}}{\sigma_{\mathrm{SHOT}}(V_{\mathrm{SN}})}\right]^{-1}$$

COL AI: *False* sense node gain

$$A_{\rm SN} = [S({\rm DN}) \times K_{\rm ADC}({\rm e^-/DN})/S(V_{\rm SN})]^{-1}\ (false)$$

Figure A.10:
$S_{\rm SN}({\rm e^-}/V_{\rm SN})$, $N_{\rm SN}({\rm e^-}/V_{\rm SN})$ versus S
Figure A.11:
$S_{\rm SN}(V_{\rm SN}/{\rm e^-})$, $N_{\rm SN}(V_{\rm SN}/{\rm e^-})$ versus S

Table A.8: Calculated results.

COL AJ: Sense node sensitivity ratio

$$\text{Sensitivity ratio} = \frac{S_{\rm SN}({\rm e^-}/V_{\rm SN})}{N_{\rm SN}({\rm e^-}/V_{\rm SN})}$$

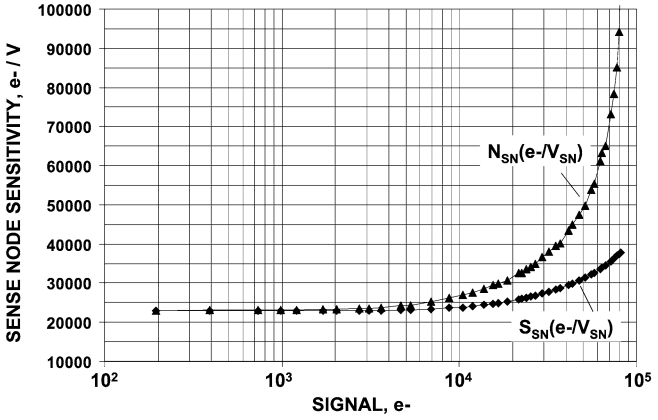

Figure A.10 $S_{\rm ADC}({\rm e^-/DN})$ and $N_{\rm ADC}({\rm e^-/DN})$ sensitivities versus signal.

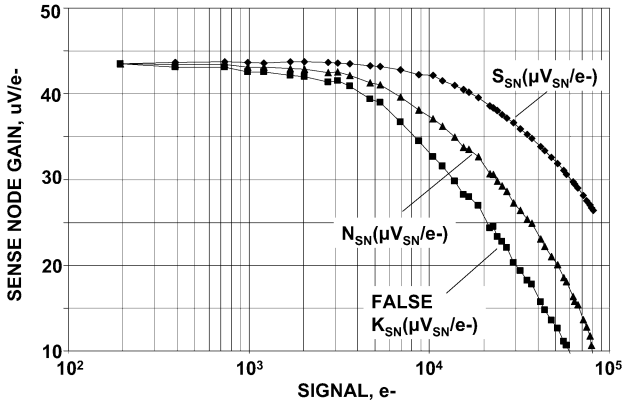

Figure A.11 Signal and noise sense node gains with signal.

Table A.8 Calculated results.

	AJ	**AK**	**AL**	**AM**	**AN**	**AO**
Data Points	Sense Node Sensitivity Ratio	Sense Node Cap. (fF)	*False* Sense Cap. (fF)	Shot Noise S/N	Shot+FPN S/N	*False* Shot Noise S/N
1	9.99E−01	3.68E+00	3.68E+00	1.40E+01	1.39E+01	1.40E+01
2	9.94E−01	3.69E+00	3.71E+00	1.97E+01	1.95E+01	1.99E+01
3	9.92E−01	3.69E+00	3.71E+00	2.71E+01	2.66E+01	2.73E+01
4	9.87E−01	3.71E+00	3.76E+00	3.14E+01	3.05E+01	3.18E+01
5	9.88E−01	3.71E+00	3.76E+00	3.48E+01	3.36E+01	3.53E+01
6	9.82E−01	3.73E+00	3.80E+00	4.12E+01	3.92E+01	4.20E+01
7	9.80E−01	3.73E+00	3.81E+00	4.51E+01	4.26E+01	4.61E+01
8	9.73E−01	3.77E+00	3.87E+00	5.24E+01	4.84E+01	5.38E+01
9	9.76E−01	3.76E+00	3.85E+00	5.57E+01	5.11E+01	5.70E+01
10	9.70E−01	3.79E+00	3.91E+00	6.01E+01	5.40E+01	6.20E+01
11	9.54E−01	3.88E+00	4.07E+00	6.85E+01	5.99E+01	7.19E+01
12	9.50E−01	3.90E+00	4.10E+00	7.31E+01	6.30E+01	7.69E+01
13	9.25E−01	4.04E+00	4.36E+00	8.33E+01	6.93E+01	9.00E+01
14	9.03E−01	4.19E+00	4.64E+00	9.37E+01	7.52E+01	1.04E+02
15	8.81E−01	4.31E+00	4.90E+00	1.02E+02	7.91E+01	1.16E+02
16	8.71E−01	4.42E+00	5.08E+00	1.09E+02	8.22E+01	1.25E+02
17	8.53E−01	4.58E+00	5.37E+00	1.18E+02	8.61E+01	1.38E+02
18	8.35E−01	4.74E+00	5.67E+00	1.24E+02	8.88E+01	1.49E+02
19	8.34E−01	4.78E+00	5.73E+00	1.29E+02	9.08E+01	1.55E+02
20	8.26E−01	4.90E+00	5.94E+00	1.37E+02	9.28E+01	1.66E+02
21	7.94E−01	5.22E+00	6.57E+00	1.47E+02	9.58E+01	1.85E+02
22	7.99E−01	5.22E+00	6.54E+00	1.50E+02	9.68E+01	1.88E+02
23	7.83E−01	5.37E+00	6.86E+00	1.54E+02	9.78E+01	1.97E+02
24	7.77E−01	5.48E+00	7.04E+00	1.59E+02	9.92E+01	2.05E+02
25	7.70E−01	5.59E+00	7.25E+00	1.64E+02	9.94E+01	2.13E+02
26	7.44E−01	5.87E+00	7.89E+00	1.71E+02	1.01E+02	2.30E+02
27	7.34E−01	6.07E+00	8.27E+00	1.79E+02	1.03E+02	2.44E+02
28	7.19E−01	6.31E+00	8.77E+00	1.87E+02	1.03E+02	2.60E+02
29	7.16E−01	6.43E+00	8.99E+00	1.93E+02	1.05E+02	2.69E+02
30	6.81E−01	6.94E+00	1.02E+01	2.03E+02	1.09E+02	2.98E+02
31	6.65E−01	7.21E+00	1.08E+01	2.09E+02	1.08E+02	3.14E+02
32	6.46E−01	7.61E+00	1.18E+01	2.18E+02	1.08E+02	3.38E+02
33	6.30E−01	7.97E+00	1.27E+01	2.27E+02	1.10E+02	3.59E+02
34	5.98E−01	8.62E+00	1.44E+01	2.36E+02	1.10E+02	3.94E+02

Table A.8 (Continued.)

Data Points	**AJ** Sense Node Sensitivity Ratio	**AK** Sense Node Cap. (fF)	**AL** *False* Sense Cap. (fF)	**AM** Shot Noise S/N	**AN** Shot+FPN S/N	**AO** *False* Shot Noise S/N
35	5.89E−01	8.87E+00	1.50E+01	2.40E+02	1.10E+02	4.08E+02
36	5.50E−01	9.79E+00	1.78E+01	2.50E+02	1.12E+02	4.55E+02
37	5.36E−01	1.01E+01	1.89E+01	2.53E+02	1.12E+02	4.72E+02
38	5.30E−01	1.04E+01	1.96E+01	2.59E+02	1.12E+02	4.88E+02
39	4.86E−01	1.17E+01	2.41E+01	2.68E+02	1.14E+02	5.50E+02
40	4.63E−01	1.25E+01	2.71E+01	2.73E+02	1.12E+02	5.90E+02
41	4.35E−01	1.36E+01	3.13E+01	2.79E+02	1.16E+02	6.40E+02
42	3.97E−01	1.51E+01	3.80E+01	2.82E+02	1.14E+02	7.10E+02
43	3.39E−01	1.79E+01	5.29E+01	2.85E+02	1.15E+02	8.42E+02

COL AK: Sense capacitance

$$C_{\mathrm{SN}} = N_{\mathrm{SN}}(\mathrm{e}^{-}/V_{\mathrm{SN}}) \times (1.6 \times 10^{-19})$$

COL AL: *False* sense node capacitance

$$C_{\mathrm{SN}} = K_{\mathrm{SN}}(\mathrm{e}^{-}/V_{\mathrm{SN}}) \times (1.6 \times 10^{-19})\ (false)$$

COL AM: Shot noise S/N

$$\mathrm{S/N} = \frac{S}{\sigma_{\mathrm{SHOT}}}$$

COL AN: Shot and FPN S/N

$$\mathrm{S/N} = \frac{S}{(\sigma^2_{\mathrm{SHOT}} + \sigma^2_{\mathrm{FPN}})^{1/2}}$$

COL AO: Shot noise S/N

$$\mathrm{S/N} = [S(\mathrm{DN}) \times K_{\mathrm{ADC}}(\mathrm{e}^{-}/\mathrm{DN})]^{1/2}\ (false)$$

Figure A.12:

Sensitivity ratio $\dfrac{S_{\mathrm{SN}}(\mathrm{e}^{-}/V_{\mathrm{SN}})}{N_{\mathrm{SN}}(\mathrm{e}^{-}/V_{\mathrm{SN}})}$ versus S

Figure A.13:

C_{SN} versus V_{SN}

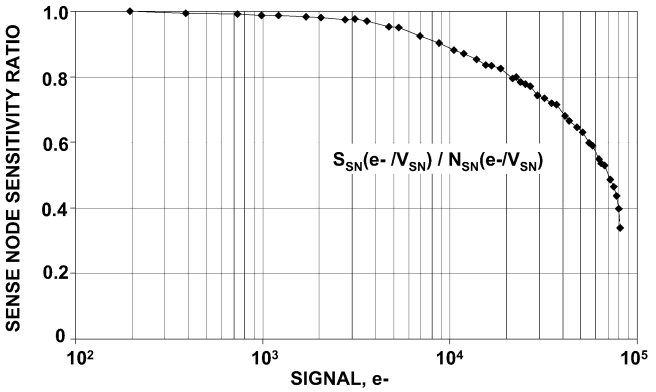

Figure A.12 Signal and noise sensitivity ratio with signal.

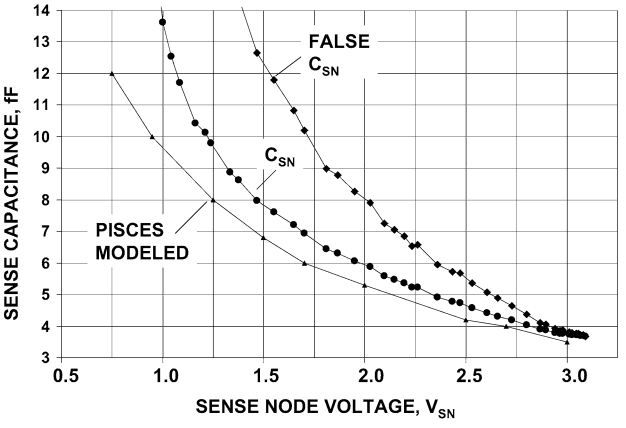

Figure A.13 Sense capacitance versus sense node voltage showing measured and modeled results.

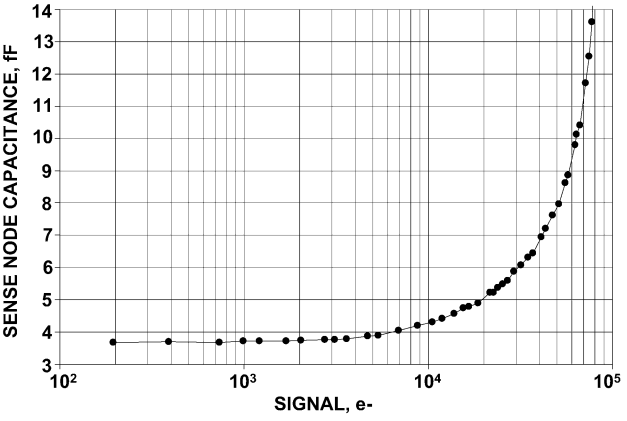

Figure A.14 Sense node capacitance versus signal.

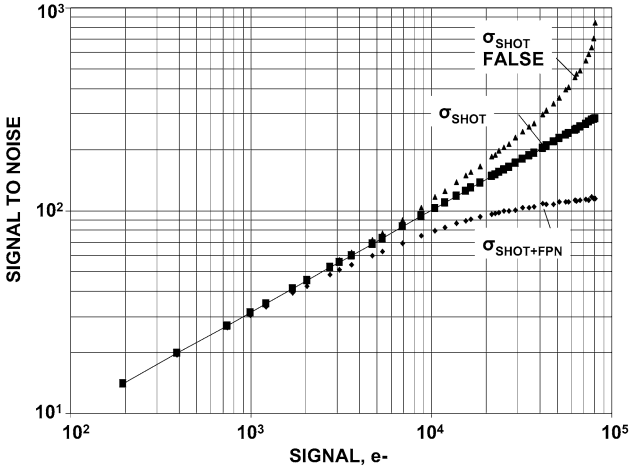

Figure A.15 S/N versus signal with and without FPN.

Figure A.14:
C_{SN} versus S
Figure A.15:
S/N($\sigma_{\mathrm{SHOT+FPN}}$, σ_{SHOT}) versus S

Appendix B
PTC Simulation Program with Thermal Dark Current

The Matlab^{TM} simulation program below generates a PTC using a random number noise generator to simulate read noise, shot noise, and FPN. The program also includes thermal dark current shot noise and FPN, which could influence the read noise floor depending on the parameters (e.g., operating temperature). Figure B.1 shows a typical plot without dark current present, whereas Fig. B.2 includes dark current noise. The plots shown are in DN units. A plotting routine in electron units is also supplied. Refer to Chapter 5 for PTC relations used in the program. Dark current equations are given in Chapter 11.

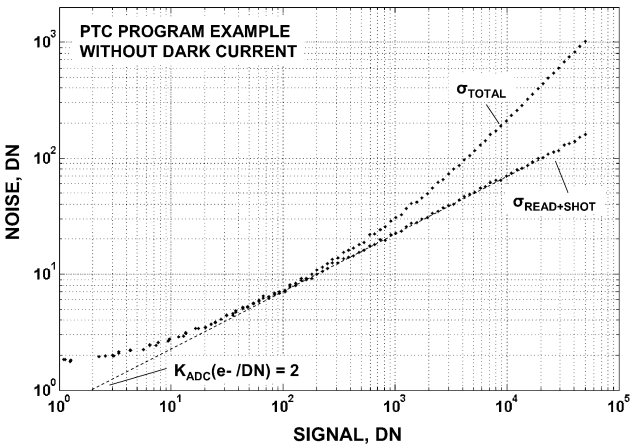

Figure B.1 Total noise and read+shot noise PTC responses.

```
% PTC simulation program with dark current
clear all;                                  % clear workspace

PIX=1000;                                   % number of pixels sampled
DATA=100;                                   % number of data points
```

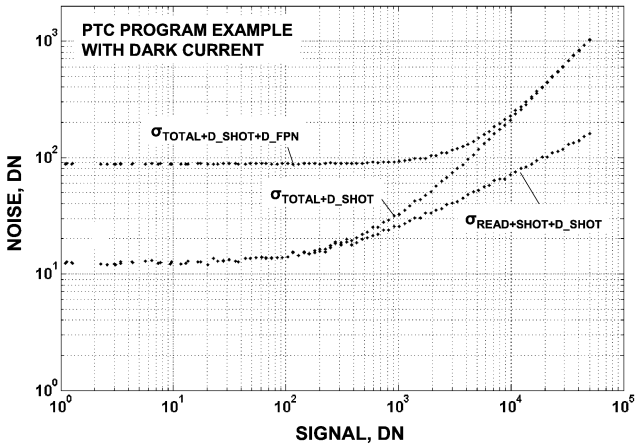

Figure B.2 Total noise and read+shot noise PTC responses with thermal dark current.

```
% Parameters
edn=2;                                  % e⁻/DN
RN_e=3;                                 % read noise (e⁻)
RN=RN_e/edn;                            % read noise (DN)
FW_e=10^5;                              % full well (e⁻)
FW=FW_e/edn;                            % full well (DN)
SCALE=DATA/log10(FW);                   % full well scale factor
PN = 0.02;                              % FPN factor

T=300;                                  % operating temperature (K)
k1=8.62*10^-5;                          % Boltzmann's constant
DFM=0.5;                                % dark current figure of merit
                                        (nA/cm^2)
DN=0.30;                                % dark FPN factor
PA=(8*10^-4)^2;                         % pixel area (cm^2)
t=.3;                                   % integration time
Eg=1.1557-(7.021*10^-4*T^2)/(1108+T);   % silicon band gap energy (eV)
DARK_e=t*2.55*10^15*PA*DFM*T^1.5*       % dark current (e⁻)
          *exp(-Eg/(2*k1*T));
DARK=DARK_e/edn;                        % dark current (DN)

% Program
randn('state',sum(100*clock))           % randomize number generator
C=randn(PIX,1);                         % random number generator for FPN
F=randn(PIX,1);                         % random number generator for dark FPN

      for i=1:DATA

sig=10^(i/SCALE);                       % signal step (DN)

A=randn(PIX,DATA);                      % random number generator
B=randn(PIX,DATA);                      % random number generator
D=randn(PIX,DATA);                      % random number generator
```

```
read = RN*A(1:PIX,i);                          % read noise (DN)
shot =(sig/edn)^0.5*B(1:PIX,i);                % shot noise (DN)

FPN=sig*PN*C(1:PIX,1);                         % FPN (DN)
Dshot=(DARK/edn)^0.5*D(1:PIX,i);               % dark shot noise (DN)
DFPN=DARK*DN*F(1:PIX,1);                       % dark FPN (DN)

SIG1(1:PIX,i)=sig+read+shot+FPN                % read+shot+FPN+dark shot+dark
+Dshot+DFPN;                                   FPN (DN)
SIG2(1:PIX,i)=sig+read+shot+FPN+Dshot;         % read+shot+FPN+dark shot (DN)
SIG3(1:PIX,i)=sig+read+shot+Dshot;             % read+shot+dark shot (DN)
SIG4(1:PIX,i)=sig+read+shot;                   % read+shot (DN)
SIG5(1:PIX,i)=sig+read+shot+FPN;               % read+shot+FPN+dark shot
                                               +dark FPN (DN)

    end

SIGNAL=mean(SIG1);                 % signal(DN)
NOISE1=std(SIG1);                  % read+shot+FPN+dark shot+dark FPN (DN)
NOISE2=std(SIG2);                  % read+shot+FPN+dark shot (DN)
NOISE3=std(SIG3);                  % read+shot+dark shot (DN)
NOISE4=std(SIG4);                  % read+shot (DN)
NOISE5=std(SIG5);                  % read+shot+FPN (DN)

SIGNAL_e=mean(SIG1)*edn;           % signal (e⁻)
NOISE1_e=std(SIG1)*edn;            % read+shot+FPN+dark shot+dark FPN (e⁻)
NOISE2_e=std(SIG2)*edn;            % read+shot+FPN+dark shot (e⁻)
NOISE3_e=std(SIG3)*edn;            % read+shot+dark shot (e⁻)
NOISE4_e=std(SIG4)*edn;            % read+shot (e⁻)
NOISE5_e=std(SIG1)*edn;            % read+shot+FPN (e⁻)

% PTC Plot (DN)
plot(SIGNAL,NOISE1,'k.',SIGNAL,NOISE2,'k.',SIGNAL,NOISE3,'k.',SIGNAL,
NOISE4,'k.',SIGNAL,NOISE5,'k.');

% PTC Plot (e⁻)
plot(SIGNAL_e,NOISE1_e,'k.',SIGNAL_e,NOISE2_e,'k.',SIGNAL_e,NOISE3_
e,'k.',SIGNAL_e,NOISE4_e,'k.',SIGNAL_e,NOISE5_e,'k.');
```

Appendix C
PTC Simulation Program with FPN Removal through Flat Fielding

The Matlab^{TM} simulation program below generates a PTC before and after FPN noise is removed by the flat-fielding technique described in Chapter 8. Figure C.1 is a typical output showing total noise and the ideal shot noise response. The third curve shows the noise response after FPN is removed.

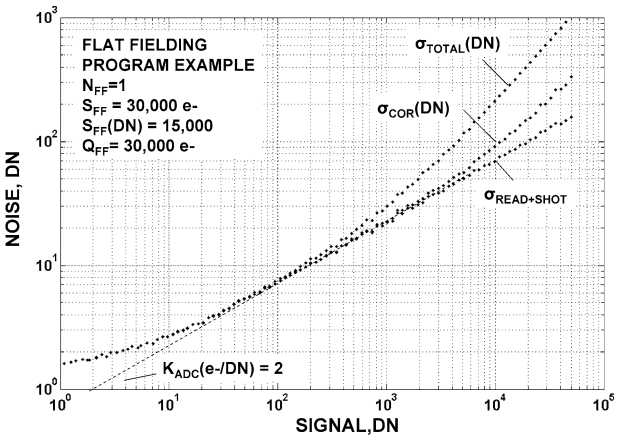

Figure C.1 PTC responses before and after flat fielding.

```
% PTC simulation program with FPN removal through flat fielding
clear all;                                  % clear workspace

% Parameters
PIX=1000;                                   % number of pixels sampled
DATA=100;                                   % number of data points
```

```
edn=2;                                          % e⁻/DN
RN_e=3;                                         % read noise (e⁻)
RN=RN_e/edn;                                    % read noise (DN)
FW_e=10^5;                                      % full well (e⁻)
FW=FW_e/edn;                                    % full well (DN)
SCALE=DATA/log10(FW);                           % full well scale factor
PN = 0.02;                                      % FPN factor
FF=3*10^4;                                      % flat field for FPN removal (e⁻)
FF_DN=FF/edn;                                   % flat field for FPN removal (DN)
NFF=1;                                          % number of flat fields
Q=FF*NFF;                                       % flat fielding quality factor

% Program
randn('state',sum(100*clock))                   % randomize number generators
C=randn(PIX,1);                                 % random number generator for FPN

        for i=1:DATA

sig=10^(i/SCALE);                               % signal step (DN)

A=randn(PIX,DATA);                              % random number generator
B=randn(PIX,DATA);                              % random number generator
D=randn(PIX,DATA);                              % random number generator

read = RN*A(1:PIX,i);                           % read noise (DN)
shot =(sig/edn)^0.5*B(1:PIX,i);                 % shot noise (DN)
FPN=sig*PN*C(1:PIX,1);                          % FPN

SIG1(1:PIX,i)=sig+read+shot+FPN;                % read+shot+FPN+ (DN)
SIG2(1:PIX,i)=sig+read+shot;                    % read+shot (DN)

shot_FF =(FF_DN/edn)^0.5*D(1:PIX,i)/NFF^0.5;    % flat field shot noise (DN)
FPN_FF=FF_DN*PN*C(1:PIX,1);                     % flat field FPN(DN)

CAL(1:PIX,i) = FF_DN+read+shot_FF+FPN_FF;       % flat field calibration frame (DN)

        end

COR=FF_DN.*SIG1./CAL;                           % corrected frame without
                                                FPN (DN)
SIGNAL=mean(SIG1);                              % signal(DN)

NOISE1=std(SIG1);                               % read+shot+FPN (DN)
NOISE2=std(SIG2);                               % read+shot (DN)
NOISE3=std(COR);                                % read+shot (DN) CORRECTED

SIGNAL_e=SIGNAL*edn;                            % signal (e⁻)
NOISE1_e=NOISE1*edn;                            % read+shot+FPN (e⁻)
NOISE2_e=NOISE2*edn;                            % read+shot (e⁻)
```

```
NOISE3_e=NOISE3*edn;                    % read+shot (e⁻) CORRECTED

% PTC PLOT (DN)
plot (SIGNAL,NOISE1,'k.',SIGNAL,NOISE2,'k.',SIGNAL,NOISE3,'k.');

%PTC PLOT (e⁻)
plot(SIGNAL_e,NOISE1_e,'k.',SIGNAL_e,NOISE2_e,'k.',SIGNAL_e,NOISE3_e,'k.');
```

Appendix D
LTC Simulation Program with Thermal Dark Current

The Matlab^{TM} simulation program below generates a LTC with and without FPN. Figure D.1 is a typical LTC for the parameters specified. Refer to Chapter 12 for lux transfer relations used in this program.

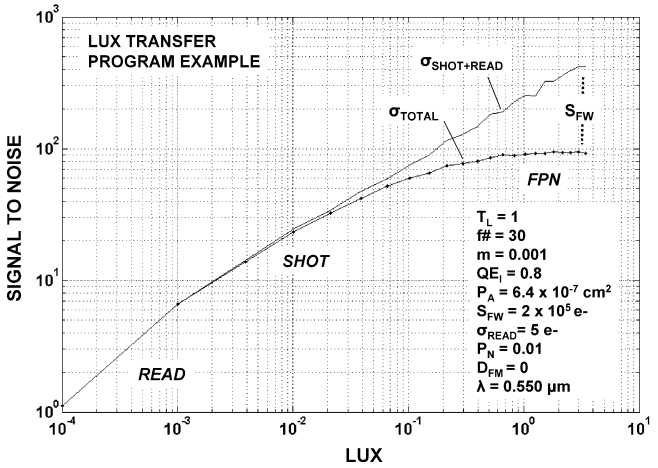

Figure D.1 LTC responses with and without FPN.

```
% Lux transfer simulation program
clear all;                          % clear workspace

% Parameters
QE=0.8;                             % quantum efficiency
PA=(8*10^-4)^2;                     % pixel area (cm^2)
FW = 2*10^5;                        % full well (e⁻)
RN=5;                               % read noise (e⁻)
PN=0.01;                            % pixel nonuniformity
```

```
k1=8.62*10^-5;                          % Boltzmann's constant
T=300;                                  % operating temperature
DFM=0;                                  % dark current figure of merit
DN=0;                                   % dark current FPN
Eg=1.1557-(7.021*10^-4*T^2)/(1108+T);   % silicon band gap (eV)
t=1000;                                 % integration time (sec)
DARK = t*2.55*10^15*PA*DFM*T^1.5*       % dark current (e⁻)
exp(-Eg/(2*k1*T));

TL=1;                                   % transmission of lens
fn=30;                                  % f-number of the lens
mag=.001;                               % magnification of the lens
lense=TL*(4*fn^2*(1+mag)^2)^-1;         % lens equation

row=20;                                 % number of rows (pixels)
column=20;                              % number of columns (pixels)
Num =1000;                              % Number of exposures

% Program
randn('state',sum(100*clock));          % randomize number generators

C=randn(row,column);                    % random number generator for FPN
D=randn(row,column);                    % random number generator for dark FPN

  for k=1:Num;

A=randn(row,column);                    % random number generator for shot noise
B=randn(row,column);                    % random number generator of read noise
E=randn(row,column);                    % random array for dark shot noise

LUX(k)=10^(10/3*log10(k)-4);            % lux light level (lux)

  for j =1:row;
  for i=1:column;


sig(j,i)=LUX(k)*4*10^11*t*QE*PA*lense;  % signal (e⁻)
read(j,i) = RN*B(j,i);                  % read noise (e⁻)
shot(j,i) =A(j,i).* (sig(j,i)).^.5;     % shot noise (e⁻)

FPN(j,i) = C(j,i).*sig(j,i).*PN;        % FPN (e⁻)
Dshot(j,i)= E(j,i).*DARK^.5;            % dark shot noise (e⁻)
DFPN(j,i) = D(j,i).*DN.*DARK;           % dark FPN (e⁻)

  end
  end
```

```
SIG1=sig+read+shot+FPN+Dshot+DFPN;   % read+shot+FPN+dark shot+dark
                                     FPN (e−)
SIG2=sig+read+shot+Dshot+DFPN;       % read+shot+dark shot+dark FPN (e−)

S1(k)=mean(mean(SIG1)');             % average signal for SIG1
N1(k)=mean(std(SIG1)');              % average noise for SIG1

if S1(k)>FW;                         % full well limit
    S1(k)=0;
   end

S2(k)=mean(mean(SIG2)');             % average signal for SIG2
N2(k)=mean(std(SIG2)');              % average noise for SIG2

if S2(k)>FW;                         % full well limit
   S2(k)=0;
   end

StoN(k)=S1(k)./N1(k);                % S/N for SIG1
S2toN2(k)=S2(k)./N2(k);              % S/N for SIG2

   end

%Lux Tranfer Plot
plot(LUX,StoN,'k',LUX,S2toN2,'k');
```

Table of Symbols

Symbol	Parameter	Units	Chapter
$[S/N]_{A\_FF}$	Absolute flat field S/N		12
$[S/N]_{A\_I}$	Absolute image S/N		12
$[S/N]_{FF}$	Flat field S/N		10
$[S/N]_{FF\_COR}$	FPN corrected flat-field S/N		10
$[S/N]_{FF\_SUM}$	Flat-field S/N with on-chip summing		10
$[S/N]_{I}$	Image S/N		10
$[S/N]_{I\_AV}$	Image S/N with frame averaging		10
$[S/N]_{I\_COR}$	FPN corrected image S/N		10
$[S/N]_{I\_MAX}$	Maximum image S/N		10
$[S/N]_{SIN}$	Sinusoidal S/N		10
$[S/N]_{SIN\_AV}$	Sinusoidal S/N with frame averaging		10
$[S/N]_{SIN\_COR}$	FPN corrected sinusoidal S/N		10
$[S/N]_{SIN\_MAX}$	Maximum sinusoidal S/N		10
$A(\mathrm{DN}/V_{\mathrm{SN}})$	Sense node to ADC gain	DN/V	7
A_{ADC}	ADC gain	DN/V	4
A_{CDS}	CDS gain	V/V	4
A_{D}	Standard diode area	cm^2	2
A_{SF}	Source follower gain	V/V	4
A_{SN}	Sense node gain	$\mathrm{V/e}^-$	4
B	Equivalent noise bandwidth	Hz	11
c	Speed of light	cm/sec	3
CCE	Charge collection efficiency		4
C_{D}	Detector contrast		9
C_{P}	Photon scene contrast		9
C_{SN}	Sense node capacitance	F	4
D	Dark current signal	e^-	11
$D(\mathrm{DN})$	Dark current signal	DN	11
D_{FM}	Dark current figure of merit	$\mathrm{nA/cm}^2$	11
DN	Digital number	DN	4
D_{N}	Dark current FPN quality factor		11

Continued

Symbol	Parameter	Units	Chapter
$\mathrm{DN_{ADC}}$	Raw ADC signal	DN	4
DR	Dynamic range		5
D_{R}	Dark current rate	$\mathrm{e^-}$/sec	11
$E_{\text{e-h}}$	Energy to generate $\mathrm{e^-}$/hole pair	eV/$\mathrm{e^-}$	2
E_{g}	Silicon band gap energy	eV	11
f	Normalized spatial frequency	cycles/cm	9
f	Electrical frequency	Hz	11
$f\#$	Lens f-number		12
f_{c}	Flicker noise corner frequency	Hz	11
F_{F}	Fano factor		3
f_{N}	Nyquist spatial frequency	cycles/cm	9
f_{S}	Spatial frequency	cycles/cm	9
h	Planck's constant	J-sec	3
$H_{\mathrm{CDS}}(f)$	CDS transfer function		11
h_ν	Photon energy	eV	2
$\mathrm{I_{LAG}}$	Image lag		5
k	Boltzmann's constant	J/K	3
$K_{\mathrm{ADC}}(\mathrm{e^-/DN})$	ADC sensitivity	$\mathrm{e^-}$/DN	2
$K_{\mathrm{ADC}}(P/\mathrm{DN})$	ADC sensitivity	incident photon/DN	4
$K_{\mathrm{ADC}}(P_{\mathrm{I}}/\mathrm{DN})$	ADC sensitivity	interacting photon/DN	4
$K_{\mathrm{CDS}}(\mathrm{e^-}/V_{\mathrm{CDS}})$	CDS sensitivity	$\mathrm{e^-}$/V	4
$K_{\mathrm{PI}}(P/P_{\mathrm{I}})$	Incident photon sensitivity		4
$K_{\mathrm{SF}}(\mathrm{e^-}/V_{\mathrm{SF}})$	Source follower sensitivity	$\mathrm{e^-}$/V	4
$K_{\mathrm{SN}}(\mathrm{e^-}/V_{\mathrm{SN}})$	Sense node sensitivity	$\mathrm{e^-}$/V	4
$K_{\mathrm{SN}}(P_{\mathrm{I}}/\mathrm{e^-})$	Interacting photon sensitivity	interacting photon/$\mathrm{e^-}$	4
L	Luminance light level	lux	12
L_{A}	Photon absorption length	μm	2
L_{MIN}	Minimum luminance for S/N = 1	lux	12
L_{Q}	Image luminance for S/N = 10	lux	12
m	Lens magnification		12
M_{I}	Image modulation constant	$\mathrm{e^-}$	9
M_{SIN}	Sinusoidal modulation constant	$\mathrm{e^-}$	9
$\mathrm{MTF_D}$	Detector MTF		9
N_{ADC}	Number of ADC DN levels	DN	11
$N_{\mathrm{ADC}}(\mathrm{e^-/DN})$	ADC noise sensitivity	$\mathrm{e^-}$/DN	7

Continued

Symbol	Parameter	Units	Chapter
N_{AV}	Number of frames averaged		10
N_{BITS}	Number of ADC bits	bits	11
N_{FF}	Number of flat fields averaged		8
N_{L}	Number of photons for 1 lux	photons	12
$\mathrm{NL_D}$	Dark current nonlinearity		11
$\mathrm{NL_K}$	V/V nonlinearity		7
$\mathrm{NL_N}$	V/e^- noise nonlinearity		7
$\mathrm{NL_S}$	V/e^- signal nonlinearity		7
N_{P}	Photon rate area density	photons/cm^2-sec	12
N_{PIX}	Number of pixels sampled	pixels	5
$N_{\mathrm{SN}}(e^-/V_{\mathrm{SN}})$	Sense node noise sensitivity	e^-/V	7
OFF(DN)	Offset frame	DN	5
P	Incident photons	photons	2
P_{A}	Pixel area	cm^2	2
P_{I}	Interacting photons	photons	2
p_{ix}	Pixel pitch	cm	9
P_{N}	FPN quality factor		3
q	Electron charge	C	4
QE	Quantum efficiency	e^-/incident photon	2
$\mathrm{QE_D}$	Standard diode QE	e^-/incident photon	2
$\mathrm{QE_I}$	Interacting quantum efficiency	interacting photons/ incident photons	2
Q_{FF}	Flat-field quality factor	e^-	8
R	Reset MOSFET channel resistance	R	11
R_{e}	Standard diode responsivity	A/W	2
R_{e}	Absolute responsivity	e^-/lux-sec	12
$R_{\mathrm{e}}(V_{\mathrm{SN}})$	Relative responsivity	V/lux-sec	12
R_{REF}	Silicon reflection factor		2
S	Flat-field signal	e^-	2
S(DN)	ADC signal	DN	2
$S(V_{\mathrm{CDS}})$	CDS signal	V	4
$S(V_{\mathrm{SF}})$	Source follower signal	V	4
$S(V_{\mathrm{SN}})$	Sense node signal	V	4
S_{A}	Absolute signal	e^-	12
$S_{\mathrm{A\_MIN}}$	Minimum detectable signal for S/N = 1	e^-	12
$S_{\mathrm{ADC}}(e^-/\mathrm{DN})$	ADC signal sensitivity	e^-/DN	7
$S_{\mathrm{ADC\_OFF}}$(DN)	ADC offset	DN	4

Continued

Symbol	Parameter	Units	Chapter
S_{D}	Standard photo diode signal	e^-/sec	2
$S_{\mathrm{DET}}(f)$	Detector noise power spectrum		11
S_{FW}	Full well	e^-	5
S_{I}	Average image signal level	e^-	9
S_{iCOR}	Signal after FPN is removed	e^-	8
S_{iFF}	Flat-field correction signal level	e^-	8
SIN	Sinusoidal pixel output signal	e^-	9
S_{iRAW}	Signal before FPN is removed	e^-	8
S_{MAX}	Maximum sinusoidal signal	e^-	9
$S_{\mathrm{MAX}}(P)$	Maximum sinusoidal photon input	photons	9
S_{MIN}	Minimum sinusoidal signal	e^-	9
$S_{\mathrm{MIN}}(P)$	Minimum sinusoidal photon input	photons	9
$S_{\mathrm{RTS}}(f)$	RTS noise power spectrum		11
S_{SIN}	Average sinusoidal signal level	e^-	9
$S_{\mathrm{SN}}(e^-/V_{\mathrm{SN}})$	Sense node signal sensitivity	e^-/V	7
T	Temperature	K	3
T_{EPI}	Silicon epi thickness	μm	2
t_{I}	Integration time	sec	2
T_{L}	Transmission of lens		12
t_{s}	CDS sample-to-sample time	sec	11
V_{CDS}	CDS voltage	V	4
$V_{\mathrm{CDS\_OFF}}$	CDS offset voltage	V	4
V_{REF}	Sense node reference voltage	V	4
V_{SF}	Source follower voltage	V	4
$V_{\mathrm{SF\_OFF}}$	Source follower offset voltage	V	4
V_{SN}	Sense node voltage	V	4
$W(f)$	Source follower white noise	V/Hz$^{1/2}$	11
δ_{I}	Image signal modulation	rms e^-	9
ΔI	RTS current modulation	A	11
p_{f}	Pixel fill factor		9
δ_{SIN}	Sinusoidal signal modulation	rms e^-	9
η_{E}	Effective quantum yield	e^-/interacting photons	4
η_{i}	Quantum yield	e^-/interacting photons	2
λ	Wavelength	A	2
μ_{FF}	Average flat-field signal level	e^-	8
σ_{ADC}	ADC quantizing noise	rms e^-	11
σ_{COR}	Noise after FPN is removed	rms e^-	8

Continued

Symbol	Parameter	Units	Chapter
$\sigma_{\mathrm{D\_FPN}}$	Dark current FPN	rms e^-	11
$\sigma_{\mathrm{D\_FPN}}$(DN)	Dark current FPN	rms DN	11
$\sigma_{\mathrm{D\_SHOT}}$	Dark current shot noise	rms e^-	11
$\sigma_{\mathrm{D\_SHOT}}$(DN)	Dark current shot noise	rms DN	11
σ_{FN}	Fano noise	rms e^-	3
σ_{FPN}	Pixel FPN	rms e^-	3
σ_{FPN}(DN)	Pixel FPN	rms DN	5
$\sigma_{\mathrm{I\_FPN}}$	Image FPN	rms e^-	9
$\sigma_{\mathrm{I\_M}}$	Total image modulation	rms e^-	9
$\sigma_{\mathrm{I\_SHOT}}$	Image shot noise	rms e^-	9
$\sigma_{\mathrm{I\_TOTAL}}$	Total image noise	rms e^-	9
σ_{K}	ADC sensitivity standard deviation	rms e^-/DN	6
σ_{OFF}	Offset FPN noise	rms e^-	11
σ_{READ}	Read noise	e^- rms	5
σ_{READ}(DN)	Read noise	rms DN	5
$\sigma_{\mathrm{READ+SHOT}}$(DN)	Read and shot noise	rms DN	5
σ_{RESET}	Sense node reset noise	rms e^-	11
$\sigma_{\mathrm{RESET}}(V_{\mathrm{SN}})$	Sense node reset noise voltage	V	11
$\sigma_{\mathrm{SF}}(V_{\mathrm{SF}})$	Pixel source follower noise voltage	rms V	11
σ_{SHOT}	ADC shot noise	e^- rms	3
σ_{SHOT}(DN)	ADC shot noise	rms DN	4
$\sigma_{\mathrm{SHOT}}(P)$	Incident photon shot noise	rms photons	4
$\sigma_{\mathrm{SHOT}}(P_{\mathrm{I}})$	Interacting photon shot noise	rms photons	3
$\sigma_{\mathrm{SHOT}}(V_{\mathrm{CDS}})$	CDS shot noise voltage	rms V	4
$\sigma_{\mathrm{SHOT}}(V_{\mathrm{SF}})$	Source follower shot noise voltage	rms V	4
$\sigma_{\mathrm{SHOT}}(V_{\mathrm{SN}})$	Sense node shot noise voltage	rms V	4
$\sigma_{\mathrm{SIN\_FPN}}$	Sinusoidal FPN	rms e^-	9
$\sigma_{\mathrm{SIN\_M}}$	Total sinusoidal modulation	rms e^-	9
$\sigma_{\mathrm{SIN\_SHOT}}$	Sinusoidal shot noise	rms e^-	9
$\sigma_{\mathrm{SIN\_TOTAL}}$	Total sinusoidal noise	rms e^-	9
σ_{SY}	System noise	rms e^-	11
σ_{TOTAL}	Total noise	rms e^-	3
σ_{TOTAL}(DN)	Total noise	rms DN	5
τ_{D}	CDS dominate time constant	sec	11
τ_{RTS}	RTS characteristic time constant	sec	11

References

1. J. Janesick, *Scientific Charge-Coupled Devices*, SPIE Press, Bellingham, WA (2001).
2. K. Seyrafi, *Electro-Optical Systems Analysis*, Electro-Optical Research Company, Los Angeles, p. 115 (1973).
3. M. Garbuny, *Optical Physics*, Academic Press, Inc., New York (1963).
4. J. Jamieson, R. McFee, G. Plass, R. Grube, and R. Jamieson, *Infrared Physics and Engineering*, McGraw-Hill, New York (1963).
5. J. Janesick, J. Andrews, and T. Elliott, "Fundamental performance differences between CMOS and CCD imagers: Part 1," *Proc. SPIE* 6276, 62760M (2006).
6. J. Janesick, J. Cheng, J. Bishop, J. Andrews, J. Tower, J. Walker, M. Grygon, and T. Elliot, "CMOS minimal array," *Proc. SPIE* 6295, 62950O (2006).
7. J. Janesick and G. Putnam, "Developments and applications of high-performance CCD and CMOS imaging arrays," *Annual Review of Nuclear and Particle Science*, Vol. 53, pp. 263–300 (2003).
8. J. Janesick, J. Andrews, J. Tower, T. Elliott, and J. Cheng, "Fundamental performance differences between CMOS and CCD imagers: Part 2," *Proc. SPIE* 6690-2, yet to be published (2007).
9. J. Janesick, "Lux transfer: Complementary metal oxide semiconductors versus charge-coupled devices," *Optical Engineering*, Vol. 41, Issue 6, pp. 1203–1215 (2002).

Index

James R. Janesick is a Distinguished Engineer and group leader at Sarnoff Inc., developing high-performance CMOS imagers for various scientific and government projects. Previously, he was group leader for Advanced Development Personal Imaging Systems at Conexant Systems Inc., developing commercial CMOS imagers. He founded and directed the Advanced Systems Division of Pixel Vision, Inc., developing high-speed backside illuminated CCDs for scientific and cinematographic applications. He was with the Jet Propulsion Laboratory for 22 years, where he was group leader of the Advanced CCD Sensors Development Group. He pioneered scientific CCD and support electronic designs for several NASA space-borne imaging systems, including the Hubble Space Telescope, Galileo, Cassini, the Multi-Imaging Spectral Radiometer, the Solar X-ray Telescope, the Mars Orbital Camera, Mars Pathfinder, Deep Space I, Pluto Horizons, and Star Dust. He has authored 77 publications on CCD and CMOS imagers and contributed to 17 *NASA Tech Briefs*. Additionally, he holds 10 patents for various CCD and CMOS innovations and has authored the text books *Scientific Charge-Coupled Devices* and *Photon Transfer*. He received NASA medals for Exceptional Engineering Achievement in 1982 and 1992, was the recipient of the SPIE Educator Award in 2004, and is a SPIE fellow. He also has presented over 75 short courses on CCDs and CMOS imagers for UCLA Extension and SPIE.